

**EFFECTS OF DIMETHYL ETHER  
ON N-BUTANE OXIDATION**

**A Thesis Submitted to  
the Graduate School of Engineering and Sciences of  
İzmir Institute of Technology  
in Partial Fulfillment of the Requirements for the Degree of  
MASTER OF SCIENCE  
in Chemical Engineering**

**by  
Tuğçe BEKAT**

**December 2011  
İZMİR**

We approve the thesis of **Tuğçe BEKAT**

---

**Assoc. Prof. Dr. Fikret İNAL**  
Supervisor

---

**Prof. Dr. Devrim BALKÖSE**  
Committee Member

---

**Assist. Prof. Dr. Ali ÇAĞIR**  
Committee Member

**15 December 2011**

---

**Prof. Dr. Mehmet POLAT**  
Head of the Department of  
Chemical Engineering

---

**Prof. Dr. R. Tuğrul SENGER**  
Dean of the Graduate School of  
Engineering and Sciences

## **ACKNOWLEDGEMENTS**

I would like to express my gratitude to my supervisor Dr. Fikret İnal for his guidance and support during my graduate studies, and for his patience, motivation, encouragement and immense knowledge. I also would like to thank my mother Serap Hiçyılmaz for supporting me throughout my life.

# ABSTRACT

## EFFECTS OF DIMETHYL ETHER ON N-BUTANE OXIDATION

Effects of dimethyl ether on the oxidation of n-butane were investigated using Detailed Chemical Kinetic Modeling approach. Oxidation process was carried out in a tubular reactor under laminar flow conditions. The formations of various oxidation products, especially toxic species were investigated for the addition of dimethyl ether in different mole fractions to n-butane. Pure dimethyl ether oxidation was also investigated for comparison. Pure dimethyl ether oxidation resulted in lower mole fractions of carbon monoxide, methane, acetaldehyde and aromatic species, but higher mole fractions of formaldehyde when compared to pure n-butane oxidation. The addition of dimethyl ether to n-butane in different mole fractions was observed to decrease mole fractions of acetaldehyde and aromatic species and increase the mole fraction of formaldehyde, while other toxic species investigated were not affected significantly.

The effects of three important process parameters on the formations of oxidation products were also investigated. Inlet temperatures between 500 and 1700 K, pressures of 1 and 5 atm, and equivalence ratios of 2.6 and 3.0 were studied. Increasing pressure and equivalence ratio were observed to increase the mole fractions of toxic species in general. The effect of temperature was more complicated depending on the species and the temperature interval.

Reaction path analysis indicated that the most important precursors playing role in the formation of the first ring benzene were acetylene, ethylene, propargyl, allene, allyl, propene and fulvene during n-butane/dimethyl ether oxidation.

Finally, a skeletal chemical kinetic mechanism was developed and validated for the oxidation of n-butane/dimethyl ether mixture.

# ÖZET

## DİMETİL ETERİN N-BÜTAN OKSİDASYONUNA ETKİLERİ

Dimetil eterin n-bütan oksidasyonuna olan etkileri kimyasal kinetik modellemeyle teorik olarak incelenmiştir. Oksidasyon, bir borusal akış reaktörde ve laminer akış koşullarında çalışılmış, değişik oranlardaki dimetil eterin n-bütana ilavesinin, oksidasyon ürünlerinin oluşumlarına etkileri araştırılmıştır. Ayrıca saf dimetil eter oksidasyonu da karşılaştırma amacıyla incelenmiştir. Saf dimetil eter oksidasyonunda, saf n-bütan oksidasyonuna göre, karbon monoksit, metan, asetaldehit ve aromatik bileşikler gibi zararlı bileşiklerin daha düşük oranlarda oluştukları, formaldehitin ise daha yüksek oranlarda oluştuğu gözlenmiştir. Dimetli eterin n-bütana farklı oranlarda ilave edilmesi durumunda ise, yine formaldehit mol kesrinde artış, asetaldehit ve aromatik bileşiklerin mol kesirlerinde ise azalma görülmüş, incelenen diğer zararlı bileşiklerin mol kesirlerinde ise önemli bir değişiklik gerçekleşmemiştir.

Çalışmada sıcaklık, basınç ve eşdeğerlik oranının dimetil eter/n-bütan oksidasyonu üzerine olan etkileri de incelenmiştir. Sıcaklık aralığı olarak 500-1700 K, basınç değeri olarak 1 ve 5 atm, ve eşdeğerlik oranı olarak da 2.6 ve 3.0 değerleri seçilmiş ve bu koşullarda ürün oluşumları incelenmiştir. Basınç ve eşdeğerlik oranı artışının genel olarak zararlı oksidasyon ürünlerinde artışlara neden olduğu bulunmuştur. Sıcaklığın etkisi ise oluşan ürüne ve sıcaklık aralığına göre farklılıklar göstermektedir.

Zararlı oksidasyon ürünlerinden en küçük halkalı aromatik bileşik olan benzenin oluşumunda rol oynayan en önemli öncü bileşikler asetilen, etilen, proparjil, allen, allil, propen ve fulven olarak belirlenmiştir.

Son olarak, dimetil eter/n-bütan karışımının oksidasyonunu temsil etmek üzere bir iskelet kimyasal kinetik mekanizma geliştirilmiş ve bu mekanizma literatür ve detaylı mekanizmayla karşılaştırılarak doğrulanmıştır.

# TABLE OF CONTENTS

LIST OF FIGURES.....	vii
LIST OF TABLES.....	xiii
CHAPTER 1. INTRODUCTION.....	1
CHAPTER 2. LITERATURE REVIEW.....	3
2.1. General Mechanism of Hydrocarbon Oxidation.....	3
2.1.1. Formations of CO and CO <sub>2</sub> during the Oxidation of Hydrocarbons.....	5
2.1.2. Formation of PAHs during the Oxidation of Hydrocarbons.....	6
2.2. n-Butane and its Oxidation Mechanism.....	7
2.3. DME and its Oxidation Mechanism.....	15
2.4. Studies of DME as a Fuel Additive.....	21
CHAPTER 3. METHOD.....	26
3.1. Theory of Chemical Kinetic Modeling Using Chemkin <sup>®</sup> .....	26
3.1.1. Chemical Rate Expressions.....	27
3.1.2. Thermodynamic Properties.....	29
3.1.3. Transport Properties.....	30
3.1.4. Validation of the Detailed Chemical Kinetic Mechanism.....	31
3.1.5. Reactor Model.....	32
3.1.5.1. Validation of the Plug-Flow Assumption.....	37
3.2. Reduction of the Detailed Mechanism into a Skeletal Mechanism for the Oxidation of n-Butane/DME Mixture.....	38
CHAPTER 4. RESULTS AND DISCUSSION.....	40
4.1. Investigation of the Effects of DME Addition to n-Butane Oxidation.....	41

4.2. The Effects of Process Parameters on n-Butane/DME Oxidation.....	65
4.2.1. The Effects of Temperature and Pressure.....	65
4.2.2. The Effects of Equivalence Ratio.....	88
4.3. The Formation Pathways of the Aromatic Species in n-Butane and n-Butane/DME Oxidations.....	108
4.4. Skeletal Mechanism for n-Butane/DME Oxidation.....	122
CHAPTER 5. CONCLUSIONS.....	126
REFERENCES.....	129
APPENDICES	
APPENDIX A. DETAILED CHEMICAL KINETIC MECHANISM.....	134
APPENDIX B. SKELETAL CHEMICAL KINETIC MECHANISM.....	155

## LIST OF FIGURES

<b><u>Figure</u></b>		<b><u>Page</u></b>
Figure 2.1.	Reaction pathway diagrams for the reaction sequences leading to aromatic species and aliphatic products that occur in n-butane oxidation.....	14
Figure 2.2.	Overall reaction scheme for dimethyl ether oxidation.....	20
Figure 3.1.	Validation of the detailed chemical kinetic mechanism for C <sub>4</sub> H <sub>10</sub> oxidation by comparison with the results of Chakir et al. (1989)....	33
Figure 3.2.	Validation of the detailed chemical kinetic mechanism for CH <sub>3</sub> OCH <sub>3</sub> oxidation by comparison with the results of Fischer et al. (2000).....	34
Figure 3.3.	Validation of the detailed chemical kinetic mechanism for CH <sub>4</sub> /CH <sub>3</sub> OCH <sub>3</sub> and C <sub>2</sub> H <sub>6</sub> /CH <sub>3</sub> OCH <sub>3</sub> oxidation by comparison with the results of Yoon et al. (2008).....	35
Figure 4.1.	Temperature profiles for different concentrations of CH <sub>3</sub> OCH <sub>3</sub> added to C <sub>4</sub> H <sub>10</sub> /O <sub>2</sub> /Ar oxidation versus reactor distance.....	46
Figure 4.2.	Concentration profiles of (a) C <sub>4</sub> H <sub>10</sub> and (b) CH <sub>3</sub> OCH <sub>3</sub> for different concentrations of CH <sub>3</sub> OCH <sub>3</sub> added to C <sub>4</sub> H <sub>10</sub> /O <sub>2</sub> /Ar oxidation versus reactor distance.....	47
Figure 4.3.	Concentration profile of O <sub>2</sub> for different concentrations of CH <sub>3</sub> OCH <sub>3</sub> added to C <sub>4</sub> H <sub>10</sub> /O <sub>2</sub> /Ar oxidation versus reactor distance.....	48
Figure 4.4.	Concentration profiles of (a) CO <sub>2</sub> and (b) CO for different concentrations of CH <sub>3</sub> OCH <sub>3</sub> added to C <sub>4</sub> H <sub>10</sub> /O <sub>2</sub> /Ar oxidation versus reactor distance.....	49
Figure 4.5.	Concentration profiles of (a) H <sub>2</sub> O and (b) H <sub>2</sub> for different concentrations of CH <sub>3</sub> OCH <sub>3</sub> added to C <sub>4</sub> H <sub>10</sub> /O <sub>2</sub> /Ar oxidation versus reactor distance.....	50
Figure 4.6.	Concentration profiles of (a) CH <sub>4</sub> (b) C <sub>2</sub> H <sub>6</sub> and (c) C <sub>3</sub> H <sub>8</sub> for different concentrations of CH <sub>3</sub> OCH <sub>3</sub> added to C <sub>4</sub> H <sub>10</sub> /O <sub>2</sub> /Ar oxidation versus reactor distance.....	51



Figure 4.7.	Concentration profiles of (a) CH <sub>2</sub> O and (b) C <sub>2</sub> H <sub>4</sub> O for different concentrations of CH <sub>3</sub> OCH <sub>3</sub> added to C <sub>4</sub> H <sub>10</sub> /O <sub>2</sub> /Ar oxidation versus reactor distance.....	52
Figure 4.8.	Concentration profiles of (a) C <sub>2</sub> H <sub>2</sub> and (b) C <sub>2</sub> H <sub>4</sub> for different concentrations of CH <sub>3</sub> OCH <sub>3</sub> added to C <sub>4</sub> H <sub>10</sub> /O <sub>2</sub> /Ar oxidation versus reactor distance.....	53
Figure 4.9.	Concentration profiles of (a) C <sub>3</sub> H <sub>3</sub> and (b) C <sub>3</sub> H <sub>6</sub> for different concentrations of CH <sub>3</sub> OCH <sub>3</sub> added to C <sub>4</sub> H <sub>10</sub> /O <sub>2</sub> /Ar oxidation versus reactor distance.....	54
Figure 4.10.	Concentration profiles of (a) aC <sub>3</sub> H <sub>4</sub> and (b) pC <sub>3</sub> H <sub>4</sub> for different concentrations of CH <sub>3</sub> OCH <sub>3</sub> added to C <sub>4</sub> H <sub>10</sub> /O <sub>2</sub> /Ar oxidation versus reactor distance.....	55
Figure 4.11.	Concentration profiles of (a) C <sub>4</sub> H <sub>2</sub> and (b) C <sub>4</sub> H <sub>4</sub> for different concentrations of CH <sub>3</sub> OCH <sub>3</sub> added to C <sub>4</sub> H <sub>10</sub> /O <sub>2</sub> /Ar oxidation versus reactor distance.....	56
Figure 4.12.	Concentration profiles of (a) 1,3-C <sub>4</sub> H <sub>6</sub> and (b) 1-C <sub>4</sub> H <sub>6</sub> for different concentrations of CH <sub>3</sub> OCH <sub>3</sub> added to C <sub>4</sub> H <sub>10</sub> /O <sub>2</sub> /Ar oxidation versus reactor distance.....	57
Figure 4.13.	Concentration profiles of (a) C <sub>4</sub> H <sub>8</sub> -1 and (b) C <sub>4</sub> H <sub>8</sub> -2 for different concentrations of CH <sub>3</sub> OCH <sub>3</sub> added to C <sub>4</sub> H <sub>10</sub> /O <sub>2</sub> /Ar oxidation versus reactor distance.....	58
Figure 4.14.	Concentration profiles of c-C <sub>5</sub> H <sub>6</sub> for different concentrations of CH <sub>3</sub> OCH <sub>3</sub> added to C <sub>4</sub> H <sub>10</sub> /O <sub>2</sub> /Ar oxidation versus reactor distance.....	59
Figure 4.15.	Concentration profiles of C <sub>6</sub> H <sub>5</sub> for different concentrations of CH <sub>3</sub> OCH <sub>3</sub> added to C <sub>4</sub> H <sub>10</sub> /O <sub>2</sub> /Ar oxidation versus reactor distance.....	59
Figure 4.16.	Concentration profiles of (a) C <sub>6</sub> H <sub>6</sub> and (b) C <sub>7</sub> H <sub>8</sub> for different concentrations of CH <sub>3</sub> OCH <sub>3</sub> added to C <sub>4</sub> H <sub>10</sub> /O <sub>2</sub> /Ar oxidation versus reactor distance.....	60
Figure 4.17.	Concentration profiles of (a) C <sub>8</sub> H <sub>6</sub> and (b) C <sub>9</sub> H <sub>8</sub> for different concentrations of CH <sub>3</sub> OCH <sub>3</sub> added to C <sub>4</sub> H <sub>10</sub> /O <sub>2</sub> /Ar oxidation versus reactor distance.....	61

Figure 4.18. Concentration profiles of (a) $C_{10}H_8$ (b) $C_{12}H_8$ and (c) $C_{12}H_{10}$ for different concentrations of $CH_3OCH_3$ added to $C_4H_{10}/O_2/Ar$ oxidation versus reactor distance.....	62
Figure 4.19. Concentration profiles of (a) $aC_{14}H_{10}$ and (b) $pC_{14}H_{10}$ for different concentrations of $CH_3OCH_3$ added to $C_4H_{10}/O_2/Ar$ oxidation versus reactor distance.....	63
Figure 4.20. Concentration profiles of $C_{16}H_{10}$ for different concentrations of $CH_3OCH_3$ added to $C_4H_{10}/O_2/Ar$ oxidation versus reactor distance.....	64
Figure 4.21. Final reaction temperatures versus reactor inlet temperatures at different pressures and different concentrations of $CH_3OCH_3$ .....	66
Figure 4.22. Final mole fractions of (a) $C_4H_{10}$ and (b) $CH_3OCH_3$ versus reactor inlet temperatures at different pressures and different concentrations of $CH_3OCH_3$ .....	67
Figure 4.23. Final mole fractions of $O_2$ versus reactor inlet temperatures at different pressures and different concentrations of $CH_3OCH_3$ .....	68
Figure 4.24. Final mole fractions of (a) $CO_2$ and (b) $CO$ versus reactor inlet temperatures at different pressures and different concentrations of $CH_3OCH_3$ .....	69
Figure 4.25. Final mole fractions of (a) $H_2O$ and (b) $H_2$ versus reactor inlet temperatures at different pressures and different concentrations of $CH_3OCH_3$ .....	70
Figure 4.26. Final mole fractions of (a) $CH_4$ (b) $C_2H_6$ and (c) $C_3H_8$ versus reactor inlet temperatures at different pressures and different concentrations of $CH_3OCH_3$ .....	71
Figure 4.27. Final mole fractions of (a) $CH_2O$ and (b) $C_2H_4O$ versus reactor inlet temperatures at different pressures and different concentrations of $CH_3OCH_3$ .....	72
Figure 4.28. Final mole fractions of (a) $C_2H_2$ and (b) $C_2H_4$ versus reactor inlet temperatures at different pressures and different concentrations of $CH_3OCH_3$ .....	73

Figure 4.29.	Final mole fractions of (a) $C_3H_3$ and (b) $C_3H_6$ versus reactor inlet temperatures at different pressures and different concentrations of $CH_3OCH_3$ .....	74
Figure 4.30.	Final mole fractions of (a) $aC_3H_4$ and (b) $pC_3H_4$ versus reactor inlet temperatures at different pressures and different concentrations of $CH_3OCH_3$ .....	75
Figure 4.31.	Final mole fractions of (a) $C_4H_2$ and (b) $C_4H_4$ versus reactor inlet temperatures at different pressures and different concentrations of $CH_3OCH_3$ .....	76
Figure 4.32.	Final mole fractions of (a) 1,3- $C_4H_6$ and (b) 1- $C_4H_6$ versus reactor inlet temperatures at different pressures and different concentrations of $CH_3OCH_3$ .....	77
Figure 4.33.	Final mole fractions of (a) $C_4H_8-1$ and (b) $C_4H_8-2$ versus reactor inlet temperatures at different pressures and different concentrations of $CH_3OCH_3$ .....	78
Figure 4.34.	Final mole fractions of $c-C_5H_6$ versus reactor inlet temperatures at different pressures and different concentrations of $CH_3OCH_3$ .....	79
Figure 4.35.	Final mole fractions of $C_6H_5$ versus reactor inlet temperatures at different pressures and different concentrations of $CH_3OCH_3$ .....	79
Figure 4.36.	Final mole fractions of (a) $C_6H_6$ and (b) $C_7H_8$ versus reactor inlet temperatures at different pressures and different concentrations of $CH_3OCH_3$ .....	80
Figure 4.37.	Final mole fractions of (a) $C_8H_6$ and (b) $C_9H_8$ versus reactor inlet temperatures at different pressures and different concentrations of $CH_3OCH_3$ .....	81
Figure 4.38.	Final mole fractions of (a) $C_{10}H_8$ (b) $C_{12}H_8$ and (c) $C_{12}H_{10}$ versus reactor inlet temperatures at different pressures and different concentrations of $CH_3OCH_3$ .....	82
Figure 4.39.	Final mole fractions of (a) $aC_{14}H_{10}$ and (b) $C_{14}H_{10}$ versus reactor inlet temperatures at different pressures and different concentrations of $CH_3OCH_3$ .....	83
Figure 4.40.	Final mole fractions of $C_{16}H_{10}$ versus reactor inlet temperatures at different pressures and different concentrations of $CH_3OCH_3$ .....	84

Figure 4.41.	Final reaction temperatures versus reactor inlet temperatures at different equivalence ratios and different concentrations of $\text{CH}_3\text{OCH}_3$ .....	89
Figure 4.42.	Final mole fractions of (a) $\text{C}_4\text{H}_{10}$ and (b) $\text{CH}_3\text{CH}_3$ versus reactor inlet temperatures at different equivalence ratios and different concentrations of $\text{CH}_3\text{OCH}_3$ .....	90
Figure 4.43.	Final mole fractions of (a) $\text{O}_2$ versus reactor inlet temperatures at different equivalence ratios and different concentrations of $\text{CH}_3\text{OCH}_3$ .....	91
Figure 4.44.	Final mole fractions of (a) $\text{CO}_2$ and (b) $\text{CO}$ versus reactor inlet temperatures at different equivalence ratios and different concentrations of $\text{CH}_3\text{OCH}_3$ .....	92
Figure 4.45.	Final mole fractions of (a) $\text{H}_2\text{O}$ and (b) $\text{H}_2$ versus reactor inlet temperatures at different equivalence ratios and different concentrations of $\text{CH}_3\text{OCH}_3$ .....	93
Figure 4.46.	Final mole fractions of (a) $\text{CH}_4$ (b) $\text{C}_2\text{H}_6$ and (c) $\text{C}_3\text{H}_8$ versus reactor inlet temperatures at different equivalence ratios and different concentrations of $\text{CH}_3\text{OCH}_3$ .....	94
Figure 4.47.	Final mole fractions of (a) $\text{CH}_2\text{O}$ and (b) $\text{C}_2\text{H}_4\text{O}$ versus reactor inlet temperatures at different equivalence ratios and different concentrations of $\text{CH}_3\text{OCH}_3$ .....	95
Figure 4.48.	Final mole fractions of (a) $\text{C}_2\text{H}_2$ and (b) $\text{C}_2\text{H}_4$ versus reactor inlet temperatures at different equivalence ratios and different concentrations of $\text{CH}_3\text{OCH}_3$ .....	96
Figure 4.49.	Final mole fractions of (a) $\text{C}_3\text{H}_3$ and (b) $\text{C}_3\text{H}_6$ versus reactor inlet temperatures at different equivalence ratios and different concentrations of $\text{CH}_3\text{OCH}_3$ .....	97
Figure 4.50.	Final mole fractions of (a) $\text{aC}_3\text{H}_4$ and (b) $\text{pC}_3\text{H}_4$ versus reactor inlet temperatures at different equivalence ratios and different concentrations of $\text{CH}_3\text{OCH}_3$ .....	98
Figure 4.51.	Final mole fractions of (a) $\text{C}_4\text{H}_2$ and (b) $\text{C}_4\text{H}_4$ versus reactor inlet temperatures at different equivalence ratios and different concentrations of $\text{CH}_3\text{OCH}_3$ .....	99

Figure 4.52.	Final mole fractions of (a) 1,3-C <sub>4</sub> H <sub>6</sub> and (b) 1-C <sub>4</sub> H <sub>6</sub> versus reactor inlet temperatures at different equivalence ratios and different concentrations of CH <sub>3</sub> OCH <sub>3</sub> .....	100
Figure 4.53.	Final mole fractions of (a) C <sub>4</sub> H <sub>8</sub> -1 and (b) C <sub>4</sub> H <sub>8</sub> -2 versus reactor inlet temperatures at different equivalence ratios and different concentrations of CH <sub>3</sub> OCH <sub>3</sub> .....	101
Figure 4.54.	Final mole fractions of c-C <sub>5</sub> H <sub>6</sub> versus reactor inlet temperatures at different equivalence ratios and different concentrations of CH <sub>3</sub> OCH <sub>3</sub> .....	102
Figure 4.55.	Final mole fractions of C <sub>6</sub> H <sub>5</sub> versus reactor inlet temperatures at different equivalence ratios and different concentrations of CH <sub>3</sub> OCH <sub>3</sub> .....	102
Figure 4.56.	Final mole fractions of (a) C <sub>6</sub> H <sub>6</sub> and (b) C <sub>7</sub> H <sub>8</sub> versus reactor inlet temperatures at different equivalence ratios and different concentrations of CH <sub>3</sub> OCH <sub>3</sub> .....	103
Figure 4.57.	Final mole fractions of (a) C <sub>8</sub> H <sub>6</sub> and (b) C <sub>9</sub> H <sub>8</sub> versus reactor inlet temperatures at different equivalence ratios and different concentrations of CH <sub>3</sub> OCH <sub>3</sub> .....	104
Figure 4.58.	Final mole fractions of (a) C <sub>10</sub> H <sub>8</sub> (b) C <sub>12</sub> H <sub>8</sub> and (c) C <sub>12</sub> H <sub>10</sub> versus reactor inlet temperatures at different equivalence ratios and different concentrations of CH <sub>3</sub> OCH <sub>3</sub> .....	105
Figure 4.59.	Final mole fractions of (a) aC <sub>14</sub> H <sub>10</sub> and (b) pC <sub>14</sub> H <sub>10</sub> versus reactor inlet temperatures at different equivalence ratios and different concentrations of CH <sub>3</sub> OCH <sub>3</sub> .....	106
Figure 4.60.	Final mole fractions of C <sub>16</sub> H <sub>10</sub> versus reactor inlet temperatures at different equivalence ratios and different concentrations of CH <sub>3</sub> OCH <sub>3</sub> .....	107
Figure 4.61.	Concentration profiles of (a) C <sub>6</sub> H <sub>6</sub> and C <sub>2</sub> precursor species C <sub>2</sub> H <sub>2</sub> and C <sub>2</sub> H <sub>4</sub> , and (b) C <sub>6</sub> H <sub>6</sub> and C <sub>3</sub> precursor species C <sub>3</sub> H <sub>3</sub> , aC <sub>3</sub> H <sub>4</sub> , pC <sub>3</sub> H <sub>4</sub> , and C <sub>3</sub> H <sub>6</sub> , for the neat oxidation of n-butane.....	111
Figure 4.62.	Concentration profiles of (a) C <sub>6</sub> H <sub>6</sub> and C <sub>4</sub> precursor species C <sub>4</sub> H <sub>2</sub> , 1,3-C <sub>4</sub> H <sub>6</sub> and 1-C <sub>4</sub> H <sub>6</sub> , and (b) C <sub>6</sub> H <sub>6</sub> and C <sub>4</sub> precursor species C <sub>4</sub> H <sub>4</sub> , C <sub>4</sub> H <sub>8</sub> -1, and C <sub>4</sub> H <sub>8</sub> -2, for the neat oxidation of n-butane.....	112

Figure 4.63.	Concentration profiles of $C_6H_6$ and $C_5$ precursor species $c-C_5H_6$ , for the neat oxidation of n-butane.....	113
Figure 4.64.	Concentration profiles of (a) one-ring aromatics (b) two-ring aromatics and (c) three-and four-ring aromatics, for the neat oxidation of n-butane.....	114
Figure 4.65.	Concentration profiles of (a) $C_6H_6$ and $C_2$ precursor species $C_2H_2$ and $C_2H_4$ , and (b) $C_6H_6$ and $C_3$ precursor species $C_3H_3$ , $aC_3H_4$ , $pC_3H_4$ , and $C_3H_6$ , for the oxidation of n-butane/DME mixture.....	115
Figure 4.66.	Concentration profiles of (a) $C_6H_6$ and $C_4$ precursor species $C_4H_2$ , 1-3, $C_4H_6$ and 1- $C_4H_6$ , and (b) $C_6H_6$ and $C_4$ precursor species $C_4H_4$ , $C_4H_8-1$ , and $C_4H_8-2$ , for the oxidation of n-butane/DME mixture...	116
Figure 4.67.	Concentration profiles of $C_6H_6$ and $C_5$ precursor species $c-C_5H_6$ , for the oxidation of n-butane/DME mixture.....	117
Figure 4.68.	Concentration profiles of (a) one-ring aromatics (b) two-ring aromatics and (c) three-and four-ring aromatics, for the oxidation of n-butane/DME mixture.....	118
Figure 4.69.	Main formation paths of $C_6H_6$ from $C_4H_{10}$ during the oxidations of (a) neat $C_4H_{10}$ and (b) $C_4H_{10}/CH_3OCH_3$ mixture at $T=1100K$ .....	119
Figure 4.70.	Main formation paths of $C_6H_6$ from $C_4H_{10}$ during the oxidations of (a) neat $C_4H_{10}$ and (b) $C_4H_{10}/CH_3OCH_3$ mixture at $T=950K$ .....	120
Figure 4.71.	Main formation paths of $C_6H_6$ from $C_4H_{10}$ during the oxidations of (a) neat $C_4H_{10}$ and (b) $C_4H_{10}/CH_3OCH_3$ mixture at $T=1350K$ .....	120
Figure 4.72.	Total number of elementary reactions for different threshold values of normalized reaction contribution coefficients.....	123
Figure 4.73.	Validation of the skeletal chemical kinetic mechanism for $CH_4/CH_3OCH_3$ and $C_2H_6/CH_3OCH_3$ oxidation by comparison with the results of Yoon et al. (2008).....	124
Figure 4.74.	Comparison of the results of the skeletal mechanism with the results of the detailed mechanism, showing the mole fractions of (a) $C_2H_2$ (b) $C_3H_3$ (c) $C_6H_6$ and (d) $C_{16}H_{10}$ versus inlet temperatures for the oxidation of n-butane/DME(50:50) mixture...	125

## LIST OF TABLES

<b><u>Table</u></b>		<b><u>Page</u></b>
Table 2.1.	Physical and chemical properties of DME compared with the properties of diesel fuel .....	16
Table 4.1.	Parameters investigated for the oxidation of n-butane/DME mixture.....	40
Table 4.2.	Inlet mole fractions of n-butane, DME, O <sub>2</sub> , and Ar for various concentrations of DME added to n-butane oxidation for an equivalence ratio of 2.6.....	41
Table 4.3.	List of the major and minor oxidation products investigated.....	43
Table 4.4.	List of investigated aromatic species and PAHs.....	44

# CHAPTER 1

## INTRODUCTION

Emissions from combustion and oxidation processes utilized in transportation, manufacturing and power generation are the major sources of environmental pollution. Environmental concerns and dependency on fossil fuel reserves result in growing demand of alternative fuels and advanced energy technologies which will fulfill the requirements of low hazardous emissions and higher energy efficiencies.

The pollutants emitted from oxidation processes can be classified as carbon monoxide (CO), nitrogen oxides (NO<sub>x</sub>), sulfur oxides (SO<sub>x</sub>), organic compounds (unburned and partially burned hydrocarbons), and particulates (soot, fly ash, and aerosols). The formation of these oxidation products are related to the oxidation chemistry of fuels as well as process conditions. Thus, the need to control the emission levels of oxidation products requires better physical and chemical understanding of oxidation processes.

In the last decades, numerical modeling has rapidly become an essential part of the research carried out on oxidation processes. Detailed chemical kinetic mechanisms are routinely used to describe the transformation of reactants into products at the molecular level. Detailed chemical kinetic mechanisms describing oxidation chemistry are structured in a hierarchical manner including elementary reactions and kinetic parameters of these reactions. Given the wide range of operating parameters experienced in most oxidation systems, also a suitable physical and numerical model for each of the physical and chemical processes (such as turbulence, heat transfer, diffusive transport etc.) should be included in the representations of these systems. The sets of differential equations describing the rates of formation and destruction of each species and other physical processes are then integrated; and the computed concentrations of reactants, intermediates, and products are compared to experimental results. This procedure, known as modeling, is widely used in oxidation studies.

The bulk of fuels utilized currently are almost totally comprised of hydrocarbons and hydrocarbons are by far the most studied class of compounds for which reliable and detailed chemical information exists. One of the most important types of emissions from



these fuels is organic and carbonaceous emissions which represent not only fuel loss but also, in some cases, a significant pollution problem.

n-Butane ( $C_4H_{10}$ ), one type of hydrocarbon fuel, is an alkane that is produced by the fractionation of crude oil in refinery operations or during natural gas processing. Large amounts of n-butane are consumed as fuel or fuel component in internal combustion engines, industrial burners, and residential heating. It is also one of the two main components of liquefied petroleum gas (LPG). Although n-butane is known to be a cleaner fuel producing lower emissions compared to gasoline and diesel; there are still some types of emissions such as CO, polycyclic aromatic hydrocarbons (PAHs), and soot, associated with the usage of n-butane, especially in fuel-rich conditions. There are fundamental reasons for examining the fuel-rich oxidation process of n-butane, since the reaction sequences leading to the formations of CO, PAHs, and soot compromise a very complicated process. These compounds are known to be toxic or carcinogenic and their emissions are subject to regulatory control.

Currently, the most used alternative fuels are natural gas, LPG, and biofuels. Some types of alternative fuels may also be used as fuel additives, instead of being directly applied as neat fuels. Dimethyl ether (DME), alcohols, and other oxygenates are examples to these types of fuel additives. Oxygenated organic compounds are added to fuels in small amounts in order to promote the oxidation of rich mixtures and to reduce emissions.

Among these oxygenated fuel additives, DME ( $CH_3OCH_3$ ) is the simplest ether containing two methyl groups linked by an oxygen atom. It does not contain any C-C bonds and it has the lowest possible C/H ratio after methane. These properties of DME are related to smokeless and low-emission oxidation characteristics of DME, and make it an attractive fuel additive.

In this study, the addition of DME to the oxidation of n-butane was studied using detailed chemical kinetic modeling approach. The effects of DME addition on the formations of main oxidation products and emissions from the oxidation of n-butane were analyzed. The effects of various process parameters, such as temperature, pressure and equivalence ratio, were also investigated. The formation pathways of the first aromatic ring benzene was tried to be identified for the oxidations of n-butane and n-butane/DME mixture. Finally, a skeletal kinetic mechanism that represents n-butane/DME oxidation was developed.

## CHAPTER 2

### LITERATURE REVIEW

#### 2.1. General Mechanism of Hydrocarbon Oxidation

The behavior of the chemical oxidation mechanism of hydrocarbons change from one mechanism to another as the reaction parameters change, due to the temperature and pressure dependence of various elementary reactions. Depending on initial conditions, the same initial reactants may yield different products. The mechanisms of hydrocarbon oxidation are somewhat different at low and high temperatures.

During the oxidations of hydrocarbons, after the initiation steps have created some radicals, the radical pool is rapidly established. Once the radical pool is established, the most important reactions are the H-abstraction reactions from the fuel molecules. The most important radicals that participate in H-abstraction reactions from the fuel are OH, O, H, CH<sub>3</sub>, and HO<sub>2</sub> radicals (Westbrook and Pitz, 1989).

At temperatures below 423 K, the oxidation of hydrocarbons is very slow. The most important intermediate species produced are hydroperoxides. Above 373 K, the hydroperoxides formed produce alcohols (RC-OH), ketones (RC=O) or aldehydes (R-CHO). Further reaction of the aldehydes rapidly produces acids (RC=O-OH). Above about 573 K, the gas phase oxidation of hydrocarbons is a slow process that mainly yields olefins (RC=CH<sub>2</sub>) and H<sub>2</sub>O<sub>2</sub> (Bartok and Sarofim, 1991).

At temperatures around 500–600 K, alkyl radicals react rapidly with O<sub>2</sub> molecules and form peroxy radicals. Peroxy radicals then lead to the formation of peroxide species and small radicals, which then react with alkane molecules to reproduce alkyl radicals. The propagation of the reaction is a chain reaction and the main carriers are the OH radicals. The degenerate branching steps involving formation of alkyl radicals from peroxides are related to the exponential acceleration of the overall reaction rate due to multiplication of the number of radicals. When the temperature increases to the benefit of the formation of alkenes, the reversibility of the alkyl addition to O<sub>2</sub> leads a reduction in the overall reaction rate. This is the main cause of the

appearance of the “negative temperature coefficient” (NTC) region that signifies a zone of temperature in which the overall rate of reaction decreases with increasing temperature (Battin-Leclerc, 2008). The range of temperatures where NTC region occurs is a function of pressure, but generally is around 650–700 K (Bartok and Sarofim, 1991).

The existence of the NTC region results in another characteristic of the oxidation of hydrocarbons, which is the occurrence of “cool flames”. During occurrence of cool flames, temperature and pressure increase strongly over a limited temperature range, but the reaction stops before completion as a result of the decrease of reactivity in the NTC region. Cool flames play an important role in two-stage autoignition (Griffiths and Mohamed, 1997; Battin-Leclerc, 2008). These phenomena occur for all alkanes, except for methane and ethane (Bartok and Sarofim, 1991).

The low-temperature oxidation region ends with the transition through NTC zone to intermediate-temperature oxidation region. The key feature of the low-temperature kinetic mechanism is the production of OH radicals, since these radicals then react with the fuel molecules producing H<sub>2</sub>O and releasing a significant amount of heat (Westbrook and Pitz, 1989). Also, it should be noted that, in addition to the intermediate species characteristics, there are significant productions of CO and CO<sub>2</sub> accompanying the formation and oxidation of the reactant intermediates (Bartok and Sarofim, 1991).

As the intermediate-temperature region begins, reactions such as  $\text{H}_2\text{O}_2 \rightarrow 2\text{OH}$  and  $\text{H} + \text{O}_2 \rightarrow \text{O} + \text{OH}$  result in the multiplication of the number of radicals (Battin-Leclerc, 2008). At temperatures above 800 K, the oxidation chemistry of most hydrocarbons begins to change. Alkyl radicals formed through H-abstraction start to decompose to smaller hydrocarbon radicals and small olefins. Methyl, ethyl, and propyl radicals formed in this region are important since they are the only radicals likely to yield H atoms through further reaction (Bartok and Sarofim, 1991).

At temperatures above 900–1000 K, the alkyl radicals that contain more than 3 atoms of carbon decompose to give a smaller alkyl radical and a 1-alkene molecule. H-abstractions followed by isomerizations and decompositions of alkyl radicals until the chemistry of C<sub>1</sub> - C<sub>2</sub> species (Simmie, 2003) is reached (Warnatz, 1983; Westbrook and Dryer, 1984; Battin-Leclerc, 2008). In this high-temperature regime, the chain branching features of the oxidation mechanism are dominated by the reaction  $\text{H} + \text{O}_2 \rightarrow \text{O} + \text{OH}$  and the overall rate of reaction is very fast (Westbrook and Pitz, 1989).

Finally, as severe conditions are approached (1800 K and 1 atm), decomposition of reactants, including very stable ones such as aromatics and more stable radicals, becomes significant (Bartok and Sarofim, 1991).

The oxidations of alkanes follow the general mechanisms for hydrocarbon oxidation mentioned above. The chemistry of the oxidation of ethers is also very close to that of alkanes. The only characteristic of the oxidation of ethers is a molecular reaction involving the transfer of a H-atom bound to a C-atom into the  $\beta$  position of an O-atom, to form an alcohol molecule and an alkyl radical. The presence of an atom of oxygen also favors the decomposition of radicals derived from ethers, which occurs at a lower temperature compared to alkanes. This easier decomposition, as well as the molecular reaction, produces alkenes that have a strong inhibiting effect on the formation of hydroperoxides and explains the lower reactivity of these compounds (Battin-Leclerc, 2008).

### **2.1.1. Formations of CO and CO<sub>2</sub> during the Oxidation of Hydrocarbons**

In terms of CO and CO<sub>2</sub>, the oxidation of hydrocarbons can be characterized as a two-step process. The first step is the breakdown of the fuel to CO, and the second step is the oxidation of this CO to CO<sub>2</sub> (Turns, 2006).

CO formation is one of the principal reaction paths in the oxidation mechanism of hydrocarbons. The primary CO formation mechanism can be shown as  $RH \rightarrow R' \rightarrow RO_2 \rightarrow RCHO \rightarrow RC'O \rightarrow CO$  where RH represents the parent hydrocarbon fuel and R' is a hydrocarbon radical produced by removing one or more H-atoms from the fuel molecule. Subsequent oxidation of the hydrocarbon radical leads to the formation of aldehydes (RCHO), which in turn react to form acyl (RC'O) radicals. Acyl then forms CO (Bartok and Sarofim, 1991).

The existence of the OH radical accelerates the oxidation of CO to CO<sub>2</sub> during the oxidation of hydrocarbons.  $CO + OH \rightarrow CO_2 + H$  reaction is the key reaction in the formation of CO<sub>2</sub> from CO (Turns, 2006).

## 2.1.2. Formation of PAHs during the Oxidation of Hydrocarbons

PAHs are high molecular weight aromatic hydrocarbons that contain two or more benzene (C<sub>6</sub>H<sub>6</sub>) rings. PAHs are produced by most practical combustion and oxidation systems. The main concern with this class of compounds is that some members are known mutagens, co-carcinogens, or carcinogens (Kaden et al., 1979; Fu et al., 1980; Lafleur et al., 1993). After the formation of the first aromatic ring, aromatic species combine to form PAHs which are the potential precursors to soot formation.

The formation of PAHs during hydrocarbon oxidation is especially observed for fuel-rich oxidation conditions. There have been many studies on the formation of PAHs in the oxidation of both aliphatic and aromatic hydrocarbons, but many details of the PAHs and soot formation remain unclear. The reason of this uncertainty is the complexity of the reaction mixtures in which a large number of PAHs are present together. Another reason is the existence of soot together with the PAH molecules in many cases (Bartok and Sarofim, 1991). Although some details of the PAH formation remains poorly understood, there is considerable agreement on the general features of the processes involved.

The pyrolysis of acetylene (C<sub>2</sub>H<sub>2</sub>) around temperatures of 1000 K has long been known to give rise to C<sub>6</sub>H<sub>6</sub> (Badger et al., 1960; Homann, 1967; Bockhorn et al., 1983; Colket, 1986; Frenklach and Warnatz, 1987; Richter and Howard, 2000). Another species proposed to play role in the formation of aromatic rings is 1,3-butadiene (C<sub>4</sub>H<sub>6</sub>) (Cole et al., 1984; Bartok and Sarofim, 1991).

It has been proposed that the initial formation of ring compounds occurs through the addition of the 1,3-butadienyl (C<sub>4</sub>H<sub>5</sub>) radical to the various C<sub>2</sub>H<sub>2</sub> species (Cole et al., 1984; Bartok and Sarofim, 1991):



R=H; acetylene, C<sub>2</sub>H<sub>2</sub> → benzene, C<sub>6</sub>H<sub>6</sub>

R=CH<sub>3</sub>; methylacetylene, C<sub>3</sub>H<sub>4</sub> → toluene, C<sub>6</sub>H<sub>5</sub>CH<sub>3</sub>

R=C<sub>2</sub>H; diacetylene, C<sub>4</sub>H<sub>2</sub> → phenylacetylene, C<sub>6</sub>H<sub>5</sub>C<sub>2</sub>H

R=C<sub>2</sub>H<sub>3</sub>; vinylacetylene, C<sub>4</sub>H<sub>4</sub> → styrene, C<sub>6</sub>H<sub>5</sub>C<sub>2</sub>H<sub>3</sub>

The most important radical in the formation of the first aromatic ring has been suggested as the propargyl ( $C_3H_3$ ) radical by Miller and Melius (1992), Hidaka et al. (1989), Stein (1991), Marinov et al. (1996), and Dagaut and Cathonnet (1998).

Other species that are proposed to play a role in the formation of aromatic species; i.e. aromatic precursors, are allene and propyne (methylacetylene,  $C_3H_4$ ) (Wu and Kern, 1987), ethylene ( $C_2H_4$ ) (Hague and Wheeler, 1929; Dente et al., 1979), and cyclopentadiene ( $C_5H_6$ ) (Dente et al., 1979; Roy, 1998).

## 2.2. n-Butane and its Oxidation Mechanism

Unlike hydrocarbon fuels with simpler structures such as methane or ethane, the thermochemical and combustion properties of n-butane are similar in many ways to more complex practical fuels. Therefore, n-butane can be used as a reference fuel for the oxidation of higher carbon number alkanes. Various studies have been performed in order to identify the oxidation mechanism of n-butane.

Allara and Shaw (1980) assembled a list of several hundred free-radical reactions which occur during the low temperature (700–850 K) pyrolysis of small n-alkane molecules up to pentane ( $C_5H_{12}$ ). A set of Arrhenius parameters was assigned on the basis of experiment, theory, thermochemical estimates and structural analogy. Rate parameters were recommended for initiation, recombination, disproportionation, H-transfer, decomposition, addition and isomerization reactions, giving a total of 505 reactions. Their compilation was intended for use in assembling reaction matrices in computational modeling studies of the thermal reactions of hydrocarbon molecules.

Cathonnet et al. (1981) studied the oxidation of propane and n-butane experimentally and analytically near 1000 K between 1 and 6 bars. Experiments were performed in a laminar flow quartz reactor on highly diluted mixtures (less than 2% of fuel by volume), over the range of equivalence ratios of 0.05 to 25. They suggested that the initial oxygen concentration had very little influence on ethene and propene yields, but an appreciable one on methane yields. A numerical model incorporating detailed chemical kinetics and thermal effects was proposed for the interpretation of the experiments, and the reaction mechanism used for the simulation was able to predict most of the experimental results. Most important steps in this detailed mechanism were

identified and assembled in a simplified kinetic scheme describing the reaction processes.

Warnatz (1983) developed a general reaction scheme for the simulation of lean and rich, high-temperature combustion of hydrocarbons up to C<sub>4</sub>-species, by combination of a mechanism describing lean and moderately rich combustion of alkanes and alkenes with a mechanism describing rich combustion and formation of soot precursors in acetylene flames. He compared the results of the simulations to the experimental data, and discussed some consequences of the reaction scheme with respect to rich flames of propane and butane.

Pitz et al. (1985) developed a detailed chemical kinetic reaction mechanism for the intermediate and high temperature oxidation of n-butane. The mechanism consisted of 238 elementary reactions among 47 chemical species and it was validated by comparison between computed and experimental results from shock tubes, turbulent flow reactor, and premixed laminar flames. The model accurately reproduced n-butane combustion kinetics for wide ranges of pressure, temperature, and fuel-air equivalence ratios. In spite of the large number of species and reactions, it was found that computed results were most sensitive to reactions involving the H<sub>2</sub>-O<sub>2</sub>-CO submechanism, in agreement with other modeling studies of hydrocarbon oxidation.

In another study, Pitz et al. (1986) added a low temperature submechanism to their previously developed high temperature mechanism in order to examine the importance of low temperature reaction paths in autoignition related to engine knock. Reactions that involve the production and consumption of HO<sub>2</sub> and H<sub>2</sub>O<sub>2</sub> were found to play a crucial role in high pressure autoignition.

The model of Pitz et al. (1986) was modified and extended to incorporate reactions which are important at low and intermediate temperatures and utilized subsequently to model autoignition engines, rapid compression machines (RCM), and two-stage flames (Cernansky et al., 1986; Green et al., 1987; Pitz et al., 1988; Carlier et al., 1991; Corre et al., 1992; Minetti et al., 1994).

Cernansky et al. (1986) made a comparison between measured concentrations in a spark ignition (SI) engine and predictions from a numerical model using detailed chemical kinetics, for the oxidation of n-butane/air and isobutene/air mixtures. Concentration histories of stable species were obtained through gas chromatographic analysis. A detailed chemical kinetics model was used to predict species concentration in an idealized end gas. The chemical reactions leading to formation of the relevant

species were identified. The relative distribution of intermediate products predicted by the model was in good agreement with the experimental measurements. Chemical kinetic differences between autoignition of n-butane, a straight chain hydrocarbon, and iso-butane, a branched chain hydrocarbon were discussed.

Green et al. (1987) studied the chemical aspects of the compression ignition of n-butane experimentally in a SI engine and theoretically using computer simulations with a detailed chemical kinetic mechanism. The results of their studies demonstrated the effect of initial charge composition on autoignition. They assessed how well the detailed kinetic model could predict the autoignition and modified the model to better simulate the experimental observations.

Pitz et al. (1988) used a detailed chemical kinetic mechanism to simulate the oxidation of n-butane/air mixture in an engine. The modeling results were compared to species measurements obtained from the exhaust of the engine and to measured critical compression ratios. Pressures, temperatures and residence times were considered that are in the range relevant to automotive engine knock. The relative yields of intermediate species calculated by the model matched the measured yields generally to within a factor of two. The influence of different components in the residual fraction, such as the peroxides, on fuel oxidation chemistry during the engine cycle was investigated.

Carlier et al. (1991) studied the autoignition of n-butane by two techniques. At a relatively low pressure (1.8 bar), a two-stage flame was fully described by stable-species and peroxy-radical evolution. At higher pressures, studies were conducted in a RCM in order to investigate the evolution of the autoignition delay times with temperature. These experimental results were compared with predictions obtained from the n-butane oxidation mechanism of Pitz et al. (1986). In a reduced version (45 species and 272 reactions) the model agreed with the measured major species produced in the second stage of a burner-stabilized, two-stage flame. In its complete conversion, it also predicted the NTC observed at high pressure in the RCM. However, to account for the ignition delay, it was necessary to modify the rate constants associated with the low-temperature mechanism as suggested by Pitz et al. (1988).

Corre et al. (1992) investigated two-stage flame processes to achieve a better understanding of the low temperature and high temperature chemistry responsible for two-stage type of autoignition behavior. A stabilized n-butane two-stage flame was simulated, utilizing a detailed kinetic mechanism involving 141 species and 850 elementary reactions, and the results were compared with experimental data from the



literature. With the exception of those for butenes and hydroperoxyl radicals, calculated and experimental profiles were found to agree within a factor of two over the entire flame region. In the second stage region, predicted reaction profiles were in general agreement with the experiment, with the exception of formaldehyde ( $\text{CH}_2\text{O}$ ) and  $\text{C}_4$ -oxygenated species, for which consumptions were substantially underestimated.

Minetti et al. (1994) studied the oxidation and autoignition of stoichiometric, lean ( $\phi = 0.8$ ), and rich ( $\phi = 1.2$ ) n-butane/air mixtures in a RCM between 700–900 K and 9–11 bar. Information was obtained concerning cool flames and ignition delays. Product profiles for selected major and minor species were measured during a two-stage ignition process. They suggested that the presence of  $\text{C}_4$  heterocyclic species could be connected to isomerization and decomposition of butylperoxy radicals. The experimental results were compared with numerical predictions of a homogeneous adiabatic model based on the mechanism of Pitz et al. (1988). The experimental and predicted delays were in the same order of magnitude. A relatively good agreement was found for the major species profiles. Improvement of the mechanism was needed to account for the minor products. The different paths of OH formation were discussed.

Chakir et al. (1989) performed an analytical study of n-butane oxidation in a jet-stirred reactor (JSR). Experimental measurements were made in the temperature range 900–1200 K, at pressures extending from 1 to 10 atm, for a 0.15 to 4.0 range of equivalence ratios. The mechanism they developed consisted of 344 reversible reactions among 51 species. Good agreement between computed and measured concentrations of major chemical species was obtained. The major reaction paths for n-butane consumption and for the formation of main products were identified, showing the influence of pressure and equivalence ratios. The same mechanism was also used to model the ignition of n-butane in a shock tube. Experimental ignition delays measured behind reflected shock waves were accurately reproduced, extending the validation of the mechanism up to 1400 K.

Kojima (1994) proposed two versions of a detailed chemical kinetic model of n-butane autoignition. The key distinctions between the two versions were the exclusion or inclusion of the direct abstraction or apparently bimolecular path of the reaction  $\text{HO}_2 + \text{HO}_2 \rightarrow \text{H}_2\text{O}_2 + \text{O}_2$ , and the selection of rate parameters for the reaction  $\text{C}_2\text{H}_5 + \text{O}_2 \rightarrow \text{C}_2\text{H}_4 + \text{HO}_2$ . Both versions were evaluated over 1200–1400 K for a stoichiometric mixture and over 720–830 K for lean to rich mixtures by comparing the computed autoignition delays with the results of a shock-tube experiment

(representative of high-temperature chemistry) and the results of a RCM (representative of low-temperature chemistry). The experiments demonstrated the ability of the models to predict autoignition delays at high pressures typical of automobile engines. The two model versions provided the same behavior of autoignition delay (a macroscopic phenomenon), but the sensitivities of the delays to reaction rate constants (a microscopic aspect of the autoignition mechanism) were remarkably different. Therefore, while the two models were shown to reproduce the macroscopic experimental data, it was stated that more research was required to determine which model was valid at the microscopic level.

Ranzi et al. (1994) discussed a scheme of n-butane oxidation consisting of more than 100 species involved in about 2000 reactions. Low temperature, primary oxidation reactions of propane and butane were added to a comprehensive kinetic scheme already available for methane and C<sub>2</sub> species. They also applied a method of formalizing the large quantity of mechanistic rate data for the application and the extension of their scheme. Several comparisons with experimental data, obtained over a wide range of temperatures (550–1200 K), pressures and oxygen concentrations supported and validated their proposed kinetic model.

Wilk et al. (1995) conducted an experimental investigation of the transition in the oxidation chemistry of n-butane across the region of NTC from low to intermediate temperatures. The experimental study was carried out using a conventional static reactor system for a fuel-rich ( $\phi = 3.25$ ) n-butane/O<sub>2</sub>/N<sub>2</sub> system at a total pressure of 550 torr. The initial reaction temperature was varied from 554 to 737 K encompassing the NTC region and portions of each of the low and intermediate temperature regimes. The experimental results indicated a region of NTC between approximately 640 and 695 K and a shift in the nature of the reaction intermediates and products across the region. On the basis of experimental results and some previous kinetic modeling results, they presented a mechanism for n-butane to describe the observed phenomena. The mechanism was consistent with the experimental results and predicted the NTC and the shift in product distribution with temperature. They suggested that oxygenated species dominated the hydrocarbon intermediates and products at low temperatures while alkanes and alkenes were the primary hydrocarbon species produced at intermediate temperatures.

Marinov et al. (1998) performed experimental and detailed chemical kinetic modeling work to investigate aromatic and polycyclic aromatic hydrocarbon formation

pathways in a premixed, rich, sooting, n-butane/O<sub>2</sub>/Ar burner stabilized flame. An atmospheric pressure, laminar flat flame operated at an equivalence ratio of 2.6 was used to acquire experimental data for model validation. Experimental measurements were made in the main reaction and post-reaction zones for a number of low molecular weight species, aliphatics, aromatics, and PAHs ranging from two to five-fused aromatic rings. Reaction flux and sensitivity analysis were used to identify the important reaction sequences leading to aromatic and PAH growth and destruction in the n-butane flame. Reaction flux analysis showed the C<sub>3</sub>H<sub>3</sub> recombination reaction was the dominant pathway to benzene formation. The consumption of C<sub>3</sub>H<sub>3</sub> by H atoms was shown to limit C<sub>3</sub>H<sub>3</sub>, benzene, and naphthalene formation in flames as exhibited by the large negative sensitivity coefficients. Many of the low molecular weight aliphatics, combustion by-products, aromatics, branched-aromatics and PAHs were fairly simulated by the model. The model was able to reasonably predict the concentrations of benzene, naphthalene, phenanthrene, anthracene, toluene, ethyl benzene, styrene, o-xylene, indene, and biphenyl; but it was unable to simulate properly the concentration profiles of phenyl acetylene, fluoranthene, and pyrene.

Marinov et al. (1998) explains the formation pathways of the oxidation products in the n-butane rich oxidation scheme, as shown in Figure 2.1. These reaction pathways are proposed to serve as the underlying foundation for aromatics, PAHs, and potential soot growth. The principal pathway to the formation of aromatic precursors in the n-butane flame is represented in Figure 2.1.a. This pathway is described by H-abstraction from n-butane to form isobutyl (sC<sub>4</sub>H<sub>9</sub>) radical followed by decomposition to propene (C<sub>3</sub>H<sub>6</sub>) and methyl (CH<sub>3</sub>). C<sub>3</sub>H<sub>6</sub> is primarily dehydrogenated by H atoms and leads to the production of resonantly stabilized allyl (aC<sub>3</sub>H<sub>5</sub>) and propargyl (H<sub>2</sub>CCCH) radicals. These radicals play role in the formation of aromatic species. Figure 2.1.b represents the formations of the low molecular weight aliphatics and major oxidation by-products. n-Butane decomposes to n-butyl (pC<sub>4</sub>H<sub>9</sub>), n-propyl (nC<sub>3</sub>H<sub>7</sub>), CH<sub>3</sub>, and ethyl (C<sub>2</sub>H<sub>5</sub>) radicals, and in turn, these radicals are primarily removed by the reactions shown in Figure 2.1.b.

Warth et al. (1998) developed a system that permits the computer-aided formulation of comprehensive primary mechanisms and simplified secondary mechanisms, coupled with the relevant thermochemical and kinetic data in the case of the gas-phase oxidation of alkanes and ethers. The system was demonstrated by modeling the oxidation of n-butane at temperatures between 554 and 737 K, i.e. in the

NTC regime, and at a higher temperature of 937 K. The automatically generated mechanism for n-butane oxidation and combustion includes 168 species and 797 reactions. The system yielded satisfactory agreement between the computed and the experimental values for the rates, the induction period and conversion, and also for the distribution of the products formed.

The work of Warth et al. (1998) was later updated and expanded by Buda et al. (2005) for a range of hydrocarbons especially with a view to low temperature oxidation. The validations were based on recent data of the literature obtained in shock tubes and in RCM. The compounds studied were n-butane, n-pentane, iso-pentane, neo-pentane, 2-methylpentane, n-heptane, iso-octane, n-decane, and mixtures of n-heptane and iso-octane. Investigated conditions were temperature range of from 600 to 1200 K, including the NTC region, pressures range from 1 to 50 bar, and equivalence ratios range from 0.5 to 2.

Yamasaki and Iida (2003) studied the combustion mechanism of the homogeneous-charge compression-ignition (HCCI) engine in order to control ignition and combustion as well as to reduce hydrocarbon and CO emissions and to maintain high combustion efficiency by calculating the chemical kinetics of elementary reactions. For the calculations, n-butane was selected as fuel since it is a fuel with the smallest carbon number in the alkane family that shows two-stage autoignition similarly to higher hydrocarbons such as gasoline. They used the elementary reaction scheme of Kojima (1994) which consisted of 161 species and 461 reactions. The results revealed the heat release mechanism of the low- and high-temperature reactions, the control factor of ignition timing and combustion speed, and the condition affecting the hydrocarbon and CO emissions, and the combustion efficiency.

Basevich et al. (2007) suggested a compact kinetic mechanism of the oxidation of n-butane with 54 species and 288 reversible reactions, including the main processes and intermediate and final reaction products. The mechanism did not contain reactions of the double addition of oxygen and intermediate species in the form of isomeric compounds and their derivatives. The calculation results were compared with the experimental data over wide ranges of initial temperatures, pressures, and compositions of n-butane mixtures with air and oxygen; and satisfactory qualitative agreement with measurements was observed.

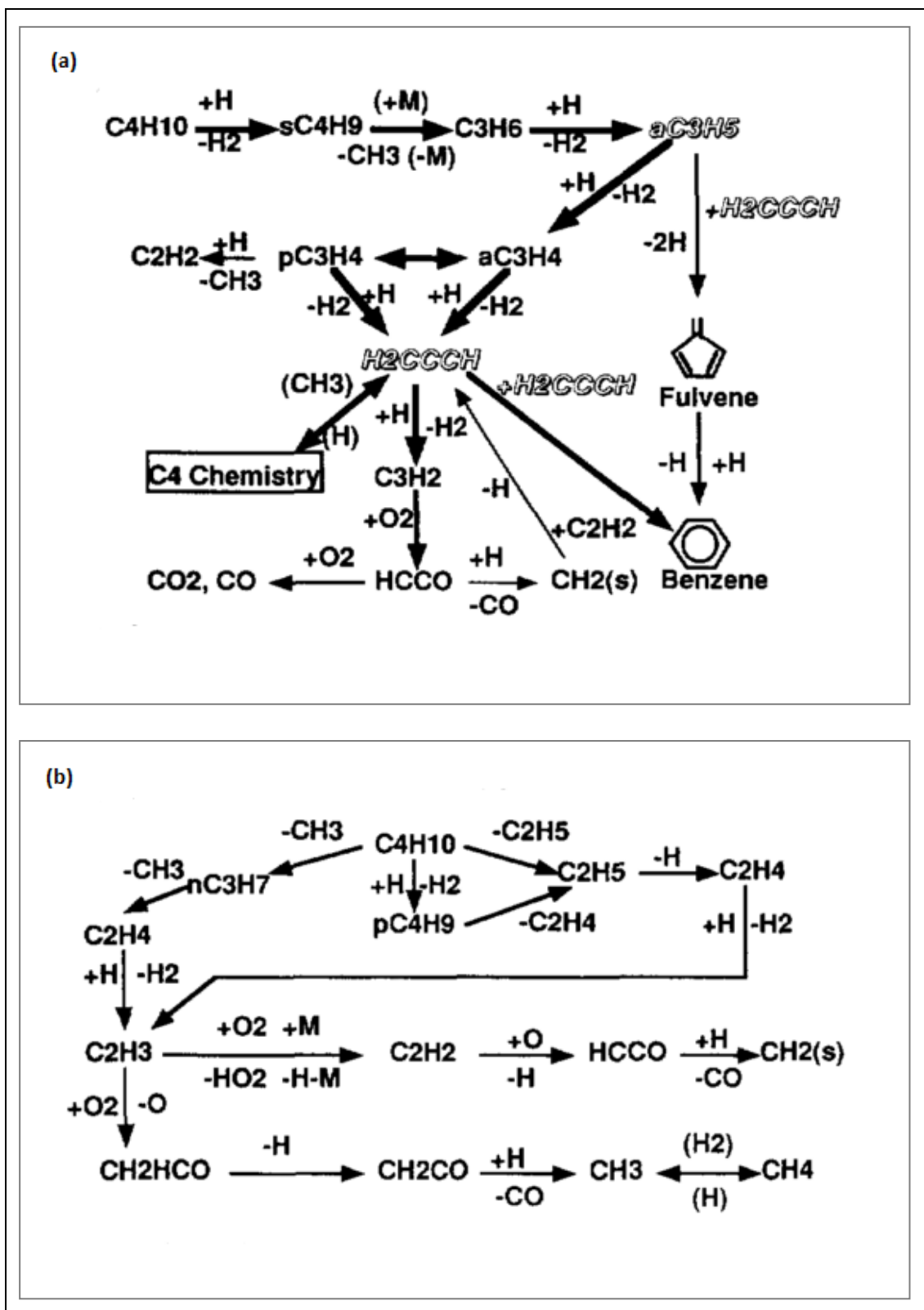


Figure 2.1. Reaction pathway diagrams for the reaction sequences leading to (a) aromatic species and (b) aliphatic oxidation products that occur in n-butane oxidation (Source: Marinov et al., 2000)

Strelkova et al. (2010) derived a skeletal mechanism (54 species and 94 reactions) for low-temperature (500–800 K) ignition of n-butane in air, using the detailed mechanism of Warth et al. (1998). The skeletal mechanism obtained accurately reproduced n-butane combustion kinetics for the practically important ranges of pressure, temperature and fuel-air equivalence ratio, especially in the low-temperature range. The model was validated against available experimental results for normal and elevated initial pressure (1–15 atm) and a good agreement with experiments was found.

Healy et al. (2010) performed ignition delay time measurements at equivalence ratios of 0.3, 0.5, 1, and 2 for n-butane, at pressures of approximately 1, 10, 20, 30 and 45 atm, at temperatures from 690 to 1430 K, in both a RCM and in a shock tube. A detailed chemical kinetic model consisting of 1328 reactions involving 230 species was constructed and used to validate the delay times. Arrhenius-type ignition delay correlations were developed for temperatures greater than 1025 K which relate ignition delay time to temperature and concentration of the mixture. A detailed sensitivity analysis and a reaction pathway analysis were performed to give further insight to the chemistry at various conditions. The model performed quite well when compared to the existing data from the literature and the experimental results.

### **2.3. DME and its Oxidation Mechanism**

DME is in the gas phase at ambient temperature and pressure, but is easily liquefied under pressure. Its handling characteristics are very similar to those of LPG. It has a high cetane number of approximately 55–60, and this makes DME ideal for usage in diesel engines. DME does not have the tendency to form particulates and has a low toxicity. It can be produced from natural gas (dehydration of methanol) or from biomass (gasification). Beside these advantages of DME, it has the disadvantages of having low combustion enthalpy and low viscosity. The main physical and chemical properties of DME compared with diesel fuel are shown in Table 2.1.

DME has been featured in the combustion literature as a neat fuel and as a fuel additive. It has been shown that, DME oxidation results in lower emissions of  $\text{NO}_x$  and hydrocarbons, compared to diesel (Rouhi, 1995; Ying et al., 2005; Crookes and Bob-Manuel, 2007; Arcoumanis et al., 2008; Zhang et al., 2008), propane and n-butane (Frye et al., 1999) and n-heptane (Park, 2009). DME was also found to result in lower

emissions of PAHs and other soot precursors, and soot compared to methane (Kaiser et al., 2000; Hayashida et al., 2011), propane (Hayashida et al., 2011) and n-heptane (Kitamura et al., 2001; Park, 2009). Smoke emissions of DME are also lower than that of diesel (Ying et al., 2005; Crookes and Bob-Manuel, 2007; Zhang et al., 2008). CO emissions of DME were observed to be higher than that of diesel fuel (Arcoumanis et al., 2008; Zhang et al., 2008) and n-heptane (Park, 2009), but lower than that of propane and n-butane (Frye et al., 1999). Emissions of CH<sub>2</sub>O and other aldehydes were observed to be increased with the usage of DME, compared to diesel (Rouhi, 1995; Arcoumanis, 2008) and methane (Kaiser et al., 2000).

Table 2.1. Physical and chemical properties of DME compared with the properties of diesel fuel (Source: Hewu and Longbao, 2002)

Properties	DME	Diesel fuel
General formula	CH <sub>3</sub> OCH <sub>3</sub>	C <sub>x</sub> H <sub>y</sub>
Molecular weight (g/mol)	46.07	190 – 220
Carbon content (% mass)	52.2	86
Hydrogen content (% mass)	13	14
Oxygen content (% mass)	34.8	0
Density in the liquid state (g/cm <sup>3</sup> )	0.668	0.84
Kinematic viscosity at 40°C (mm <sup>2</sup> /s)	0.15	2.0 – 4.5
Boiling point (°C)	-24.9	189 – 360
Autoignition point (°C)	235	250
Heating value (MJ/kg)	28.43	42.5
Heat of vaporization (kJ/kg)	410	250
Stoichiometric ratio (kg/kg)	9.0	14.6
Cetane number	55 – 60	40 – 55

Various studies exist in the literature about identification of the mechanism of DME oxidation. Dagaut et al. (1996) studied the oxidation of DME in a JSR. The experiments covered a wide range of conditions; pressures between 1–10 atm, equivalence ratios between 0.2–2.0, and temperatures between 800–1300 K. These results represented the first detailed kinetic study of DME oxidation in a reactor. The results demonstrated that the oxidation of DME did not yield higher molecular weight compounds. A numerical model consisting of a detailed kinetic reaction mechanism

with 286 reactions among 43 species was developed in order to describe DME oxidation in a JSR. Generally good agreement between the data and the model was observed.

Curran et al., (1998) studied the oxidation of DME experimentally and theoretically, over a wide range of conditions. Experimental results obtained in a JSR at pressures of 1 and 10 atm, equivalence ratios between 0.2 and 2.5, and temperatures between 800–1300 K, were modeled in addition to those generated in a shock tube at pressures of 13 and 40 bar, equivalence ratio of  $\phi = 1.0$  and temperatures between 650–1300 K. These data were used to test the kinetic model they developed, which consisted of 78 chemical species and 336 chemical reactions.

Fischer et al. (2000) studied the DME reaction kinetics at high temperature in two different flow reactors under highly dilute conditions. Pyrolysis of DME was studied in a variable–pressure flow reactor at 2.5 atm and 1118 K. Studies were also conducted in an atmospheric pressure flow reactor at about 1085 K. These experiments included trace–oxygen–assisted pyrolysis, as well as full oxidation experiments, with the equivalence ratio varying from 0.32 to 3.4. Species concentrations were correlated against residence time in the reactor and species evolution profiles were compared to the predictions of previously published detailed chemical kinetic mechanism (Curran et al., 1998). Some changes were made to the model in order to improve agreement with the experimental data.

In a companion paper, Curran et al. (2000) studied low and intermediate temperature kinetics of DME as well. They studied the oxidation of DME in a variable–pressure flow reactor over an initial reactor temperature range of 550–850 K, in the pressure range 12–18 atm, at equivalence ratios of 0.7–4.2 with nitrogen diluent of approximately 98.5%. They observed formic acid as a major intermediate of DME oxidation at low temperatures. The experimental species profiles were compared to the predictions of the previously published mechanism of Curran et al. (1998), which could not predict the formation of formic acid. Therefore, the chemistry leading to formic acid formation and oxidation was included into the mechanism. The new mechanism was able to produce the experimental observations with good accuracy.

Curran et al. (2000) describe the oxidation mechanism of DME as shown in Figure 2.2. At high temperatures, the fuel consumption pathway is quite simple with unimolecular fuel decomposition, forming methoxy ( $\text{CH}_3\text{O}$ ) and methyl ( $\text{CH}_3$ ) radicals, and  $\beta$ -scission of the methoxy-methyl radical ( $\text{CH}_3\text{OCH}_2$ ) proceeding to  $\text{CH}_2\text{O}$  and  $\text{CH}_3$  radical. At low temperatures, chain branching is primarily due to the reaction pathway



leading through ketohydroperoxide species. As the temperature increases through the NTC region, the chain propagation reactions of alkyl hydroperoxide species increase in importance, leading to the formation of  $\beta$ -decomposition products, while the proportion of chain branching decreases.

Kaiser et al. (2000) measured the profiles of chemical species at atmospheric pressure for two DME/air flat flames having fuel–air equivalence ratios of 0.67 and 1.49. Species profiles for two methane/air flames with equivalence ratios and flow velocities similar to those of the DME flames were also obtained for comparison to DME results. Mole fractions of  $C_2$  product species were similar in DME and methane flames of similar equivalence ratios. However, the  $CH_2O$  mole fractions were much larger in the DME flames. They used a detailed chemical kinetic mechanism based on the previously published mechanisms of Curran et al. (1998), Fischer et al. (2000) and Curran et al. (2000). Experimental profiles they obtained were compared to profiles generated with computer modeling. The results showed that, while DME produced soot, its yellow flame luminosity was much smaller than that of an ethane flame at the same fuel volume rate, consistent with the low soot emission rate observed when DME used as a diesel fuel.

Hidaka et al. (2000) studied the high–temperature pyrolysis of DME behind reflected–shock waves experimentally. The studies were done using DME/Ar, DME/ $H_2$ /Ar, DME/CO/Ar, and DME/ $CH_2O$ /Ar mixtures in the temperature range 900–1900 K, at pressures in the range 0.83–2.9 atm. From a computer simulation, a reaction mechanism consisting of 94 reactions were constructed and used to explain their experimental data.

Yamada et al. (2003) developed a simplified reaction model for DME oxidation by extracting essential elementary reactions from previously developed mechanisms. The reduced mechanism consisted of 23 reactions for 23 species. Good agreement with the detailed model was obtained in terms of ignition timing and profiles of species such as DME,  $CH_2O$ ,  $O_2$ ,  $H_2O_2$ , and CO as functions of intake gas temperature, equivalence ratio, and intake pressure. Adding a few reactions to the mechanism, the effective range of the model was extended to rich side, where CO emission is significant.

Yao et al. (2005) investigated the autoignition and combustion mechanisms of DME in a HCCI engine using a zero–dimensional thermodynamic model coupled with a detailed chemical kinetics model. The results indicated that DME displays two–stage autoignition. Based on the sensitivity analysis of chemical reactions, the major paths of

the DME reaction occurring in the engine cylinder were clarified. The major paths of the DME reaction were reported as H-atom abstraction from DME, followed by the addition of O<sub>2</sub>, and then oxidation to CH<sub>2</sub>O, to the formyl radical (HCO), and finally to CO. CO oxidation was reported to occur by the elementary reaction CO+OH=CO<sub>2</sub>+H. They suggested that at leaner DME concentrations, CO could not be completely converted to CO<sub>2</sub>, and the process would result in high CO emissions.

Cool et al. (2007) used and enhanced the mechanism of Fischer et al. (2000) in order to identify the reaction paths of DME combustion. Mole fractions of 21 flame species were measured experimentally in a low-pressure premixed fuel-rich ( $\phi = 1.2$  and 1.68) DME/O<sub>2</sub>/Ar flames. The measurements agreed well with flame modeling predictions, using the detailed mechanism which identified reaction paths quite analogous to alkane combustion.

Zhao et al. (2008) enhanced the mechanisms of Fischer et al. (2000) and Curran et al. (2000) further. DME pyrolysis experiments were performed at 980 K in a variable-pressure flow reactor at a pressure of 10 atm, a considerably higher pressure than previous validation data. Since both unimolecular decomposition and radical abstraction are significant in describing DME pyrolysis, a hierarchical methodology was applied to produce a comprehensive high-temperature model for pyrolysis and oxidation that includes the new decomposition parameters and more recent small molecule/radical kinetic and thermochemical data. The high-temperature model was combined with the low-temperature oxidation chemistry (adopted from Fischer et al., 2000) with some modifications to several important reactions. The revised construct showed good agreement against high-as well as low-temperature flow reactor and JSR data, shock tube ignition delays, and laminar flame species as well as flame speed measurements.

Huang et al. (2009) coupled a reduced chemical mechanism with a computational fluid dynamics model to investigate DME combustion in HCCI engine and emissions processes. The reduced mechanism consisted of 26 species with 28 reactions. Emission analysis indicated that unburned fuel and CH<sub>2</sub>O accounted for the majority of unburned hydrocarbons. With the increase of DME equivalence ratio, unburned fuel and CO emissions increased. However, when the DME equivalence ratio was too small, CO emissions decreased.



## 2.4. Studies of DME as a Fuel Additive

Kajitani et al. (1998) investigated DME–propane blends in a direct injection compression ignition (CI) engine. They reported that in the engine operated by DME–propane blends, there was no need for significantly increasing the complexity of the fuel system that employed in the use of neat DME. When the content of propane was increased, which accordingly increased the heating value of the blend, a delayed start of heat release occurred. When the engine load was low, the specific fuel consumption and the emissions of unburned hydrocarbons increased as the propane content increased. Mentioning other emissions with DME–propane blends, soot emission was negligible, and the specific NO<sub>x</sub> emission was in general lower than with neat DME, which decreased with an increase in both propane content and engine load.

Flowers et al. (2001) studied the simulation of a HCCI engine fueled with DME added natural gas. For the kinetic mechanism of DME, they used the detailed mechanism of Curran et al. (1998). The fraction of DME in the fuel blend changed from 0.2 to 0.6. They studied the combustion in the engine at an inlet temperature of 333 K, inlet pressures of 1 and 2 bar, and with equivalence ratios changing from 0.25 to 0.5. They suggested that autoignition timing could be controllable by blending low cetane number fuel (natural gas) with high cetane number fuel (DME). They proposed that DME is an ideal fuel additive for natural gas HCCI engine due to its short ignition delay and its well characterized chemistry.

Song et al. (2003) performed a diesel engine research in order to investigate the effects of the oxygenated compounds blended to ethane on aromatic species, which are known to be soot precursors in fuel-rich ethane combustion. 5% oxygen by mass of the fuel was added to ethane using DME and ethanol and the equivalence ratio was kept at  $\phi = 2.0$ . The temperature range was from 1000 to 2400 K. For modeling the oxidation mechanism of DME, they used the detailed mechanism of Curran et al. (1998). As a result, a significant reduction in aromatic species relative to pure ethane was observed with the addition of both DME and ethanol, but DME was found to be more effective in reducing aromatic species than ethanol. The reason for the greater effectiveness of DME was proposed as its higher enthalpy of formation which led to a higher final temperature, compared to ethanol.

Ying et al. (2006) studied the effects of DME addition (10%, 20%, and 30% by mass) to diesel on the formation of smoke, hydrocarbons, and  $\text{NO}_x$  emissions, experimentally, in a diesel engine. They suggested that at high loads, the blends reduced smoke significantly compared to diesel fuel. Little increase was observed in CO and hydrocarbon emissions with the addition of DME.  $\text{NO}_x$  and  $\text{CO}_2$  emissions of the blends were decreased somewhat. At low loads, the blends had slight effects on smoke reduction due to overall leaner mixture. They suggested that the results indicated the potential of diesel reformation for clean combustion in diesel engines.

Morsy (2007) investigated the effect of additives such as DME,  $\text{CH}_2\text{O}$ , and  $\text{H}_2\text{O}_2$  for the control of ignition in natural gas HCCI engines, numerically. The mechanism of Curran et al. (2000) was used to simulate DME oxidation. An equivalence ratio of 0.3 and an initial pressure of 1.5 bar was used. It was found that an additive-free mixture did not ignite for the intake temperature of 400 K, whereas a mixture containing a small quantity of additives at the same temperature was ignited. It was suggested that for a fixed quantity of additive,  $\text{H}_2\text{O}_2$  addition was effective in advancing the ignition timing as compared to the other two additives.

Chen et al. (2007) studied the effects of DME addition on the high temperature ignition and burning properties of methane-air mixtures, experimentally and numerically. Experiments were performed at an initial temperature of 298 K and at atmospheric pressure, with homogeneous and non-premixed flames. For modeling of the system, they used the mechanism of Zhao et al (2008). The results showed that for a homogeneous system, a small amount of DME addition to methane resulted in significant reduction in the high temperature ignition delay. For the non-premixed system, ignition enhancement was significantly less effective. The results also showed that the flame speed increased almost linearly with DME addition.

McEnally and Pfefferle (2007) measured soot volume fractions,  $\text{C}_1$ – $\text{C}_{12}$  hydrocarbon concentrations, and gas temperatures in fuel-rich ethylene/air non-premixed flames with up to 10% DME or ethanol added to fuel. Addition of both DME and ethanol increased the maximum soot volume fractions in the ethylene flames studied, even though ethylene is a much sootier fuel than either oxygenates. Furthermore, DME produced a larger increase in soot even though neat DME flames produce less soot than neat ethanol flames. They suggested that the oxygenates increased soot concentrations because they decomposed to  $\text{CH}_3$  radical, which promoted the formation of  $\text{C}_3\text{H}_3$  radical through  $\text{C}_1+\text{C}_2$  addition reactions and consequently the

formation of  $C_6H_6$  through  $C_3H_3$  self-reaction. They also suggested DME has a stronger effect than ethanol because it decomposed more completely to  $CH_3$  radical. Their findings indicated that oxygenates do not necessarily reduce particulate formation when they are added to hydrocarbon fuels.

Yoon et al. (2008) investigated the characteristics of PAH and formation in counter-flow diffusion flames of methane, ethane, propane, and ethylene fuels mixed with DME. Results showed that even though DME is known to be a clean fuel in terms of soot formation, DME mixture with ethylene fuel increased PAH and soot formation significantly as compared to the pure ethylene case. These findings of Yoon et al. were similar to the findings of McEnally and Pfefferle (2007), and they explained the reason for this increase in PAH and soot in a similar way, suggesting that it was related to the role of  $CH_3$  radicals in the formation of  $C_3H_3$  and subsequent formations of  $C_6H_6$  and PAHs. However, the mixture of DME with methane, ethane, and propane decreased PAH and soot formation.

Marchionna et al. (2008) performed a series of experimental and modeling studies to assess the potential application of DME as a substitute fuel in domestic appliances, commonly fed with LPG. They compared CO emissions for butane and butane/DME mixtures, and observed the positive effect of DME addition on reducing CO emissions. They calculated the mole fractions of  $CH_2O$  and  $C_6H_6$  for increasing DME concentrations in LPG (propane/butane = 1:1). They observed that  $CH_2O$  showed a strong increase as DME concentration increased, due to the presence of an oxygenated group which enhances its production. A significant reduction of  $C_6H_6$  was observed in the presence of DME.

Bennett et al. (2009) examined two sets of laminar co-flow flames each consisting of ethylene/air non-premixed flames with various amounts (up to 10%) of DME and ethanol added to the fuel stream, computationally and experimentally. They observed that as the level of the additive was increased, temperatures, some major species ( $CO_2$ ,  $C_2H_2$ ), flame lengths, and residence times were essentially unchanged. However, the concentrations of  $C_6H_6$  increased, and this increase was largest when DME was the additive. Computational and experimental results supported the hypothesis of McEnally and Pfefferle (2007), proposing that the dominant pathway to  $C_6H_6$  formation begins with decomposition of oxygenates into  $CH_3$  radical, which combines with  $C_2$  species to form  $C_3H_3$ , and  $C_3H_3$  reacts with itself to form  $C_6H_6$ .

Lee et al. (2011) studied a SI engine operated with DME-blended LPG fuel, experimentally. The effects of n-butane and propane on the performance and emission characteristics (including hydrocarbons, CO, and NO<sub>x</sub>) of the engine were examined. Four kinds of test fuels with different blend ratios of n-butane, propane, and DME were used (100% n-butane; 80% n-butane and 20% DME; 70% n-butane and 30% propane; and 56% n-butane, 24 % propane and 20% DME). They observed that hydrocarbon and CO emissions were the highest for n-butane and slightly decreased with DME addition. However, NO<sub>x</sub> emissions were higher for DME blends due to higher combustion and exhaust temperatures and the knocking observed in cases of LPG without DME addition.

Liu et al. (2011) investigated the effects of DME addition to fuel on the formation of PAHs and soot, experimentally and numerically, in a laminar co-flow ethylene diffusion flame at atmospheric pressure. Experiments were conducted over the entire range of DME addition from pure ethylene to pure DME in the fuel stream. The total carbon mass flow rate was maintained constant when the fraction of DME in the fuel stream was varied (0%, 6%, 12%, 18%, 25%, 37%, 50%, 75%, and 100%). Numerical calculations of nine diffusion flames of different DME fractions in the fuel stream were performed using a detailed reaction mechanism (DME mechanism obtained from Kaiser et al., 2000) and a soot model. The addition of DME to ethylene was found experimentally to increase the concentrations of both PAHs and soot. The numerical results reproduce the synergistic effects of DME addition to ethylene on both PAHs and soot. They suggest that the effects of DME addition to ethylene on many hydrocarbon species, including PAHs, and soot can be fundamentally traced to the enhanced CH<sub>3</sub> concentration with the addition of DME to ethylene. Contrary to previous findings of McEnally and Pfefferle (2007), Yoon et al. (2008), and Bennett et al. (2009), the pathways responsible for the synergistic effects on C<sub>6</sub>H<sub>6</sub>, PAHs and soot in the ethylene/DME system were proposed to be primarily due to the cyclization of 1-C<sub>6</sub>H<sub>6</sub> and n-C<sub>6</sub>H<sub>7</sub> and to a much lesser degree due to the interaction between C<sub>2</sub> and C<sub>4</sub> species for C<sub>6</sub>H<sub>6</sub> formation, rather than the C<sub>3</sub>H<sub>3</sub> self-combination reaction route.

Ji et al. (2011) carried out an experimental study aiming at improving efficiency, combustion stability and emissions performance of a SI engine, through DME addition to gasoline. Various DME fractions (0–24% energy fraction) were selected to investigate the effects of DME addition under stoichiometric conditions. The experimental results showed that thermal efficiency was improved, and NO<sub>x</sub> and

hydrocarbon emissions were decreased with increasing DME addition to gasoline. CO emissions first decreased and then increased with the increase in DME fraction.



## CHAPTER 3

### METHOD

Chemical kinetics includes investigations of how different experimental conditions can influence the rate of a chemical reaction and yields information about the mechanism of the reaction and transition states, as well as it involves the construction of mathematical models that can describe the characteristics of a chemical reaction. In this study, the effects of DME addition to n-butane were investigated theoretically by detailed chemical kinetic modeling of the reaction system.

Availability of large amounts of elementary kinetic data, improved techniques for estimating specific reaction rates, development of efficient stiff equation solution techniques, and continual growth in the size, speed, and availability of computers have resulted in increasing usage of chemical kinetic modeling in the last decades. Chemical kinetic models are very important tools in understanding the mechanisms and kinetics of the chemical reactions.

#### **3.1. Theory of Chemical Kinetic Modeling Using Chemkin<sup>®</sup>**

There are a number of different computer applications available for chemical kinetic modeling, with Chemkin<sup>®</sup> (Kee et al., 1996) being the dominant one, since the Chemkin input data format (McBride et al., 1993) is an evolving standard for describing the reactions, the rate parameters, and the thermodynamic and transport properties of each species.

The general mathematical formulation of the problem of chemically reactive flow systems consists of continuity equations for mass, momentum, energy, and chemical species, together with equation of state and other thermodynamic relationships. Chemical kinetics provides the coupling among various chemical species concentrations, and the coupling with the energy equation through the heat of reaction. In many oxidation systems the kinetic terms determine the characteristic space and time scales over which the equations must be solved.

In order to accomplish the coupling of conservation equations, with chemical kinetics and thermodynamic relationships; Chemkin utilizes three databases, namely “Chemical rate expressions database”, “Thermodynamic properties database”, and “Transport properties database”, in combination with the reactor model specifications. The theory behind the utilization of these databases and the reactor model are explained in the following sections.

### 3.1.1. Chemical Rate Expressions

The database of chemical rate expressions is utilized for introducing the software all the species and their elementary reactions constituting the overall oxidation reaction mechanism, and for calculation of the reaction rates of the elementary reactions and production rates of the species. Each species in the mechanism and all possible elementary reactions, with their kinetic parameters are defined in the chemical rate expressions database.

The reaction rates of the elementary reactions may depend on species composition, temperature, and pressure. The temperature dependence of the reaction rate constants are expressed by using the modified–Arrhenius form as:

$$k_{f,i} = A_i T^{\beta_i} \exp\left(\frac{-E_i}{RT}\right) \quad (3.1)$$

where  $A_i$  is the pre-exponential collision frequency factor,  $\beta_i$  is the temperature exponent,  $E_i$  is the activation energy, and  $R$  is the universal gas constant. The forward reaction rate constant  $k_{f,i}$  of the  $i^{\text{th}}$  reaction depends on the temperature  $T$  and in many cases all the temperature dependence can be incorporated into the exponential term (with  $\beta_i = 0$ ), since most binary elementary reactions exhibit classical Arrhenius behavior over modest ranges of temperature. However, at high temperature ranges encountered in oxidation processes, some reactions may exhibit significant non–Arrhenius behavior, and in these cases additional variation of the rate coefficient with temperature should be included in the  $\beta_i$  term.

The values of the kinetic parameters,  $A_i$ ,  $\beta_i$ , and  $E_i$ , are specified in the chemical rate expressions database for each elementary reaction in the mechanism; and by using these values, forward rate constants of these elementary reactions are calculated.

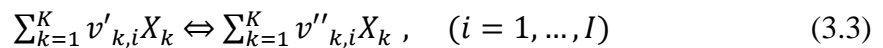
The rates of some chemical reactions may exhibit pressure dependence and these dependencies should also be defined in the chemical rate expressions database. Many unimolecular decomposition reactions and their associated recombination reactions exhibit significant pressure dependence in some experimental regimes. Other apparently bimolecular reactions actually process through an adduct state and display a dependence on pressure as well. Generally speaking, the rates of unimolecular/recombination fall-off reactions increase with increasing pressure, while the rates of chemically activated bimolecular reactions decrease with increasing pressure. The pressure dependencies of these types of reactions are expressed by Lindemann approach (Lindemann et al., 1922) or in Troe form (Gilbert et al., 1983).

For the calculation of reverse rate constants of the elementary reactions, the thermodynamic data are required for the species constituting the reactions. In thermal systems, the reverse rate constants  $k_{r,i}$  are related to the forward rate constants through the equilibrium constants by:

$$k_{r,i} = \frac{k_{f,i}}{K_{c,i}} \quad (3.2)$$

where  $K_{c,i}$  is the equilibrium constant given in concentration units.  $K_{c,i}$  can be determined from the thermodynamic properties of the species. Thermodynamic properties of species are obtained from the thermodynamic properties database that will be described in Section 3.1.2.

Considering elementary reversible reaction involving  $K$  chemical species that can be represented in the general form:



the rate-of-progress variable  $q_i$  for the  $i^{\text{th}}$  reaction is given by the difference of the forward and reverse rates as:

$$q_i = k_{f,i} \prod_{k=1}^K [X_k]^{\nu'_{k,i}} - k_{r,i} \prod_{k=1}^K [X_k]^{\nu''_{k,i}} \quad (3.4)$$

where  $X_k$  is the molar concentration of the  $k^{\text{th}}$  species and  $v_{k,i}$  are the stoichiometric coefficients for the  $k^{\text{th}}$  species. The subscript  $'$  indicates forward stoichiometric coefficients, while  $''$  indicates reverse stoichiometric coefficients.

The production rate  $\dot{w}_k$  of the  $k^{\text{th}}$  species can be written as a summation of the rate-of-progress variables for all reactions involving the  $k^{\text{th}}$  species as:

$$\dot{w}_k = \sum_{i=1}^I v_{k,i} q_i, \quad (k = 1, \dots, K) \quad (3.5)$$

where  $v_{k,i}$  is the difference between the reverse and forward stoichiometric coefficients of the species.

In summary, chemical rate expressions database consists of all the species and possible elementary reactions in the oxidation mechanism, and modified Arrhenius parameters and pressure dependence parameters of these reactions. Then these data are used for the calculation of forward reaction rates of the elementary reactions, and in turn, reverse reaction rate constants of the reactions, and production rates of the species.

### 3.1.2. Thermodynamic Properties

Another essential element in chemical kinetic modeling is the description of the thermodynamic properties of all the chemical species involved. These properties are defined in the thermodynamic properties database of Chemkin for each species in the mechanism. The thermodynamic data in this database are in the form of polynomial fits to temperature; for species enthalpy, entropy, and specific heat capacity. Once these data are defined, they can be used to determine other thermodynamic properties, thermal transport properties, and reaction equilibrium constants.

First a selection of state variables for defining the thermodynamic and chemical state of the gas mixture is required. To describe the state of the gas mixture, pressure ( $P$ ) or density ( $\rho$ ); temperature ( $T_k$ ); and mass ( $Y_k$ ) or mole fraction ( $X_k$ ) should be specified. The equation of state used is the ideal gas equation of state.

The standard-state thermodynamic properties; heat capacity ( $C_{p,k}^0$ ), enthalpy ( $H_k^0$ ), and entropy ( $S_k^0$ ), are assumed to be functions of temperature only, and are given as polynomial fits to temperature. These polynomials are in the form used in the NASA

equilibrium code (McBride et al., 1993). The coefficients of these polynomials constitute the thermodynamic properties database.

Other standard–state thermodynamic properties of the species, i.e. the specific heat at constant volume ( $C_{v,k}^0$ ), the internal energy ( $U_k^0$ ), the Gibb’s free energy ( $G_k^0$ ), and the Helmholtz free energy ( $A_k^0$ ), can be calculated from the values of  $C_{p,k}^0$ ,  $H_k^0$ , and  $S_k^0$ , if required. For the calculation of the equilibrium constants of the reactions, as mentioned in Section 3.1.1., the values of  $S_k^0$  and  $H_k^0$  are used. The mixture–averaged molar thermodynamic properties,  $\bar{C}_p, \bar{C}_v, \bar{H}, \bar{U}, \bar{S}, \bar{G}$  and  $\bar{A}$ , are calculated from the single species standard–state thermodynamic properties.

### 3.1.3. Transport Properties

In solving chemically reactive–flow problems, chemical production and destruction is often balanced by transport due to convection, diffusion, or conduction. In some cases, such as perfectly stirred reactors or plug flow reactors, the determination of composition and temperature fields are assumed to be kinetically limited. In such cases, transport is assumed to be infinitely fast within the section of gas considered and the transport effects can be neglected. For the reactor model used in this study, the transport effects are neglected; therefore, the transport properties database is not required.

The mentioned databases required by Chemkin, constitute the “Detailed chemical kinetic mechanism” of the oxidation reaction. Chemical kinetic mechanisms are available for various oxidation reactions in the literature. In the experimental and theoretical study of Marinov et al. (1998), a comprehensive chemical kinetic mechanism was given for the oxidation of n-butane, including the formations of aromatic species and larger PAHs. For the oxidation of DME, a comprehensive mechanism was given by Kaiser et al. (2000). In this study, these two mechanisms were combined in order to represent the oxidation of n-butane/DME mixture. The mechanisms of Marinov et al. (1998) and Kaiser et al. (2000) were preferred due to their validity for wide ranges of operating conditions and their comprehensiveness in terms of chemical species.

For the formation of the chemical kinetic mechanism for the oxidation of n-butane/DME mixture, the two mechanisms were merged, the kinetic parameters of the common elementary reactions were adjusted and the repetitions were excluded. As a result, a new chemical kinetic mechanism of 201 species undergoing 903 reversible

elementary reactions was obtained for the oxidation of n-butane/DME mixture. This chemical kinetic mechanism; with the list of chemical species, thermodynamic properties of the species, elementary reactions, and the kinetic parameters of the elementary reactions, is given in Appendix A.

### 3.1.4. Validation of the Detailed Chemical Kinetic Mechanism

The accuracy of the detailed mechanism developed was validated for neat n-butane oxidation by comparison with the experimental results of Chakir et al. (1989) (Figure 3.1), for neat DME oxidation by comparison with the experimental results of Fischer et al. (2000) (Figure 3.2), and for mixtures of DME with methane, ethane, propane and ethylene by comparison with theoretical results of Yoon et al. (2008) (Figure 3.3).

Chakir et al. (1989) studied n-butane oxidation in a jet-stirred reactor at 937 K and 10 atm. The detailed chemical kinetic mechanism developed in this study was used to reproduce their experimental results by theoretical modeling. Using the same reactor specifications and process conditions, mole fraction profiles of  $C_4H_{10}$ , CO,  $CO_2$ ,  $CH_4$ ,  $C_2H_4$ , and  $C_2H_6$  against space time were calculated and compared with the experimental results of Chakir et al. (1989). The results of the comparison are given in Figure 3.1. It can be observed that the detailed chemical kinetic mechanism developed can successfully reproduce mole fractions of  $C_4H_{10}$ , CO, and  $C_2H_4$ , while it slightly overpredicts mole fractions of  $CO_2$ ,  $CH_4$ , and  $C_2H_6$ .

Fischer et al. (2000) studied DME oxidation experimentally and theoretically in a flow reactor at 1086 K and 1 atm. Their experimental results were reproduced using the detailed chemical kinetic mechanism developed. Mole fractions of  $CH_3OCH_3$ ,  $H_2O$ ,  $O_2$ , CO,  $CH_2O$ , and  $CH_4$  were calculated and compared with the experimental results of Fischer et al. (2000). The results are given in Figure 3.2. It can be observed that mole fractions of  $CH_3OCH_3$ ,  $O_2$ , and  $CH_4$  are well predicted by the mechanism, while mole fractions of  $H_2O$ , CO, and  $CH_2O$  are slightly underpredicted.

Finally the results of Yoon et al. (2008) were reproduced with the detailed mechanism for the oxidations of  $CH_4/DME$  and  $C_2H_6/DME$  mixtures. Mole fractions of  $CH_3$  and  $C_2H_2$  were calculated using the detailed mechanism and compared with the findings of Yoon et al. (2008). The results are given in Figure 3.3. It can be observed

that the orders and the trends of the mole fraction profiles of  $\text{CH}_3$  and  $\text{C}_2\text{H}_2$  are successfully predicted by the detailed mechanism both for the  $\text{CH}_4/\text{DME}$  oxidation and the  $\text{C}_2\text{H}_6/\text{DME}$  oxidation.

So, it can be said that the detailed chemical kinetic mechanism developed can successfully predict mole fraction profiles of various species for the oxidations of both n-butane and DME, and the oxidation of alkane/DME mixtures.

### **3.1.5. Reactor Model**

The oxidation process in this study was modeled to be carried out in a tubular reactor, and plug flow conditions were assumed throughout the reactor. Plug-flow reactor (PFR) is the ideal form of tubular reactors with the assumptions of no mixing in the axial (flow) direction but perfect mixing in the directions transverse to this. It can be shown that the absence of axial mixing allows the achievable reactant conversion to be maximized. Likewise, the lack of transverse gradients implies that the mass-transfer limitations are absent, once again enhancing the reactor performance (Smith, 1981). Along with these practical advantages, the plug flow reactor is computationally efficient since it is modeled using first-order ordinary differential equations, and transport properties are neglected.

In PFRs, oxidation takes place at constant pressure, most often near atmospheric pressure. The flow is assumed to be linear, and all transport normal to the flow axis is neglected. This includes heat losses to the walls of the flow duct which are usually heated to the same temperature as the inlet flow. Care is taken to achieve complete and rapid gas mixing at the inlet or source end of the reactor and this mixing process is assumed to persist throughout the reactor. Combined with the neglect of radial transport, steady plug flow is achieved.

In typical flow reactors, dilute fuel or fuel-oxidizer mixtures are considered in order to keep the total temperature variation quite small. The most common temperature range encountered in PFRs is between 900 and 1300 K. An important feature of the flow reactor is that it occupies a regime roughly midway between static reactor and shock tube experiments. Most fuel and intermediate hydrocarbon consumption in flames also takes place in the same temperature range as that encountered in flow reactor experiments.

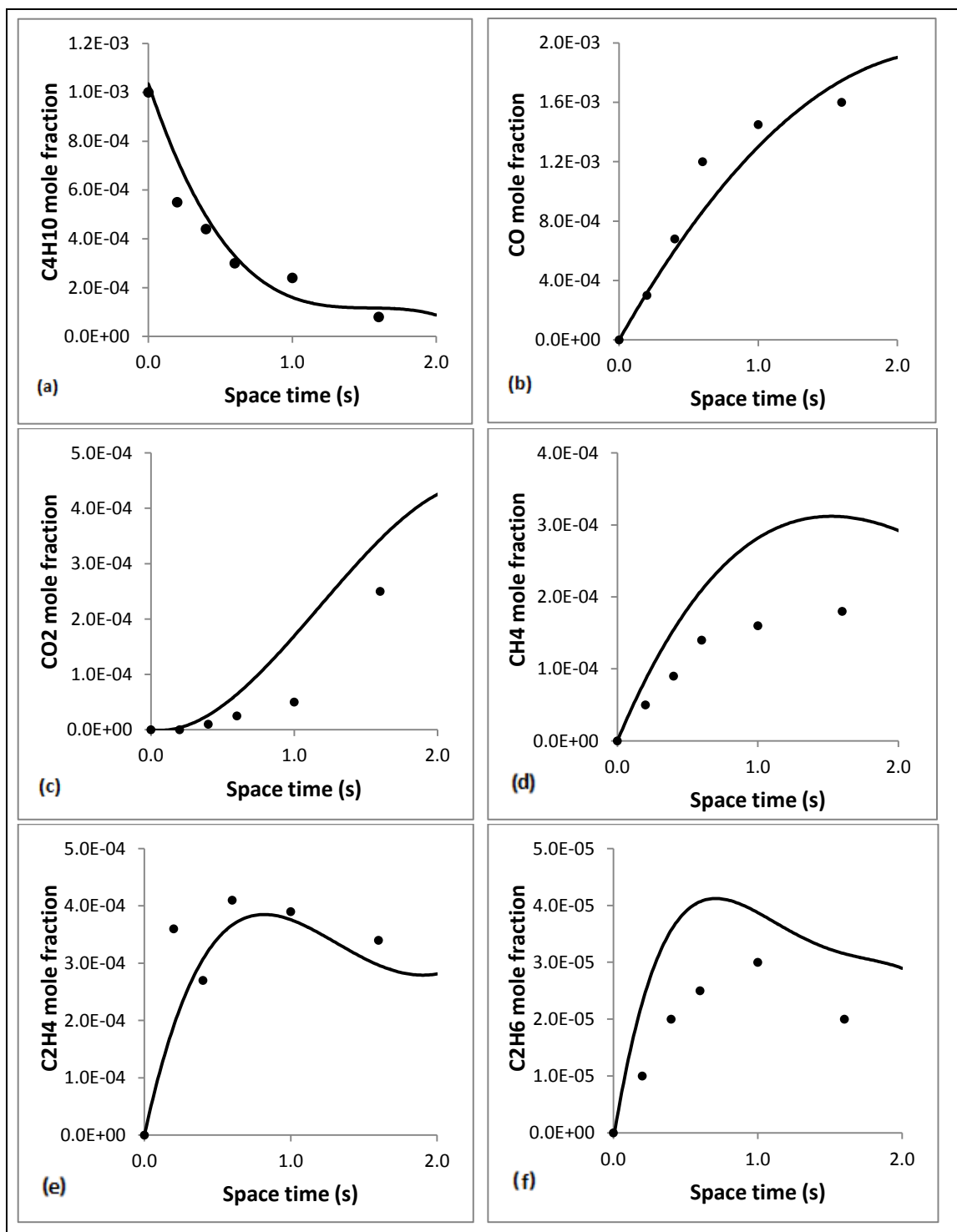


Figure 3.1. Validation of the detailed chemical kinetic mechanism for  $C_4H_{10}$  oxidation by comparison with the results of Chakir et al. (1989) ( $C_4H_{10}$  oxidation in a jet-stirred reactor at 937 K and 10 atm,  $C_4H_{10}/O_2/N_2=0.1:0.65:99.25$ ). Figures show the mole fractions of (a)  $C_4H_{10}$ , (b) CO, (c)  $CO_2$ , (d)  $CH_4$ , (e)  $C_2H_4$ , and (f)  $C_2H_6$ . Lines show modeling results and the dots correspond to experimental results.



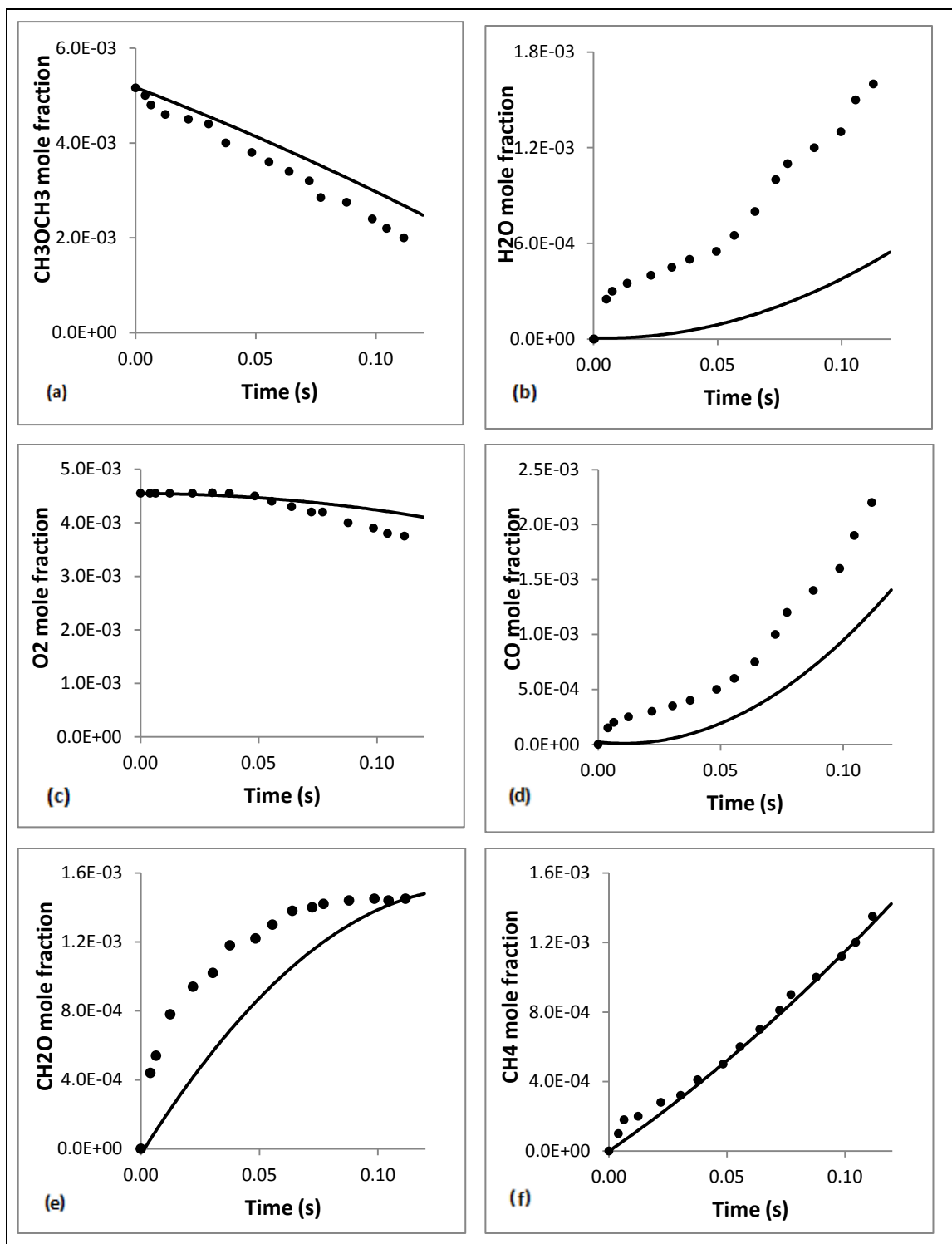


Figure 3.2. Validation of the detailed chemical kinetic mechanism for  $\text{CH}_3\text{OCH}_3$  oxidation by comparison with the results of Fischer et al. (2000) ( $\text{CH}_3\text{OCH}_3$  oxidation in a plug-flow reactor at 1086 K and 1 atm,  $\phi=3.4$ ). Figures show the mole fractions of (a)  $\text{CH}_3\text{OCH}_3$ , (b)  $\text{H}_2\text{O}$ , (c)  $\text{O}_2$ , (d)  $\text{CO}$ , (e)  $\text{CH}_2\text{O}$ , and (f)  $\text{CH}_4$ . Lines show modeling results and the dots correspond to experimental results.

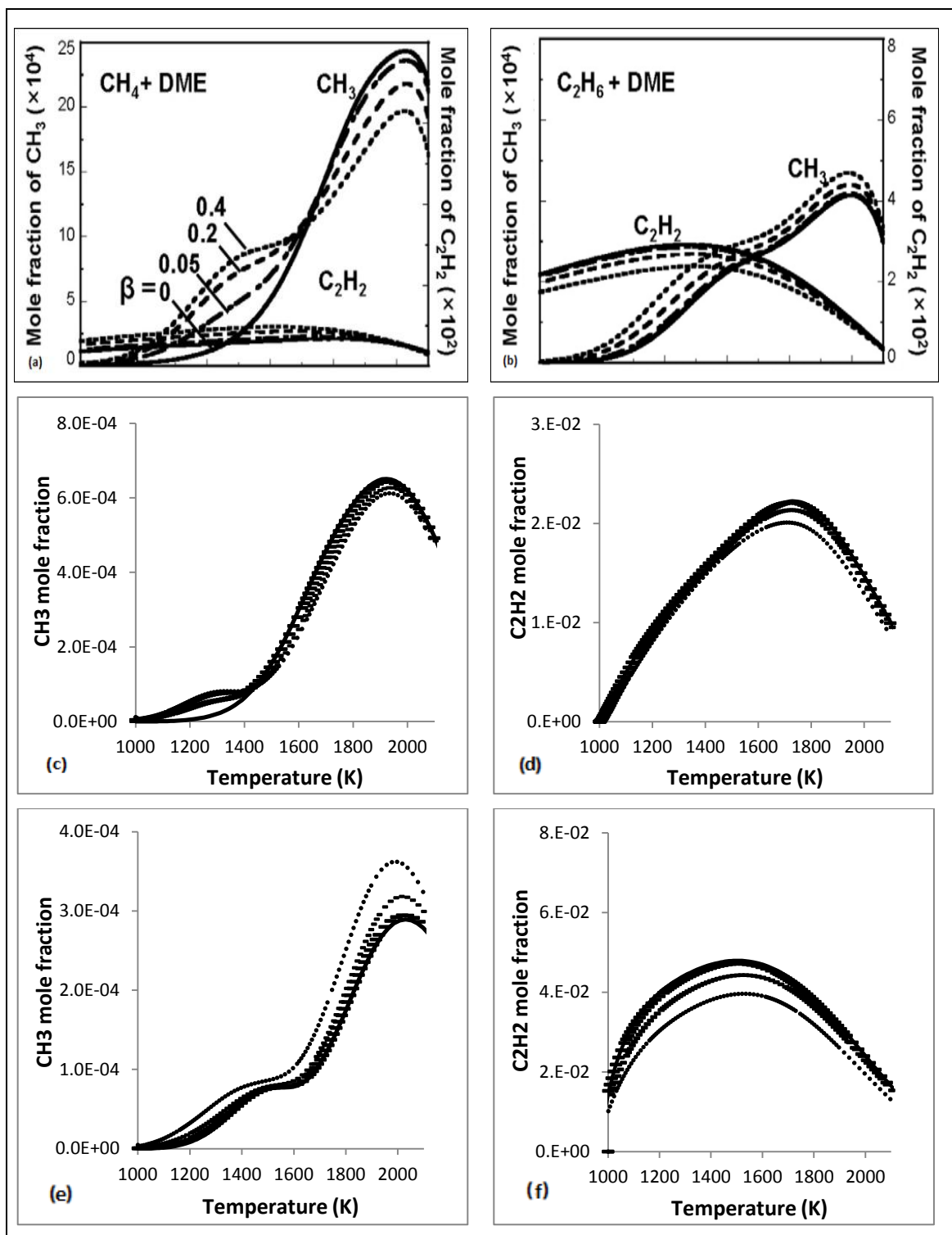


Figure 3.3. Validation of the detailed chemical kinetic mechanism for  $\text{CH}_4/\text{CH}_3\text{OCH}_3$  and  $\text{C}_2\text{H}_6/\text{CH}_3\text{OCH}_3$  oxidation by comparison with the results of Yoon et al. (2008) (Opposed-flow flames at 1 atm,  $\beta$  is the fraction of DME in the fuel mixture). Figures show the results of Yoon et al. (2008) for (a)  $\text{CH}_4/\text{CH}_3\text{OCH}_3$  oxidation and (b) for  $\text{C}_2\text{H}_6/\text{CH}_3\text{OCH}_3$  oxidation, and the results of the skeletal mechanism for (c)  $\text{CH}_3$  and (d)  $\text{C}_2\text{H}_2$  in  $\text{CH}_4/\text{CH}_3\text{OCH}_3$  oxidation and (e)  $\text{CH}_3$  and (f)  $\text{C}_2\text{H}_2$  in  $\text{C}_2\text{H}_6/\text{CH}_3\text{OCH}_3$  oxidation.

The equations governing the behavior of a PFR are simplified versions of the general relations for conservation of mass, energy, and momentum (Bird et al., 2007). These equations can be derived by writing balances over a differential slice in the flow direction  $x$ , with the stipulations that there are no variations in the radial direction, and axial diffusion of any quantity is negligible relative to the corresponding convective term. In this way, the overall mass balance is found to be:

$$\rho u \frac{dA}{dx} + \rho A \frac{du}{dx} + uA \frac{d\rho}{dx} = 0 \quad (3.6)$$

Here  $\rho$  is the mass density,  $u$  is the axial velocity of the gas mixture, and  $A$  is the cross-sectional (flow) area in the reactor. A similar equation can be written for each species individually:

$$\rho u A \frac{dY_k}{dx} = W_k \dot{w}_k A \quad (3.7)$$

Here  $W_k$  is the molecular weight and  $Y_k$  is the mass fraction of species  $k$ , and  $\dot{w}_k$  is its molar rate of production by homogeneous gas reactions. Such reactions cannot change the total mass of the gas, but they can alter its composition.

The energy equation for the PFR is given as:

$$\rho u A \left( \sum_{k=1}^K h_k \frac{dY_k}{dx} + \bar{C}_p \frac{dT}{dx} + u \frac{du}{dx} \right) = a_e Q_e \quad (3.8)$$

where  $h_k$  is the specific enthalpy of species  $k$ ,  $\bar{C}_p$  is the mean heat capacity per unit mass of the gas,  $T$  is the absolute gas temperature,  $Q_e$  is the heat flux from the surroundings to the outer tube wall, and  $a_e$  is the surface area per unit length of the tube wall.

The momentum equation expresses the balance between pressure forces, inertia, and viscous drag. Thus, can be given as:

$$A \frac{dP}{dx} + \rho u A \frac{du}{dx} + \frac{dF}{dx} = 0 \quad (3.9)$$

where  $P$  is the absolute pressure and  $F$  is the drag force exerted on the gas by the tube wall. The pressure is related to the density via the ideal-gas equation of state.

### 3.1.5.1. Validation of the Plug-Flow Assumption

Plug-flow assumption yields considerable simplifications in the solution, but a verification of the validity of this assumption is required. “The dispersion model” can be used for this purpose, for laminar flow in sufficiently long tubes (Levenspiel, 1999). In this model, a diffusion-like process superimposed on plug flow is assumed. This process is called dispersion to distinguish from molecular diffusion. The dispersion coefficient  $D$  ( $\text{m}^2/\text{s}$ ) represents this spreading process. Also,  $D/uL$  is the dimensionless group characterizing the spread in the whole reactor, where  $L$  is the length of the reactor. This dimensionless quantity is the parameter that measures the extent of axial dispersion. Thus,  $D/uL \rightarrow 0$  means negligible dispersion, hence plug flow.

The dispersion number  $D/uL$  is a product of two terms:

$$\frac{D}{uL} = \left( \begin{array}{c} \text{intensity of} \\ \text{dispersion} \end{array} \right) \left( \begin{array}{c} \text{geometric} \\ \text{factor} \end{array} \right) = \left( \frac{D}{ud} \right) \left( \frac{d}{L} \right) \quad (3.10)$$

where  $d$  is the diameter of the tubular reactor, and

$$\frac{D}{ud} = f \left( \begin{array}{c} \text{fluid} \\ \text{properties} \end{array} \right) \left( \begin{array}{c} \text{flow} \\ \text{dynamics} \end{array} \right) = f(Sc)(Re) = Bo \quad (3.11)$$

Here,  $Sc$  is the Schmidt number,  $Re$  is the Reynolds number, and  $Bo$  is the Bodenstein number.

The dispersion coefficient can be determined by using the chart given by Ananthakrishnan et al. (1965), comparing  $Bo$  versus  $L/d$ . For small extents of dispersion, i.e.  $D/uL < 0.01$ , the flow can be satisfactorily assumed as plug flow.

### 3.2. Reduction of the Detailed Mechanism into a Skeletal Mechanism for the Oxidation of n-Butane/DME Mixture

Detailed chemical kinetic mechanisms cannot be easily included in most multidimensional oxidation and combustion models because the computer speed and cost requirements of such treatments are very high. Therefore, reliable models of fuel oxidation, which are very simple and still are able to reproduce experimental data over extended ranges of operating conditions, are required. In addition, in many occasions the great amount of information that the detailed mechanism provides is unnecessary and a much simpler mechanism would be sufficient. For these purposes, detailed mechanisms are reduced into much simpler skeletal mechanisms.

One method of mechanism reduction is the “Rate of production analysis”. This analysis determines the contribution of each elementary reaction to the net production or destruction rates of a species. The contribution of reaction  $i$  to the rate of production of species  $k$  can be calculated as:

$$C_{ki} = v_{ki}q_i \quad (3.12)$$

The contributions of all the reactions to the rates of production of the selected species are calculated in this way. Then, the normalized values of these reaction contributions to the species production and destruction are calculated. The normalized production–contributions of the reactions are given by:

$$\bar{C}_{ki}^p = \frac{\max(v_{ki},0)q_i}{\sum_{i=1}^I \max(v_{ki},0)q_i} \quad (3.13)$$

and the normalized destruction–contributions of the reactions are given by:

$$\bar{C}_{ki}^d = \frac{\min(v_{ki},0)q_i}{\sum_{i=1}^I \min(v_{ki},0)q_i} \quad (3.14)$$

After the determination of the normalized contributions, a threshold value is selected for the normalized contribution coefficients. The reactions with greater contribution coefficients than this threshold value are selected to be added to the

skeletal mechanism, and the remaining reactions with smaller contributions are omitted. So that, the total number of elementary reactions is decreased by exclusion of the unimportant reactions, and the skeletal mechanism is obtained (Lu and Law, 2005). The accuracy of the skeletal mechanism developed should be verified by comparing with experimental results or with the literature.

## CHAPTER 4

### RESULTS AND DISCUSSION

The effects of DME addition to n-butane in different fractions were investigated in terms of the formations of various oxidation products. Also, the effects of important process parameters on the formations of important oxidation products during the oxidation of n-butane/DME mixture were investigated. These process parameters were temperature, pressure, and equivalence ratio. Table 4.1 summarizes the process parameters investigated and values of these parameters.

Table 4.1. Parameters investigated for the oxidation of n-butane/DME mixture

Parameter investigated	Mole fraction of DME in the fuel mixture, %	Inlet temperature, $T_0$ (K)	Pressure, P (atm)	Equivalence ratio, $\phi$
DME fraction	0, 10, 20, 50 and 100	900	1	2.6
Temperature and pressure	20 and 50	500, 700, 800, 900, 1100, 1300, 1500 and 1700	1 and 5	2.6
Equivalence ratio	20 and 50	500, 700, 800, 900, 1100, 1300, 1500 and 1700	1	2.6 and 3.0

After investigation of the effects of process parameters, formation pathways of the aromatic species during the oxidations of n-butane and n-butane/DME mixture were tried to be identified. Important precursor species and their roles in the formations of aromatic species were investigated. Finally, a skeletal chemical kinetic mechanism was developed by the reduction of the detailed chemical kinetic mechanism that was developed previously. The oxidation of n-butane/DME mixture was tried to be represented by a simpler kinetic mechanism with lower number of chemical species and elementary reactions.

## 4.1. Investigation of the Effects of DME Addition to n-Butane Oxidation

The effects of DME addition on the formations of n-butane oxidation products were investigated for three different molar concentrations of DME (10%, 20%, and 50% DME in the fuel mixture). Neat oxidations of n-butane (0% DME in the fuel mixture) and DME (100% DME in the fuel mixture) were also investigated as reference cases, for comparison purposes. The inlet fuel mixture was highly diluted with an inert gas (argon). Pure oxygen was used as the oxidizer. The inlet mole fractions of n-butane, DME, O<sub>2</sub> and Ar are given in Table 4.2.

Table 4.2. Inlet mole fractions of n-butane, DME, O<sub>2</sub>, and Ar for various concentrations of DME added to n-butane oxidation for an equivalence ratio of 2.6

% DME in the fuel mixture	X <sub>C<sub>4</sub>H<sub>10</sub></sub>	X <sub>CH<sub>3</sub>OCH<sub>3</sub></sub>	X <sub>O<sub>2</sub></sub>	X <sub>Ar</sub>
0	0.005714	0.000000	0.014286	0.980000
10	0.005349	0.000594	0.014057	0.980000
20	0.004952	0.001238	0.013810	0.980000
50	0.003537	0.003537	0.012925	0.980000
100	0.000000	0.009286	0.010714	0.980000

The oxidation process was carried out in a tubular reactor with length of  $L = 10\text{ m}$  and diameter of  $d = 0.05\text{ m}$ . The inlet velocity of the gas mixture was  $u = 0.5\text{ m/s}$ , and the flow regime was laminar. The dispersion numbers for the flow conditions studied were calculated to be below or around 0.01, and the assumption of plug flow was justified. The reactor was operated under adiabatic conditions and the inlet temperature was selected as  $T_0 = 900\text{ K}$ . The pressure was constant throughout the reactor and it was equal to atmospheric pressure ( $P = 1\text{ atm}$ ). Since it is known that the formations of aromatic species and PAHs are observed at fuel-rich conditions, equivalence ratio was selected as  $\phi = 2.6$ .

The resulting temperature profiles within the reactor for the different concentrations of DME added are given in Figure 4.1. It can be seen that temperature rise due to reaction is below 250 K in each case and is higher for the case of pure DME oxidation. The effect of DME addition at other concentrations (10%, 20%, and 50%) on the reaction temperature is not so pronounced.



The effects of DME concentration on the concentration profiles of various major, minor, and trace oxidation products were analyzed. The list of the investigated major and minor oxidation products are given in Table 4.3. First group of the oxidation products is the major species which consist of fuel (n-butane and DME), oxidizer ( $O_2$ ), and the main products of the oxidation reaction ( $H_2O$ ,  $CO_2$ ,  $CO$  and  $H_2$ ). The concentration profiles of the major products give information about the main oxidation process, the consumptions of fuels and oxidizer, and the formations of the main oxidation products. Normally, the main products of the oxidation process are  $H_2O$  and  $CO_2$ , but due to incomplete oxidation, significant formations of  $CO$  also occur.  $CO$  is a major pollutant released as a result of oxidation processes.  $H_2$  can also be considered as a major product since it is produced in relatively high amounts. This species is important in the formations of  $H$  and  $OH$  radicals which are known to be very important radicals in the decomposition reactions of the fuels.

Second group is the minor products, which are produced in lower concentrations compared to the major products. Among the minor oxidation products,  $CH_4$ ,  $C_2H_6$ , and  $C_3H_8$  are also alkane fuels with smaller carbon number compared to n-butane. The formation of  $CH_4$  is also important due to its association with global warming and climate change (EPA, 2011).  $CH_2O$  and  $C_2H_4O$  are oxygenated oxidation products, formations of which are known to be increased by the addition of oxygenated fuel additives such as DME.  $CH_2O$  is a toxic material and is classified as a human carcinogen (NIH, 2011).  $C_2H_4O$  is also a probable carcinogen for humans (EPA, 1994).

Some of the minor oxidation products are known to be the precursors of aromatic species and PAHs. These precursor species are  $C_2H_2$ ,  $C_2H_4$ ,  $C_3H_3$ ,  $aC_3H_4$ ,  $pC_3H_4$ ,  $C_3H_6$ ,  $C_4H_2$ ,  $C_4H_4$ , 1,3- $C_4H_6$ , 1- $C_4H_6$ ,  $C_4H_8-1$ ,  $C_4H_8-2$  and  $c-C_5H_6$ .

The trace species investigated were aromatic species and PAHs, which constitute an important class of emissions from the oxidation of n-butane. The formations of aromatic species and PAHs up to four-rings were analyzed. The chemical formulas, molecular weights, names, and molecular structures of the investigated aromatic species and PAHs are given in Table 4.4.

The concentration profiles of the investigated major, minor, and trace species for different mole fractions of DME in the fuel mixture are given in Figures 4.2 to 4.20.

Table 4.3. List of the major and minor oxidation products investigated

<b>Formula</b>	<b>Name</b>
<b>Major oxidation products</b>	
C <sub>4</sub> H <sub>10</sub>	n-Butane
CH <sub>3</sub> OCH <sub>3</sub>	DME
O <sub>2</sub>	Oxygen
CO <sub>2</sub>	Carbon dioxide
CO	Carbon monoxide
H <sub>2</sub> O	Water
H <sub>2</sub>	Hydrogen
<b>Minor oxidation products</b>	
CH <sub>4</sub>	Methane
C <sub>2</sub> H <sub>6</sub>	Ethane
C <sub>3</sub> H <sub>8</sub>	Propane
CH <sub>2</sub> O	Formaldehyde
C <sub>2</sub> H <sub>4</sub> O	Acetaldehyde
<b>Minor oxidation products – Precursors of aromatic species</b>	
C <sub>2</sub> H <sub>2</sub>	Acetylene
C <sub>2</sub> H <sub>4</sub>	Ethylene
C <sub>3</sub> H <sub>3</sub>	Propargyl
aC <sub>3</sub> H <sub>4</sub>	1,2-Propadiene (Allene)
pC <sub>3</sub> H <sub>4</sub>	Methylacetylene (Propyne)
C <sub>3</sub> H <sub>6</sub>	Propene
C <sub>4</sub> H <sub>2</sub>	Diacetylene
C <sub>4</sub> H <sub>4</sub>	Vinylacetylene
1,3-C <sub>4</sub> H <sub>6</sub>	1,3-Butadiene
1-C <sub>4</sub> H <sub>6</sub>	1-Butyne (Ethylacetylene)
C <sub>4</sub> H <sub>8</sub> -1	But-1-ene
C <sub>4</sub> H <sub>8</sub> -2	But-2-ene
c-C <sub>5</sub> H <sub>6</sub>	Cyclopentadiene

Table 4.4. List of aromatic species and PAHs investigated

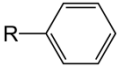

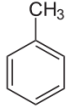
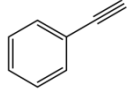
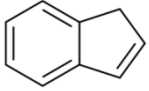
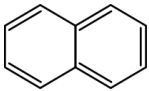
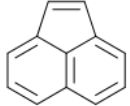
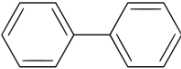
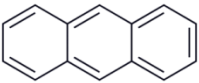
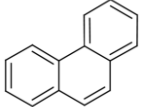
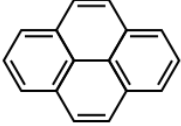
Chemical formula	Molecular weight (g/mol)	Name	Molecular structure
<b>One – ring aromatic species</b>			
$C_6H_5$	77.10	Phenyl	
$C_6H_6$	78.11	Benzene	
$C_7H_8$	92.14	Toluene	
$C_8H_6$	102.13	Phenylacetylene	
$C_9H_8$	116.16	Indene	
<b>Two – ring aromatic species</b>			
$C_{10}H_8$	128.17	Naphthalene	
$C_{12}H_8$	152.19	Acenaphthylene	
$C_{12}H_{10}$	154.21	Biphenyl	
<b>Three – ring aromatic species</b>			
$aC_{14}H_{10}$	178.23	Anthracene	
$pC_{14}H_{10}$	178.23	Phenanthrene	
<b>Four – ring aromatic species</b>			
$C_{16}H_{10}$	202.25	Pyrene	

Figure 4.2 shows the consumptions of the two fuels and Figure 4.3 shows the consumption of the oxidizer. Shift towards the shorter distances of the reactor can be observed in the concentration profiles of n-butane and  $O_2$  as the concentration of DME increases. This suggests that increasing addition of DME increases the consumption rates of n-butane and  $O_2$ , thus the overall rate of the oxidation reaction. It is also observed that increasing DME concentration decreases the requirement of  $O_2$ , since DME is an oxygenated compound.

The profiles of two major species,  $CO_2$  and  $CO$ , are given in Figure 4.4. As the DME concentration increases, an increasing trend is observed for the formation of  $CO_2$ . This effect is pronounced for pure DME oxidation. The final mole fractions of the  $CO$  formed do not seem to be different for the 0%, 10%, 20%, and 50% DME cases. But for the pure DME oxidation, the formation of  $CO$  is decreased around 20%, compared to other cases. This shows a shift in the reaction towards complete oxidation, and thus lower emissions of  $CO$ . Previously Frye et al. (1999) suggested that DME produced lower  $CO$  emissions than propane and butane; and Lee et al. (2011) suggested that DME addition to n-butane and LPG decreased the emissions of  $CO$ , in conformity with the results obtained in this study.

The concentration profiles of two other major species  $H_2O$  and  $H_2$  are given in Figure 4.5. An increasing trend is also observed for  $H_2O$ , similar to  $CO_2$ , with the increase in DME concentration. For the cases of 10%, 20%, and 50% DME addition, final mole fractions of  $H_2$  are slightly increased compared to the case of pure n-butane. However, for the case of pure DME oxidation, final mole fraction of this species is the lowest.

The concentration profiles of the three alkanes,  $CH_4$ ,  $C_2H_6$ , and  $C_3H_8$ , are given in Figure 4.6. Maximum mole fraction of  $CH_4$  seems to be increasing as the concentration of DME increases, up to 50% DME. However, in the case of 100% DME, the maximum mole fraction of  $CH_4$  produced is the lowest. The maximum mole fraction of  $C_2H_6$  increases, while the maximum mole fraction of  $C_3H_8$  decreases, as the amount of DME in the fuel mixture increases. This situation is considered to be related to the change in the oxidation chemistry of  $C_2$  species, since DME has a molecular structure with two carbons. The destruction rates are more rapid and the final mole fractions are lower for all three alkanes in the case of 100% DME, compared to other cases. For the case of 100% DME, the final mole fraction of  $CH_4$ , which is important in terms of environmental considerations, is decreased by 90% compared to pure n-butane case.

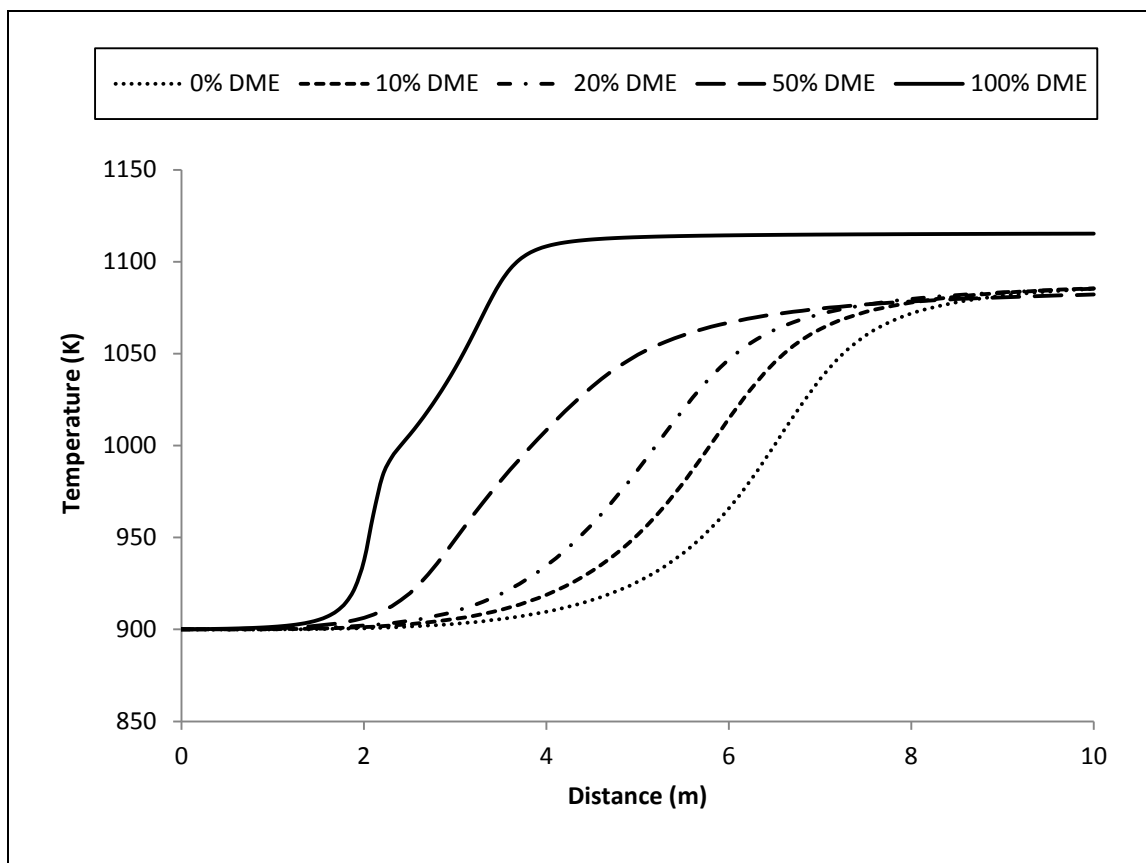


Figure 4.1. Temperature profiles for different concentrations of  $\text{CH}_3\text{OCH}_3$  added to  $\text{C}_4\text{H}_{10}/\text{O}_2/\text{Ar}$  oxidation versus reactor distance. ( $T_0 = 900\text{K}$ ,  $P = 1\text{atm}$ ,  $\phi = 2.6$ ).

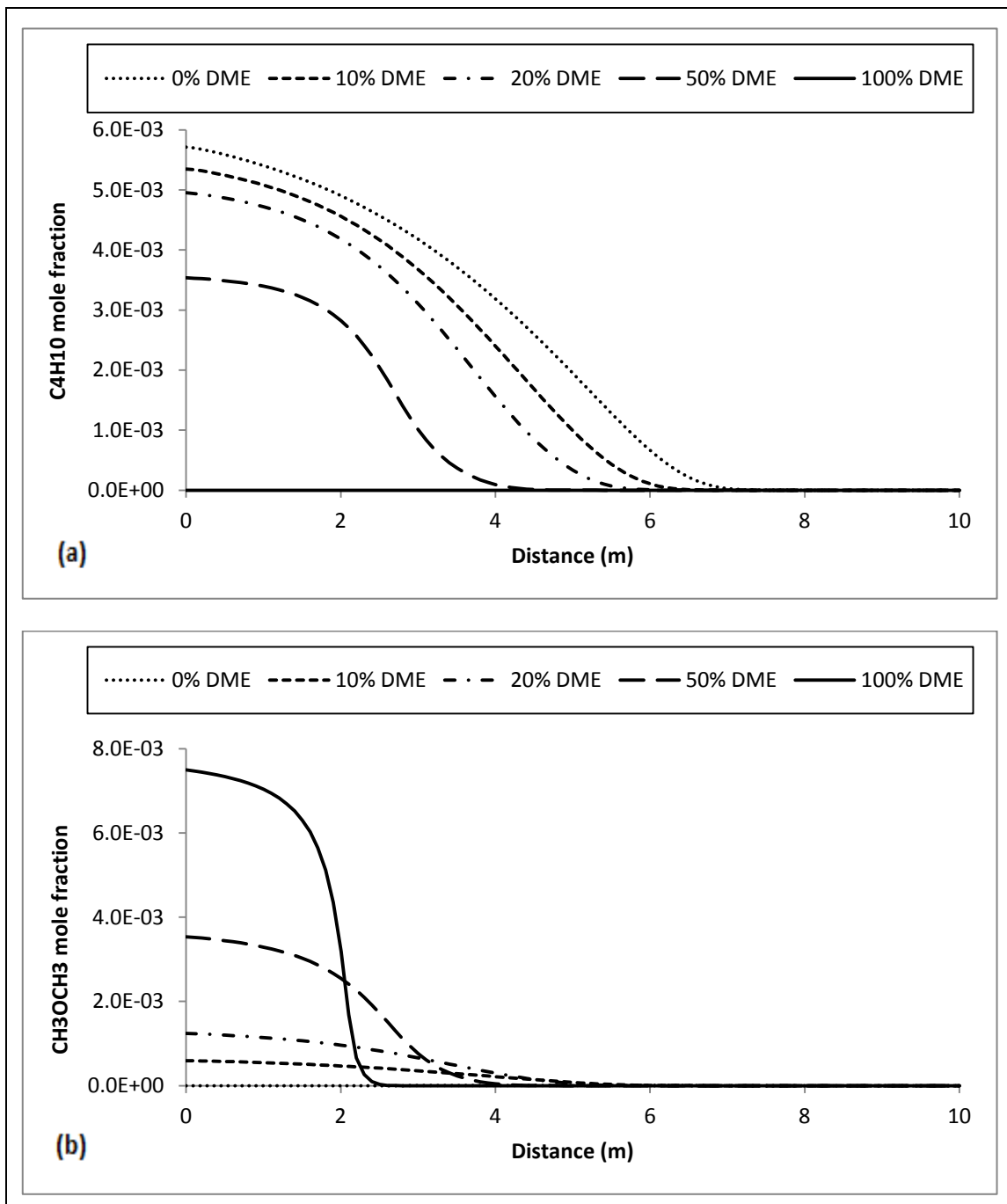


Figure 4.2. Concentration profiles of (a)  $C_4H_{10}$  and (b)  $CH_3OCH_3$  for different concentrations of  $CH_3OCH_3$  added to  $C_4H_{10}/O_2/Ar$  oxidation versus reactor distance. ( $T_0 = 900K$ ,  $P = 1atm$ ,  $\phi = 2.6$ ).

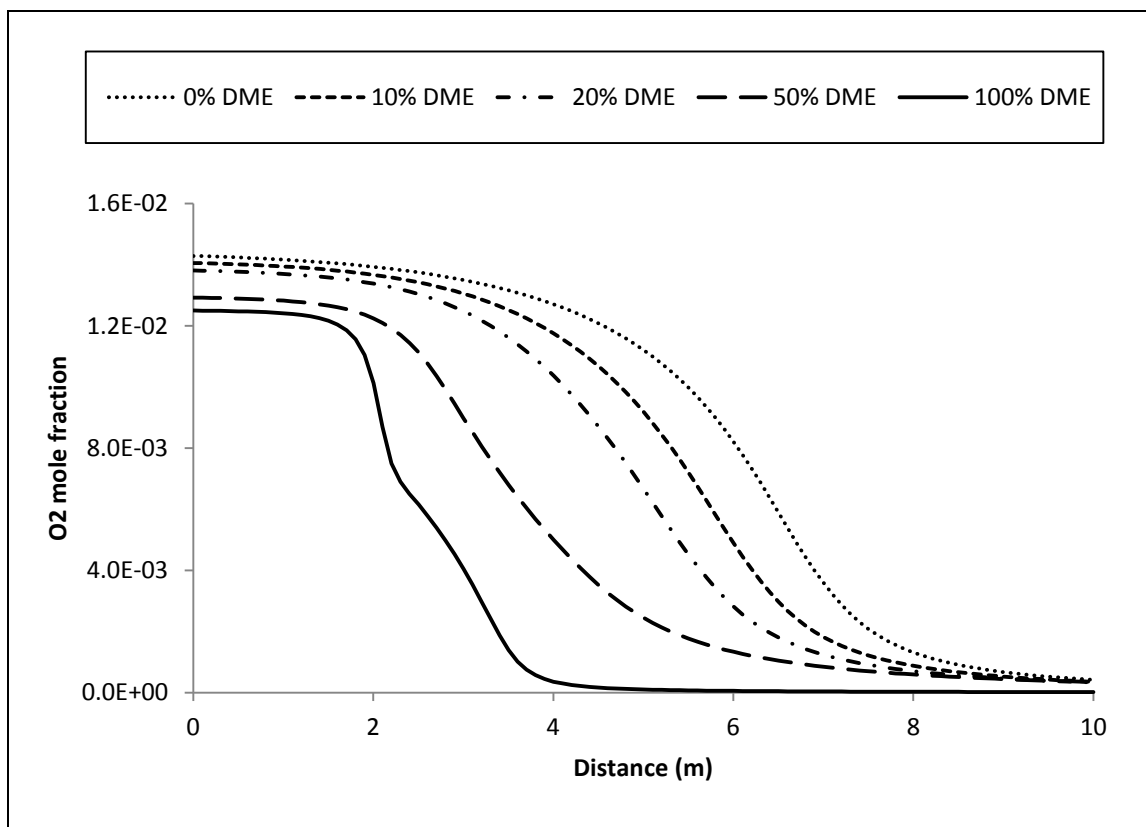


Figure 4.3. Concentration profile of O<sub>2</sub> for different concentrations of CH<sub>3</sub>OCH<sub>3</sub> added to C<sub>4</sub>H<sub>10</sub>/O<sub>2</sub>/Ar oxidation versus reactor distance. (T<sub>0</sub> = 900K, P = 1atm, φ = 2.6).

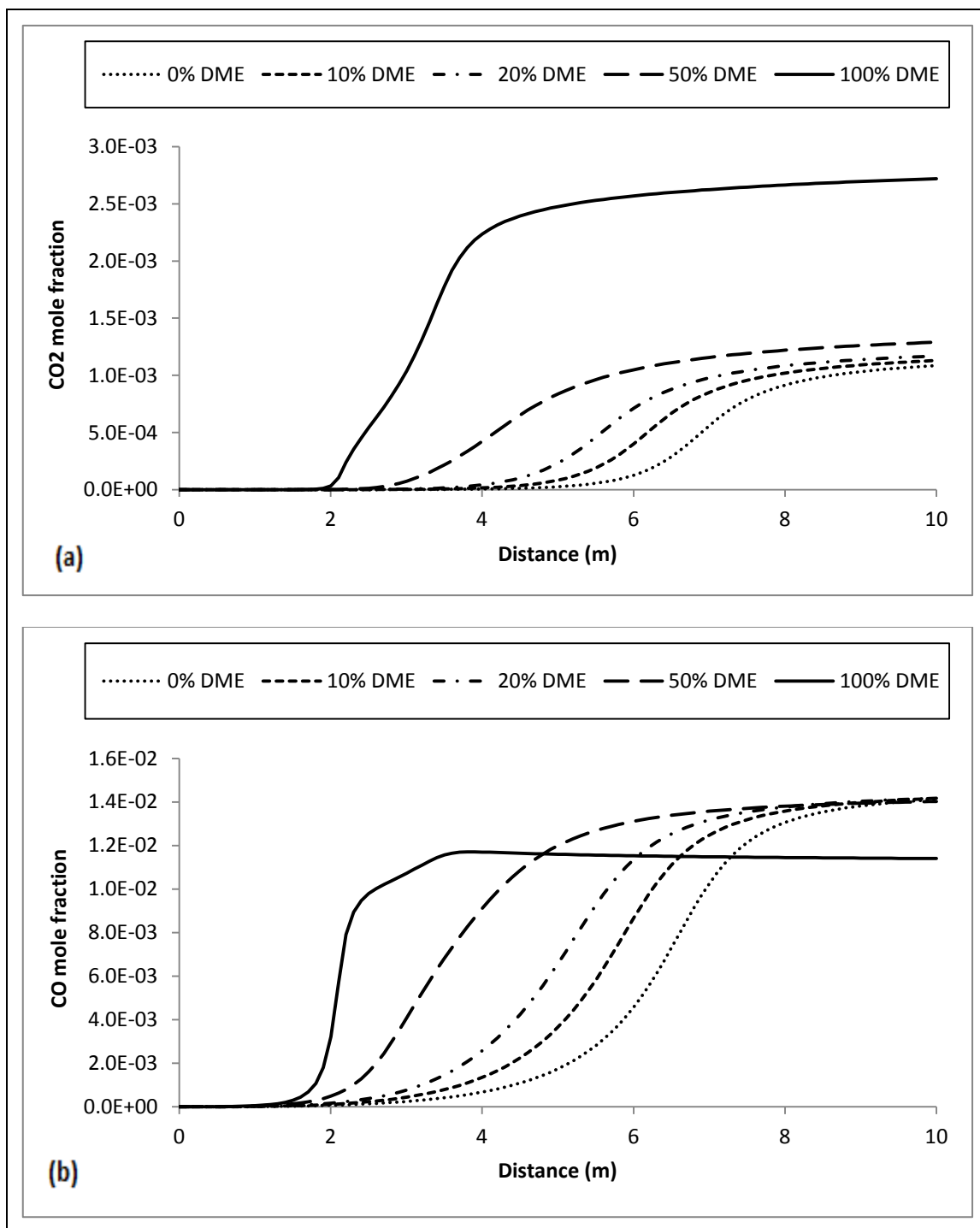


Figure 4.4. Concentration profiles of (a)  $\text{CO}_2$  and (b)  $\text{CO}$  for different concentrations of  $\text{CH}_3\text{OCH}_3$  added to  $\text{C}_4\text{H}_{10}/\text{O}_2/\text{Ar}$  oxidation versus reactor distance. ( $T_0 = 900\text{K}$ ,  $P = 1\text{atm}$ ,  $\phi = 2.6$ ).



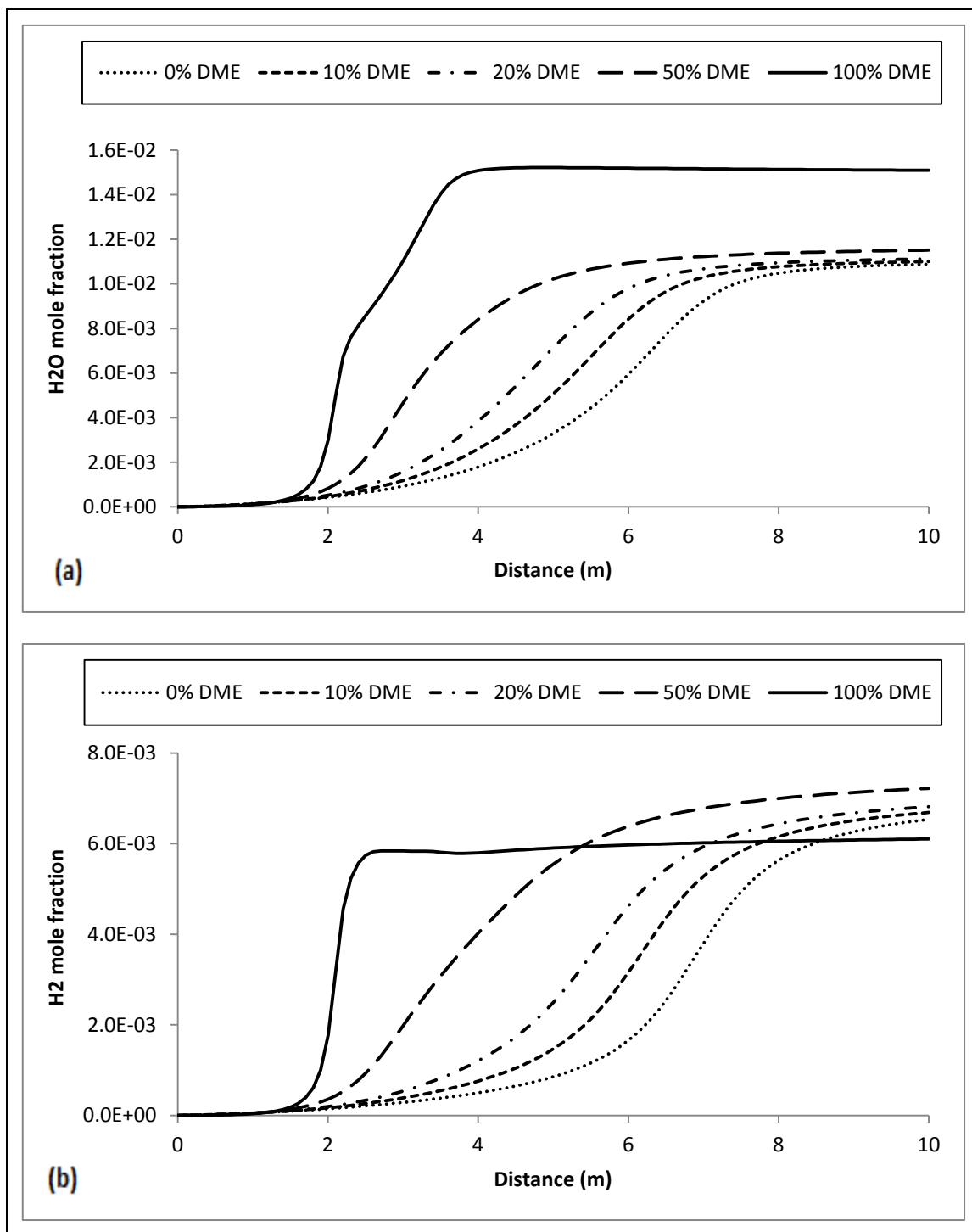


Figure 4.5. Concentration profiles of (a) H<sub>2</sub>O and (b) H<sub>2</sub> for different concentrations of CH<sub>3</sub>OCH<sub>3</sub> added to C<sub>4</sub>H<sub>10</sub>/O<sub>2</sub>/Ar oxidation versus reactor distance. (T<sub>0</sub> = 900K, P = 1atm, φ = 2.6).

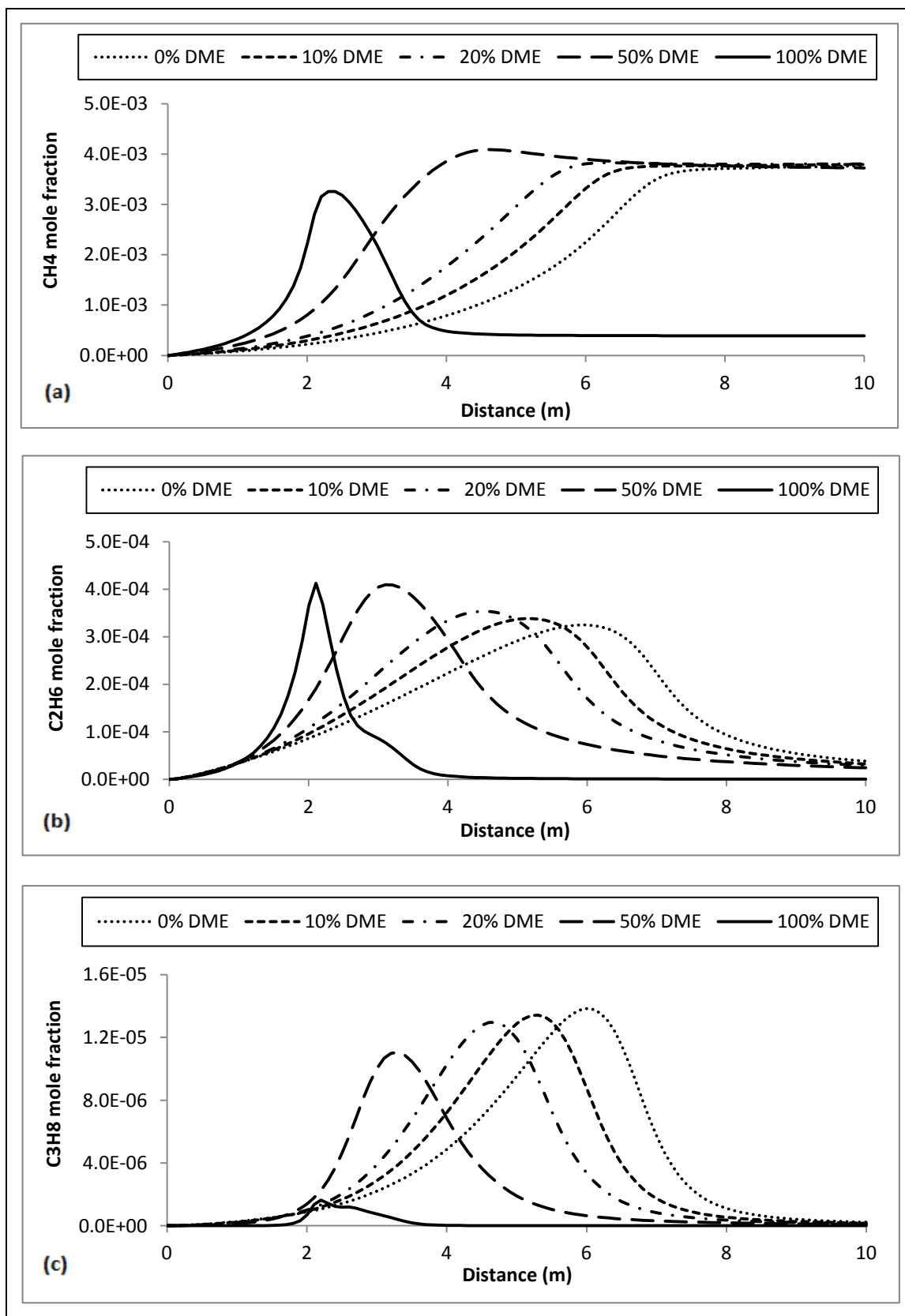


Figure 4.6. Concentration profiles of (a) CH<sub>4</sub> (b) C<sub>2</sub>H<sub>6</sub> and (c) C<sub>3</sub>H<sub>8</sub> for different concentrations of CH<sub>3</sub>OCH<sub>3</sub> added to C<sub>4</sub>H<sub>10</sub>/O<sub>2</sub>/Ar oxidation versus reactor distance. (T<sub>0</sub> = 900K, P = 1atm, φ = 2.6).

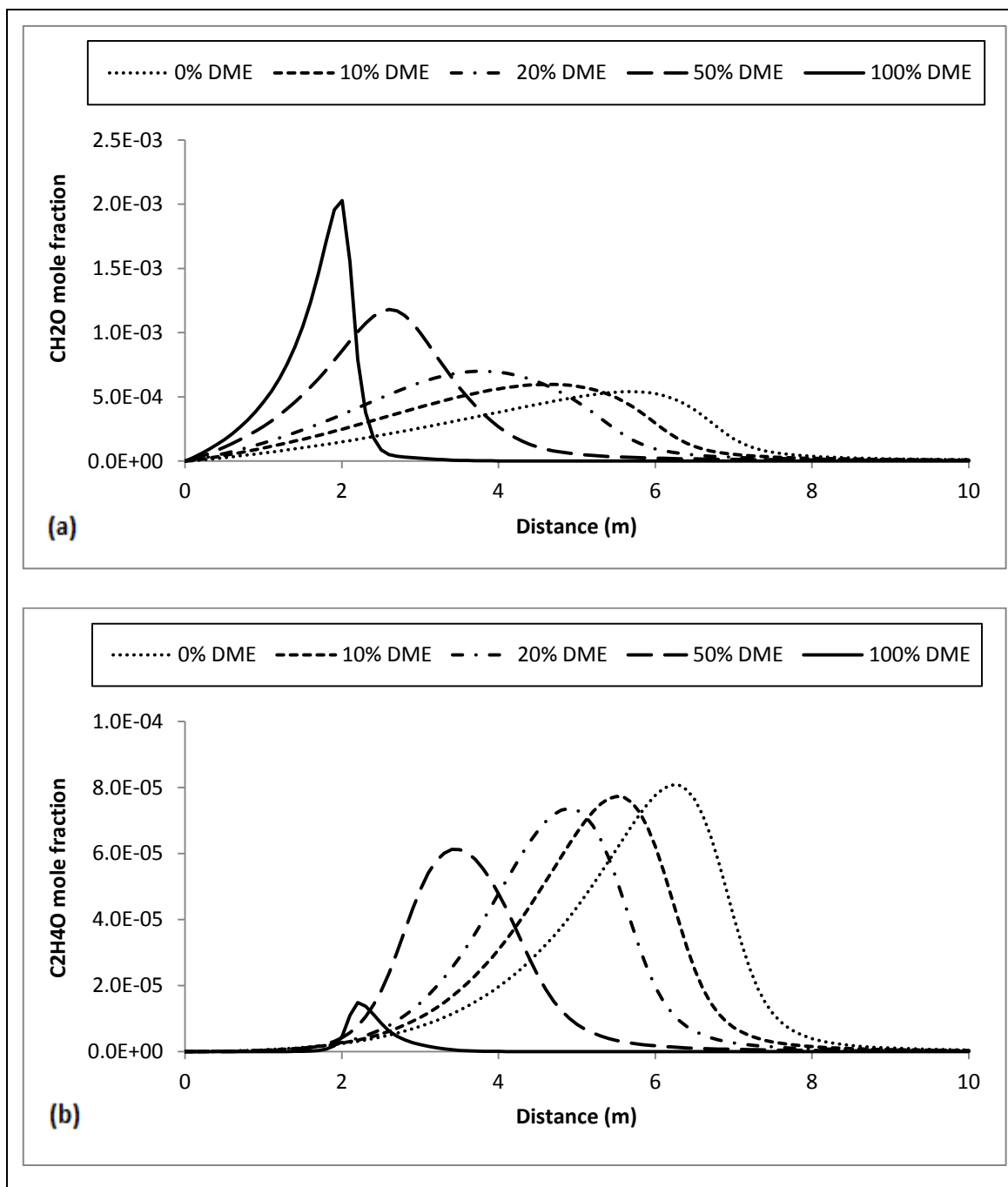


Figure 4.7. Concentration profiles of (a)  $\text{CH}_2\text{O}$  and (b)  $\text{C}_2\text{H}_4\text{O}$  for different concentrations of  $\text{CH}_3\text{OCH}_3$  added to  $\text{C}_4\text{H}_{10}/\text{O}_2/\text{Ar}$  oxidation versus reactor distance. ( $T_0 = 900\text{K}$ ,  $P = 1\text{atm}$ ,  $\phi = 2.6$ ).

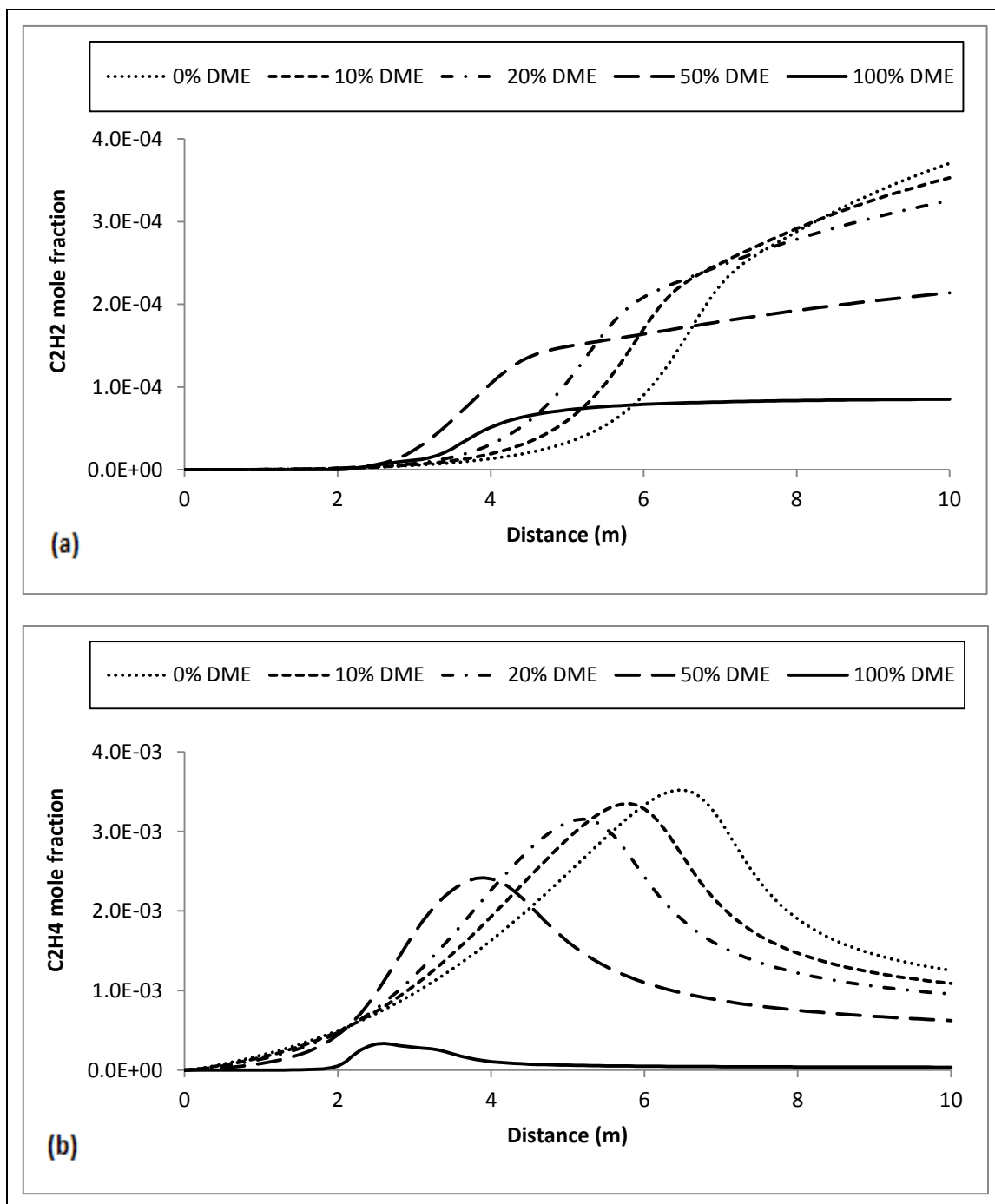


Figure 4.8. Concentration profiles of (a)  $C_2H_2$  and (b)  $C_2H_4$  for different concentrations of  $CH_3OCH_3$  added to  $C_4H_{10}/O_2/Ar$  oxidation versus reactor distance. ( $T_0 = 900K$ ,  $P = 1atm$ ,  $\phi = 2.6$ ).

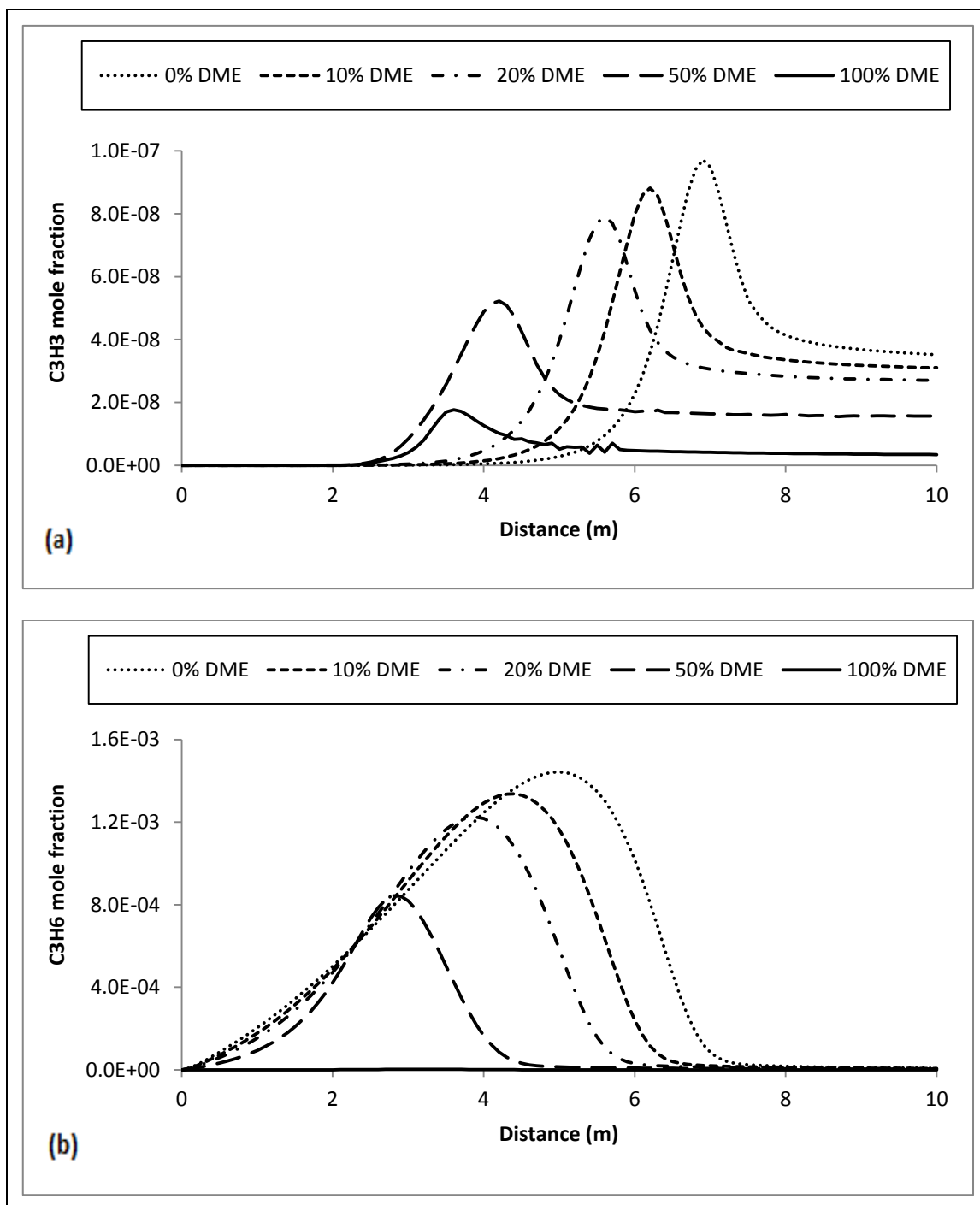


Figure 4.9. Concentration profiles of (a)  $C_3H_3$  and (b)  $C_3H_6$  for different concentrations of  $CH_3OCH_3$  added to  $C_4H_{10}/O_2/Ar$  oxidation versus reactor distance. ( $T_0 = 900K$ ,  $P = 1atm$ ,  $\phi = 2.6$ ).

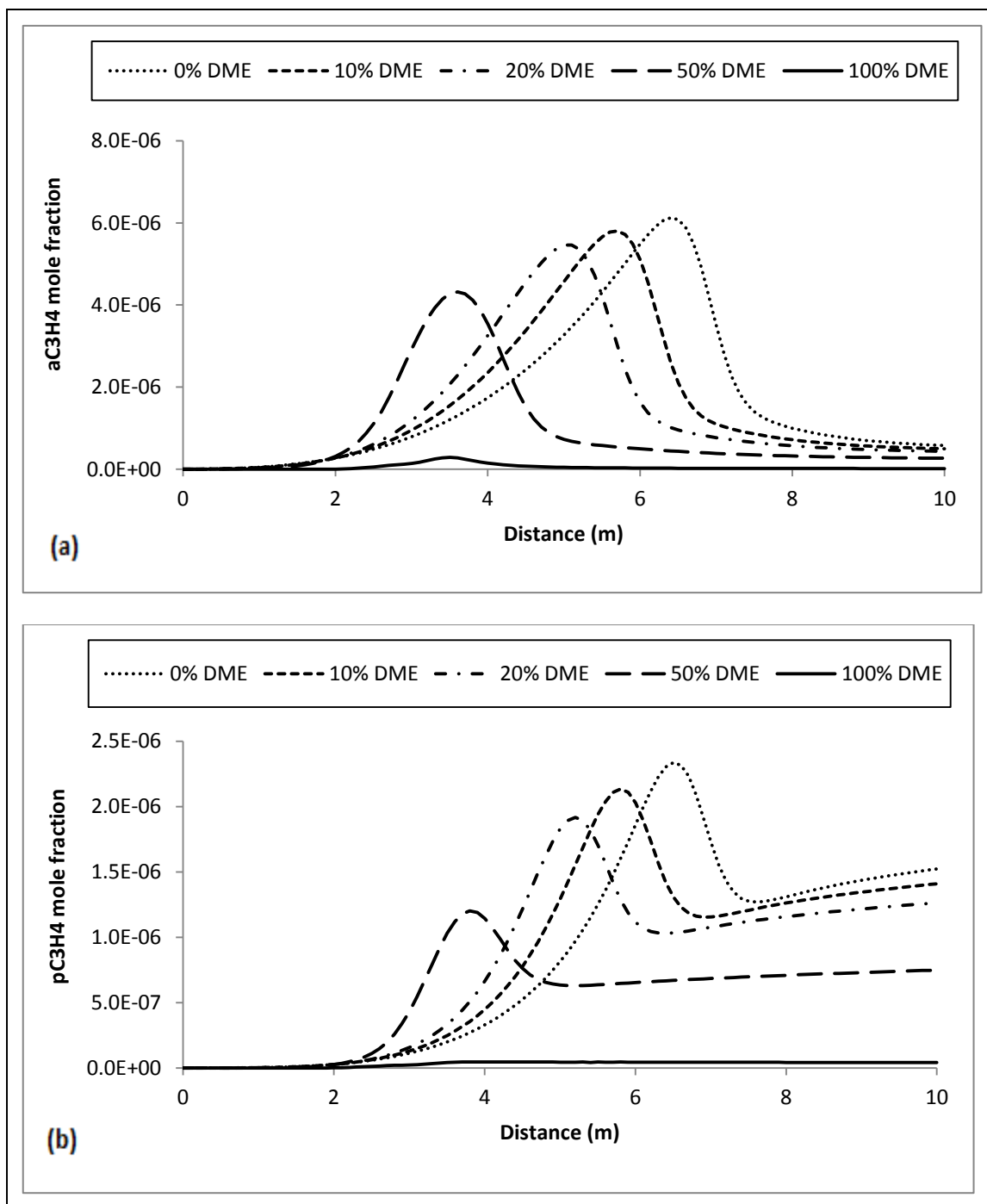


Figure 4.10. Concentration profiles of (a)  $\text{aC}_3\text{H}_4$  and (b)  $\text{pC}_3\text{H}_4$  for different concentrations of  $\text{CH}_3\text{OCH}_3$  added to  $\text{C}_4\text{H}_{10}/\text{O}_2/\text{Ar}$  oxidation versus reactor distance. ( $T_0 = 900\text{K}$ ,  $P = 1\text{atm}$ ,  $\phi = 2.6$ ).

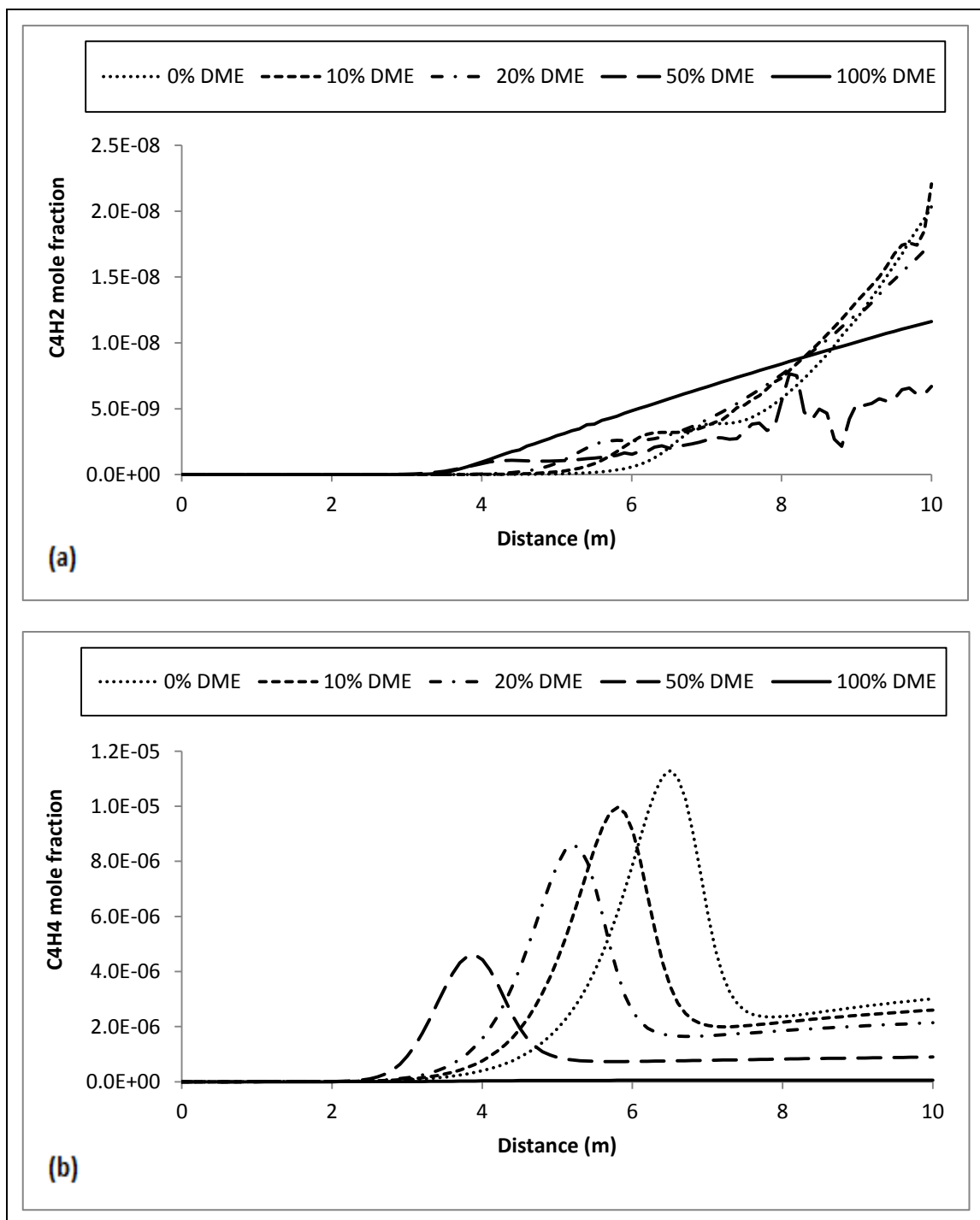


Figure 4.11. Concentration profiles of (a)  $C_4H_2$  and (b)  $C_4H_4$  for different concentrations of  $CH_3OCH_3$  added to  $C_4H_{10}/O_2/Ar$  oxidation versus reactor distance. ( $T_0 = 900K$ ,  $P = 1atm$ ,  $\phi = 2.6$ ).

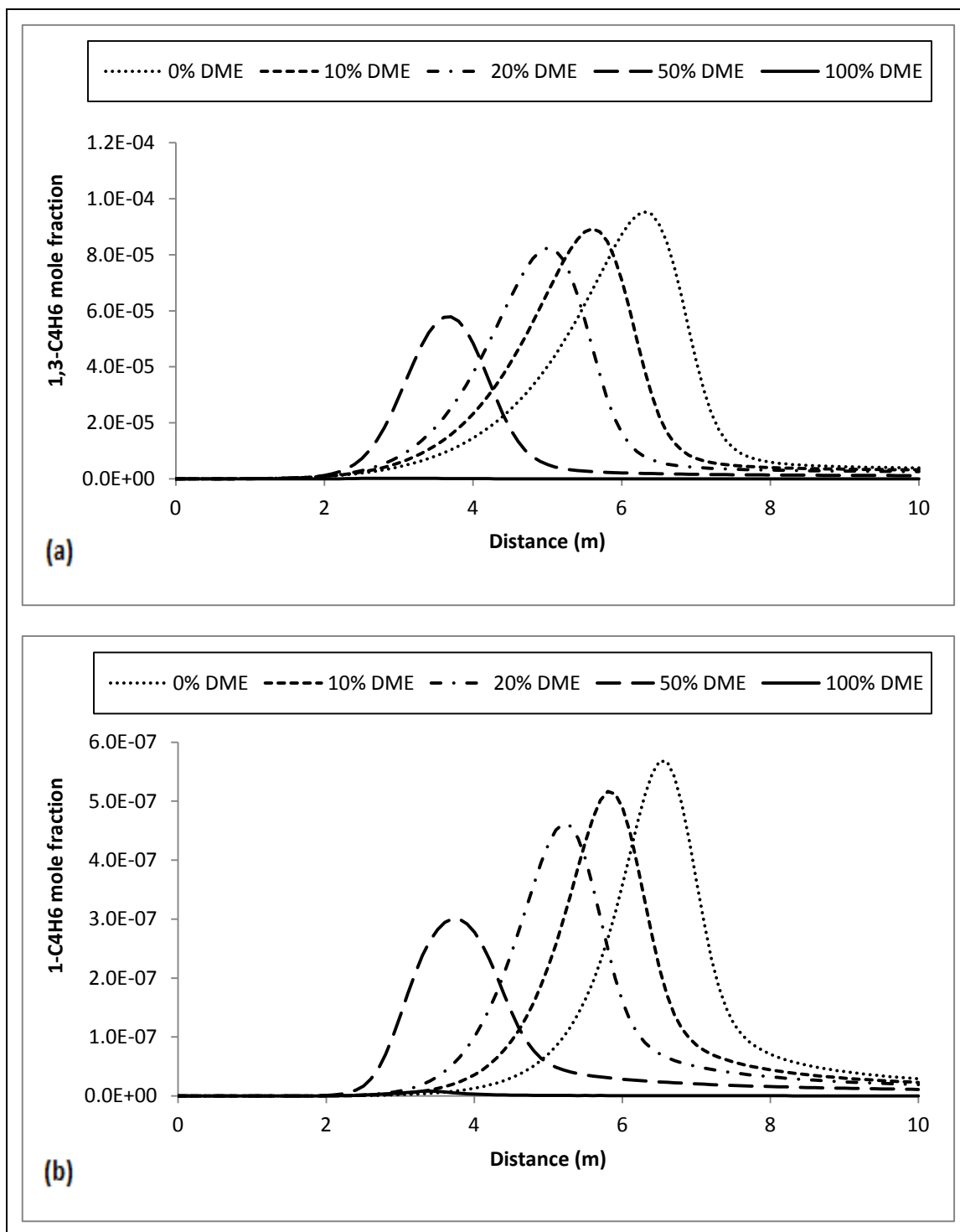


Figure 4.12. Concentration profiles of (a) 1,3-C<sub>4</sub>H<sub>6</sub> and (b) 1-C<sub>4</sub>H<sub>6</sub> for different concentrations of  $\text{CH}_3\text{OCH}_3$  added to  $\text{C}_4\text{H}_{10}/\text{O}_2/\text{Ar}$  oxidation versus reactor distance. ( $T_0 = 900\text{K}$ ,  $P = 1\text{atm}$ ,  $\phi = 2.6$ ).



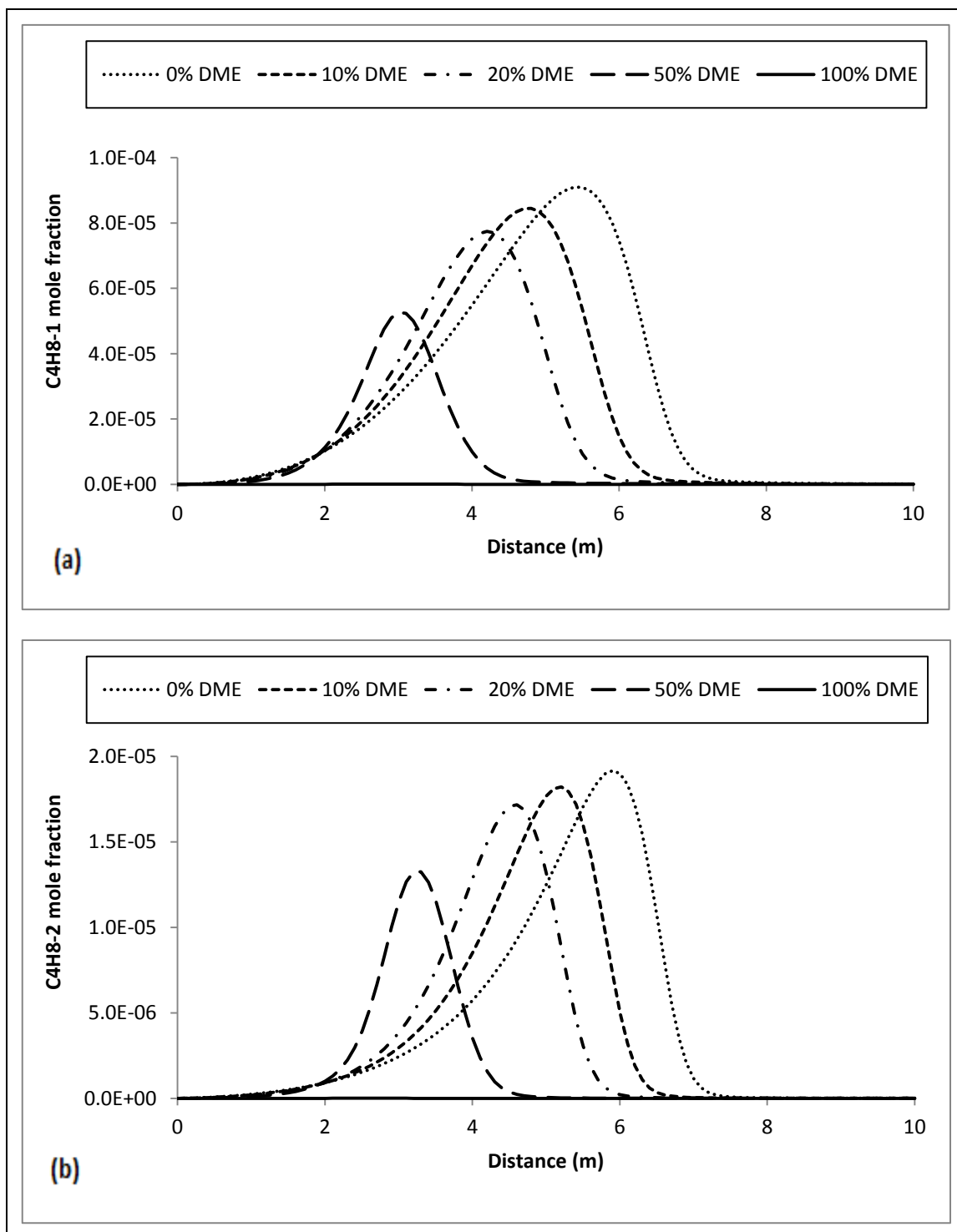


Figure 4.13. Concentration profiles of (a)  $\text{C}_4\text{H}_8-1$  and (b)  $\text{C}_4\text{H}_8-2$  for different concentrations of  $\text{CH}_3\text{OCH}_3$  added to  $\text{C}_4\text{H}_{10}/\text{O}_2/\text{Ar}$  oxidation versus reactor distance. ( $T_0 = 900\text{K}$ ,  $P = 1\text{atm}$ ,  $\phi = 2.6$ ).

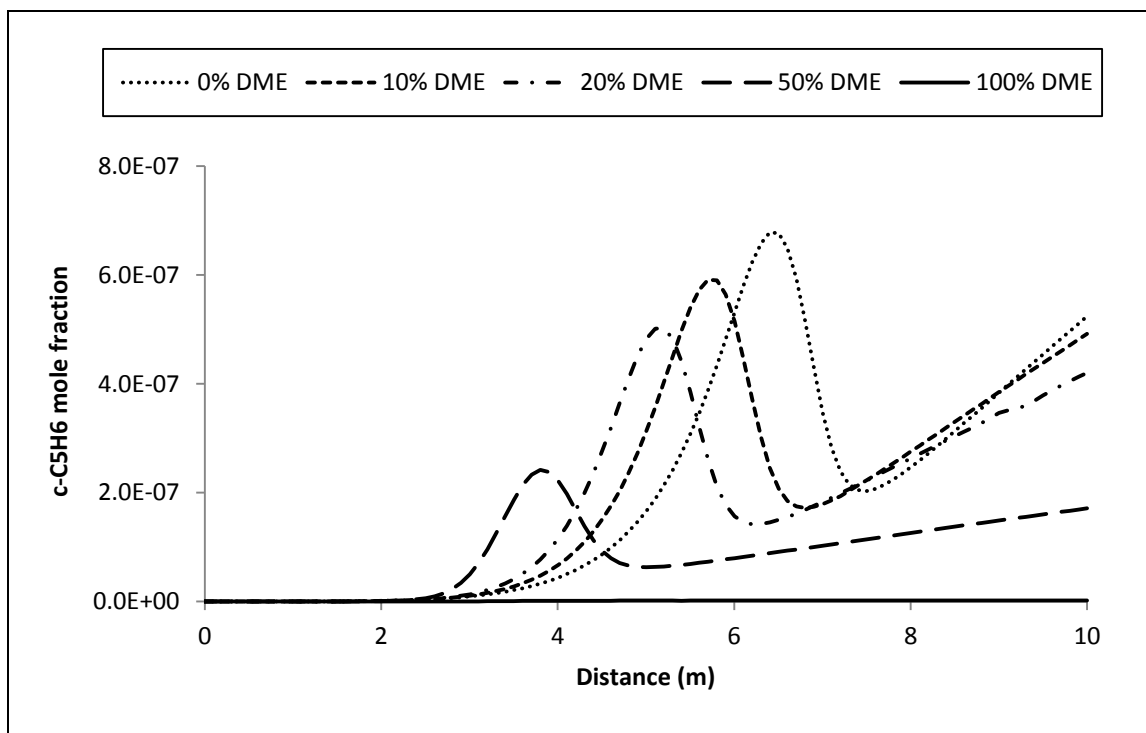


Figure 4.14. Concentration profiles of  $c\text{-C}_5\text{H}_6$  for different concentrations of  $\text{CH}_3\text{OCH}_3$  added to  $\text{C}_4\text{H}_{10}/\text{O}_2/\text{Ar}$  oxidation versus reactor distance. ( $T_0 = 900\text{K}$ ,  $P = 1\text{atm}$ ,  $\phi = 2.6$ ).

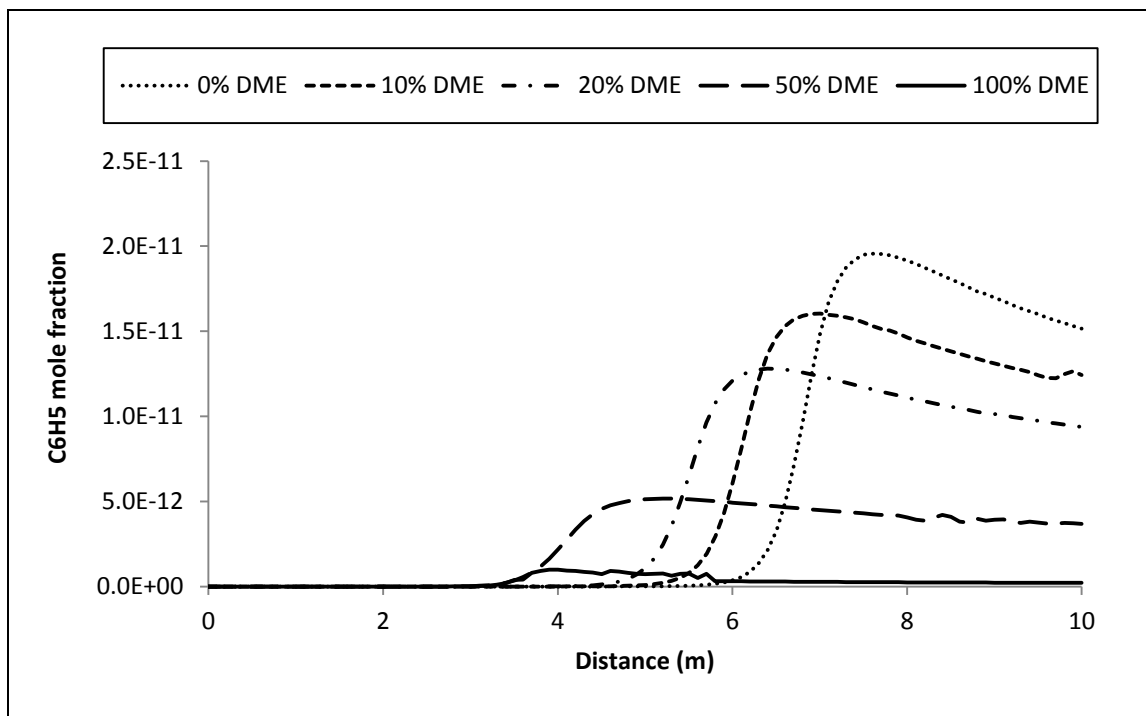


Figure 4.15. Concentration profiles of  $\text{C}_6\text{H}_5$  for different concentrations of  $\text{CH}_3\text{OCH}_3$  added to  $\text{C}_4\text{H}_{10}/\text{O}_2/\text{Ar}$  oxidation versus reactor distance. ( $T_0 = 900\text{K}$ ,  $P = 1\text{atm}$ ,  $\phi = 2.6$ ).

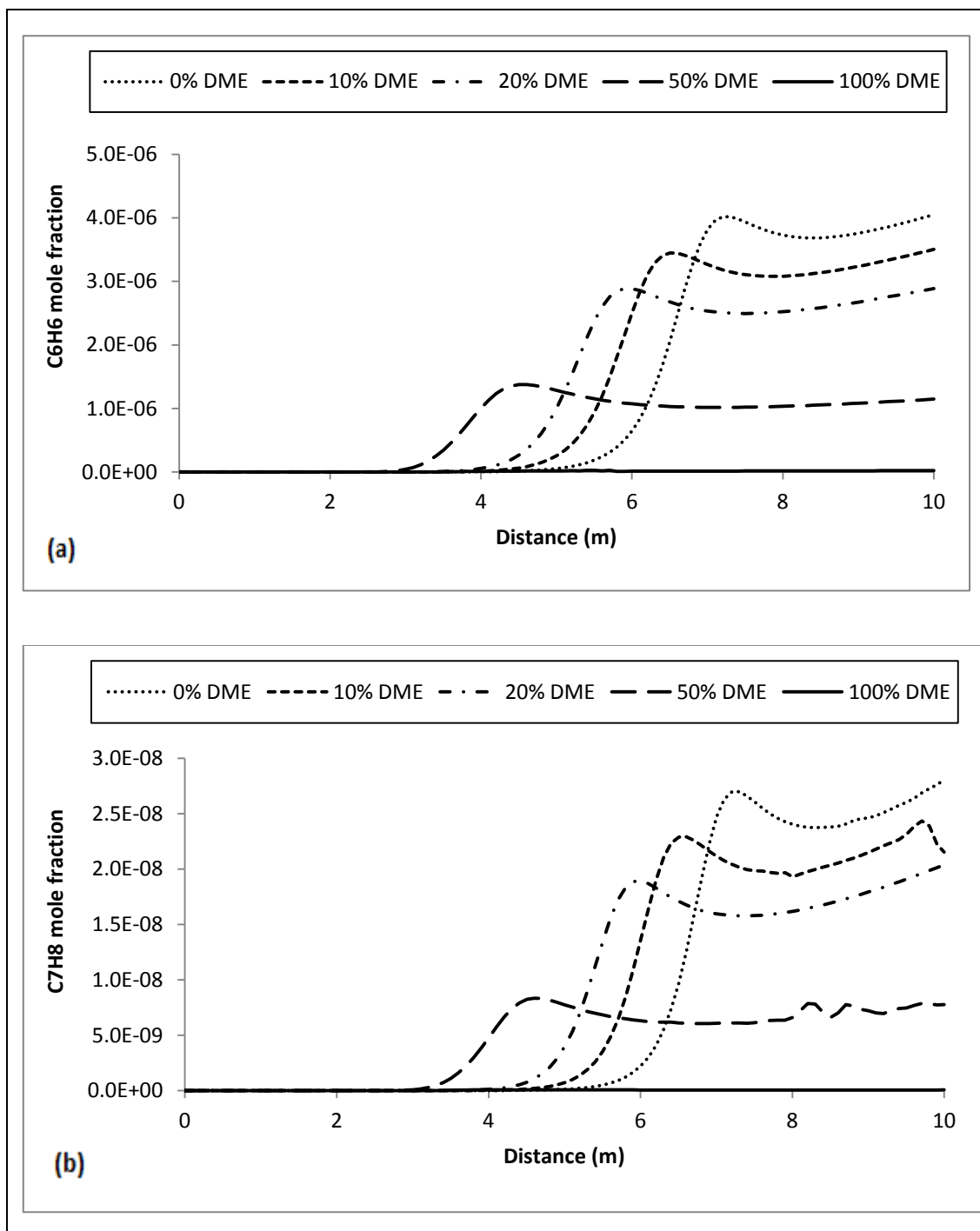


Figure 4.16. Concentration profiles of (a)  $C_6H_6$  and (b)  $C_7H_8$  for different concentrations of  $CH_3OCH_3$  added to  $C_4H_{10}/O_2/Ar$  oxidation versus reactor distance. ( $T_0 = 900K$ ,  $P = 1atm$ ,  $\phi = 2.6$ ).

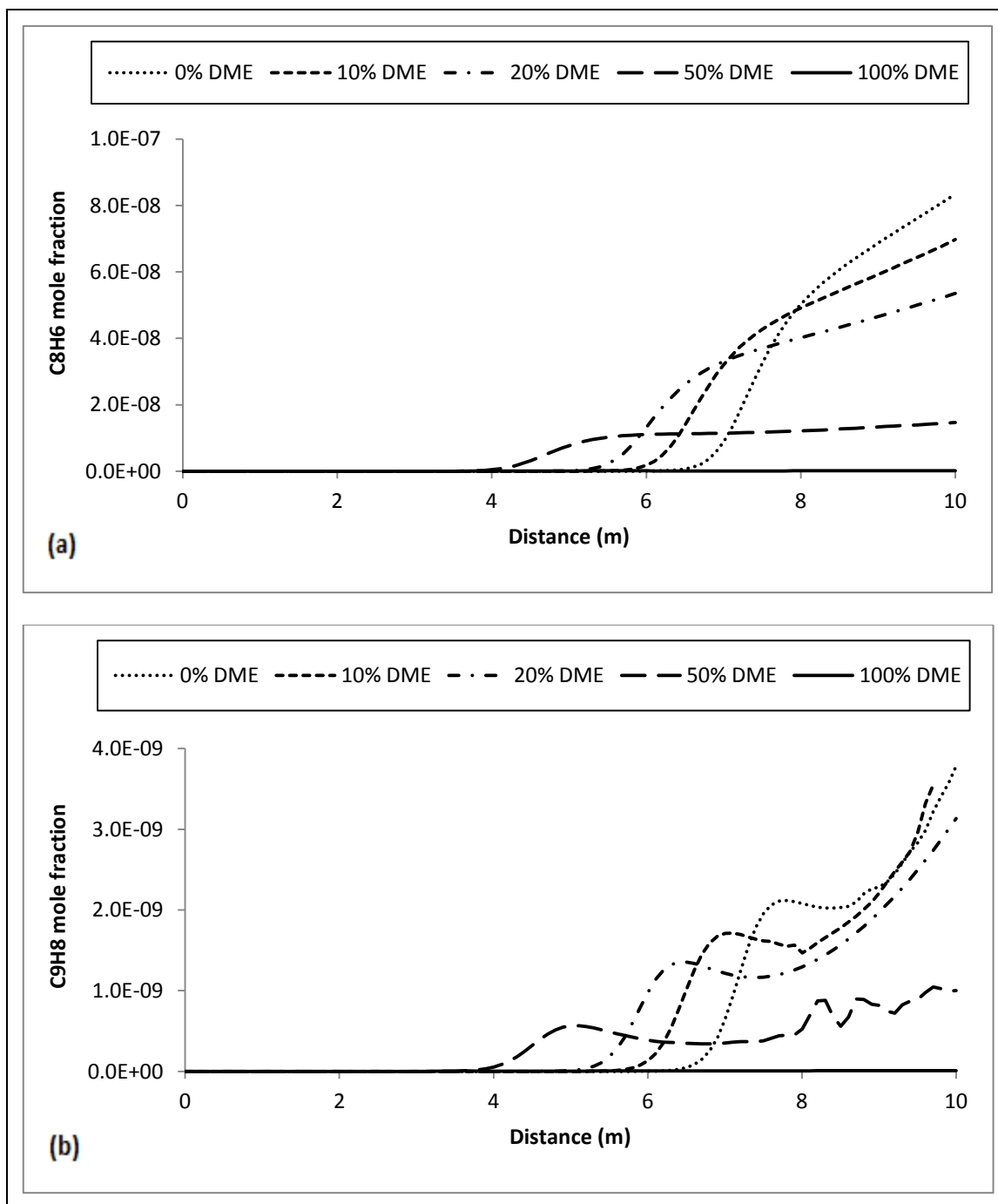


Figure 4.17. Concentration profiles of (a)  $\text{C}_8\text{H}_6$  and (b)  $\text{C}_9\text{H}_8$  for different concentrations of  $\text{CH}_3\text{OCH}_3$  added to  $\text{C}_4\text{H}_{10}/\text{O}_2/\text{Ar}$  oxidation versus reactor distance. ( $T_0 = 900\text{K}$ ,  $P = 1\text{atm}$ ,  $\phi = 2.6$ ).

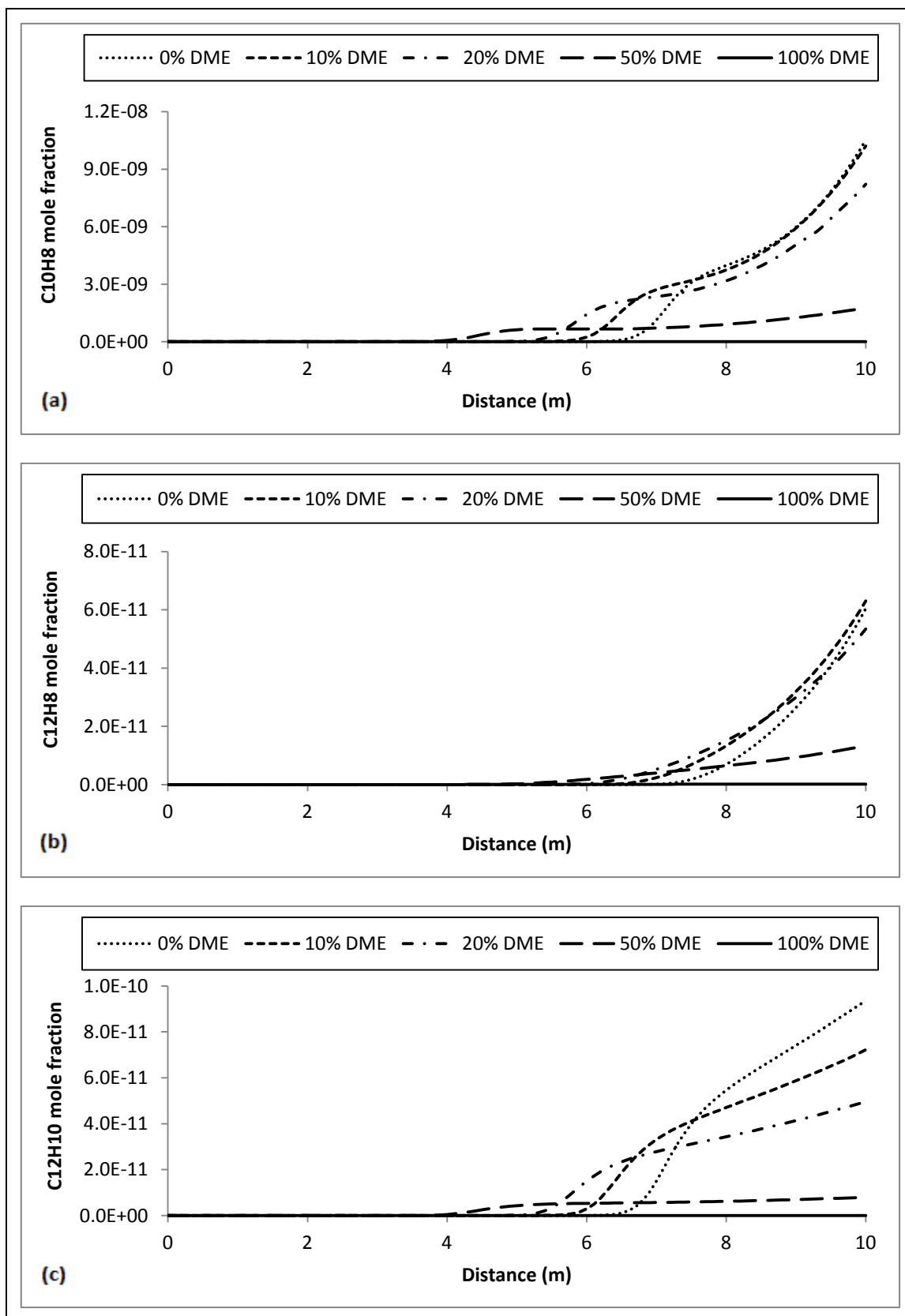


Figure 4.18. Concentration profiles of (a) C<sub>10</sub>H<sub>8</sub> (b) C<sub>12</sub>H<sub>8</sub> and (c) C<sub>12</sub>H<sub>10</sub> for different concentrations of CH<sub>3</sub>OCH<sub>3</sub> added to C<sub>4</sub>H<sub>10</sub>/O<sub>2</sub>/Ar oxidation versus reactor distance. (T<sub>0</sub> = 900K, P = 1 atm, φ = 2.6).

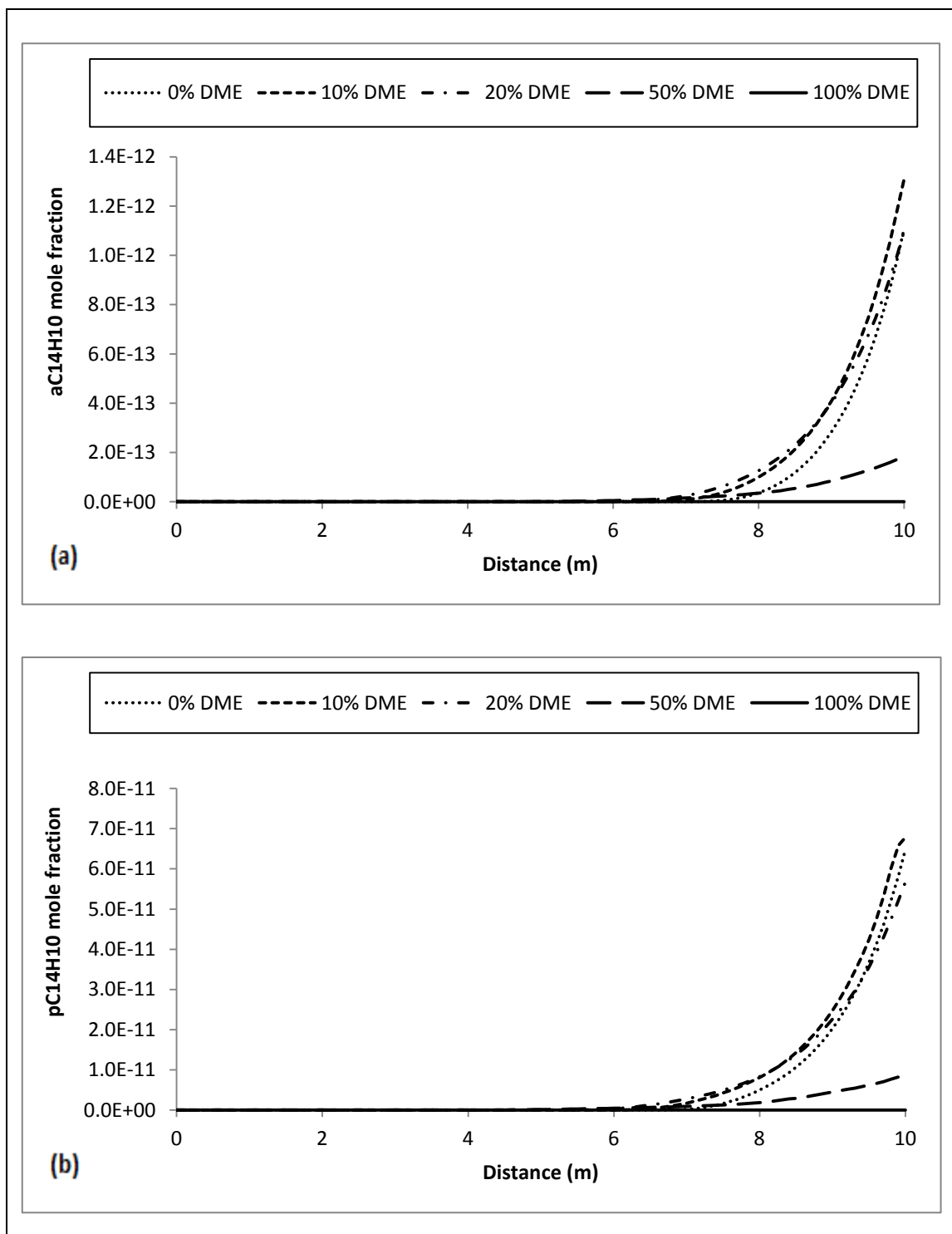


Figure 4.19. Concentration profiles of (a)  $\text{aC}_{14}\text{H}_{10}$  and (b)  $\text{pC}_{14}\text{H}_{10}$  for different concentrations of  $\text{CH}_3\text{OCH}_3$  added to  $\text{C}_4\text{H}_{10}/\text{O}_2/\text{Ar}$  oxidation versus reactor distance. ( $T_0 = 900\text{K}$ ,  $P = 1\text{atm}$ ,  $\phi = 2.6$ ).

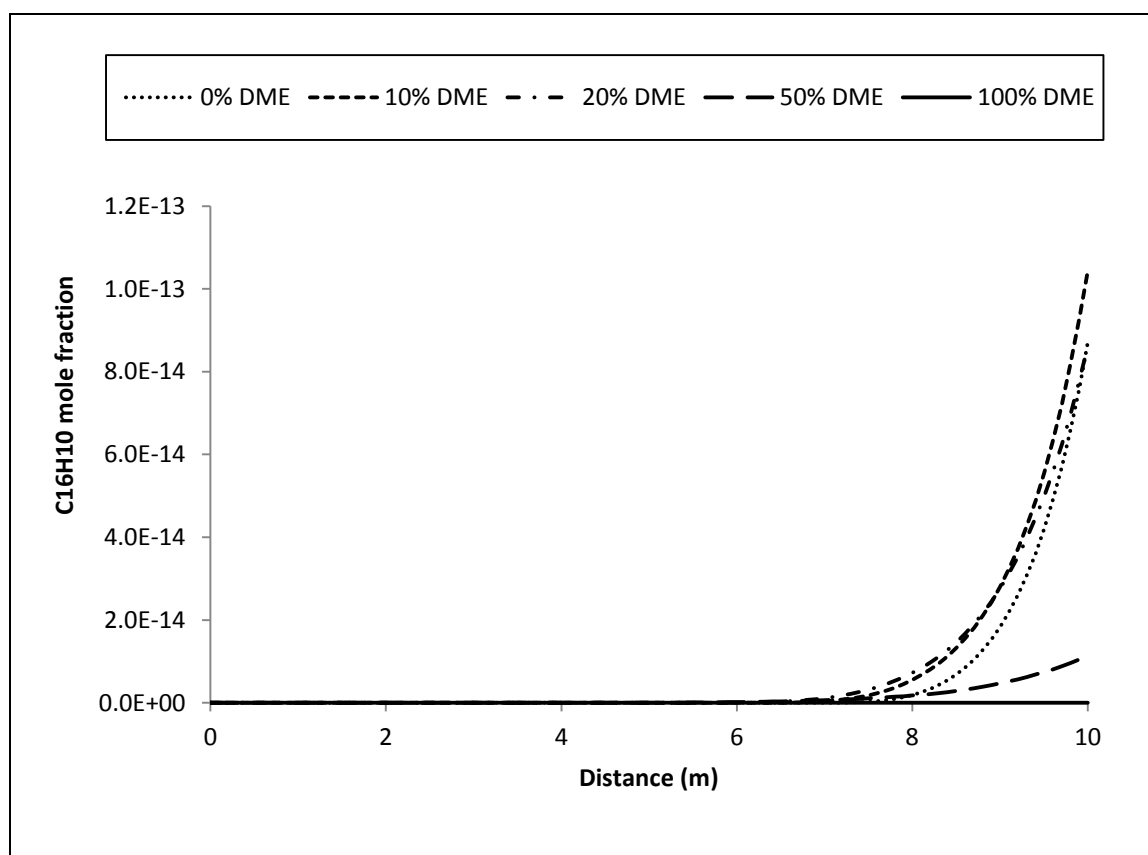


Figure 4.20. Concentration profiles of  $C_{16}H_{10}$  for different concentrations of  $CH_3OCH_3$  added to  $C_4H_{10}/O_2/Ar$  oxidation versus reactor distance. ( $T_0 = 900K$ ,  $P = 1atm$ ,  $\phi = 2.6$ ).

Figures 4.7.a and 4.7.b show the concentration profiles of  $CH_2O$  and  $C_2H_4O$ , respectively. Maximum mole fraction of  $CH_2O$  produced increases, while maximum mole fraction of  $C_2H_4O$  decreases, as the concentration of DME increases. Previous studies (Rouhi, 1995; Arcoumanis, 2008; Kaiser et al., 2000) suggested that DME resulted in higher formations of  $CH_2O$  and other aldehydes when compared with diesel and methane. In this study it was found that DME oxidation produced higher  $CH_2O$ , but lower  $C_2H_4O$  than n-butane oxidation. Also, Marchionna et al. (2008) suggested that addition of DME to LPG increased the formation of  $CH_2O$ . In this study, similar effect can be observed for DME addition to n-butane.

The concentration profiles of the species that are known to be precursors of aromatic species and PAHs are given in Figures 4.8 through 4.14. Formations of all of these species were lowered with the addition of DME. One exception to this trend is that the lowest final mole fraction of  $C_4H_2$  was observed in the 50% DME case, followed by 100%, 20%, 0% and 10% DME cases. However, as it is seen from the

graph, the complete concentration profile of this species cannot be observed for the process and reactor conditions studied.

Figures 4.15 to 4.20 show the concentration profiles of the aromatics and PAHs obtained for the different concentrations of DME added. In general, the addition of DME lowers the formations of the aromatics and PAHs investigated. This is expected since the addition of DME also lowered the formations of the precursor species. It is also observed that, the formations of all the aromatics and PAHs are dramatically decrease for the case of pure DME oxidation.

In the literature, it was found that pure DME oxidation produced PAHs in lower amounts when compared to methane, ethane, and heptane (Kaiser et al., 2000; Hayashida et al., 2011; Kitamura et al., 2001; Park, 2009). Also, it was found that addition of DME to methane, ethane, propane, and LPG lowered the formations of aromatic species and PAHs (Song et al., 2003; Yoon et al., 2008; Marchionna et al., 2008). The results obtained in this study for n-butane are conformable with the previous findings in the literature.

## **4.2. The Effects of Process Parameters on n-Butane/DME Oxidation**

Different ranges of various process parameters, which are known to be effective on the oxidation processes, were investigated for the oxidation of n-butane/DME mixture. These process parameters were temperature, pressure, and equivalence ratio.

### **4.2.1. The Effects of Temperature and Pressure**

Eight different inlet temperatures ( $T_0 = 500, 700, 800, 900, 1100, 1300, 1500,$  and  $1700 K$ ), and two different pressures ( $P = 1$  and  $5 atm$ ) were studied. Reactor and flow properties were the same as in the Section 4.1 ( $d = 0.05m$ ,  $L = 10m$ , and  $u = 0.5m/s$ ). The equivalence ratio was again selected as  $\phi = 2.6$ , and the results were shown for two different amounts of DME (20% and 50% DME in the fuel mixture) added. The final mole fractions of the same major, minor, and trace species at the reactor outlet and the final temperatures were compared for different values of inlet temperatures and pressures, for the oxidation of the n-butane/DME mixture.



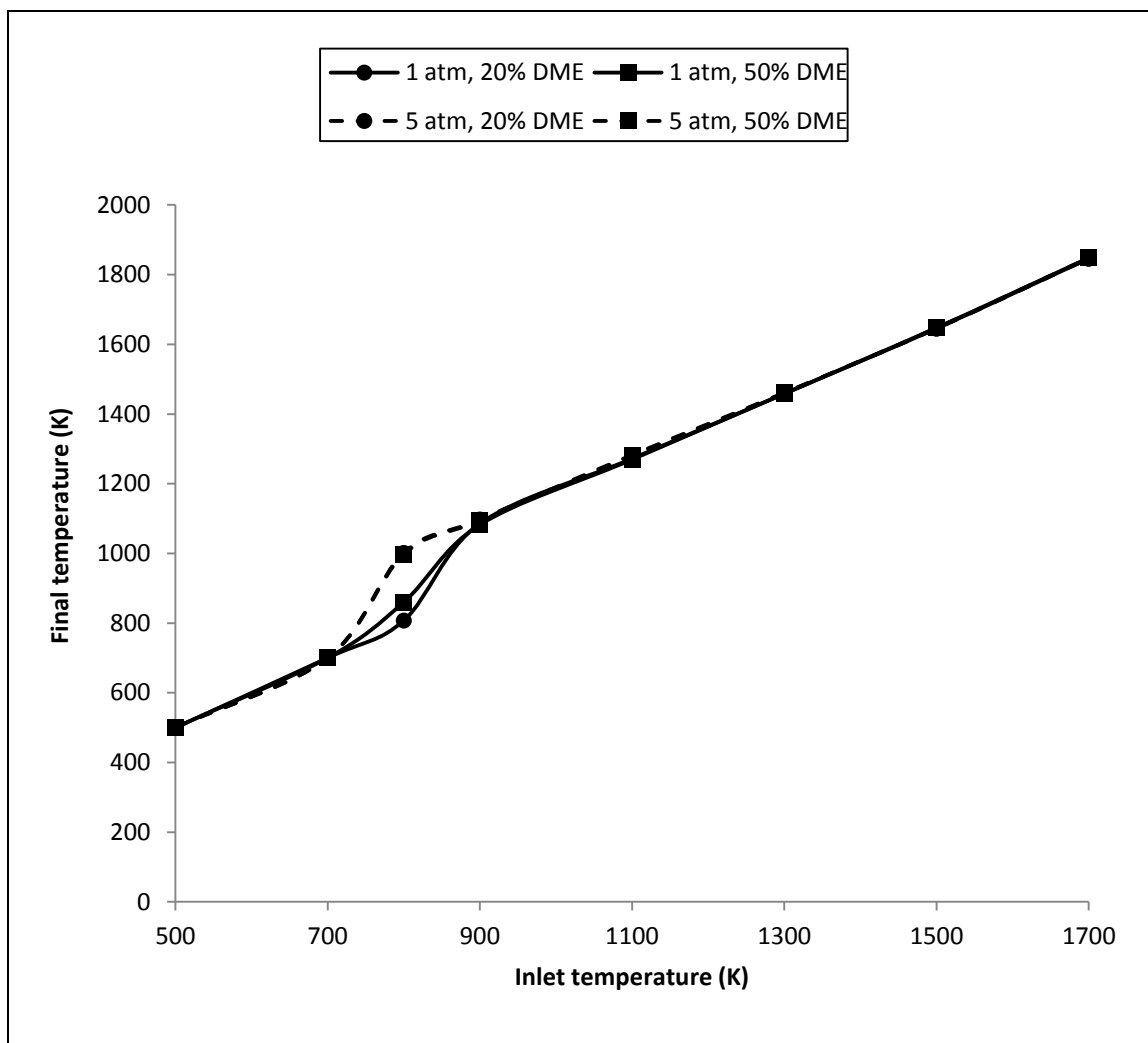


Figure 4.21. Final reaction temperatures versus reactor inlet temperatures at different pressures and different concentrations of  $\text{CH}_3\text{OCH}_3$ . ( $\phi = 2.6$ ).

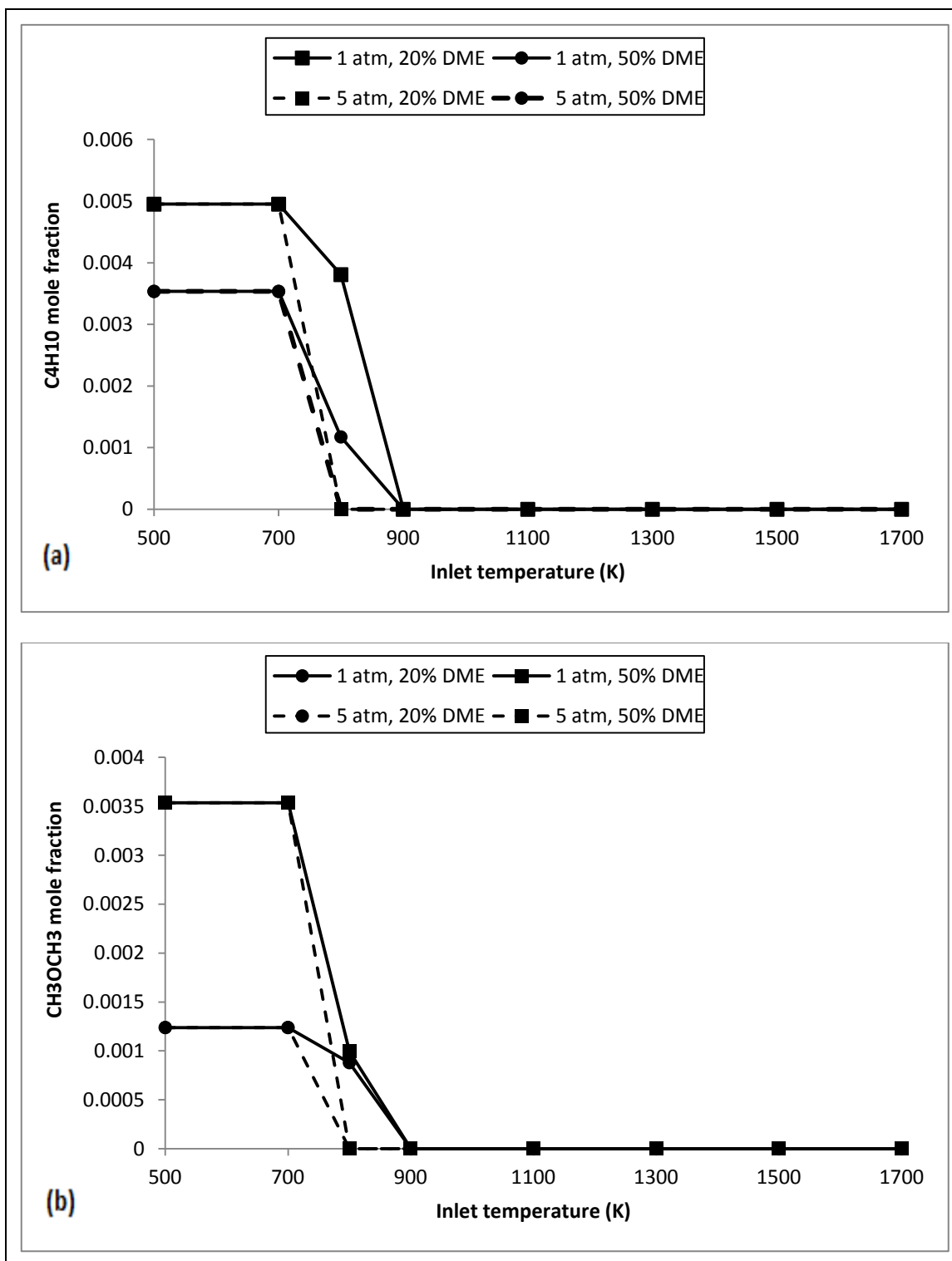


Figure 4.22. Final mole fractions of (a) C<sub>4</sub>H<sub>10</sub> and (b) CH<sub>3</sub>OCH<sub>3</sub> versus reactor inlet temperatures at different pressures and different concentrations of CH<sub>3</sub>OCH<sub>3</sub>. ( $\varphi = 2.6$ ).

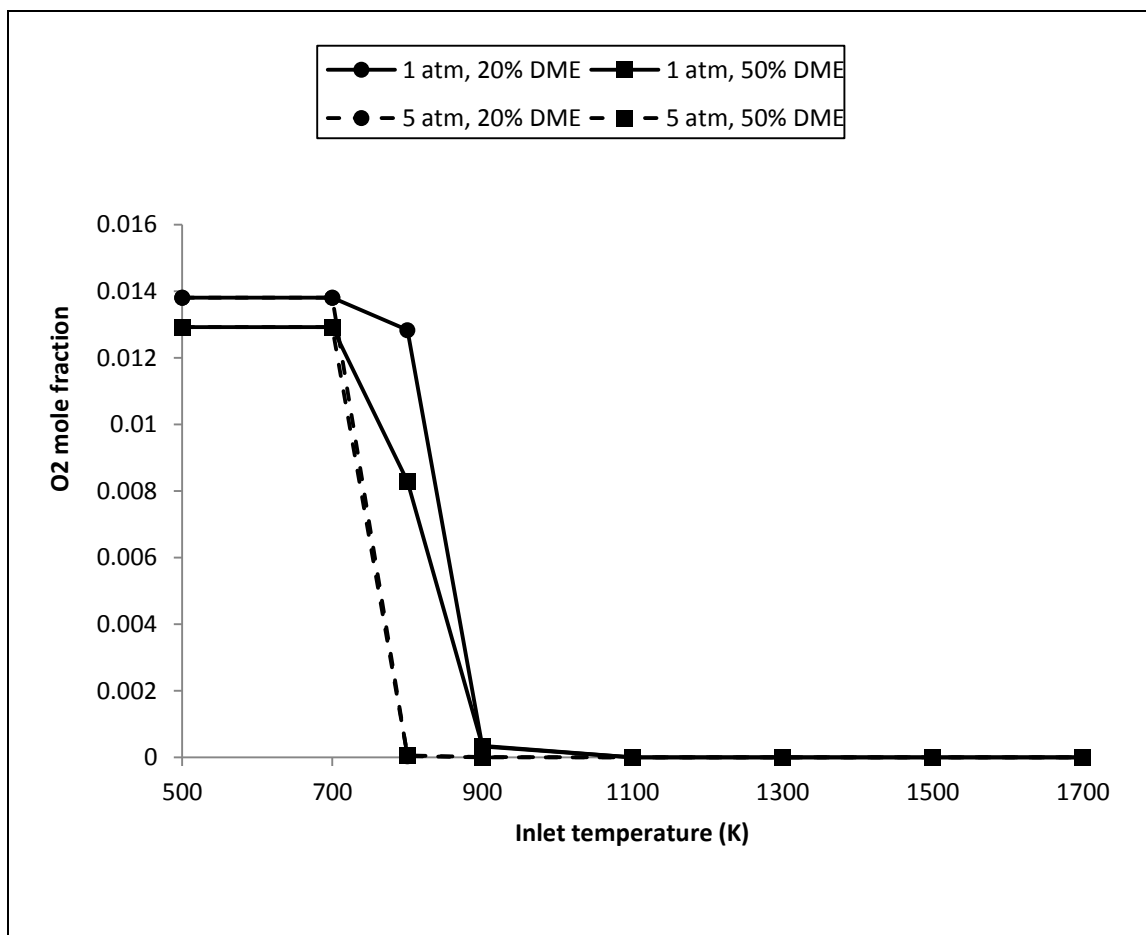


Figure 4.23. Final mole fractions of O<sub>2</sub> versus reactor inlet temperatures at different pressures and different concentrations of CH<sub>3</sub>OCH<sub>3</sub>. ( $\phi = 2.6$ ).

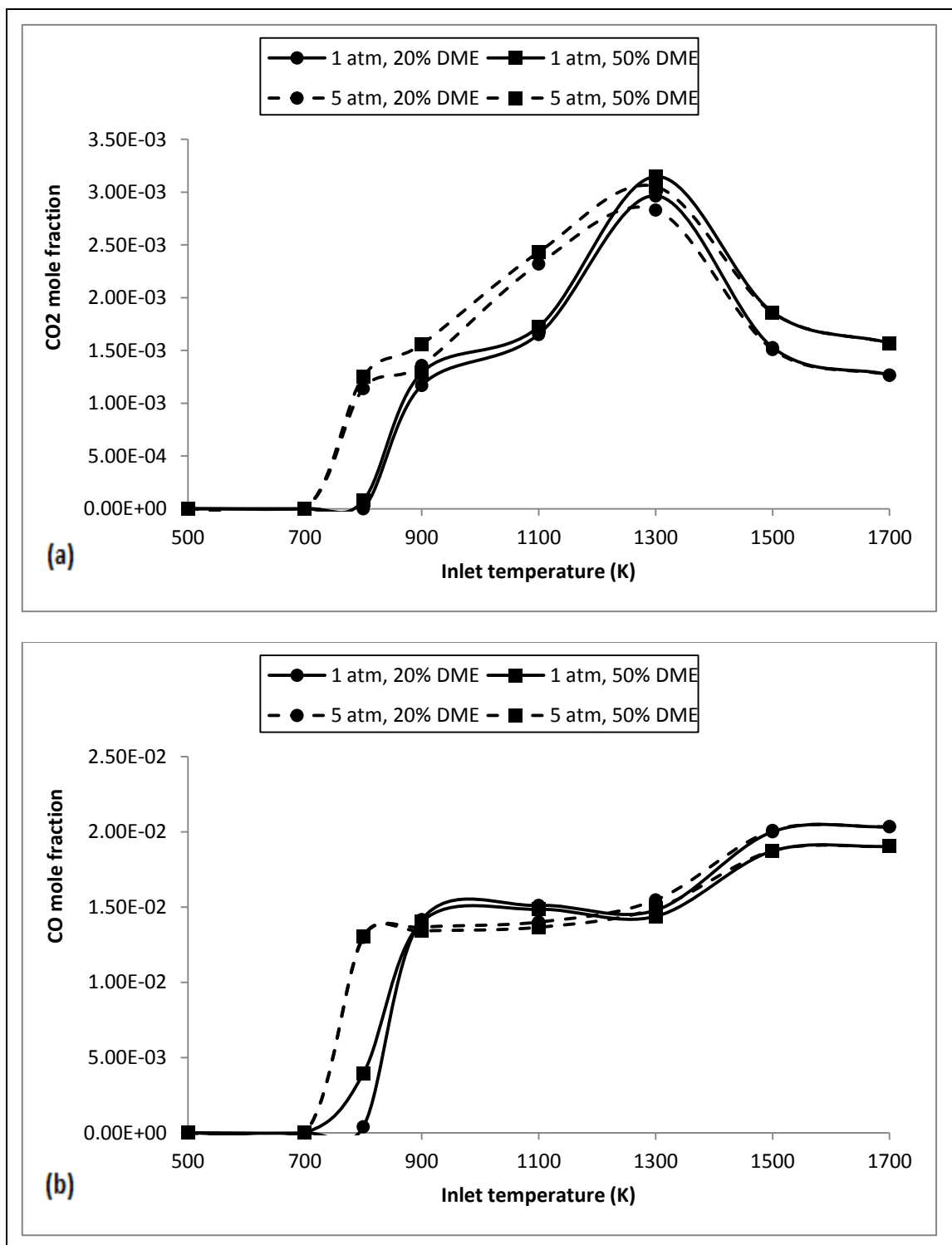


Figure 4.24. Final mole fractions of (a) CO<sub>2</sub> and (b) CO versus reactor inlet temperatures at different pressures and different concentrations of CH<sub>3</sub>OCH<sub>3</sub>. ( $\phi = 2.6$ ).

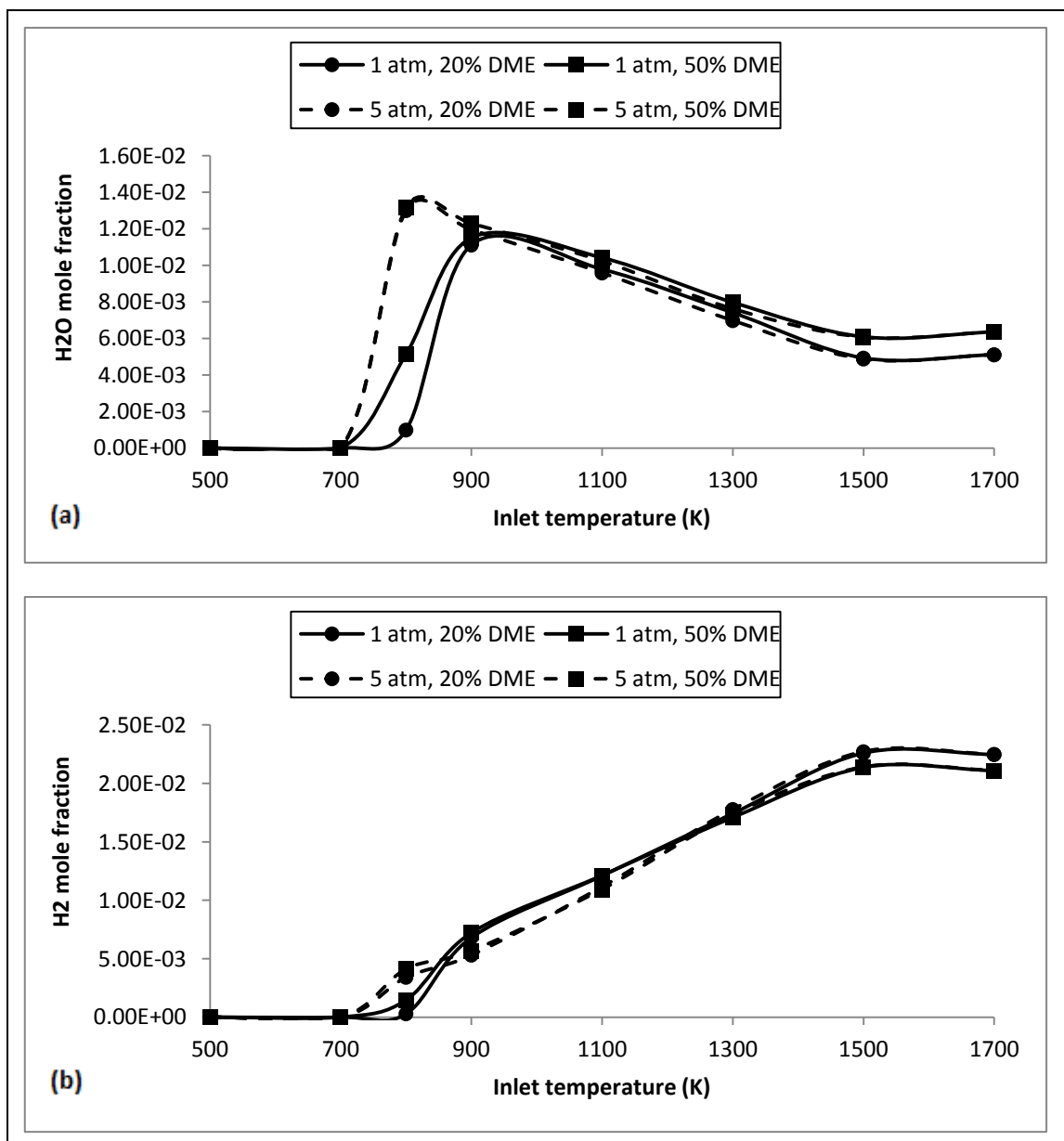


Figure 4.25. Final mole fractions of (a) H<sub>2</sub>O and (b) H<sub>2</sub> versus reactor inlet temperatures at different pressures and different concentrations of CH<sub>3</sub>OCH<sub>3</sub>. ( $\phi = 2.6$ ).

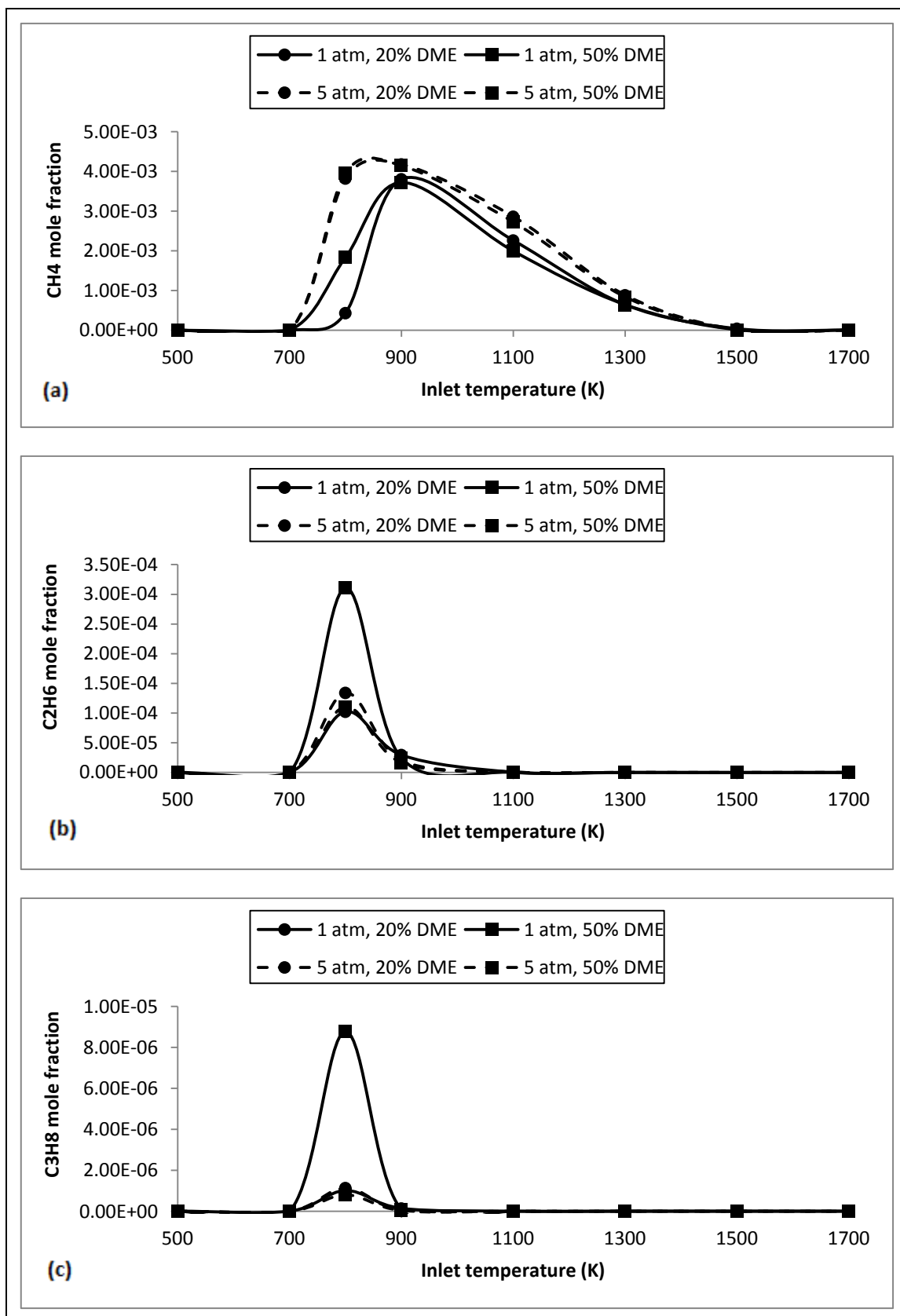


Figure 4.26. Final mole fractions of (a)  $\text{CH}_4$  (b)  $\text{C}_2\text{H}_6$  and (c)  $\text{C}_3\text{H}_8$  versus reactor inlet temperatures at different pressures and different concentrations of  $\text{CH}_3\text{OCH}_3$ . ( $\phi = 2.6$ ).

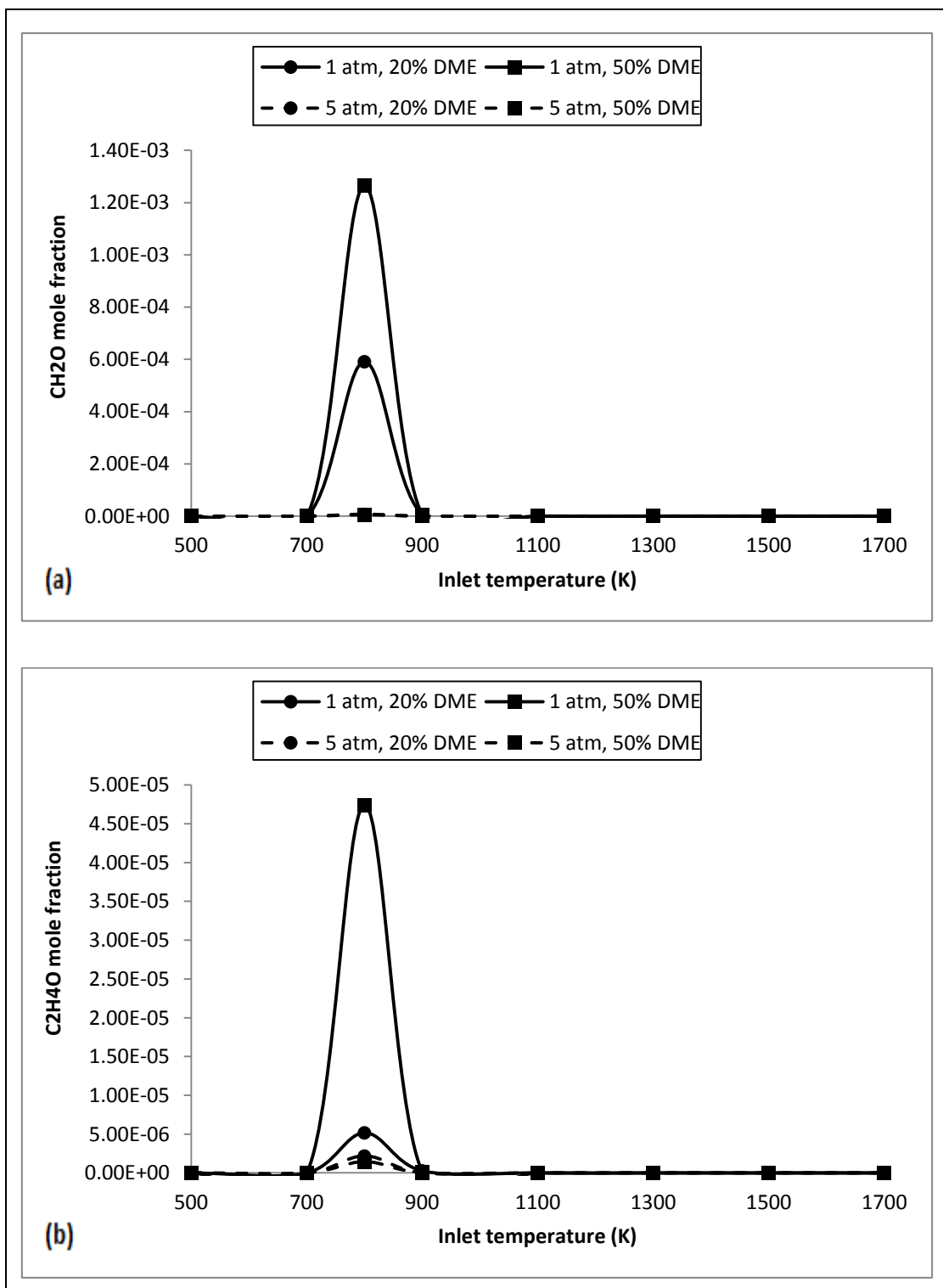


Figure 4.27. Final mole fractions of (a) CH<sub>2</sub>O and (b) C<sub>2</sub>H<sub>4</sub>O versus reactor inlet temperatures at different pressures and different concentrations of CH<sub>3</sub>OCH<sub>3</sub>. ( $\phi = 2.6$ ).

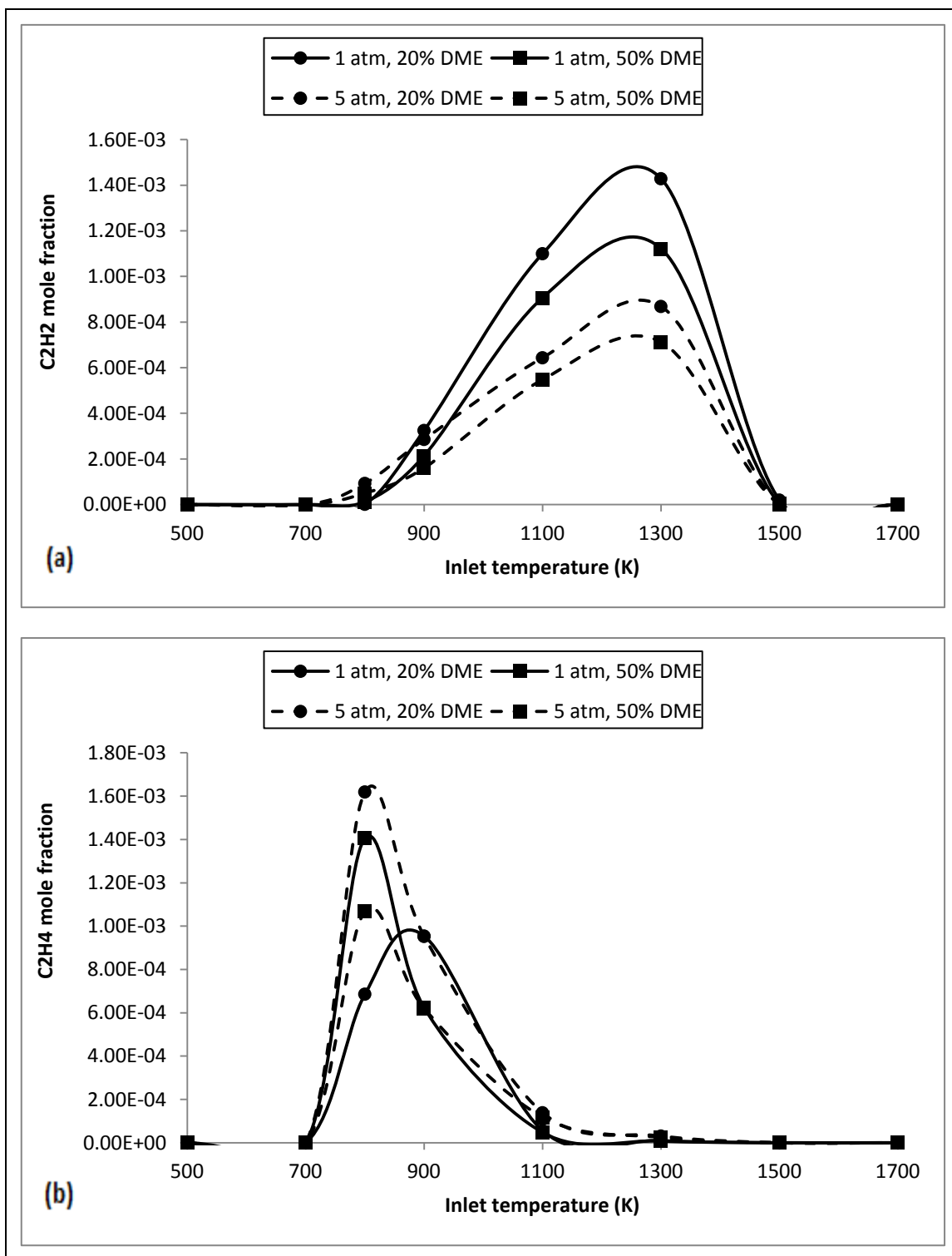


Figure 4.28. Final mole fractions of (a) C<sub>2</sub>H<sub>2</sub> and (b) C<sub>2</sub>H<sub>4</sub> versus reactor inlet temperatures at different pressures and different concentrations of CH<sub>3</sub>OCH<sub>3</sub>. ( $\phi = 2.6$ ).



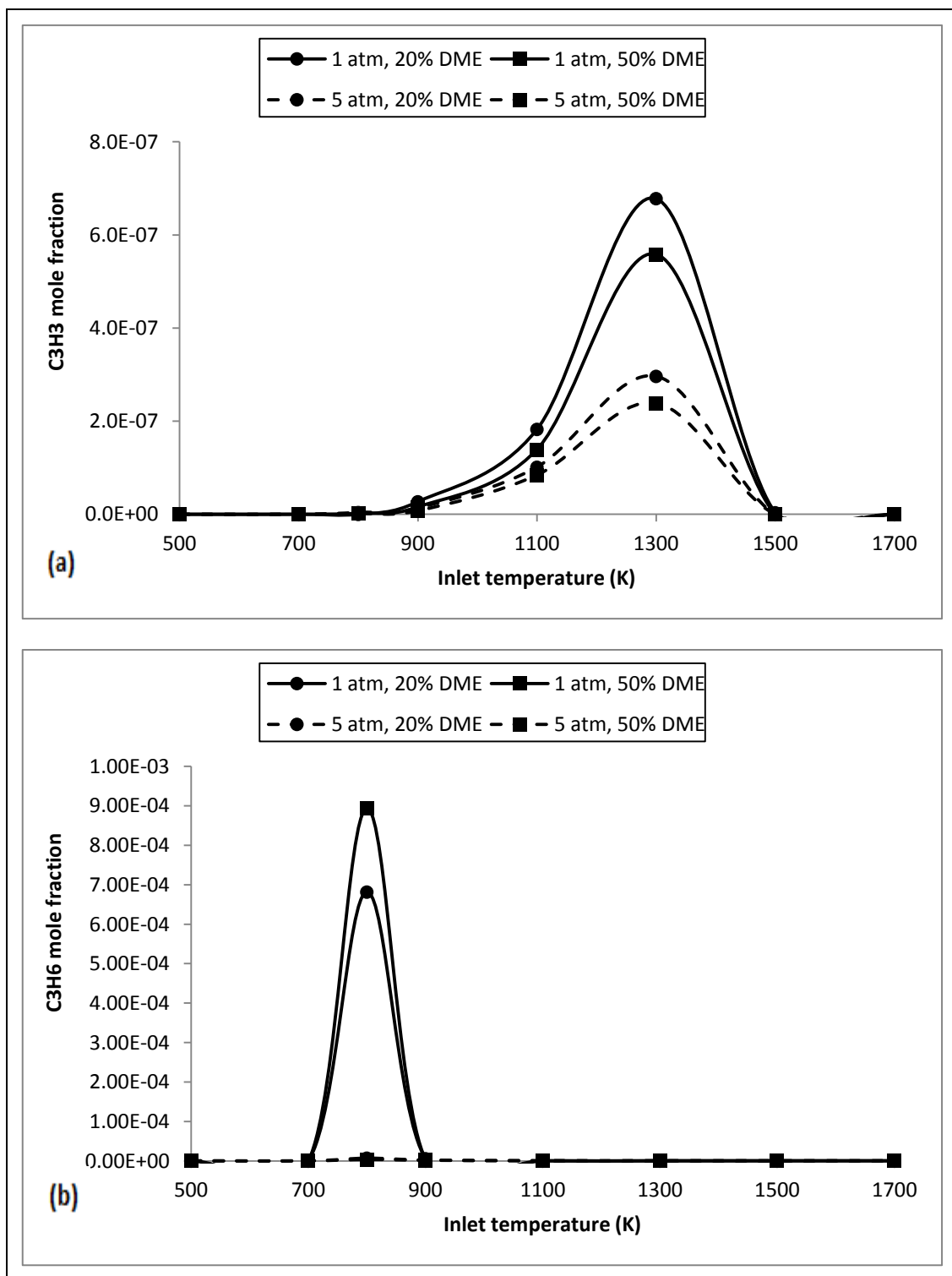


Figure 4.29. Final mole fractions of (a) C<sub>3</sub>H<sub>3</sub> and (b) C<sub>3</sub>H<sub>6</sub> versus reactor inlet temperatures at different pressures and different concentrations of CH<sub>3</sub>OCH<sub>3</sub>. ( $\phi = 2.6$ ).

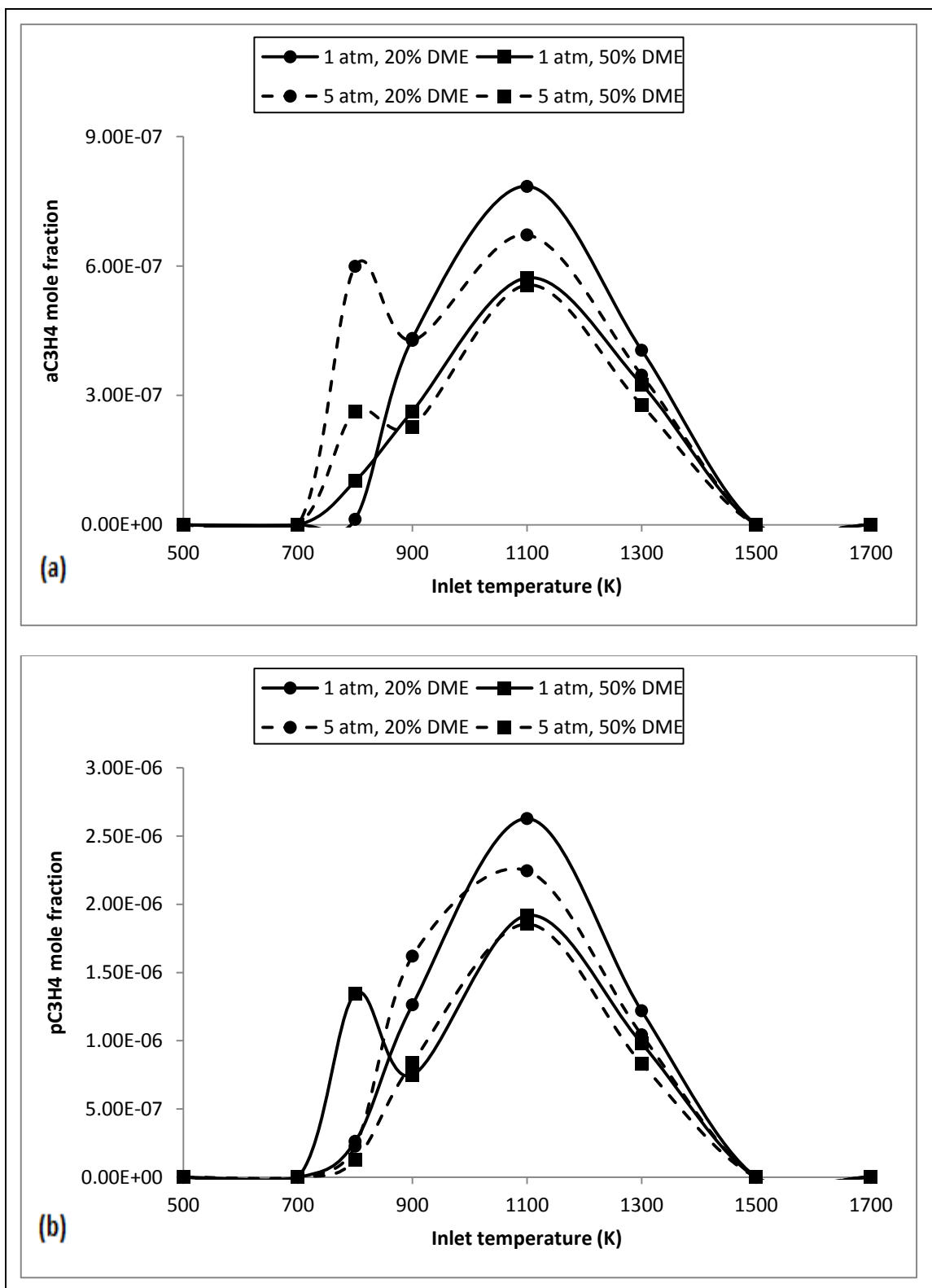


Figure 4.30. Final mole fractions of (a) aC<sub>3</sub>H<sub>4</sub> and (b) pC<sub>3</sub>H<sub>4</sub> versus reactor inlet temperatures at different pressures and different concentrations of CH<sub>3</sub>OCH<sub>3</sub>. ( $\varphi = 2.6$ ).

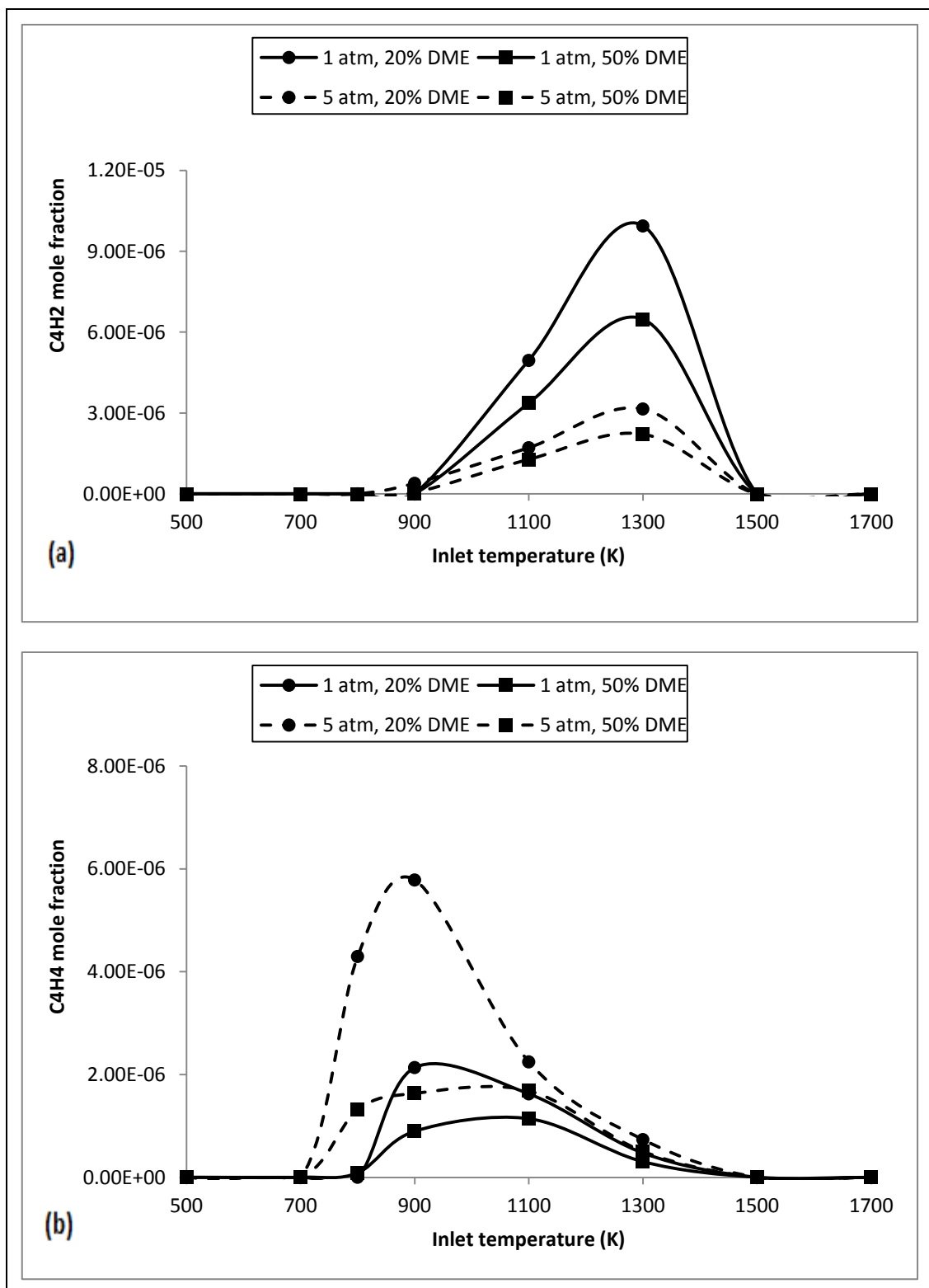


Figure 4.31. Final mole fractions of (a) C<sub>4</sub>H<sub>2</sub> and (b) C<sub>4</sub>H<sub>4</sub> versus reactor inlet temperatures at different pressures and different concentrations of CH<sub>3</sub>OCH<sub>3</sub>. ( $\phi = 2.6$ ).

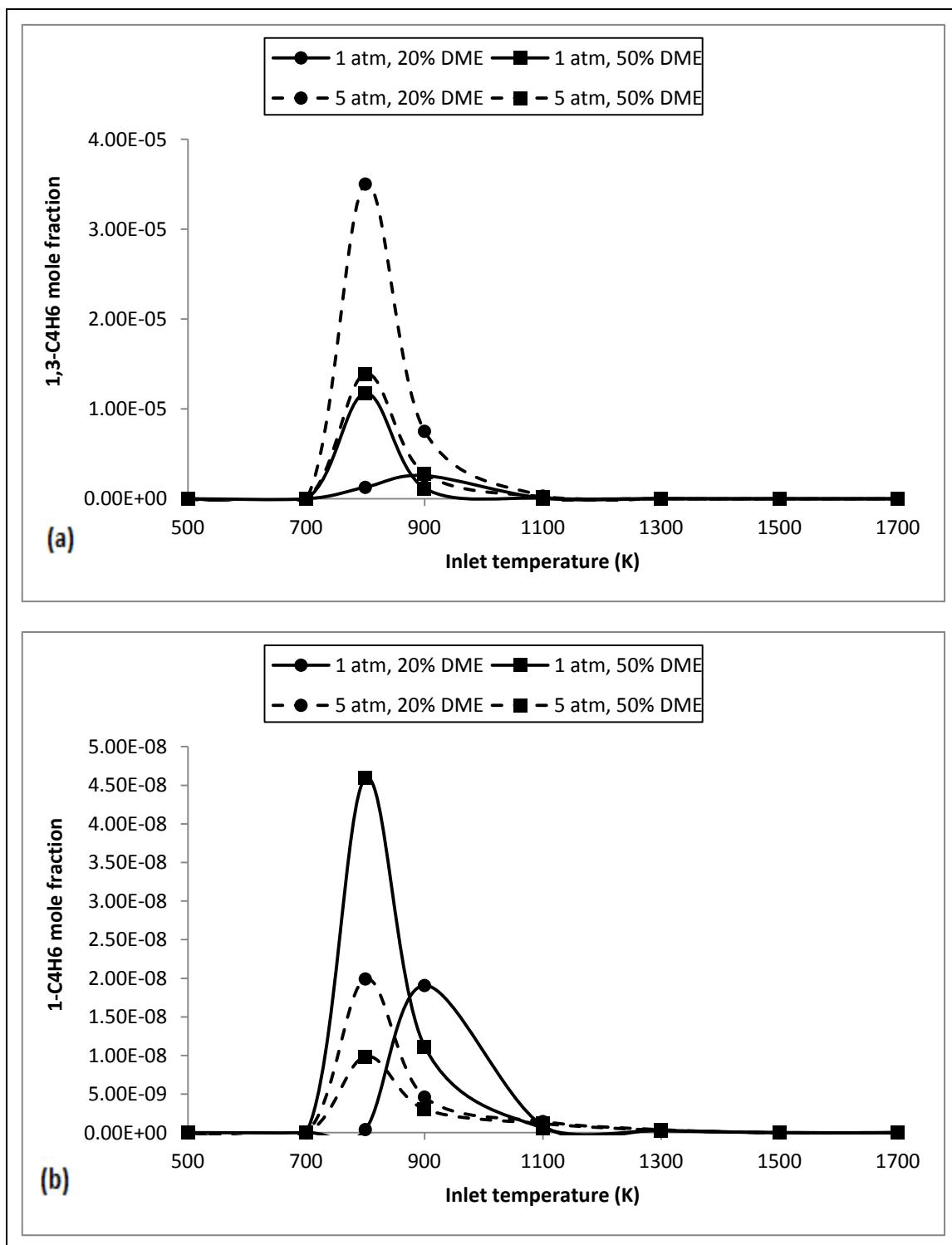


Figure 4.32. Final mole fractions of (a) 1,3-C<sub>4</sub>H<sub>6</sub> and (b) 1-C<sub>4</sub>H<sub>6</sub> versus reactor inlet temperatures at different pressures and different concentrations of CH<sub>3</sub>OCH<sub>3</sub>. ( $\phi = 2.6$ ).

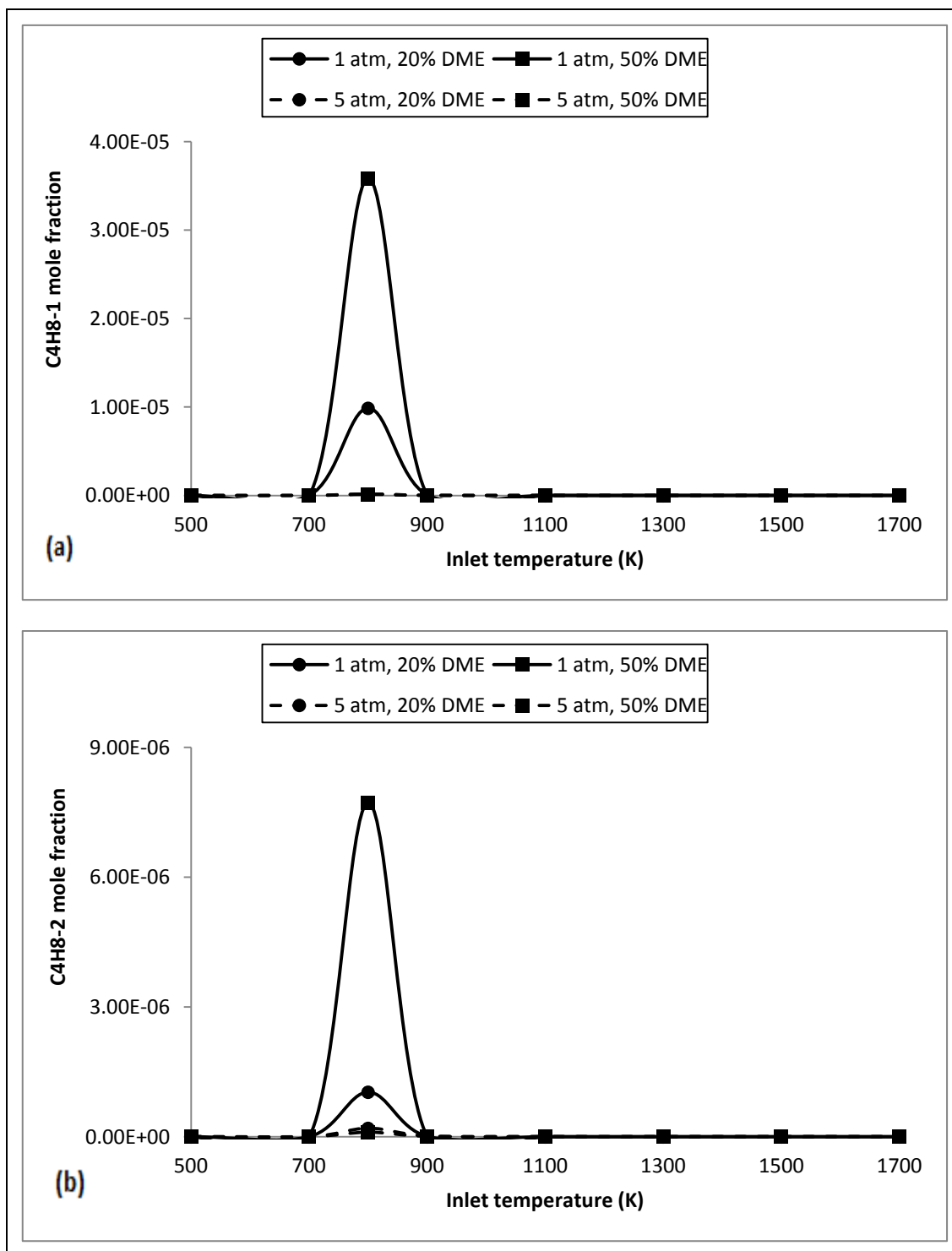


Figure 4.33. Final mole fractions of (a) C<sub>4</sub>H<sub>8</sub>-1 and (b) C<sub>4</sub>H<sub>8</sub>-2 versus reactor inlet temperatures at different pressures and different concentrations of CH<sub>3</sub>OCH<sub>3</sub>. ( $\varphi = 2.6$ ).

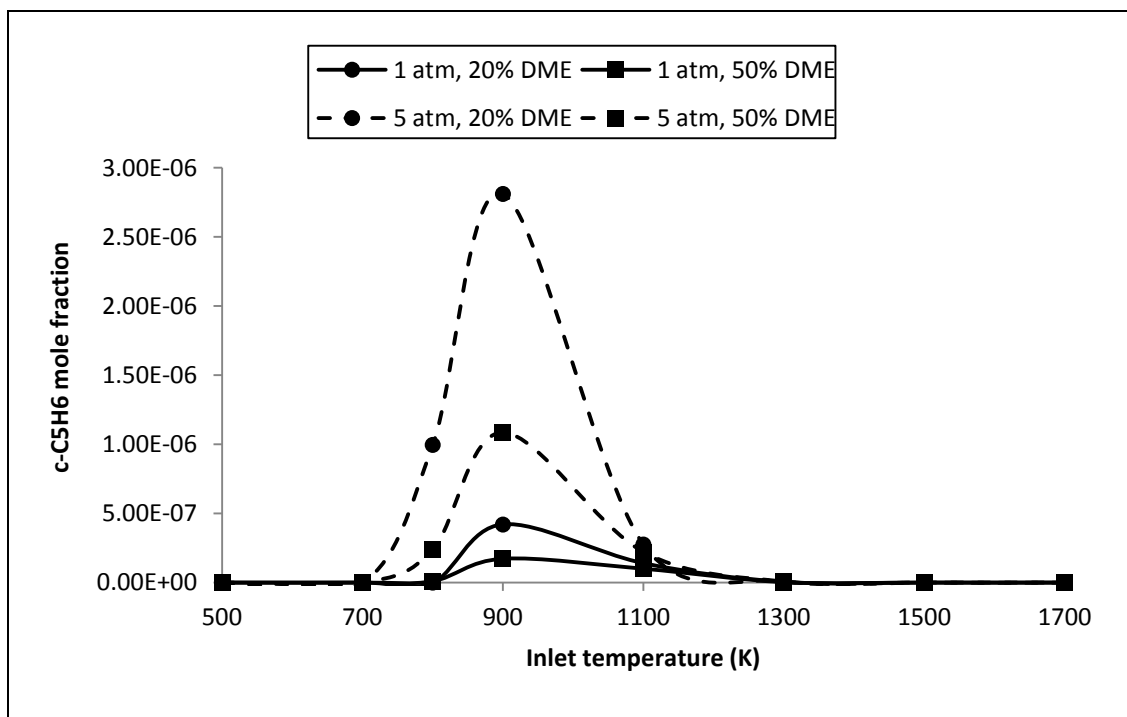


Figure 4.34. Final mole fractions of  $c\text{-C}_5\text{H}_6$  versus reactor inlet temperatures at different pressures and different concentrations of  $\text{CH}_3\text{OCH}_3$ . ( $\phi = 2.6$ ).

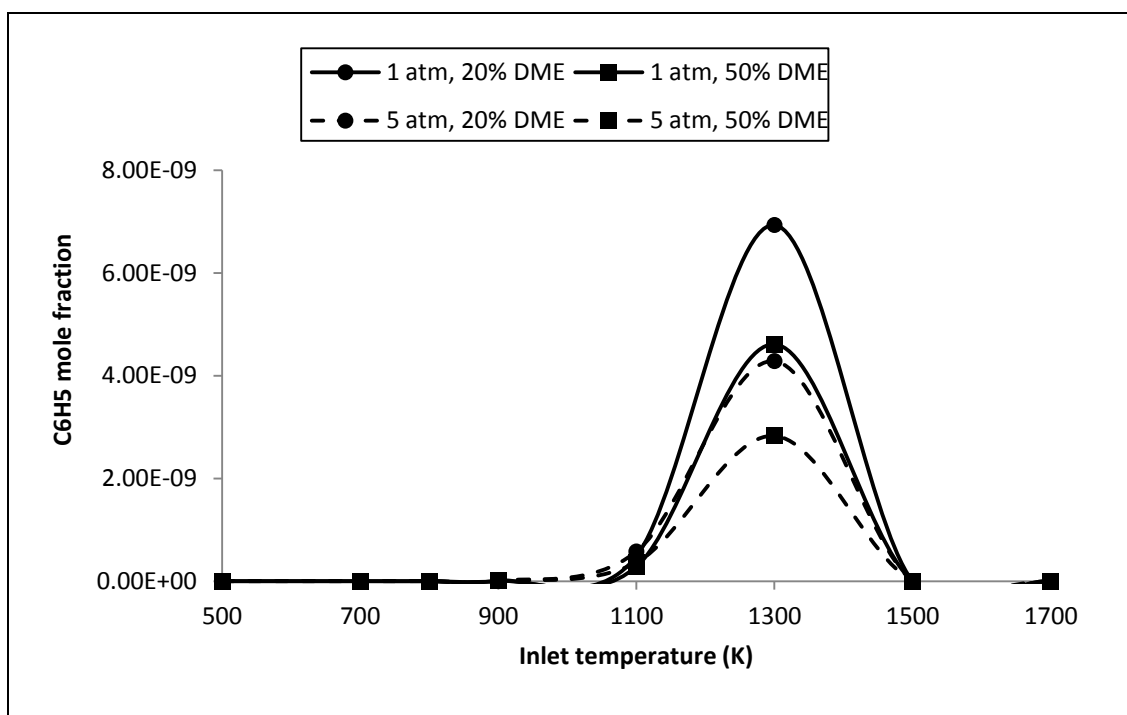


Figure 4.35. Final mole fractions of  $\text{C}_6\text{H}_5$  versus reactor inlet temperatures at different pressures and different concentrations of  $\text{CH}_3\text{OCH}_3$ . ( $\phi = 2.6$ ).

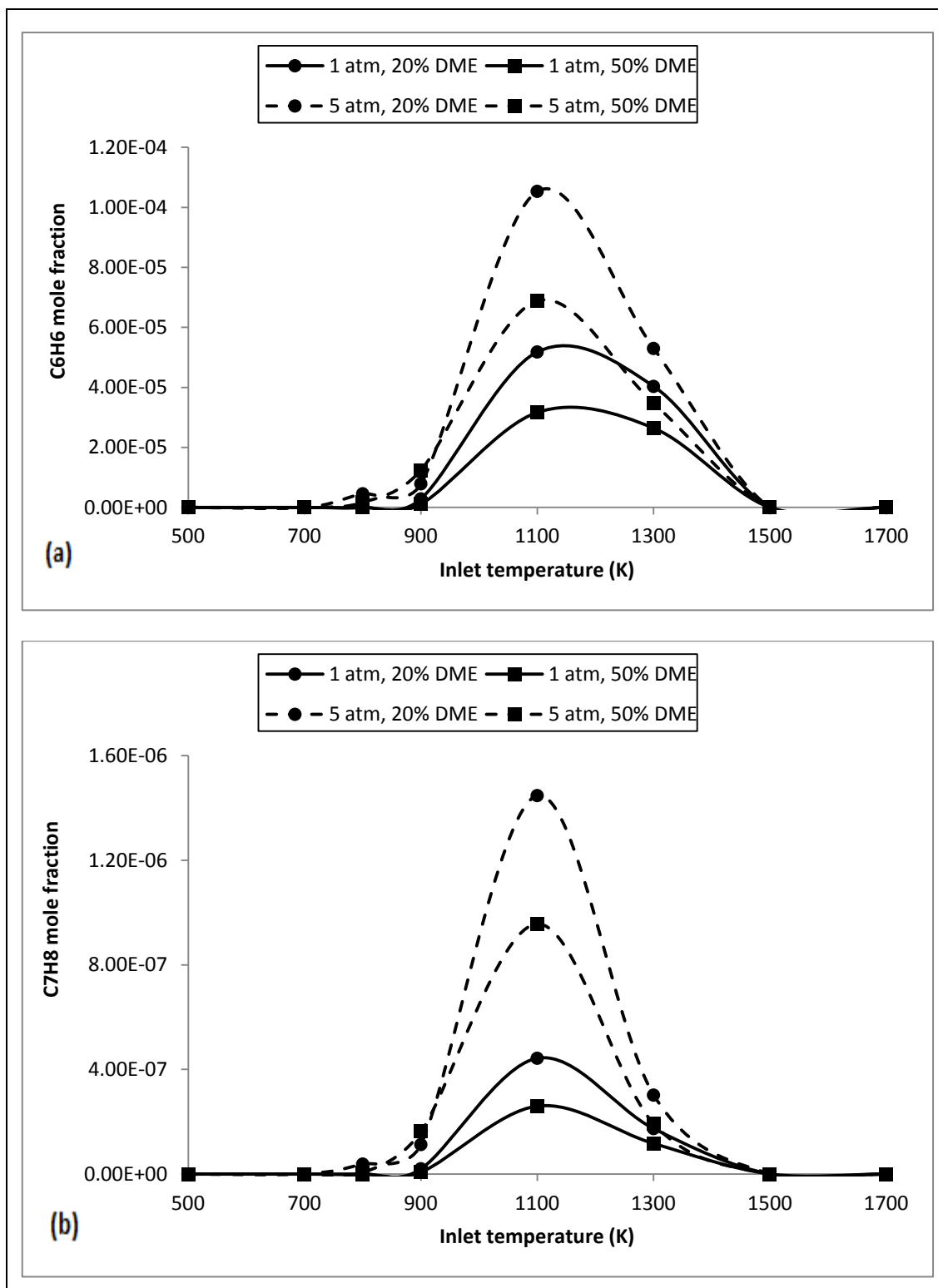


Figure 4.36. Final mole fractions of (a)  $C_6H_6$  and (b)  $C_7H_8$  versus reactor inlet temperatures at different pressures and different concentrations of  $CH_3OCH_3$ . ( $\varphi = 2.6$ ).

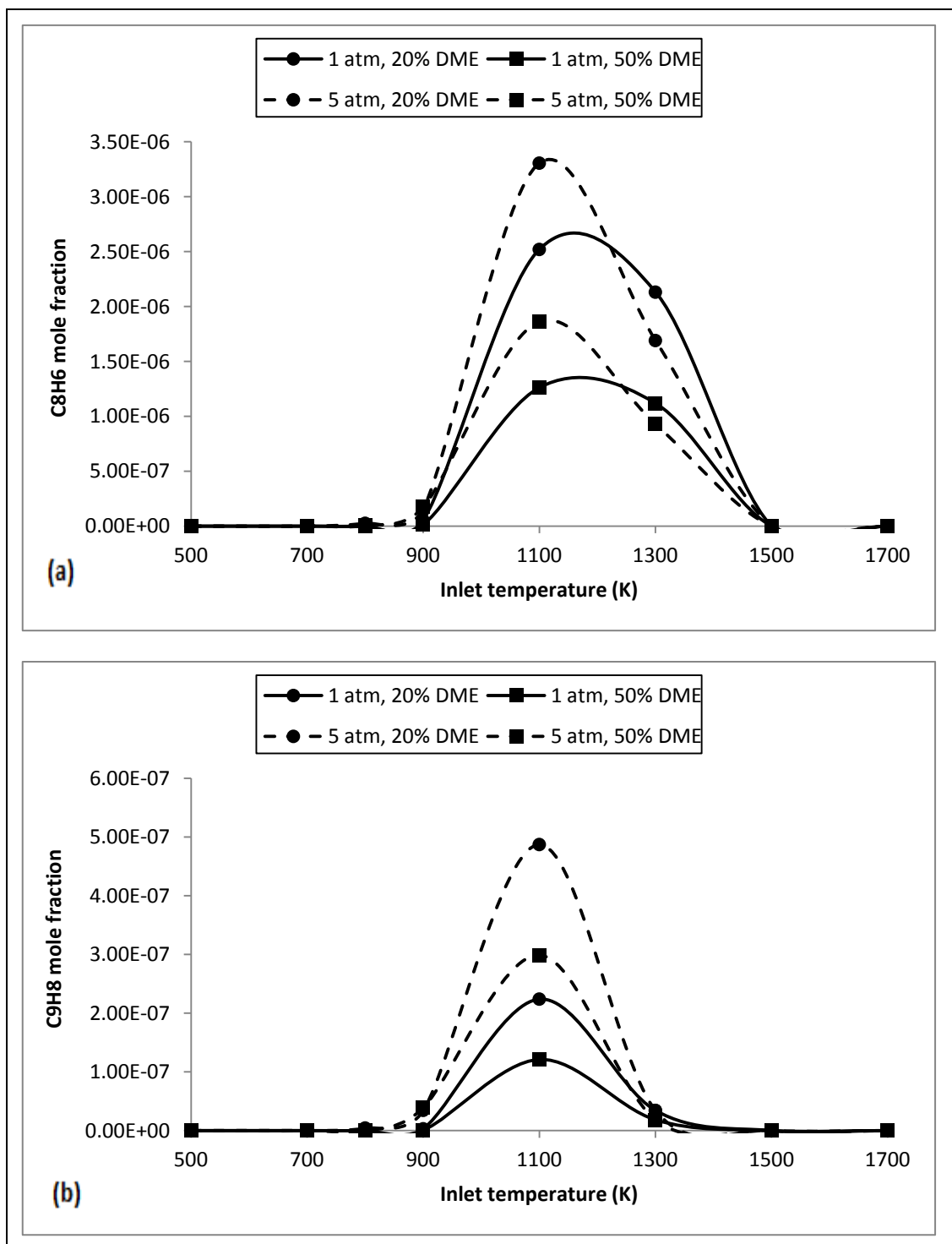


Figure 4.37. Final mole fractions of (a)  $C_8H_6$  and (b)  $C_9H_8$  versus reactor inlet temperatures at different pressures and different concentrations of  $CH_3OCH_3$ . ( $\phi = 2.6$ ).



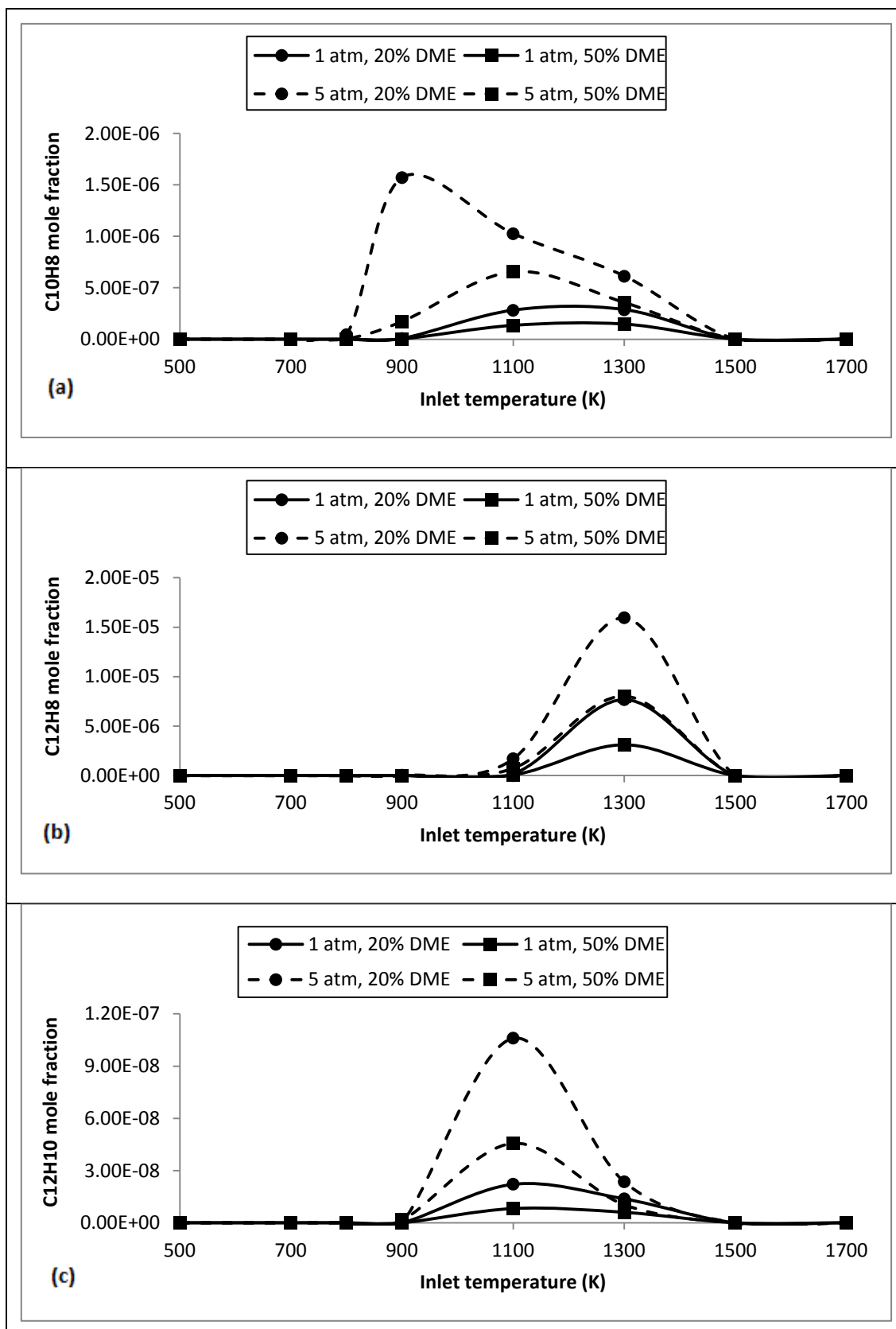


Figure 4.38. Final mole fractions of (a) C<sub>10</sub>H<sub>8</sub> (b) C<sub>12</sub>H<sub>8</sub> and (c) C<sub>12</sub>H<sub>10</sub> versus reactor inlet temperatures at different pressures and different concentrations of CH<sub>3</sub>OCH<sub>3</sub>. ( $\phi = 2.6$ ).

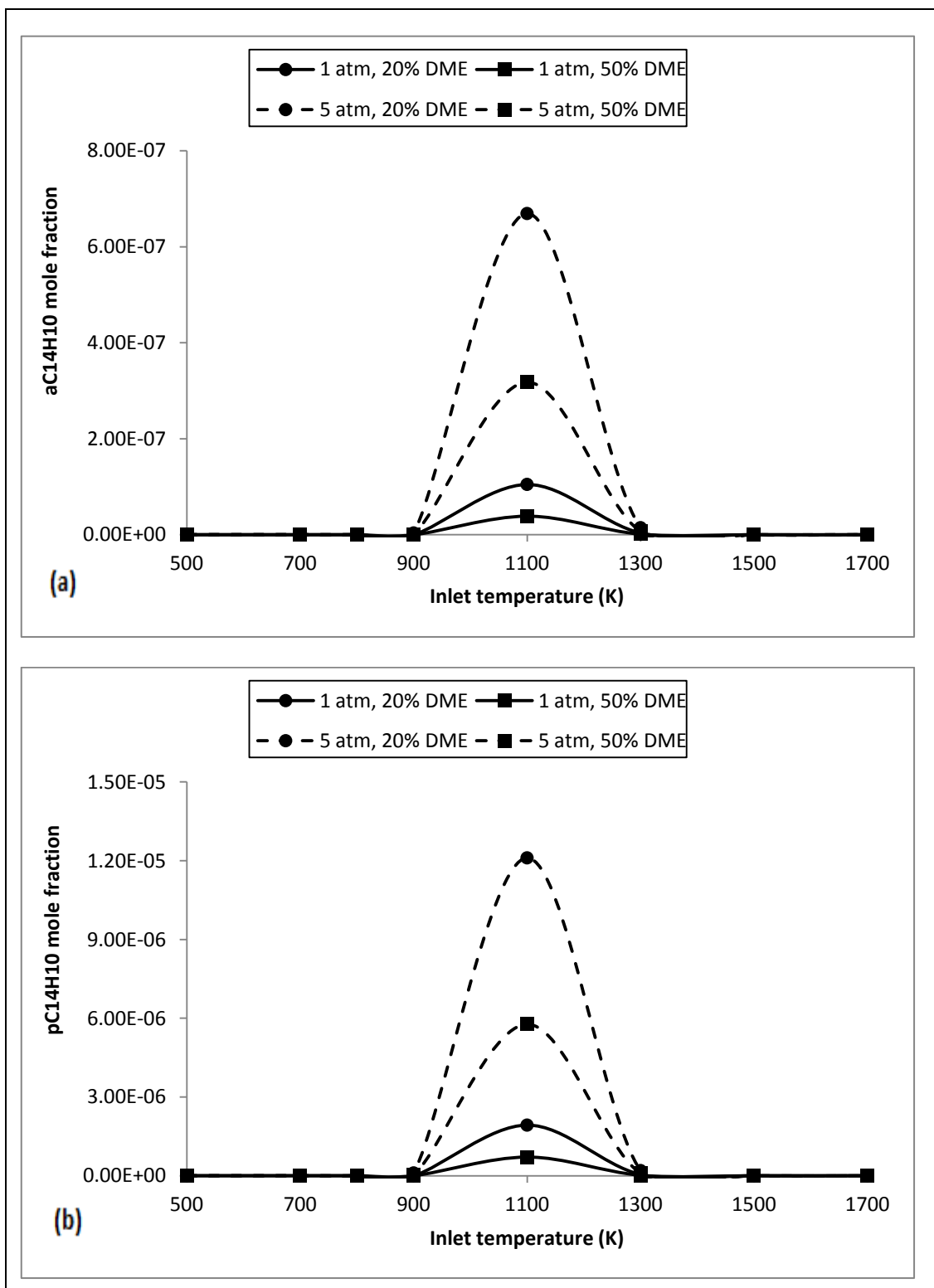


Figure 4.39. Final mole fractions of (a)  $aC_{14}H_{10}$  and (b)  $C_{14}H_{10}$  versus reactor inlet temperatures at different pressures and different concentrations of  $CH_3OCH_3$ . ( $\varphi = 2.6$ ).

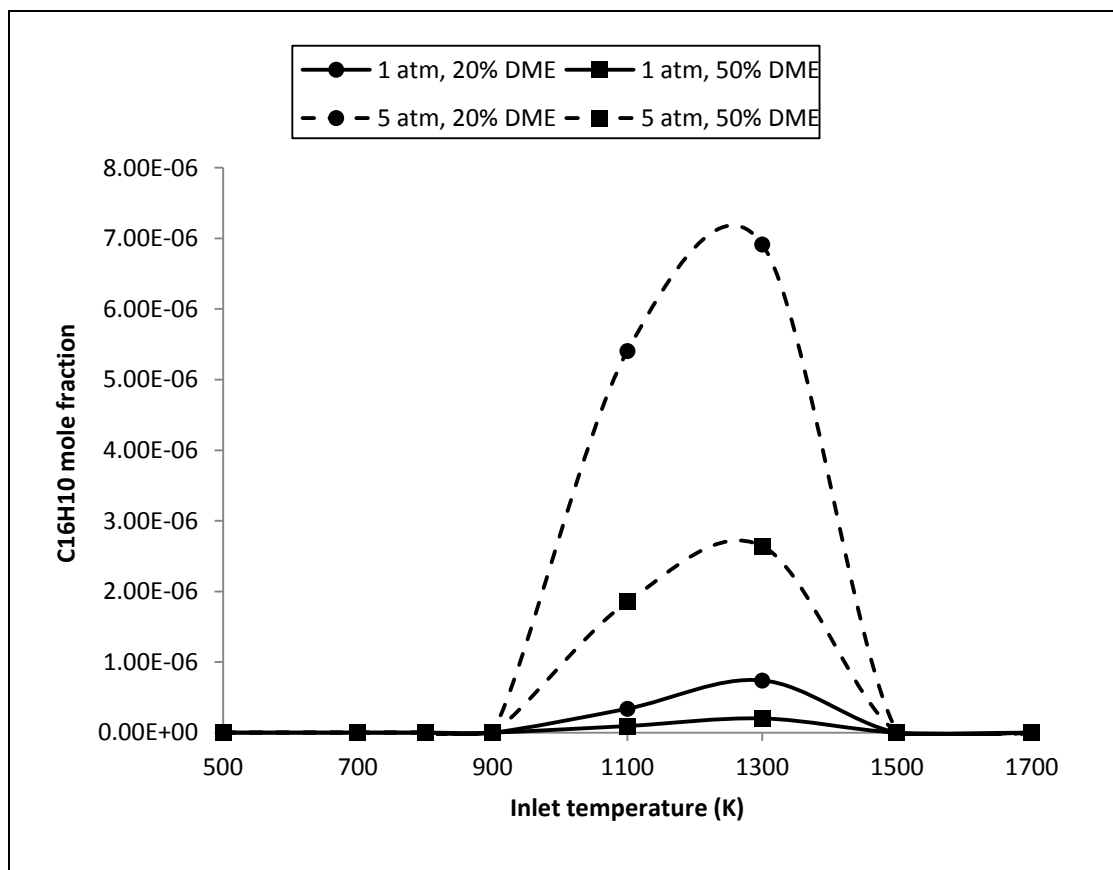


Figure 4.40. Final mole fractions of  $C_{16}H_{10}$  versus reactor inlet temperatures at different pressures and different concentrations of  $CH_3OCH_3$ . ( $\phi = 2.6$ ).

Figure 4.21 shows the final reaction temperatures for various inlet temperatures at two different pressures and two different DME concentrations. It can be seen that pressure and DME concentration do not have a significant effect on the final reaction temperature, for the parameter ranges investigated. Since the inlet fuel mixture is highly diluted with argon and the temperature increases are kept very low, the effects of these parameters on final reaction temperature cannot be observed. Due to the very slow reaction rates before 800 K, the outlet reaction temperatures are almost equal to inlet temperatures. For inlet temperatures greater than 800 K, final reaction temperatures start to increase and they increase almost linearly with increasing inlet temperature.

Figure 4.22 shows the final mole fractions of the fuels and Figure 4.23 shows the final mole fractions of the oxidizer, for various inlet temperatures at two different pressures and two different DME concentrations. It is observed that for temperatures below 700 K, the overall rate of the reaction is very small. Also, effect of pressure cannot be observed at these temperatures. The effect of pressure also cannot be observed for temperatures higher than 900 K, since after this temperature fuels and

oxidizer are totally consumed. For the inlet temperatures between 700 and 900 K, it can be observed that increasing pressure increases the consumption rates of the fuels and the oxidizer.

Final mole fractions of CO<sub>2</sub> and CO are compared in Figure 4.24. Mole fraction of CO<sub>2</sub> increases up to 1500 K, then it starts to decrease. Mole fraction of CO first increases up to 800 – 900 K, then it remains almost constant up to 1300 K, then it starts to increase again as the inlet temperature increases. At inlet temperatures of 800 and 1100 K, higher pressure results in higher formation of CO<sub>2</sub>. And at inlet temperature of 800 K, higher pressure results in higher CO mole fraction. At other inlet temperatures, pressure does not seem to affect the final mole fractions of CO<sub>2</sub> and CO significantly. Among the most important elementary reactions related to CO, the elementary reactions  $\text{HCO}+\text{M}=\text{H}+\text{CO}+\text{M}$ ,  $\text{CH}_2\text{CO}(\text{+M})=\text{CH}_2+\text{CO}(\text{+M})$ , and  $\text{CH}_3\text{CO}(\text{+M})=\text{CH}_3+\text{CO}(\text{+M})$  are known to be pressure dependent.

Final mole fractions of H<sub>2</sub>O and H<sub>2</sub> are compared in Figure 4.25. Mole fraction of H<sub>2</sub>O shows a peak around 800 K for the higher pressure and around 900 K for the lower pressure value, and then starts to decrease with increasing temperature up to 1500 K. After the inlet temperature value of 1500 K, mole fraction of H<sub>2</sub>O remains almost constant. The formation of H<sub>2</sub> increases as the inlet temperature increases, until the inlet temperature value of 1500 K. After this temperature mole fraction of H<sub>2</sub> remains almost constant. Pressure does not seem to have a significant effect.

Final mole fractions of the three alkanes, CH<sub>4</sub>, C<sub>2</sub>H<sub>6</sub>, and C<sub>3</sub>H<sub>8</sub>, are compared in Figure 4.26. Mole fraction of CH<sub>4</sub> shows a peak around 800 K at higher pressure value, and around 900 K at lower pressure value. Higher temperatures decrease mole fractions of CH<sub>4</sub>. Mole fractions of C<sub>2</sub>H<sub>6</sub> and C<sub>3</sub>H<sub>8</sub> similarly show peaks around 800 K. Lower pressure results in higher mole fractions of C<sub>2</sub>H<sub>6</sub> and C<sub>3</sub>H<sub>8</sub>, especially for the case of higher DME concentration. Among the most important elementary reactions related to the formations and destructions of CH<sub>4</sub>, C<sub>2</sub>H<sub>6</sub>, and C<sub>3</sub>H<sub>8</sub>, the reactions  $\text{CH}_3+\text{H}(\text{+M})=\text{CH}_4(\text{+M})$ ,  $2\text{CH}_3(\text{+M})=\text{C}_2\text{H}_6(\text{+M})$ , and  $\text{C}_3\text{H}_8(\text{+M})=\text{C}_2\text{H}_5+\text{CH}_3(\text{+M})$  are known to be pressure dependent.

Figure 4.27 shows the final mole fractions of the two oxygenated species, CH<sub>2</sub>O and C<sub>2</sub>H<sub>4</sub>O. Mole fractions of both species show maximum peaks around 800 K. At other inlet temperature values, significant formations of these two oxygenated species are not observed. It is known that the formations of these oxygenated compounds occur at low temperatures (Wilk et al., 1995). Increasing pressure is also observed to decrease

the formations of these two species. Among the elementary reactions related to the formation and destruction of  $\text{CH}_2\text{O}$ , the reactions  $\text{CHOCHO}(\text{+M})=\text{CH}_2\text{O}+\text{CO}(\text{+M})$  and  $\text{CH}_3\text{O}(\text{+M})=\text{CH}_2\text{O}+\text{H}(\text{+M})$  are known to be pressure dependent.

Figure 4.28 shows the final mole fractions of two-carbon-number precursor species  $\text{C}_2\text{H}_2$  and  $\text{C}_2\text{H}_4$ . Mole fraction of  $\text{C}_2\text{H}_2$  shows a maximum peak around 1300 K and mole fraction of  $\text{C}_2\text{H}_4$  shows a maximum peak around 800 K. Increasing pressure seems to decrease the formation of  $\text{C}_2\text{H}_2$  but slightly increase the formation of  $\text{C}_2\text{H}_4$ .

Figure 4.29 shows the final mole fractions of the two of the three-carbon-number precursors,  $\text{C}_3\text{H}_3$  and  $\text{C}_3\text{H}_6$ . Mole fraction of  $\text{C}_3\text{H}_3$  shows a maximum peak around 1300 K and mole fraction of  $\text{C}_3\text{H}_6$  shows a maximum peak around 800 K. Increasing pressure decreases the mole fractions of both species, especially the mole fraction of  $\text{C}_3\text{H}_6$ .

Final mole fractions of two other  $\text{C}_3$  precursor species,  $\text{aC}_3\text{H}_4$  and  $\text{pC}_3\text{H}_4$  are given in Figure 4.30. Around 800 K, mole fraction of  $\text{aC}_3\text{H}_4$ , one of the isomers, increases with increasing pressure. But the mole fraction of the other isomer  $\text{pC}_3\text{H}_4$  decreases with increasing pressure. Around 1100 K, mole fractions of both isomers show a second maximum peak. Increasing pressure seems to slightly decrease the mole fractions of these two species around this temperature.

Figure 4.31 shows the mole fractions of two of the  $\text{C}_4$  precursors  $\text{C}_4\text{H}_2$  and  $\text{C}_4\text{H}_4$ . Mole fraction of  $\text{C}_4\text{H}_2$  shows a maximum peak around 1300 K, while mole fraction of  $\text{C}_4\text{H}_4$  shows a maximum peak around 900 K. Increasing pressure decreases mole fraction of  $\text{C}_4\text{H}_2$  and increases mole fraction of  $\text{C}_4\text{H}_4$ .

Figure 4.32 shows mole fractions of two other  $\text{C}_4$  precursors 1,3- $\text{C}_4\text{H}_6$  and 1- $\text{C}_4\text{H}_6$ . Mole fractions of both isomers show maximum peaks around 800–900 K. Increasing pressure increases the mole fraction of 1,3- $\text{C}_4\text{H}_6$  while decreasing the mole fraction of the other isomer 1- $\text{C}_4\text{H}_6$ .

Figure 4.33 shows mole fractions of two other  $\text{C}_4$  precursors  $\text{C}_4\text{H}_8\text{-1}$  and  $\text{C}_4\text{H}_8\text{-2}$ . They have similar mole fraction profiles showing maximum at 800 K. Increasing pressure decreases the mole fractions of both isomers significantly.

Figure 4.34 shows the mole fractions of  $\text{c-C}_6\text{H}_5$ , a five-carbon-number aromatic precursor. Its mole fraction shows a maximum around 900 K and increasing pressure increases its mole fraction.

Figure 4.35 shows the mole fraction profiles of one-ring aromatic  $\text{C}_6\text{H}_5$  radical. Its maximum mole fraction is around 1300 K and increasing pressure decreases its mole fraction.

Figures 4.36 and 4.37 show the mole fraction profiles of one-ring aromatic species  $C_6H_6$ ,  $C_7H_8$ ,  $C_8H_6$ , and  $C_9H_8$ . Mole fractions of all one-ring aromatics are maximum around the inlet temperature of 1100 K and increasing pressure increases their mole fractions.

Figure 4.38 shows the mole fraction profiles of two-ring PAHs  $C_{10}H_8$ ,  $C_{12}H_8$ , and  $C_{12}H_{10}$ . The temperature at which the mole fraction of  $C_{10}H_8$  is maximum changes depending on other parameters. Mole fraction of  $C_{12}H_8$  is maximum around 1300 K and mole fraction of  $C_{12}H_{10}$  is maximum around 1100 K. Increasing pressure increases the mole fractions of all three PAHs.

Mole fractions of three-ring PAHs  $aC_{14}H_{10}$  and  $pC_{14}H_{10}$  are given in Figure 4.39. Their maximum mole fractions are around 1100 K and increasing pressure increases their mole fractions.

Figure 4.40 shows the mole fraction profiles of the four-ring PAH  $C_{16}H_{10}$ . Its mole fraction is maximum around 1300 K and increasing pressure increases its mole fraction.

Figures 4.28 to 4.40 showed the effects of inlet temperature and pressure on the formations of aromatic species precursors, aromatic species, and PAHs. Among the precursor species, the formations of  $C_2H_2$ ,  $C_3H_3$ ,  $aC_3H_4$ ,  $pC_3H_4$ ,  $C_3H_6$ ,  $C_4H_2$ , 1- $C_4H_6$ , and  $C_4H_8-2$  were decreased by the increase in pressure. However, the formations of the precursor species  $C_4H_4$ , 1,3- $C_4H_6$ ,  $C_4H_8-2$  and  $c-C_5H_6$  were observed to increase with increasing pressure. Also, the formations of all aromatic species and PAHs, except  $C_6H_5$ , were increased by increased pressure. This situation might be indicating that as the pressure increases, the roles of  $C_4H_4$ , 1,3- $C_4H_6$ ,  $C_4H_8-2$  and  $c-C_5H_6$  are becoming more dominant in the formations of  $C_6H_6$  and more complex aromatics. The formation of  $C_4H_2$  and its role in the formations of aromatic species and PAHs do not seem to be affected with the change in pressure.

Also, when the effects of the inlet temperature are investigated in Figures 4.28 through 4.40, it is observed that the consumptions of the precursor species  $C_2H_4$ ,  $C_3H_6$ ,  $C_4H_4$ , 1,3- $C_4H_6$ , 1- $C_4H_6$ ,  $C_4H_8-1$ ,  $C_4H_8-2$ , and  $c-C_5H_6$  start around the temperature of 900 K. This indicates that these species play role in the early formations of aromatic species and PAHs around this temperature. The formations of all aromatic species and PAHs, except  $C_6H_5$  and  $C_{12}H_8$ , start around and after the temperature of 900 K. The formations of  $C_6H_5$  and  $C_{12}H_8$  start around the temperature of 1100 K and increase until 1300 K. The precursor species  $aC_3H_4$  and  $pC_3H_4$ , consumptions of which start around

1100 K, are considered to be effective in the formations of these two aromatic species. Consumption of the precursor species  $C_2H_2$ ,  $C_3H_3$ ,  $C_4H_2$  start after 1300 K. For this reason these three species are considered to be playing role in the formations of larger PAHs.

#### 4.2.2. The Effects of Equivalence Ratio

In a fuel–oxidizer mixture, the stoichiometric quantity of oxidizer is the amount needed to completely burn a quantity of fuel. If more than a stoichiometric quantity of oxidizer is supplied, the mixture is said to be fuel–lean; while supplying less than the stoichiometric oxidizer results in a fuel–rich mixture. The equivalence ratio,  $\phi$ , is used to indicate quantitatively whether a fuel–oxidizer mixture is fuel–rich ( $\phi > 1$ ), fuel–lean ( $\phi < 1$ ), or stoichiometric ( $\phi = 1$ ). Equivalence ratio is calculated by dividing the ratio of the fuel and the oxidizer in the mixture, to the stoichiometric ratio of fuel and oxidizer.

It is known that the formations of oxidation products, especially the formations of aromatic species and PAHs strongly depend on the fuel-oxidizer equivalence ratio. Formations of aromatic species and PAHs increase with increasing equivalence ratio. In order to investigate the effects of equivalence ratio on the formation of oxidation products in the oxidation of n-butane/DME/O<sub>2</sub>/Ar system, two different equivalence ratios ( $\phi = 2.6$  and  $\phi = 3.0$ ) were studied at atmospheric pressure ( $P = 1 \text{ atm}$ ) and at various inlet temperatures ( $T_0 = 500, 700, 800, 900, 1100, 1300, 1500, \text{ and } 1700 \text{ K}$ ). The properties of the PFR and the flow conditions were the same as in Sections 4.1 and 4.2.1 ( $d = 0.05 \text{ m}$ ,  $L = 10 \text{ m}$ , and  $u = 0.5 \text{ m/s}$ ), and the results were again shown for two different fractions of DME (20% and 50% DME in the fuel mixture) added. Resulting final temperatures and final mole fractions of species at the reactor outlet, against the inlet temperature values were analyzed for the two equivalence ratio values.

The final reaction temperatures for the changing inlet temperatures at two different equivalence ratios and two different DME concentrations are given in Figure 4.41. As it can be seen from the graph; the final reaction temperature increases almost linearly, as the inlet temperature increases. The change in the equivalence ratio does not seem to have a significant effect on the final reaction temperature, since the temperature rise during the reaction is kept at very low levels with argon dilution.

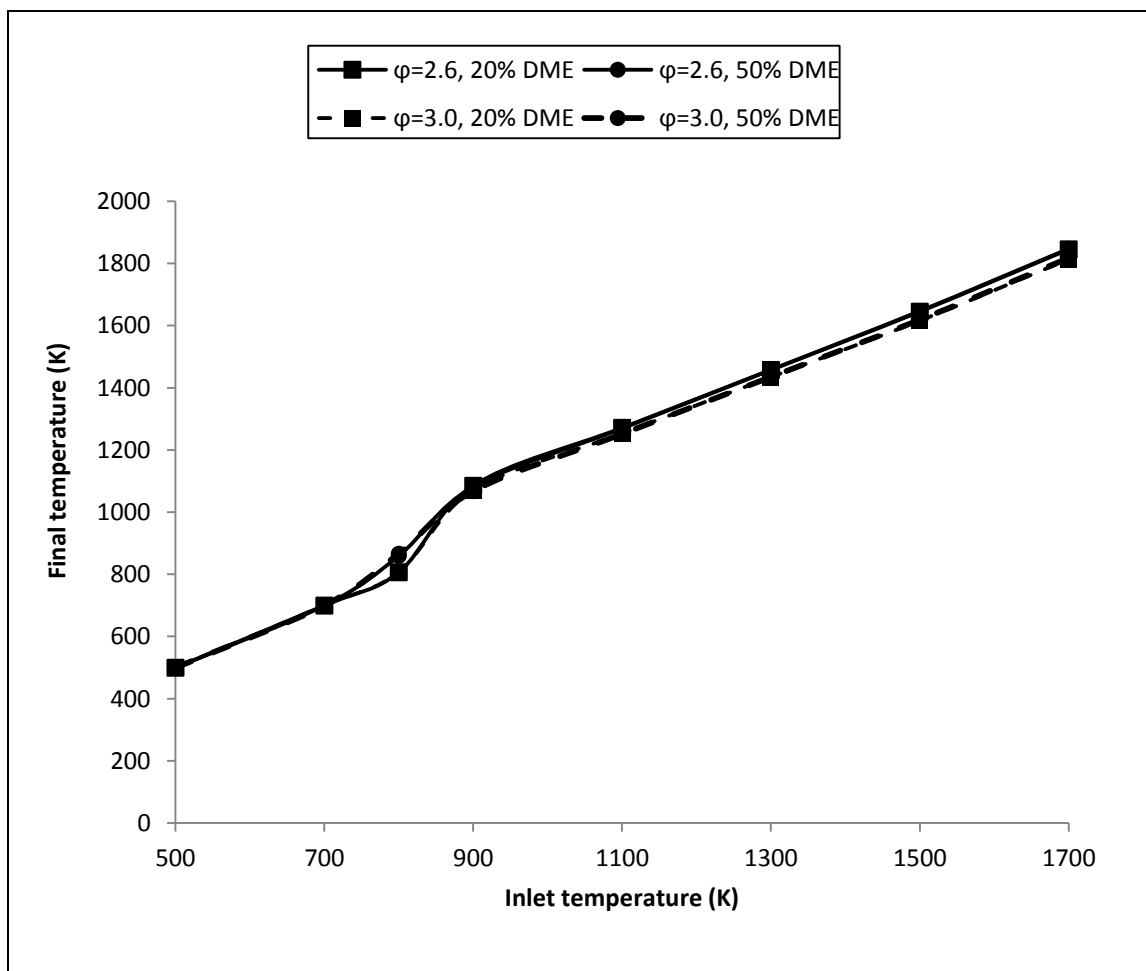


Figure 4.41. Final reaction temperatures versus reactor inlet temperatures at different equivalence ratios and different concentrations of  $\text{CH}_3\text{OCH}_3$ . ( $P=1$  atm).



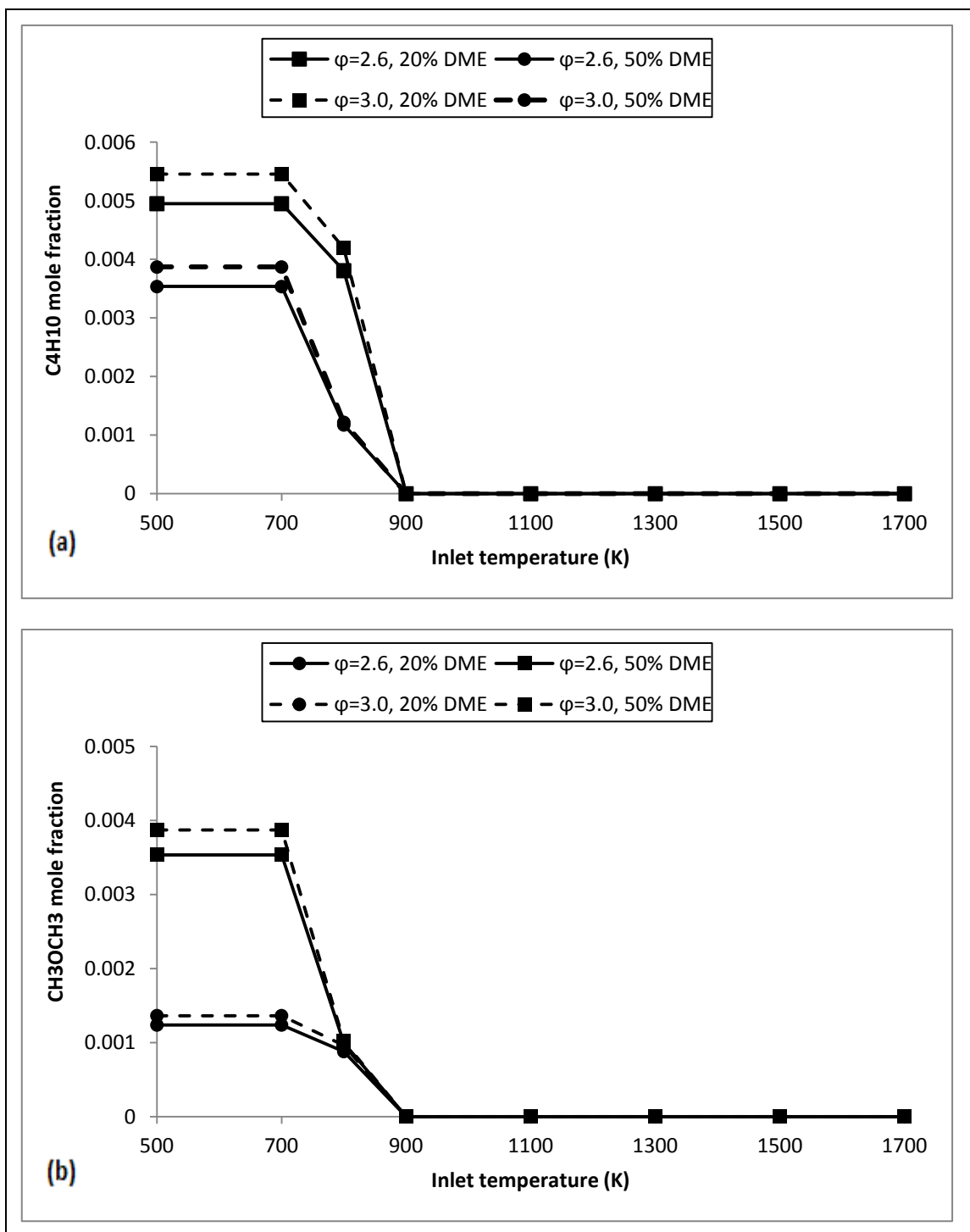


Figure 4.42. Final mole fractions of (a)  $\text{C}_4\text{H}_{10}$  and (b)  $\text{CH}_3\text{OCH}_3$  versus reactor inlet temperatures at different equivalence ratios and different concentrations of  $\text{CH}_3\text{OCH}_3$ . ( $P = 1 \text{ atm}$ ).

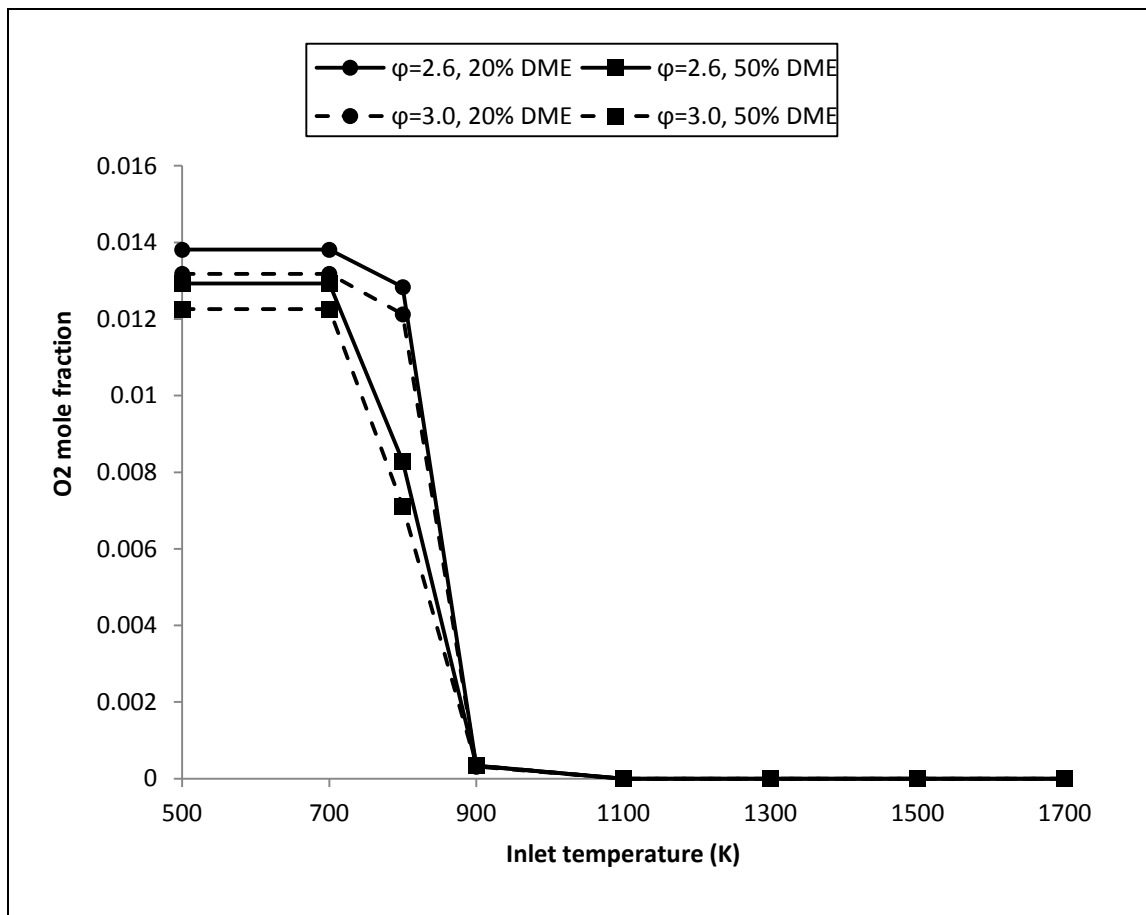


Figure 4.43. Final mole fractions of (a) O<sub>2</sub> versus reactor inlet temperatures at different equivalence ratios and different concentrations of CH<sub>3</sub>OCH<sub>3</sub>. (P = 1 atm).

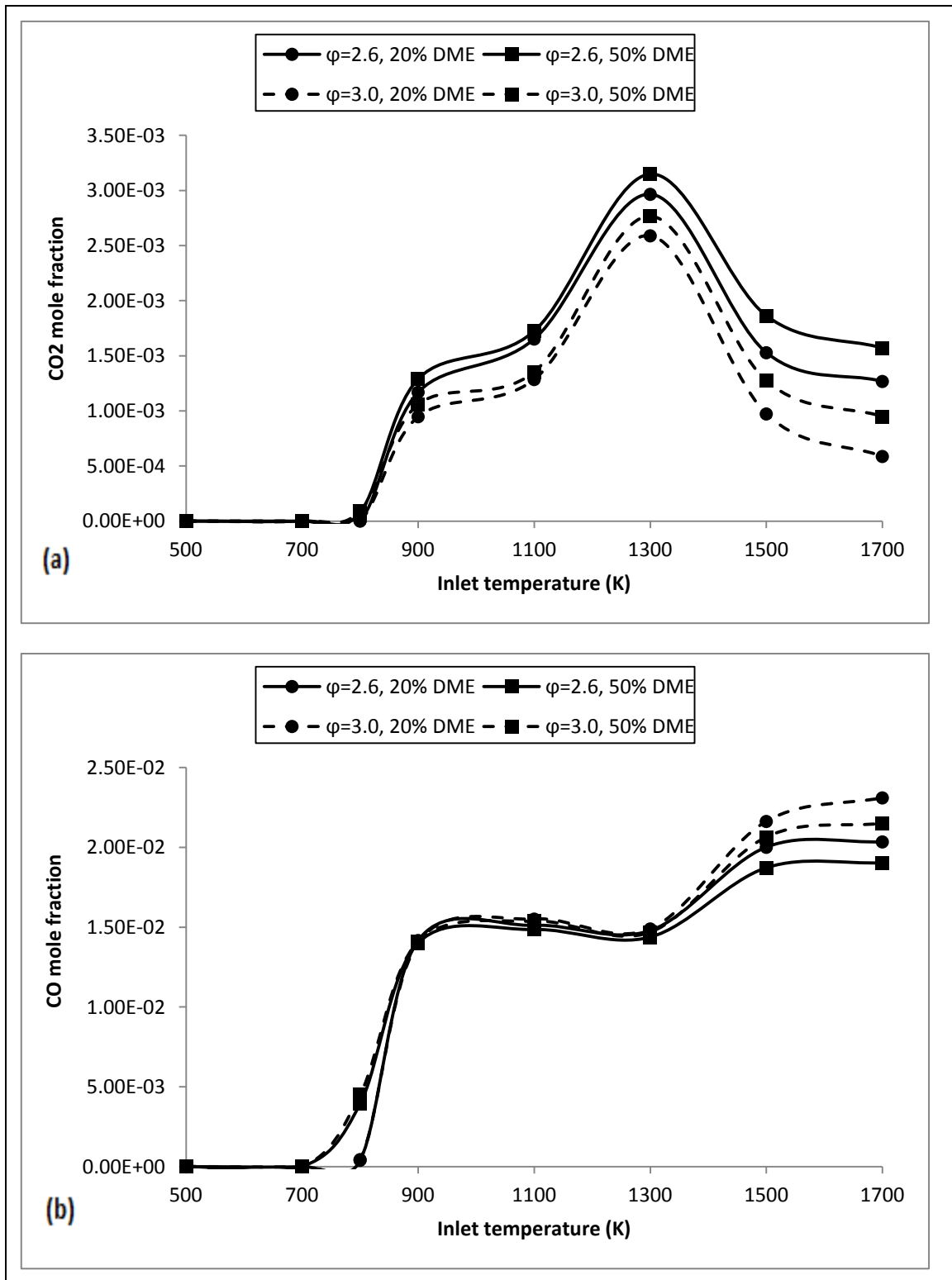


Figure 4.44. Final mole fractions of (a) CO<sub>2</sub> and (b) CO versus reactor inlet temperatures at different equivalence ratios and different concentrations of CH<sub>3</sub>OCH<sub>3</sub>. (P = 1 atm).

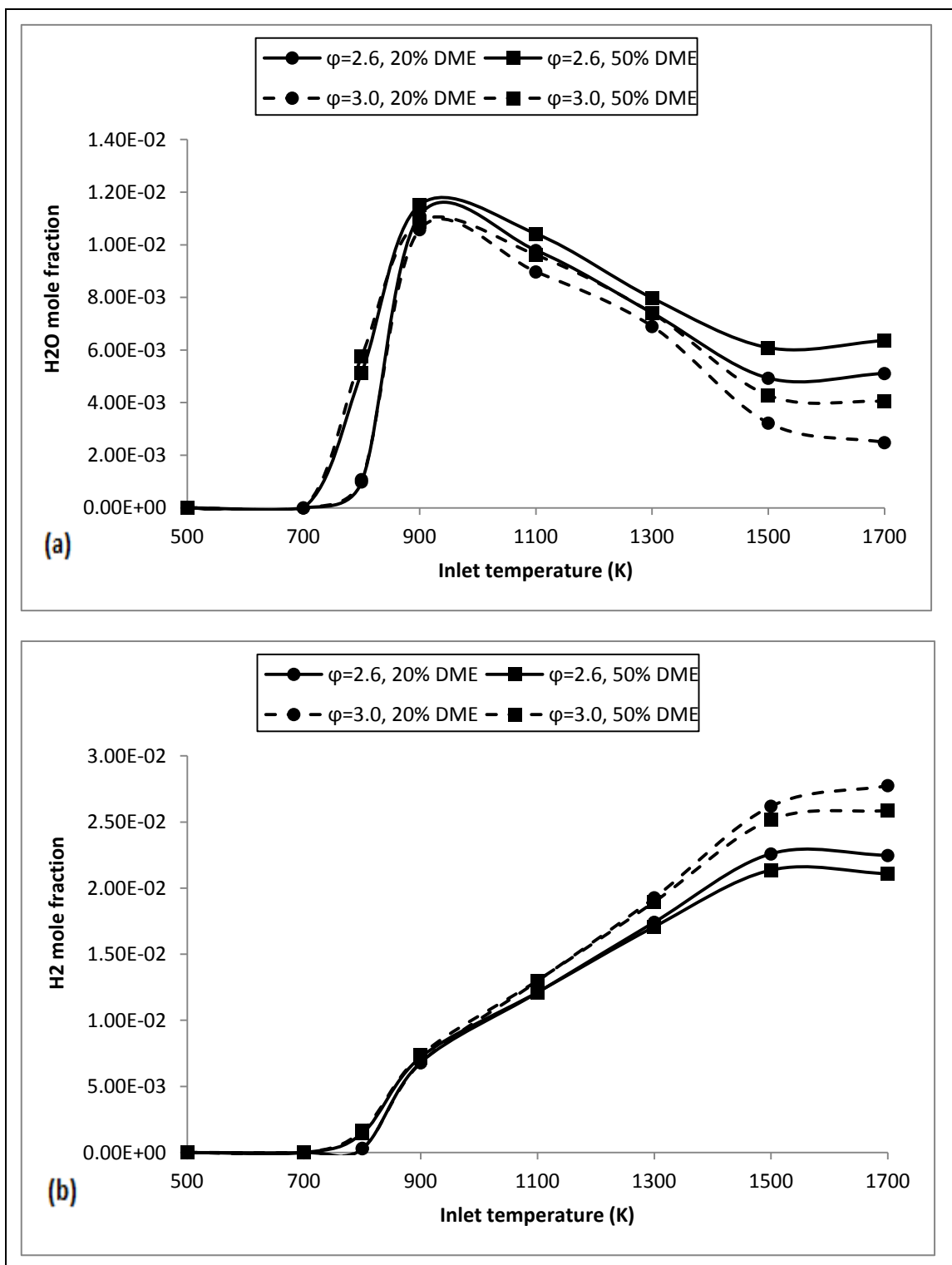


Figure 4.45. Final mole fractions of (a) H<sub>2</sub>O and (b) H<sub>2</sub> versus reactor inlet temperatures at different equivalence ratios and different concentrations of CH<sub>3</sub>OCH<sub>3</sub>. (P = 1 atm).

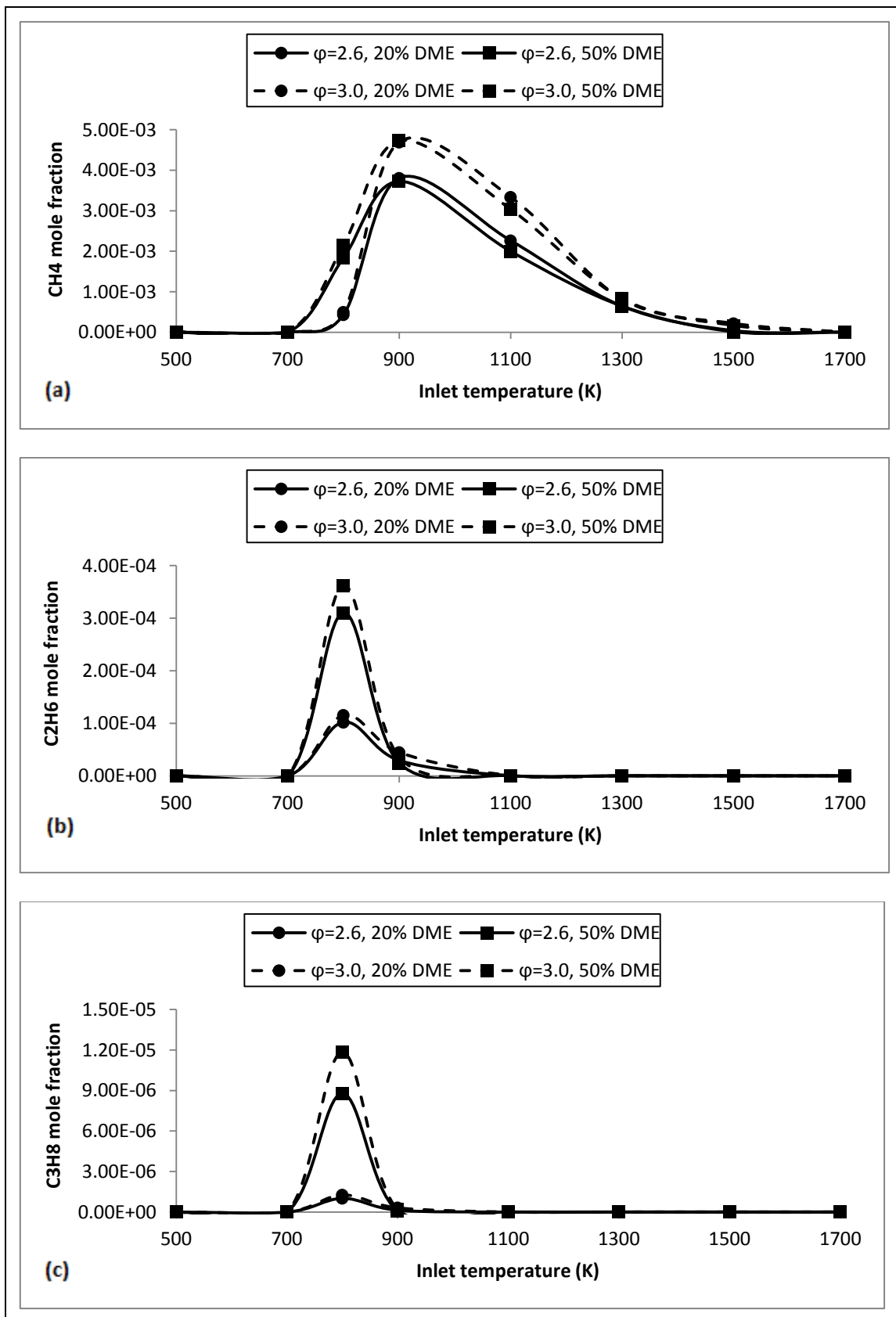


Figure 4.46. Final mole fractions of (a) CH<sub>4</sub> (b) C<sub>2</sub>H<sub>6</sub> and (c) C<sub>3</sub>H<sub>8</sub> versus reactor inlet temperatures at different equivalence ratios and different concentrations of CH<sub>3</sub>OCH<sub>3</sub>. (P = 1 atm).

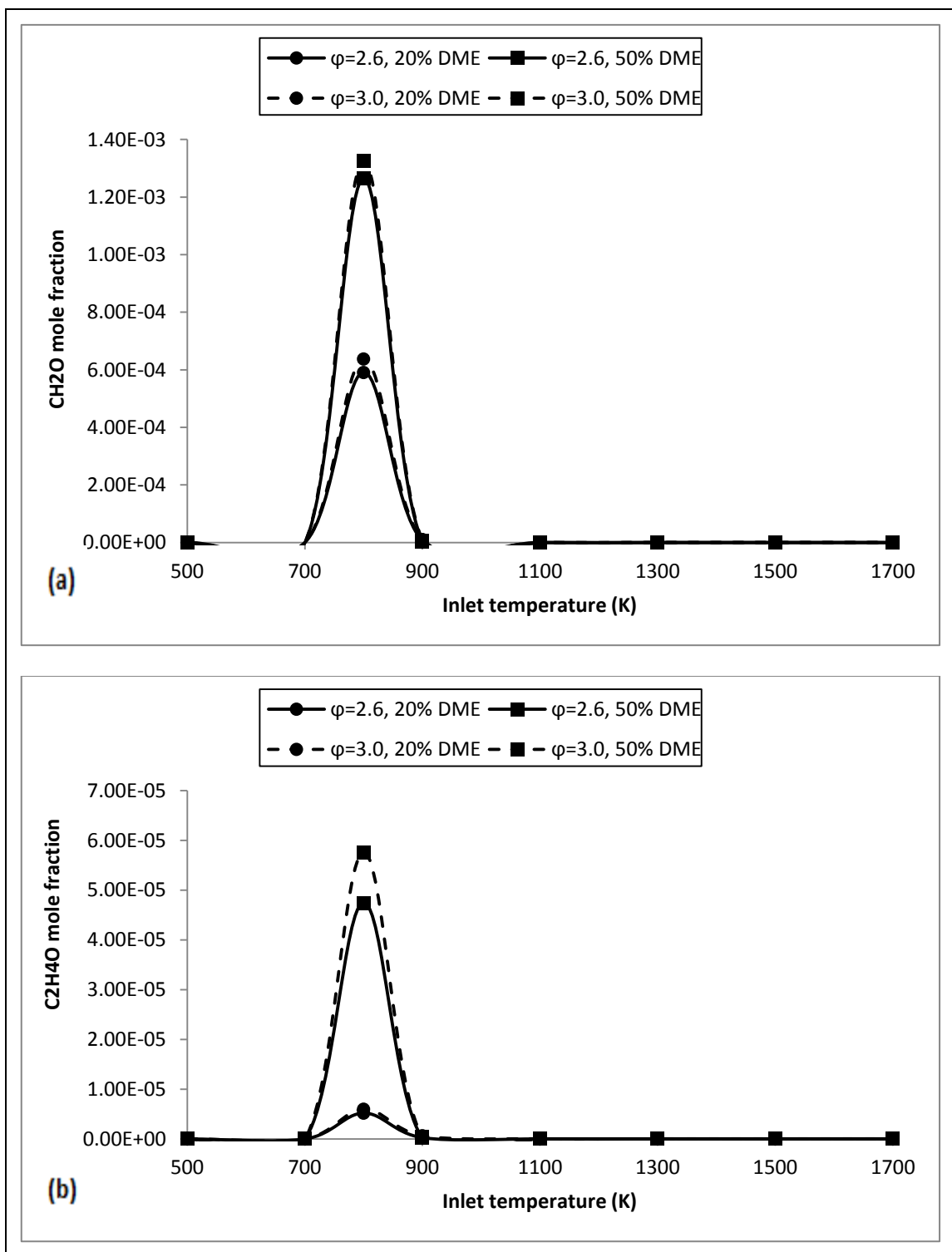


Figure 4.47. Final mole fractions of (a) CH<sub>2</sub>O and (b) C<sub>2</sub>H<sub>4</sub>O versus reactor inlet temperatures at different equivalence ratios and different concentrations of CH<sub>3</sub>OCH<sub>3</sub>. (P = 1 atm).

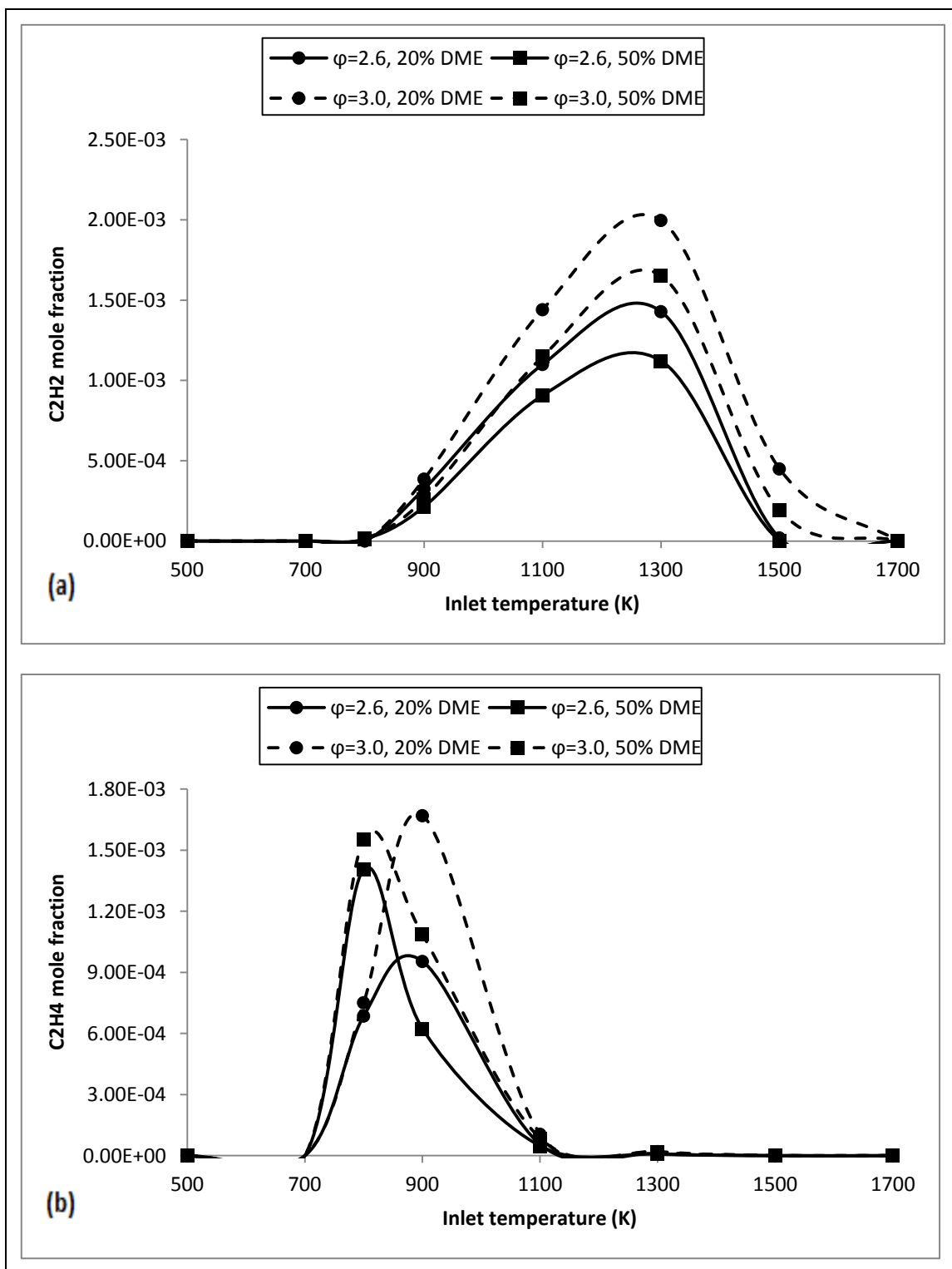


Figure 4.48. Final mole fractions of (a) C<sub>2</sub>H<sub>2</sub> and (b) C<sub>2</sub>H<sub>4</sub> versus reactor inlet temperatures at different equivalence ratios and different concentrations of CH<sub>3</sub>OCH<sub>3</sub>. (P = 1 atm).

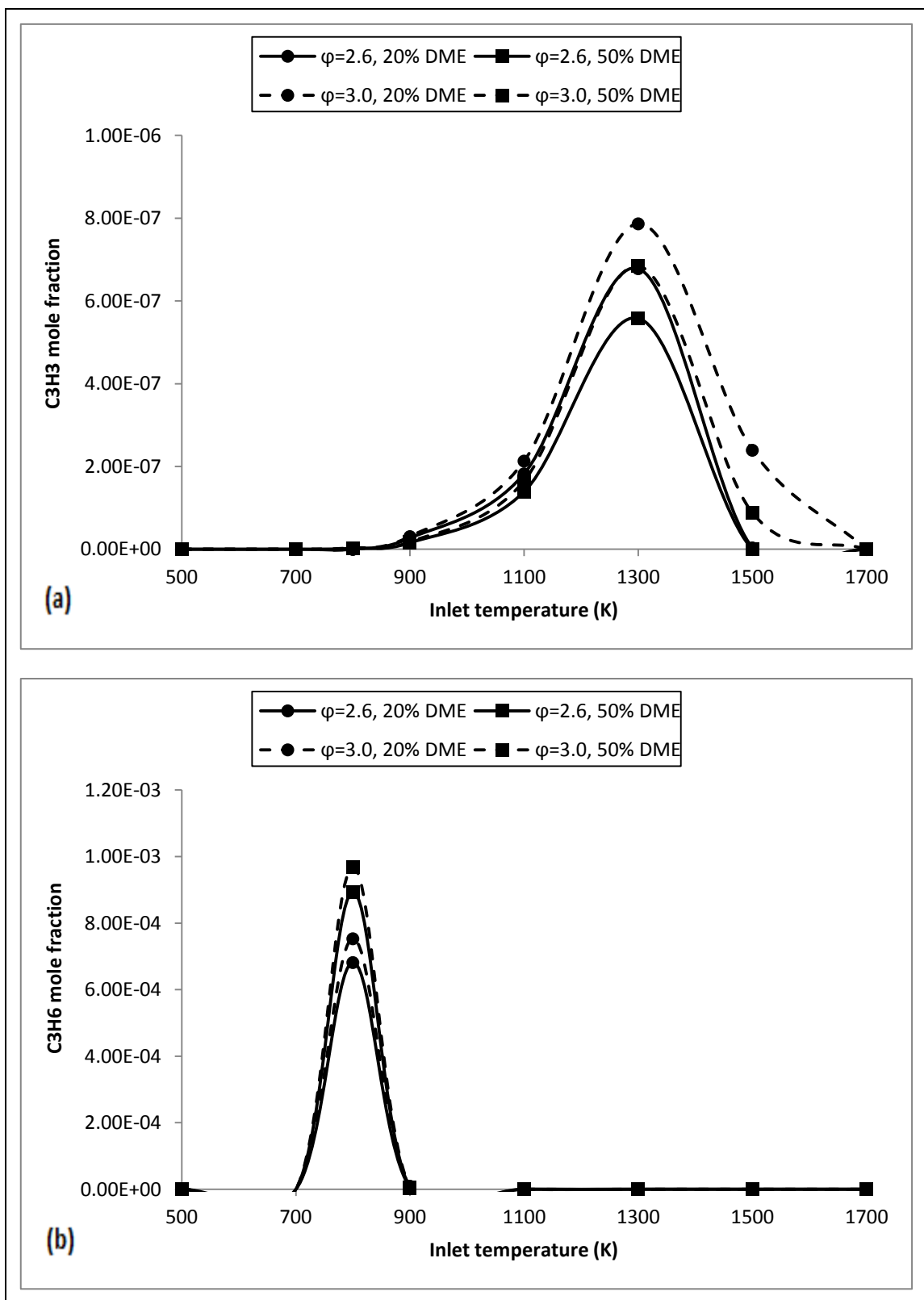


Figure 4.49. Final mole fractions of (a) C<sub>3</sub>H<sub>3</sub> and (b) C<sub>3</sub>H<sub>6</sub> versus reactor inlet temperatures at different equivalence ratios and different concentrations of CH<sub>3</sub>OCH<sub>3</sub>. (P = 1 atm).



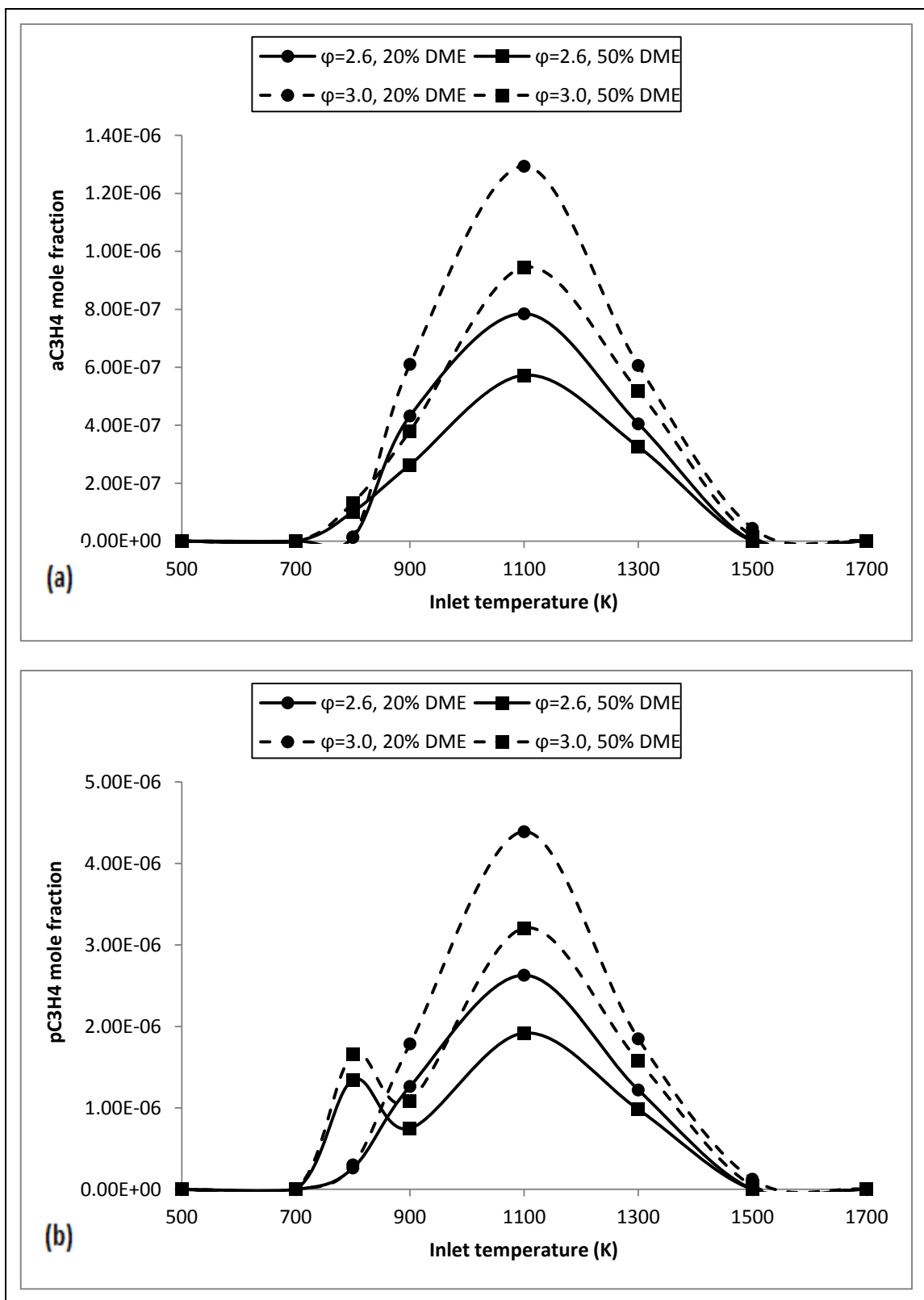


Figure 4.50. Final mole fractions of (a)  $aC_3H_4$  and (b)  $pC_3H_4$  versus reactor inlet temperatures at different equivalence ratios and different concentrations of  $CH_3OCH_3$ . ( $P = 1$  atm).

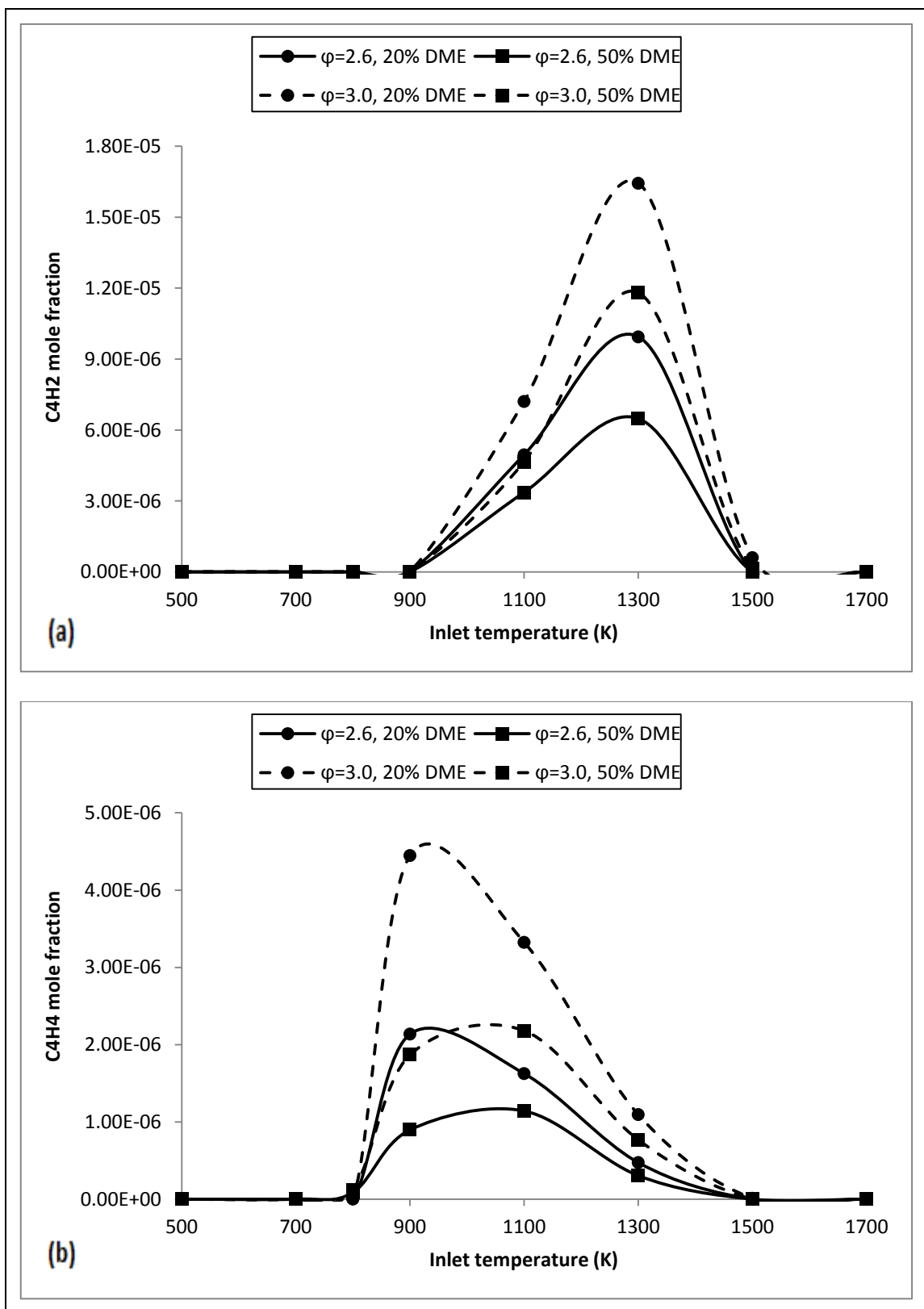


Figure 4.51. Final mole fractions of (a)  $C_4H_2$  and (b)  $C_4H_4$  versus reactor inlet temperatures at different equivalence ratios and different concentrations of  $CH_3OCH_3$ . ( $P = 1$  atm).

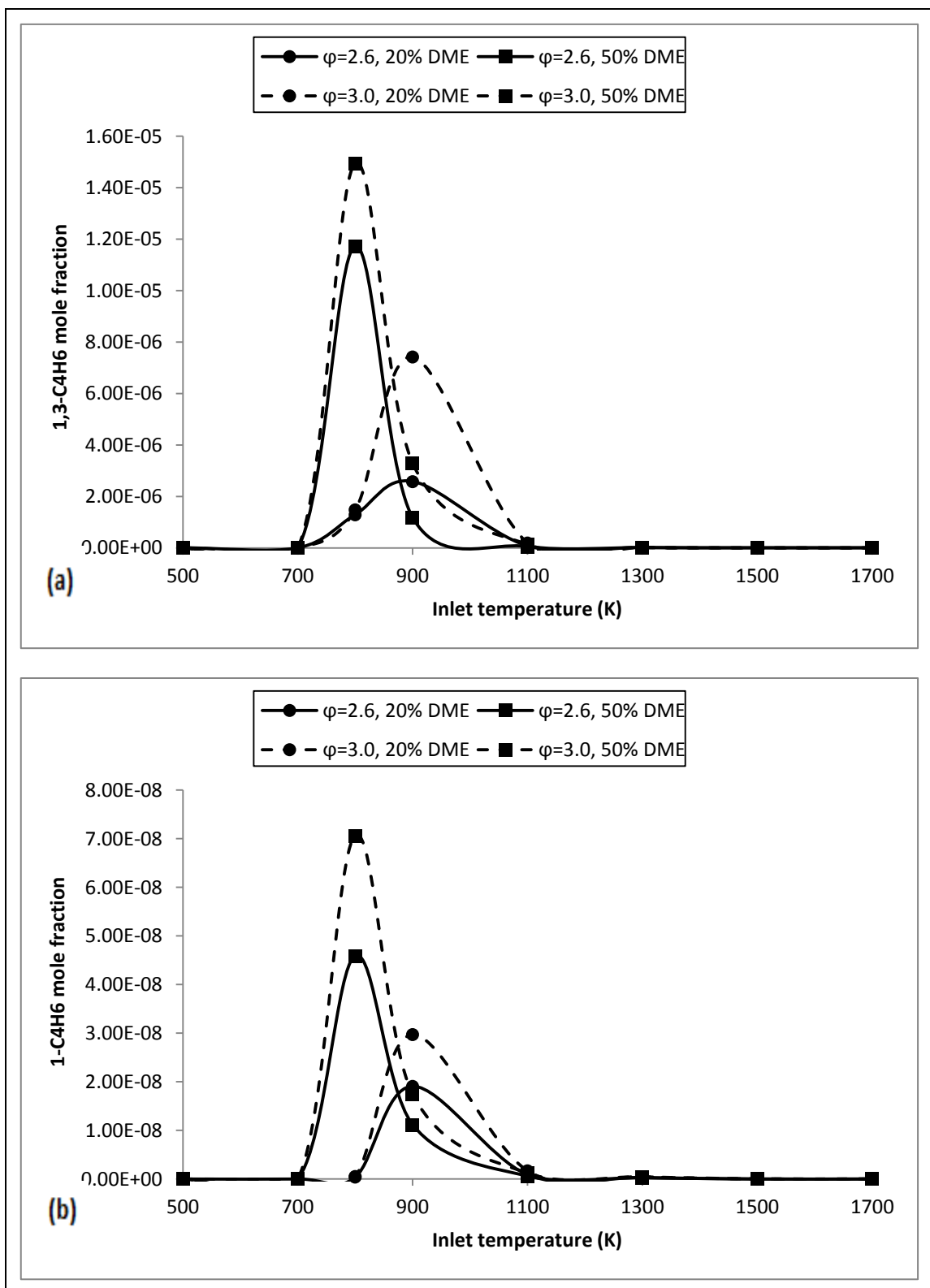


Figure 4.52. Final mole fractions of (a) 1,3-C<sub>4</sub>H<sub>6</sub> and (b) 1-C<sub>4</sub>H<sub>6</sub> versus reactor inlet temperatures at different equivalence ratios and different concentrations of CH<sub>3</sub>OCH<sub>3</sub>. (P = 1 atm).

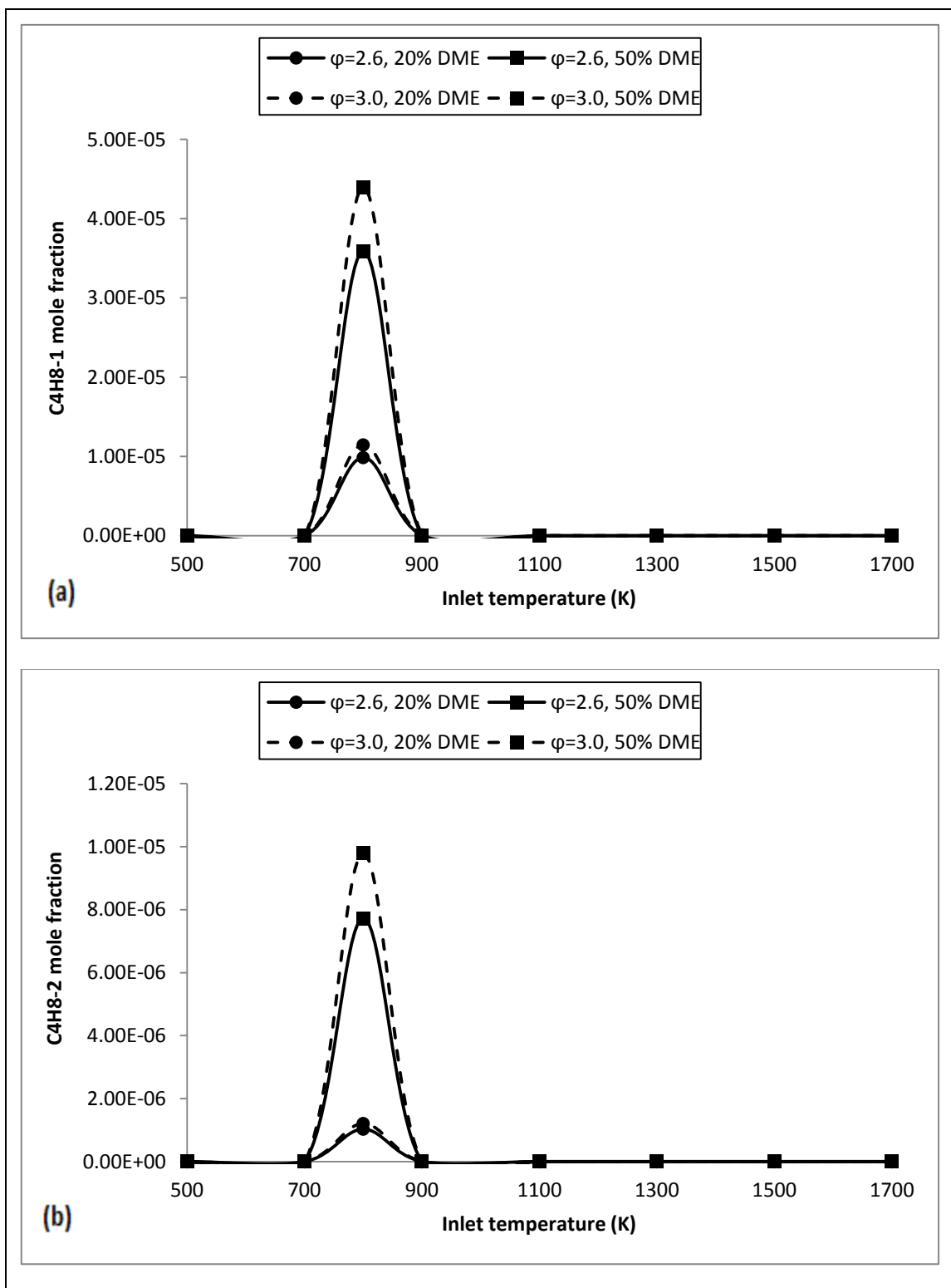


Figure 4.53. Final mole fractions of (a) C<sub>4</sub>H<sub>8</sub>-1 and (b) C<sub>4</sub>H<sub>8</sub>-2 versus reactor inlet temperatures at different equivalence ratios and different concentrations of CH<sub>3</sub>OCH<sub>3</sub>. (P = 1 atm).

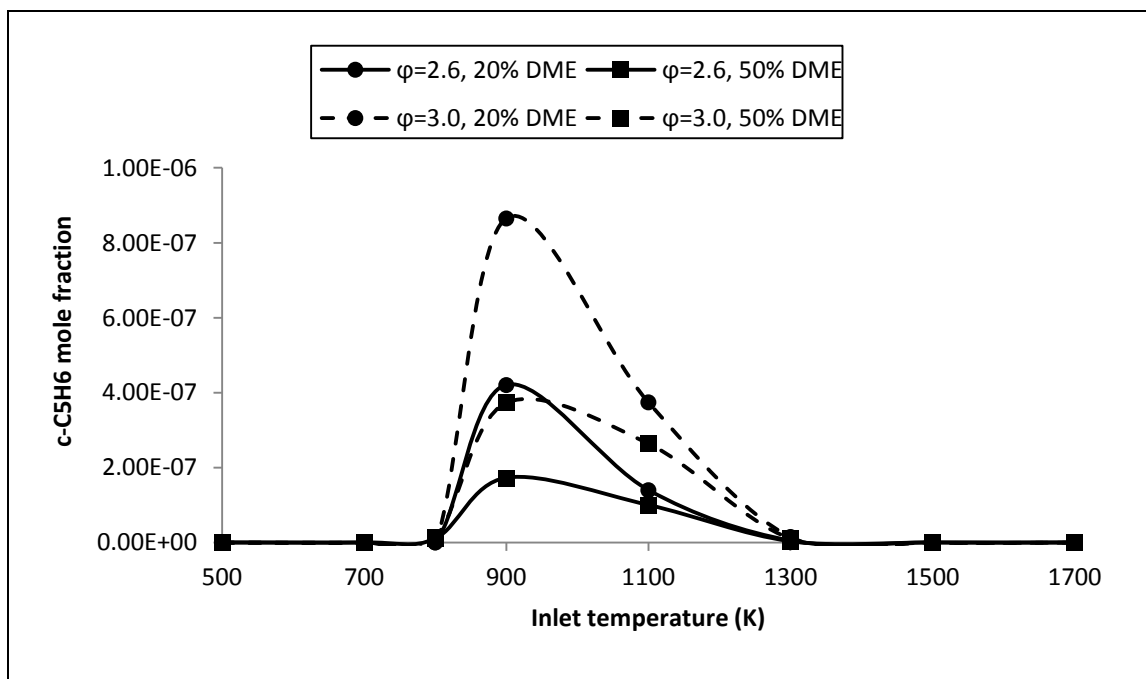


Figure 4.54. Final mole fractions of  $c\text{-C}_5\text{H}_6$  versus reactor inlet temperatures at different equivalence ratios and different concentrations of  $\text{CH}_3\text{OCH}_3$ . ( $P = 1 \text{ atm}$ ).

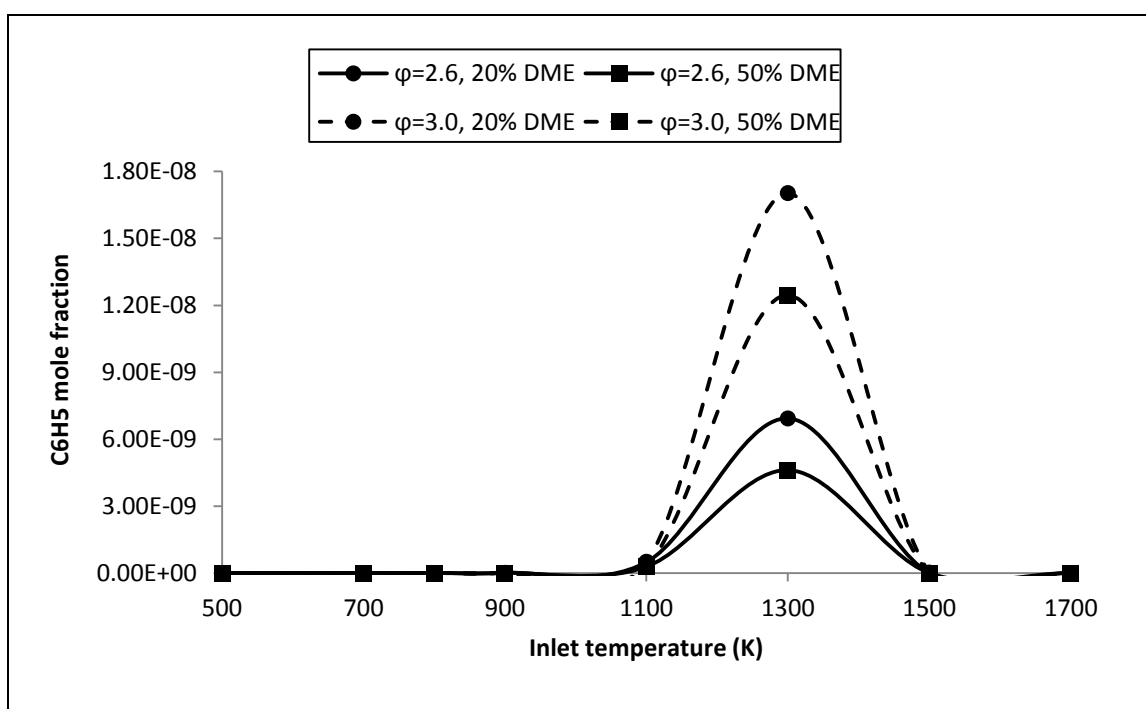


Figure 4.55. Final mole fractions of  $\text{C}_6\text{H}_5$  versus reactor inlet temperatures at different equivalence ratios and different concentrations of  $\text{CH}_3\text{OCH}_3$ . ( $P = 1 \text{ atm}$ ).

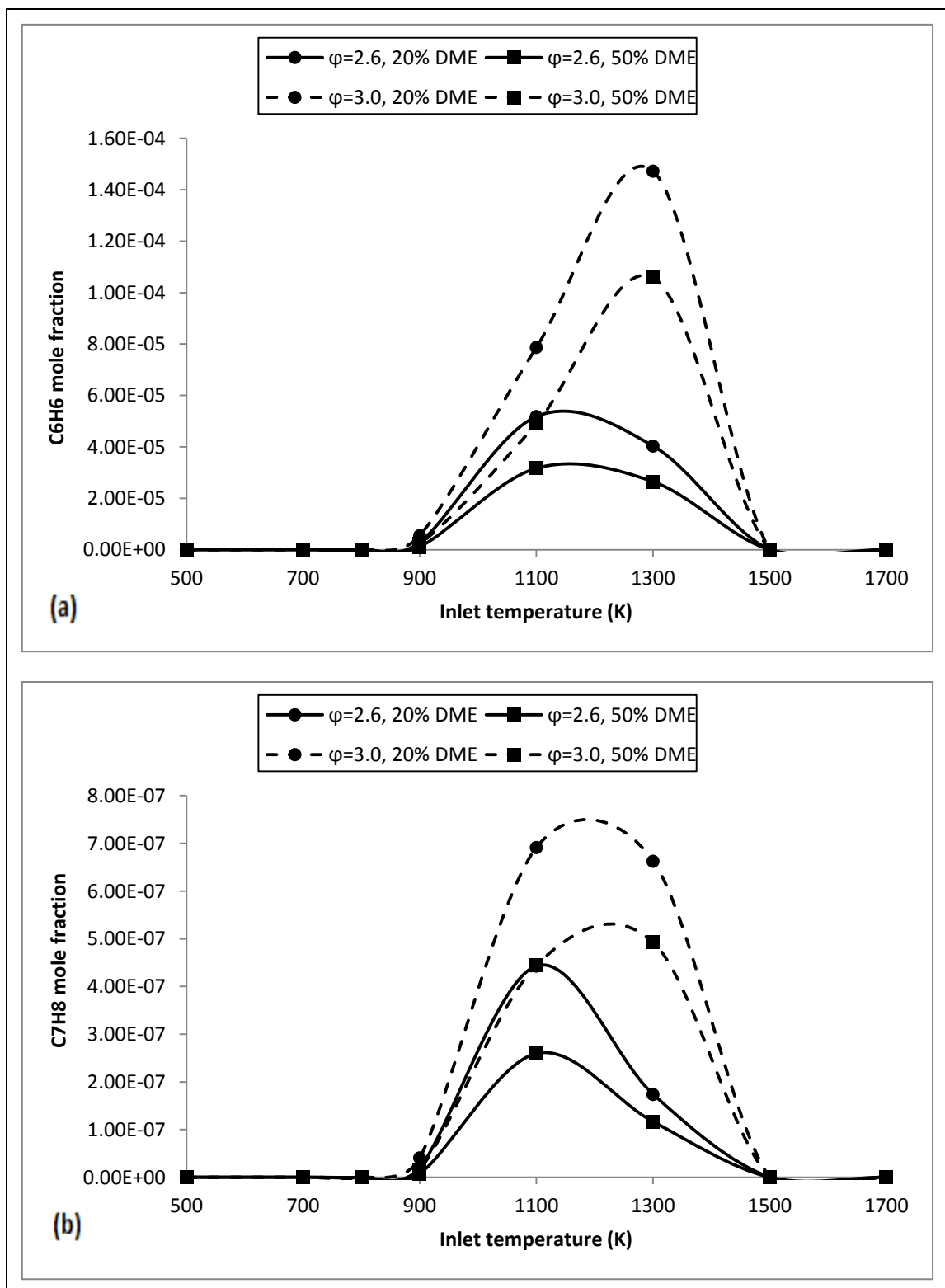


Figure 4.56. Final mole fractions of (a) C<sub>6</sub>H<sub>6</sub> and (b) C<sub>7</sub>H<sub>8</sub> versus reactor inlet temperatures at different equivalence ratios and different concentrations of CH<sub>3</sub>OCH<sub>3</sub>. (P = 1 atm).

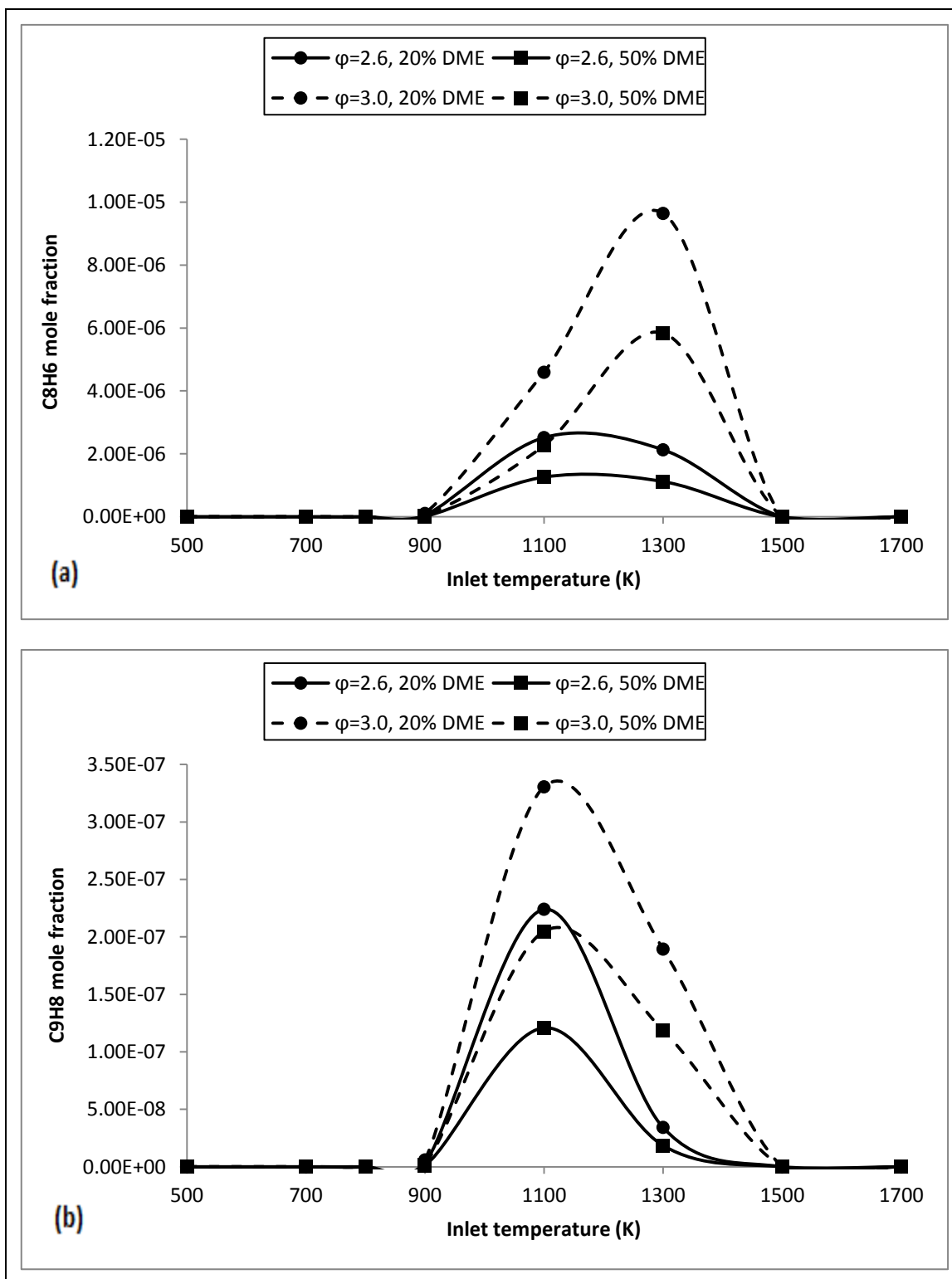


Figure 4.57. Final mole fractions of (a) C<sub>8</sub>H<sub>6</sub> and (b) C<sub>9</sub>H<sub>8</sub> versus reactor inlet temperatures at different equivalence ratios and different concentrations of CH<sub>3</sub>OCH<sub>3</sub>. (P = 1 atm).

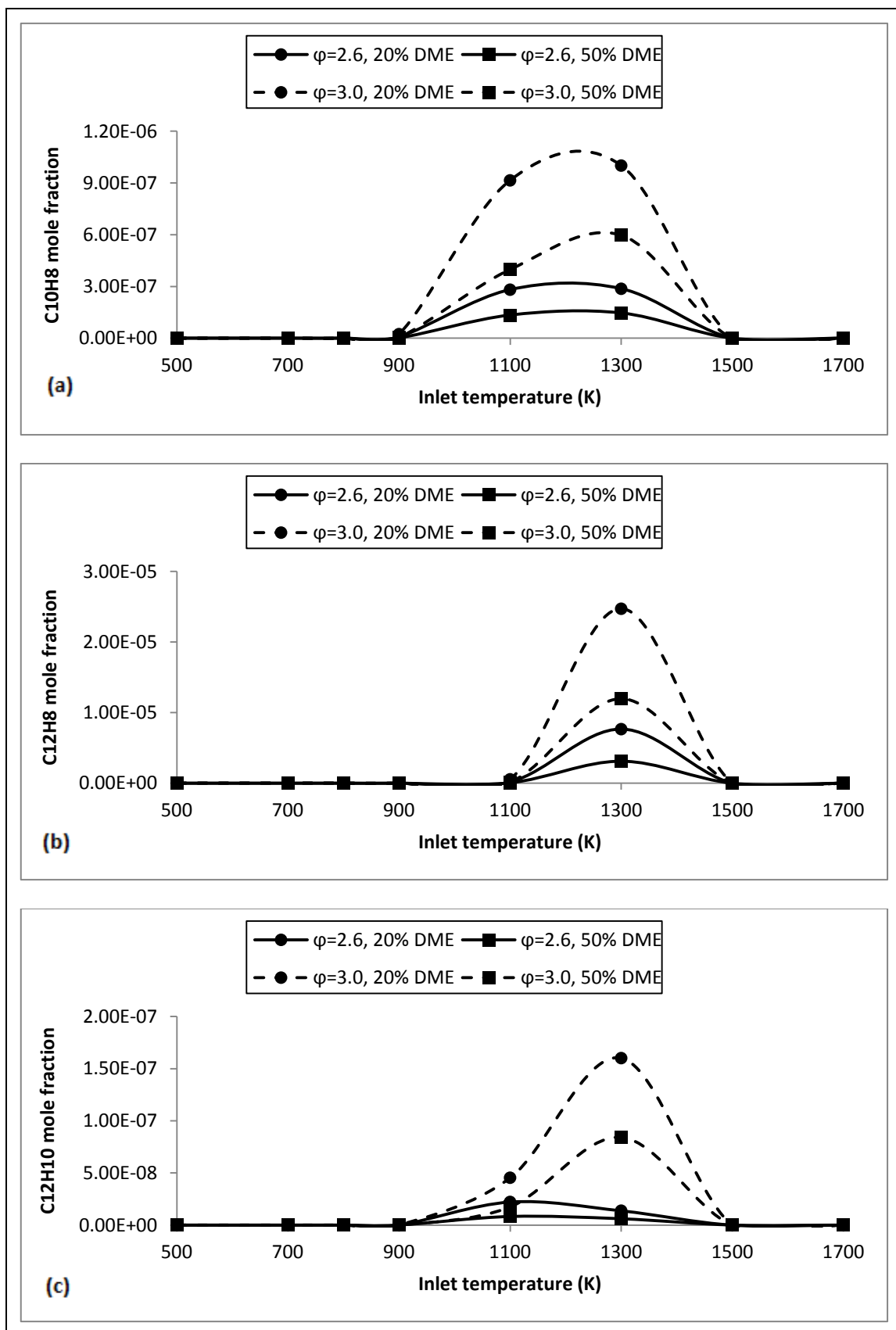


Figure 4.58. Final mole fractions of (a) C<sub>10</sub>H<sub>8</sub> (b) C<sub>12</sub>H<sub>8</sub> and (c) C<sub>12</sub>H<sub>10</sub> versus reactor inlet temperatures at different equivalence ratios and different concentrations of CH<sub>3</sub>OCH<sub>3</sub>. (P = 1 atm).



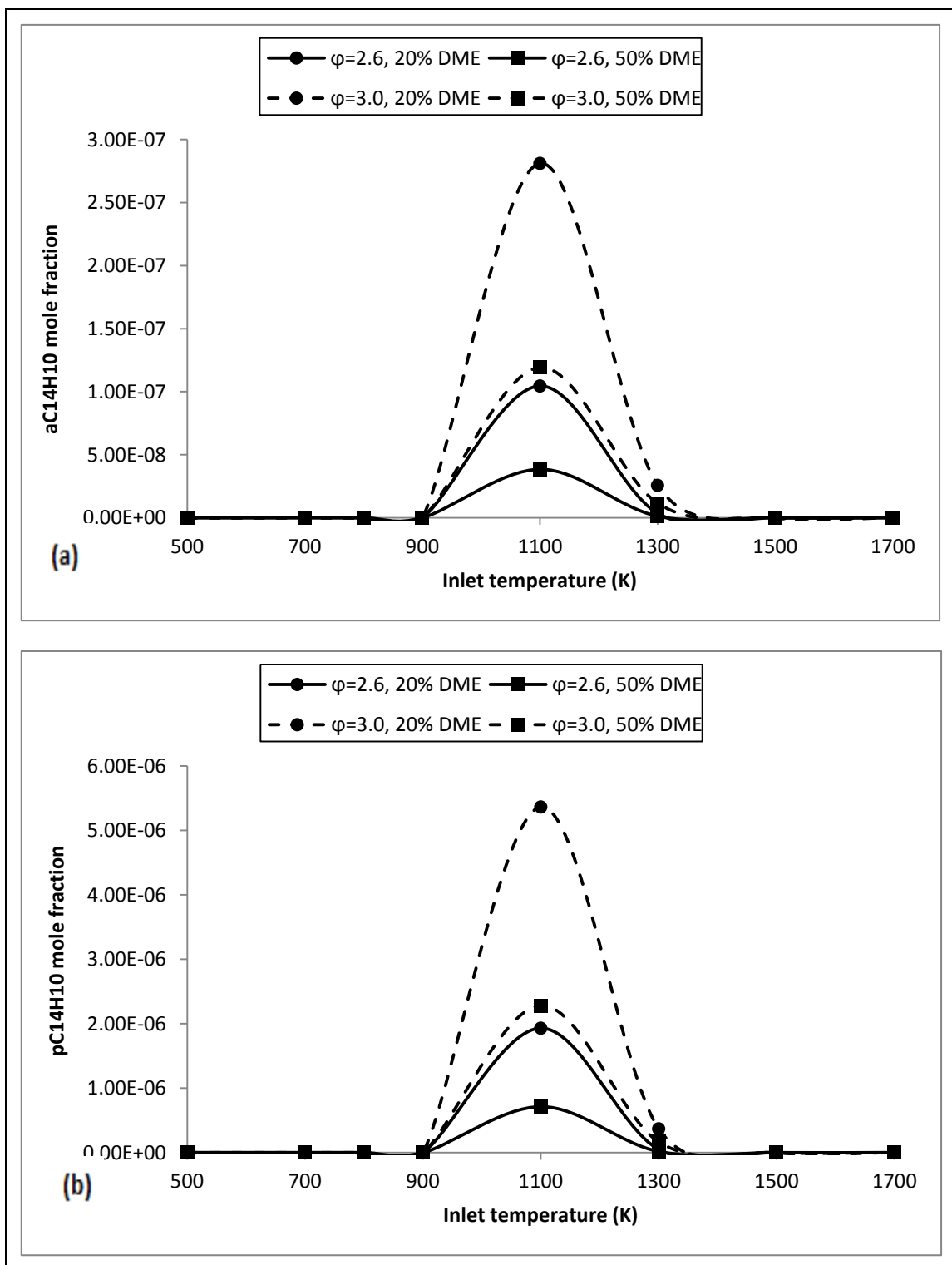


Figure 4.59. Final mole fractions of (a) aC<sub>14</sub>H<sub>10</sub> and (b) pC<sub>14</sub>H<sub>10</sub> versus reactor inlet temperatures at different equivalence ratios and different concentrations of CH<sub>3</sub>OCH<sub>3</sub>. (P = 1 atm).

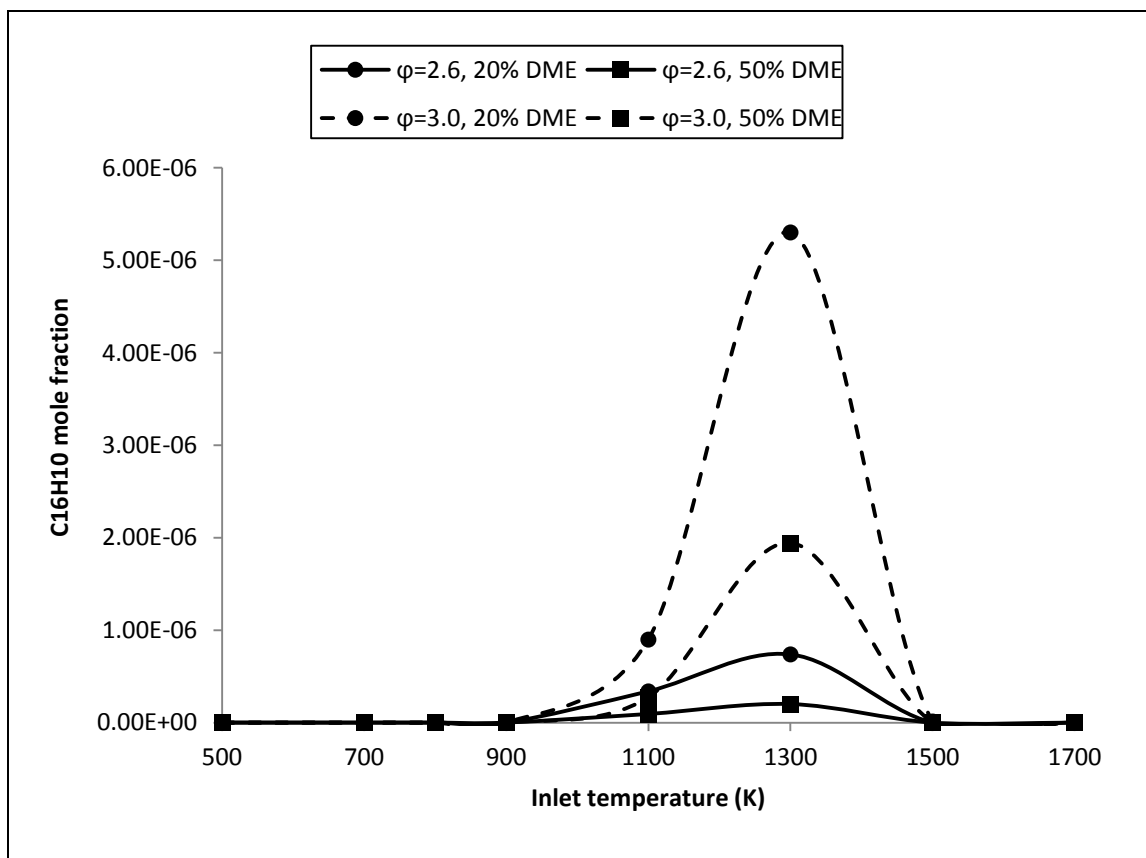


Figure 4.60. Final mole fractions of  $C_{16}H_{10}$  versus reactor inlet temperatures at different equivalence ratios and different concentrations of  $CH_3OCH_3$ . ( $P = 1$  atm).

Figure 4.42 shows the final mole fractions of the fuels,  $C_4H_{10}$  and  $CH_3OCH_3$ , and Figure 4.43 shows the final mole fractions of the oxidizer,  $O_2$ . The overall rate of reaction is again considerably slow for inlet temperatures smaller than 700 K.

Final mole fractions of major products  $CO_2$  and  $CO$  are given in Figure 4.44. It is observed that increasing equivalence ratio slightly decreases the mole fraction of  $CO_2$ . The effect of equivalence ratio on  $CO$  mole fraction is not apparent except at high temperatures, where mole fraction of  $CO$  is slightly increased with increasing equivalence ratio. Previously, Huang et al. (2009) suggested that increasing equivalence ratio increased  $CO$  emissions in DME oxidation.

Final mole fractions of other major products,  $H_2O$  and  $H_2$ , are given in Figure 4.45. Increasing equivalence ratio decreases the mole fraction of  $H_2O$  and increases the mole fraction of  $H_2$  slightly at high temperatures.

Figure 4.46 shows the mole fractions of  $CH_4$ ,  $C_2H_6$ , and  $C_3H_8$ . Increasing equivalence ratio increases mole fractions of these three species.

Figure 4.47 shows the mole fractions of  $\text{CH}_2\text{O}$  and  $\text{C}_2\text{H}_4\text{O}$ . Increasing equivalence ratio does not seem to affect the mole fractions of  $\text{CH}_2\text{O}$  and  $\text{C}_2\text{H}_4\text{O}$  significantly.

Figures 4.48 to 4.54 show the mole fractions of aromatic precursors. Increasing equivalence ratio increases mole fractions of the entire precursor species investigated. Previously it was stated by Cathonnet et al. (1981) that, during the oxidation of *n*-butane, initial  $\text{O}_2$  concentration had very little influence on the formation of  $\text{C}_3\text{H}_6$  but it affected the formation of  $\text{CH}_4$ . Very little change in the mole fraction of  $\text{C}_3\text{H}_6$  and the change in the mole fraction of  $\text{CH}_4$  with the change in equivalence ratio in this study is compatible with the findings of Cathonnet et al. (1981).

Final mole fractions of the aromatic species are given in Figures 4.55 to 4.60. Increasing equivalence ratio also increases mole fractions of the entire aromatics investigated. This result is expected since mole fractions of entire precursors investigated are also increased with increasing equivalence ratio. For some of the aromatic species, such as  $\text{C}_6\text{H}_6$ ,  $\text{C}_7\text{H}_8$ ,  $\text{C}_8\text{H}_6$ ,  $\text{C}_{10}\text{H}_8$ , and  $\text{C}_{12}\text{H}_{10}$ , changing equivalence ratio changes the temperatures at which the maximum mole fractions of these species are observed.

### **4.3. The Formation Pathways of the Aromatic Species in *n*-Butane and *n*-Butane/DME Oxidations**

The formation of the first aromatic ring and the consequent formations of higher aromatic species are attributed to the reactions of various minor species, in the literature; and the formations of these precursor species in *n*-butane and *n*-butane/DME oxidations were analyzed in Sections 4.1 and 4.2. In this section, the roles of these species were tried to be identified for the neat oxidation of *n*-butane and for the oxidation of *n*-butane/DME mixture.

First, the concentration profiles of these species were compared with the concentration profiles of the first ring  $\text{C}_6\text{H}_6$  and with other aromatics. The similarities and the differences between the cases of pure *n*-butane and *n*-butane/DME oxidations were investigated. This analysis was performed at atmospheric pressure ( $P = 1 \text{ atm}$ ) and for an inlet temperature of  $T_0 = 1100 \text{ K}$ . The inlet temperature was selected having regard to the results in Section 4.2.1, where the entire precursors and aromatics exist in

observable amounts. The equivalence ratio was selected as  $\phi = 2.6$ . The ratio of n-butane to DME was 1:1 in the n-butane/DME mixture. The profiles of all species are given for mole fractions above the order of  $10^{-8}$ .

Figures 4.61 through 4.63 show the concentration profiles of the precursors and the first aromatic ring  $C_6H_6$  against reactor distance, for the neat oxidation of n-butane. It can be seen that the formation of  $C_6H_6$  starts around the reactor distances where the consumptions of  $C_2H_4$  (Figure 4.61.a),  $aC_3H_4$ ,  $pC_3H_4$ ,  $C_3H_6$  (Figure 4.61.b), 1,3- $C_4H_6$ , (Figure 4.62.a),  $C_4H_8-1$  and  $C_4H_8-2$  (Figure 4.62.b) start. This indicates that  $C_6H_6$  is formed as a result of the reactions of these species. The consumptions of  $C_2H_2$ ,  $C_3H_3$ ,  $C_4H_2$ ,  $C_4H_4$ , and  $c-C_5H_6$  start at longer distances.

Figure 4.64 shows the concentration profiles of aromatic species in the neat oxidation of n-butane. One-ring aromatics are given in Figure 4.64.a, two-ring PAHs in Figure 4.64.b, and three- and four-rings in Figure 4.64.c. The concentration profile of the cyclic aromatic species  $C_6H_5$  is not shown because the formation of this species does not exceed the detectable level at any point throughout the reactor. The formations of all aromatic species shown in Figure 4.64 are at the reactor distances beyond the point where the formation of  $C_6H_6$  starts. In general, the formations of smaller ring aromatics occur at shorter distances, and the larger ones at the larger distances of the reactor. However, the formation of the two-ring  $C_{12}H_{10}$  is observed at the largest reactor distance, among the aromatic species observed.

The formations of  $C_{12}H_8$  and  $pC_{14}H_{10}$  start around the point where the consumption of the precursor species  $C_2H_2$  starts. This might be implying that the formations of these two PAHs are related to the reactions of  $C_2H_2$  with low molecular weight aromatic rings. When the concentration profile of  $C_4H_2$  is investigated (Figure 4.62) in the neat oxidation of n-butane, it can be observed that the consumption of this species starts at a reactor distance where the formations of all the aromatic species investigated have already started. This implies that  $C_4H_2$  may be playing role in the formations of larger PAHs that were not investigated in this study.

Figures 4.65 through 4.67 show the concentration profiles of the precursor species and  $C_6H_6$  against reactor distance, for the oxidation of n-butane/DME mixture.

When compared to the graphs given for the neat oxidation of n-butane, it can be observed that the same precursor species ( $C_2H_4$ ,  $aC_3H_4$ ,  $pC_3H_4$ ,  $C_3H_6$ , 1,3- $C_4H_6$ ,  $C_4H_8-1$  and  $C_4H_8-2$ ) are again related to the formation of the first aromatic ring  $C_6H_6$ . Similar to

neat n-butane oxidation, the consumptions of  $C_2H_2$ ,  $C_3H_3$ ,  $C_4H_2$ ,  $C_4H_4$ , and *c*- $C_5H_6$  start after the point  $C_6H_6$  formation starts.

Figure 4.68 shows the concentration profiles of the one-, two-, three-, and four-ring aromatic species for the oxidation of n-butane/DME mixture. The profiles are similar to those of neat n-butane oxidation, but are shifted towards longer reactor distances. The concentration profile of  $C_{12}H_{10}$  is not shown in this case, because the formation of this PAH does not reach observable levels. Also, the formations of all the aromatics and PAHs are lowered in this case, compared to the neat oxidation of n-butane. The relationship between the consumption of  $C_2H_2$  and the formations of  $C_{12}H_8$  and *p* $C_{14}H_{10}$  can also be observed in the oxidation of n-butane/DME, similar to the neat oxidation of n-butane.

The role of  $C_2H_2$  in the formations of large aromatics and PAHs was already revealed in the literature and was explained with H-abstraction/ $C_2H_2$ -addition mechanism (Bockhorn et al., 1983; Frenklach et al., 1983; Richter and Howard, 2000). But,  $C_2H_2$  is also known to play a role in the formation of the first aromatic ring (Badger et al., 1960; Homann, 1967; Bockhorn et al., 1983; Colket, 1986; Frenklach and Warnatz, 1987; Richter and Howard, 2000).

Similarly, the role of  $C_3H_3$  in the formations of large PAHs was suggested by Stein et al. (1991) and D'Anna and Violi (1998). But,  $C_3H_3$  was also suggested to play role in the formation of  $C_6H_6$  by Miller and Melius (1992), Hidaka et al. (1989), Stein et al. (1991), Marinov et al. (1996), and Dagaut and Cathonnet (1998).

The roles of  $C_4H_2$  and  $C_4H_4$  in the formations of large PAHs were suggested by Cole et al. (1984), and the role of *c*- $C_5H_6$  was suggested by Dean (1990).

In order to verify and extend the results of the investigation of concentration profiles of the precursors and aromatics, a “**Reaction Path Analysis**” was carried out for the identification of the precursor species that play the major role in the formation of the first aromatic ring  $C_6H_6$ . This analysis ranks the elementary reactions that take part in the formation of a particular species according to their reaction rates and determines the most important elementary reactions. The most important pathways leading to the formation of this particular species are shown in a reaction path diagram. Reaction pathway analysis was performed for the oxidations of neat n-butane and n-butane/DME mixture in order to identify the important pathways in the formation of  $C_6H_6$  from n-butane. The same operating conditions were used, i.e.  $T = 1100\text{ K}$ ,  $P = 1\text{ atm}$ , and  $\phi = 2.6$ . The ratio of n-butane to DME in the n-butane/DME mixture was 1:1.

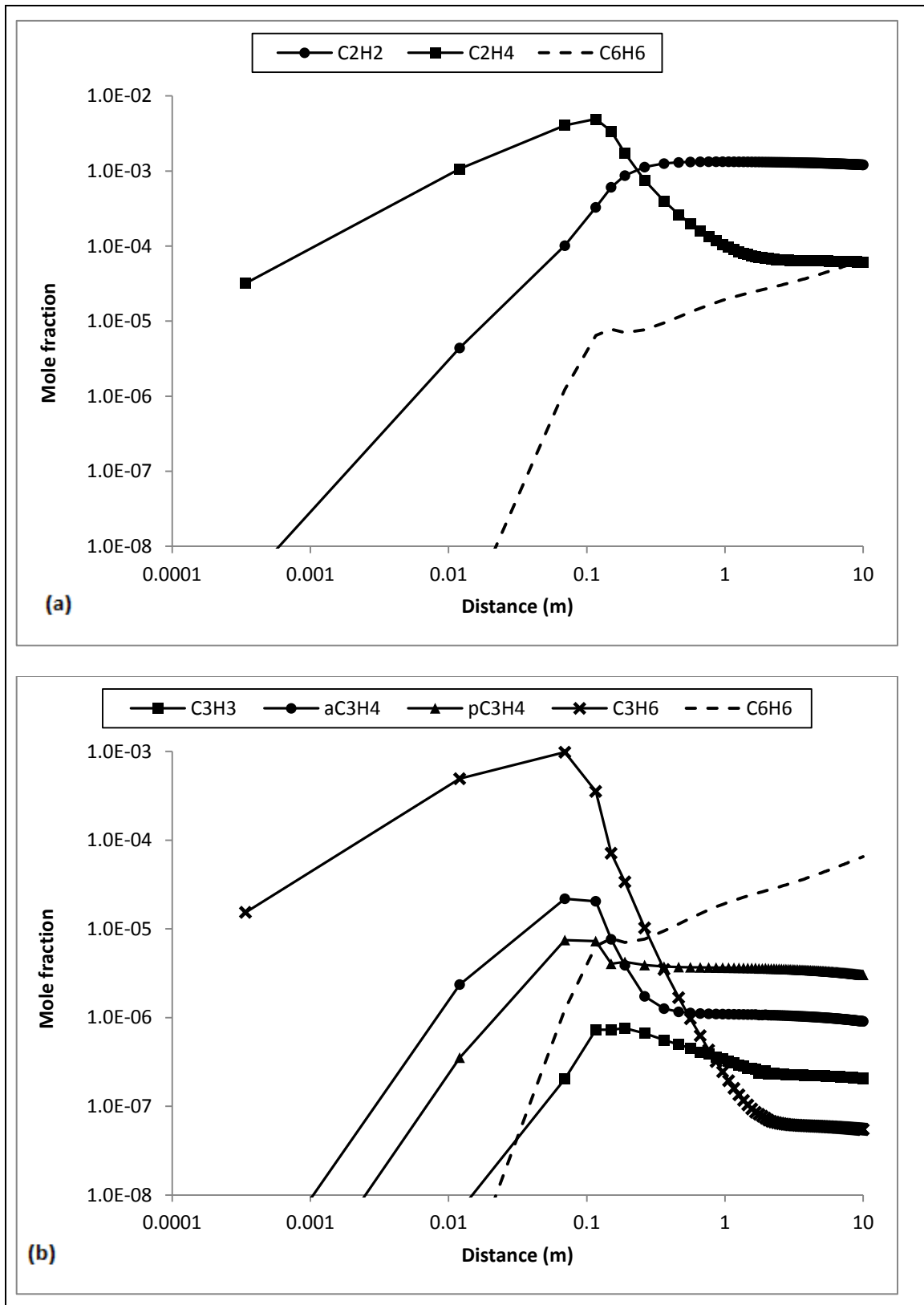


Figure 4.61. Concentration profiles of (a)  $C_6H_6$  and  $C_2$  precursor species  $C_2H_2$  and  $C_2H_4$ , and (b)  $C_6H_6$  and  $C_3$  precursor species  $C_3H_3$ ,  $aC_3H_4$ ,  $pC_3H_4$ , and  $C_3H_6$ , for the neat oxidation of n-butane. ( $T_0 = 1100 K$ ,  $P = 1 atm$ , and  $\phi = 2.6$ ). (x- and y- axes are shown in logarithmic scale).

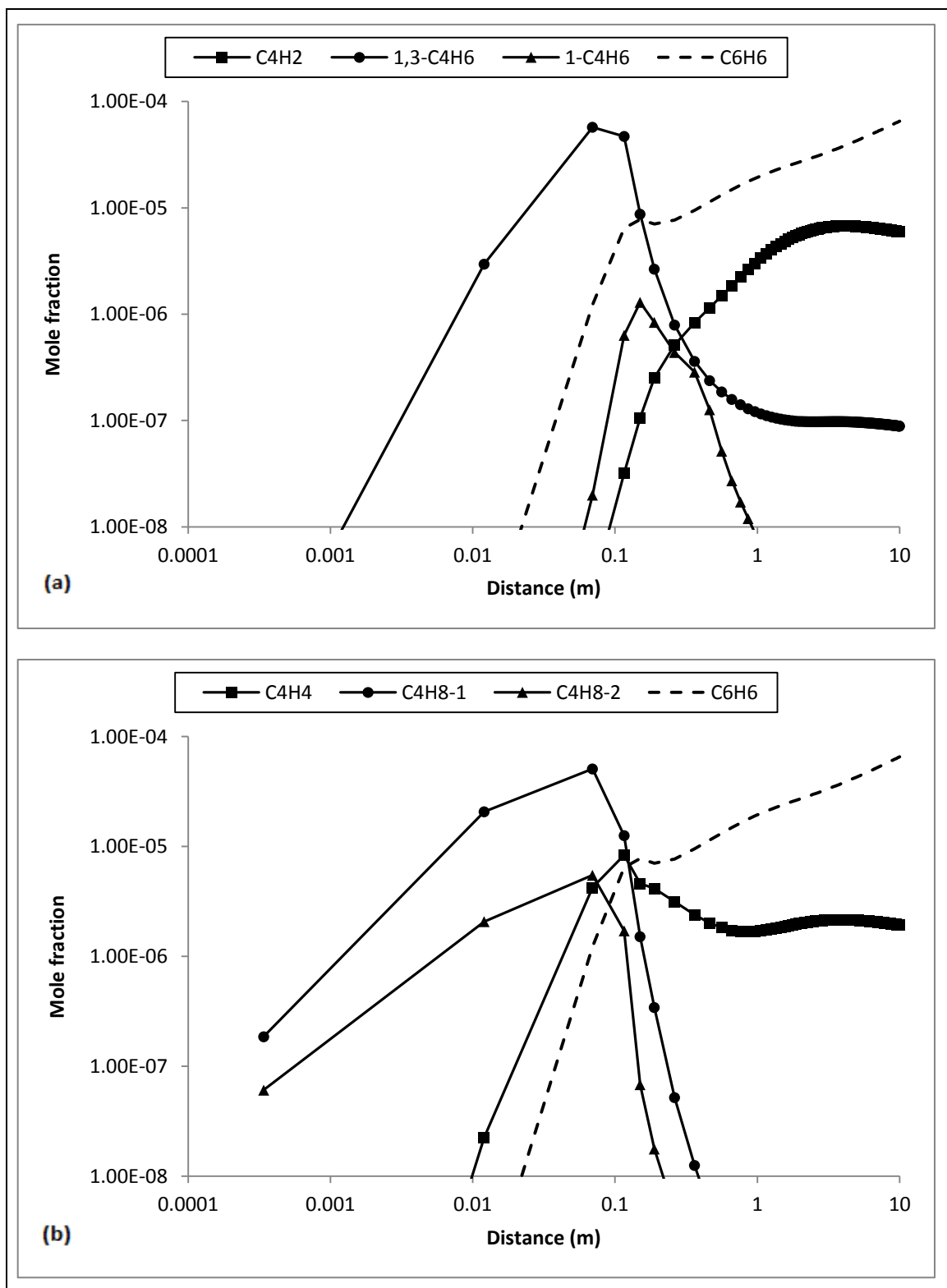


Figure 4.62. Concentration profiles of (a)  $C_6H_6$  and  $C_4$  precursor species  $C_4H_2$ , 1,3- $C_4H_6$  and 1- $C_4H_6$ , and (b)  $C_6H_6$  and  $C_4$  precursor species  $C_4H_4$ ,  $C_4H_8-1$ , and  $C_4H_8-2$ , for the neat oxidation of n-butane. ( $T_0 = 1100 K$ ,  $P = 1 atm$ , and  $\phi = 2.6$ ). (x- and y- axes are shown in logarithmic scale).

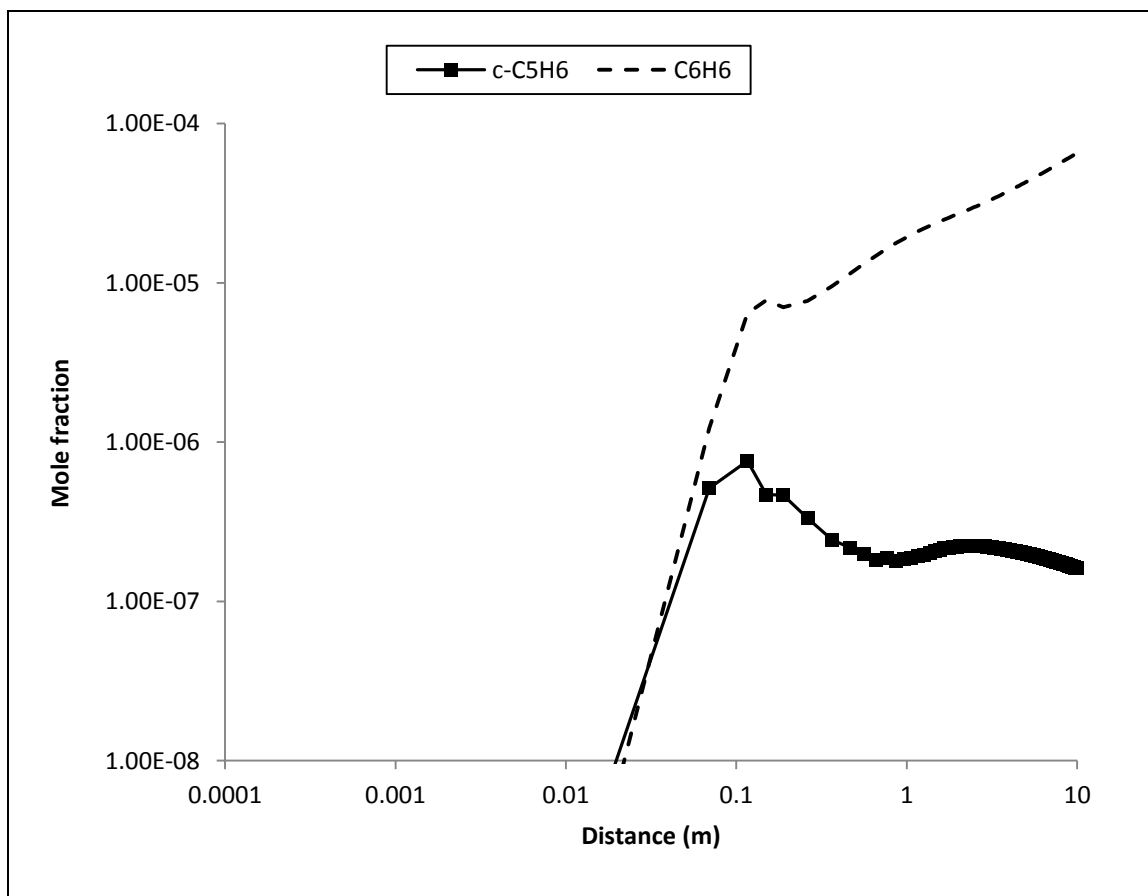


Figure 4.63. Concentration profiles of  $C_6H_6$  and  $C_5$  precursor species  $c-C_5H_6$ , for the neat oxidation of n-butane. ( $T_0 = 1100 K$ ,  $P = 1 atm$ , and  $\phi = 2.6$ ). (x- and y- axes are shown in logarithmic scale).



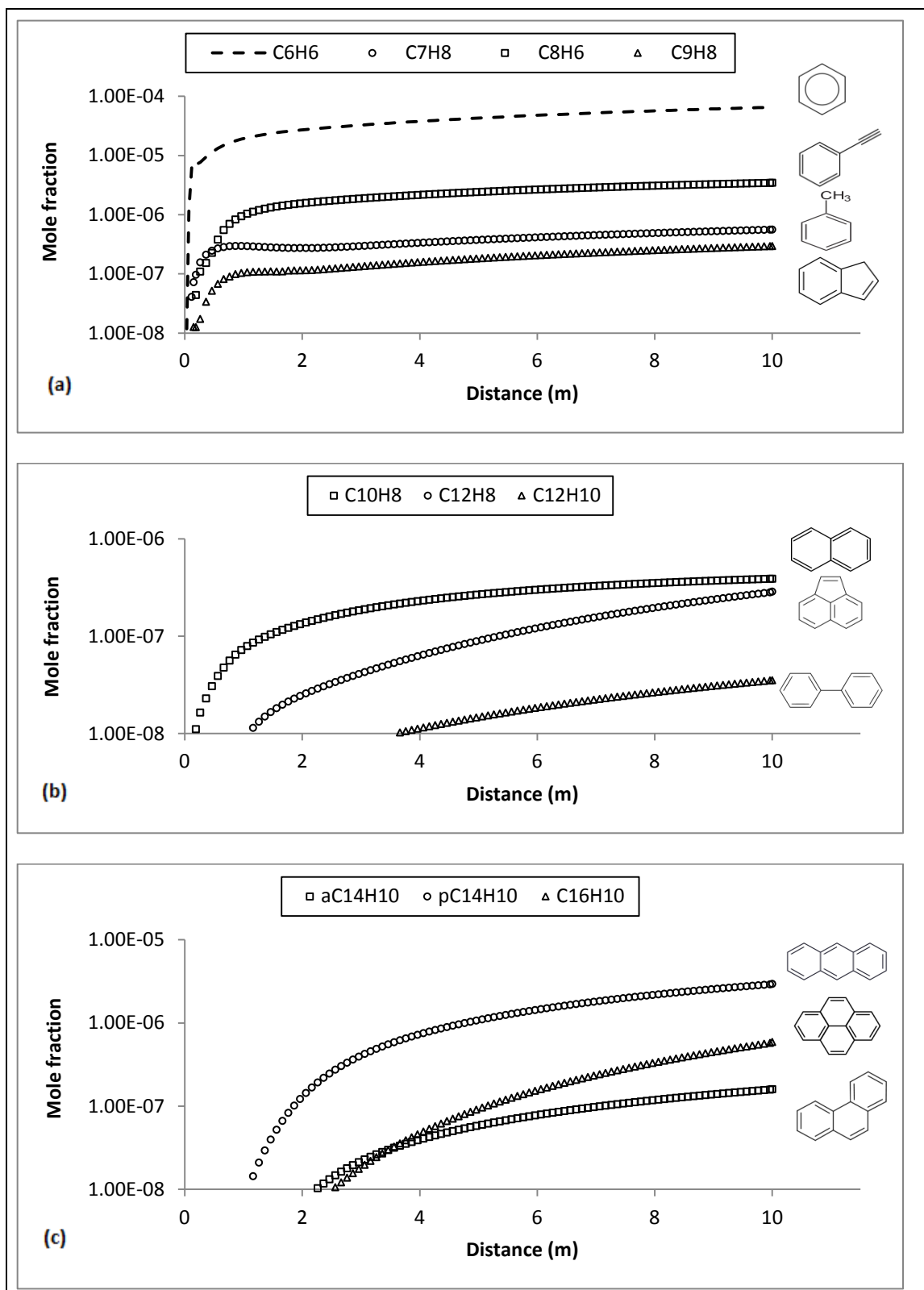


Figure 4.64. Concentration profiles of (a) one-ring aromatics (b) two-ring aromatics and (c) three- and four-ring aromatics, for the neat oxidation of n-butane. ( $T_0 = 1100\text{ K}$ ,  $P = 1\text{ atm}$ , and  $\phi = 2.6$ ). (y-axes are shown in logarithmic scale).

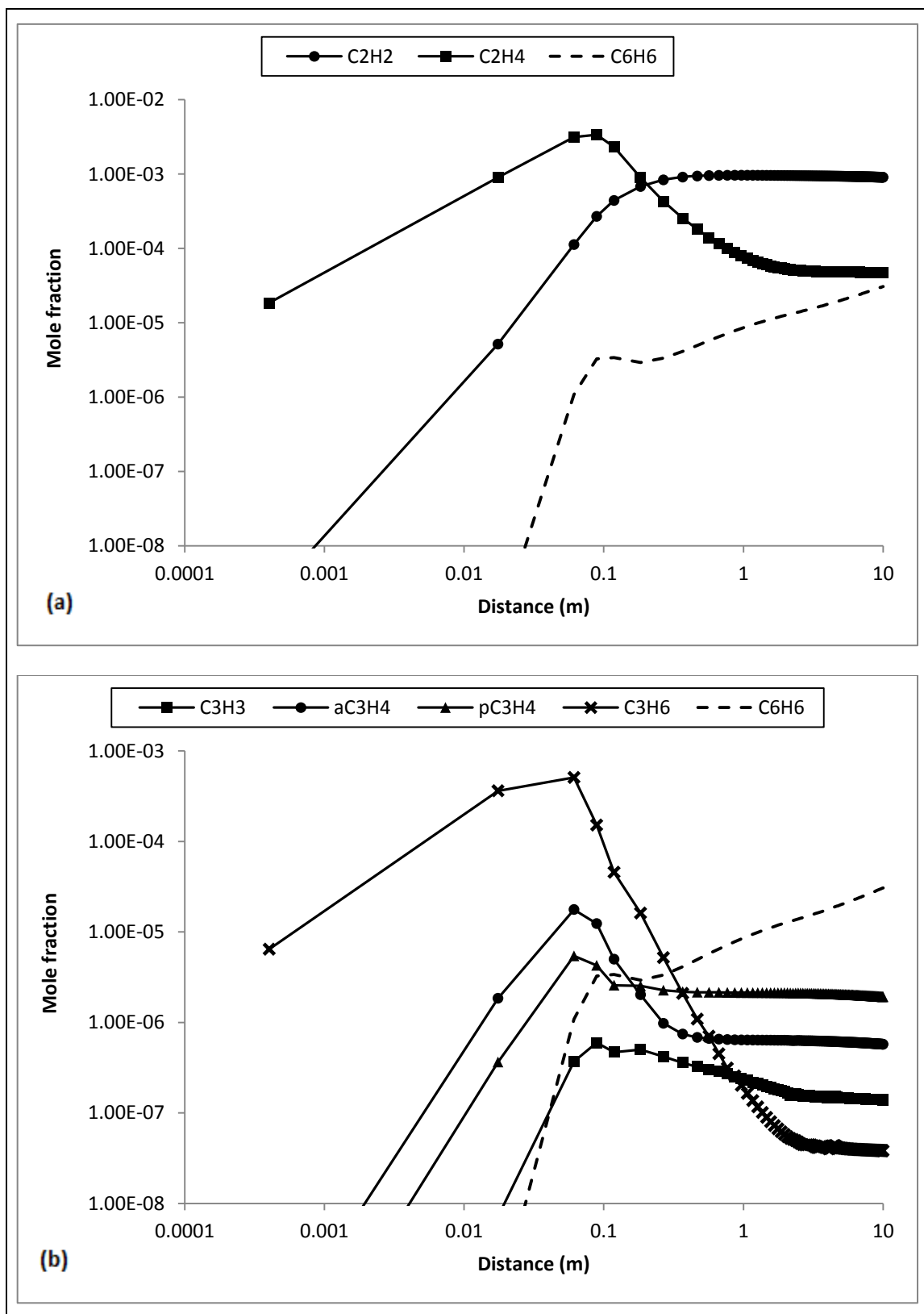


Figure 4.65. Concentration profiles of (a)  $C_6H_6$  and  $C_2$  precursor species  $C_2H_2$  and  $C_2H_4$ , and (b)  $C_6H_6$  and  $C_3$  precursor species  $C_3H_3$ ,  $aC_3H_4$ ,  $pC_3H_4$ , and  $C_3H_6$ , for the oxidation of n-butane/DME mixture. ( $X_{C_4H_{10}}/X_{CH_3OCH_3} = 1$ ,  $T_0 = 1100$  K,  $P = 1$  atm, and  $\phi = 2.6$ ). (x- and y- axes are shown in logarithmic scale).

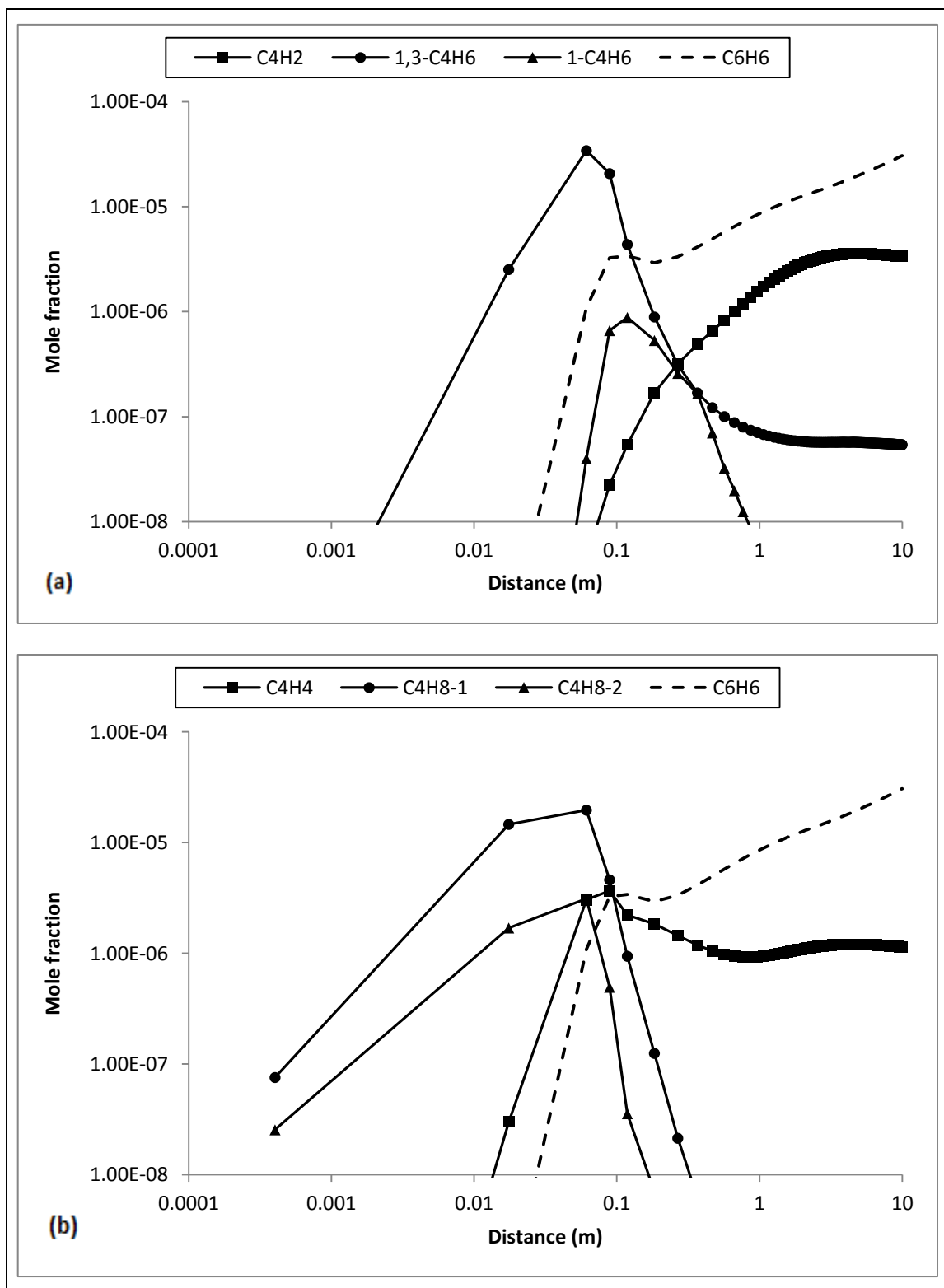


Figure 4.66. Concentration profiles of (a)  $C_6H_6$  and  $C_4$  precursor species  $C_4H_2$ , 1,3- $C_4H_6$  and 1- $C_4H_6$ , and (b)  $C_6H_6$  and  $C_4$  precursor species  $C_4H_4$ ,  $C_4H_8-1$ , and  $C_4H_8-2$ , for the oxidation of n-butane/DME mixture. ( $X_{C_4H_{10}}/X_{CH_3OCH_3} = 1$ ,  $T_0 = 1100$  K,  $P = 1$  atm, and  $\phi = 2.6$ ). (x- and y- axes are shown in logarithmic scale).

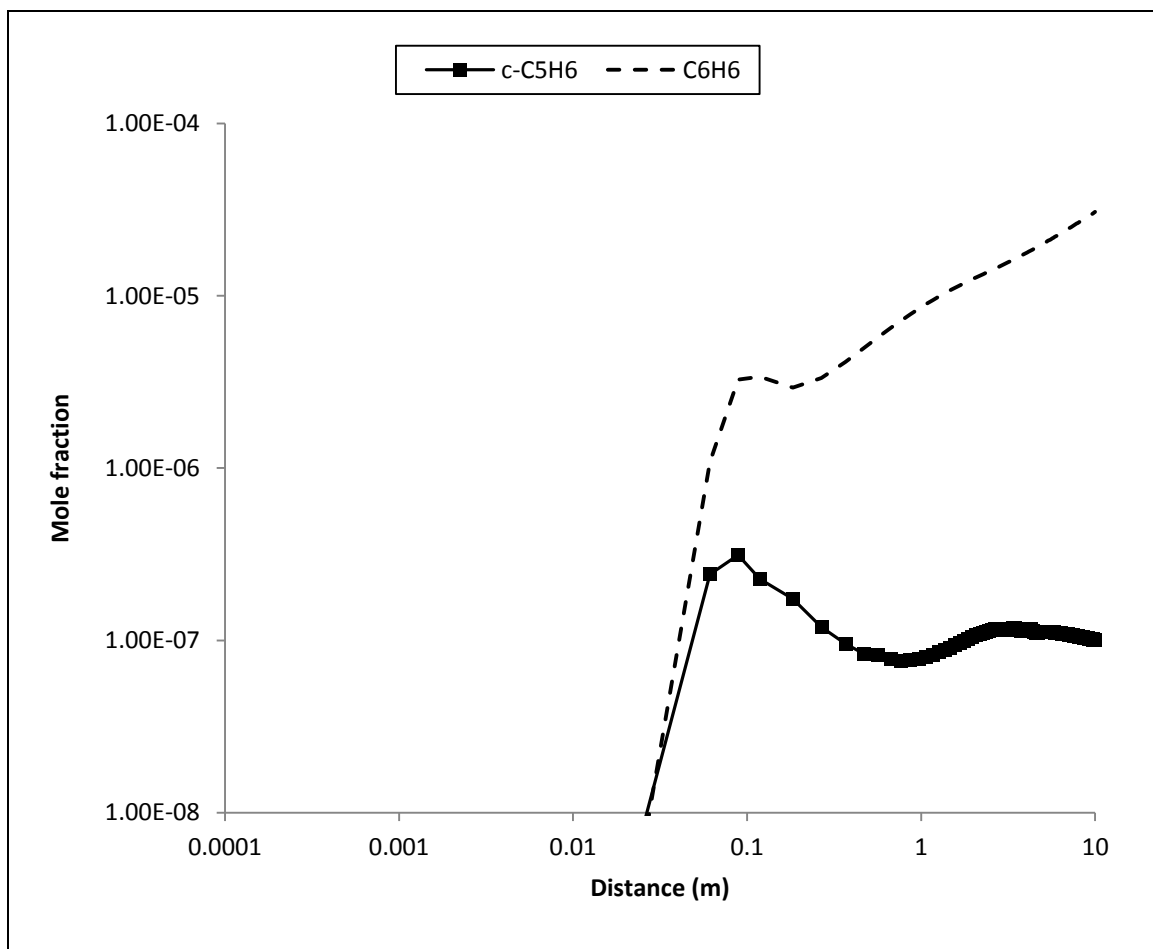


Figure 4.67. Concentration profiles of  $C_6H_6$  and  $C_5$  precursor species  $c-C_5H_6$ , for the oxidation of n-butane/DME mixture. ( $X_{C_4H_{10}}/X_{CH_3OCH_3} = 1$ ,  $T_0 = 1100\text{ K}$ ,  $P = 1\text{ atm}$ , and  $\phi = 2.6$ ). (x- and y- axes are shown in logarithmic scale).

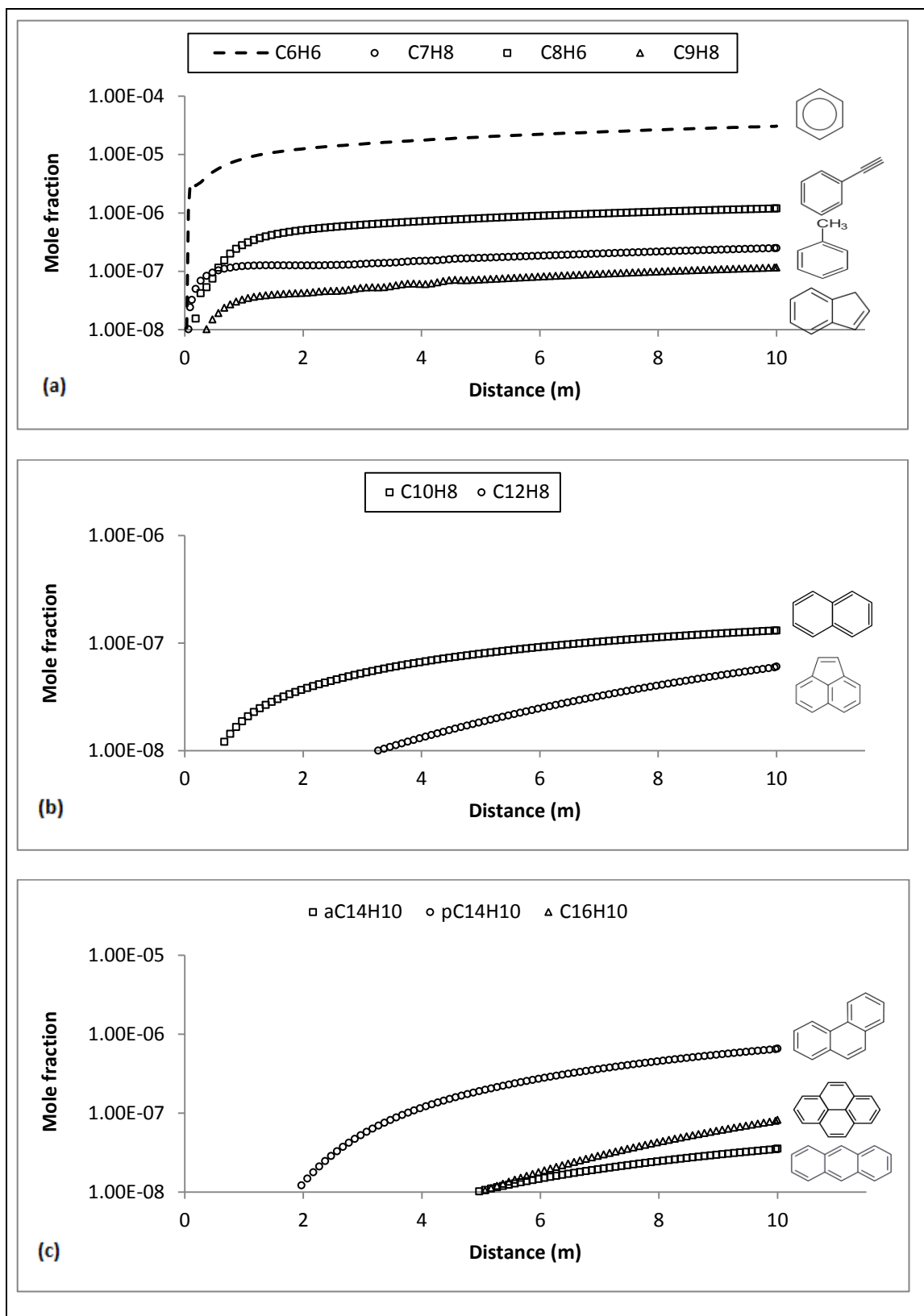


Figure 4.68. Concentration profiles of (a) one-ring aromatics (b) two-ring aromatics and (c) three- and four-ring aromatics, for the oxidation of n-butane/DME mixture. ( $X_{C_4H_{10}}/X_{CH_3OCH_3} = 1$ ,  $T_0 = 1100\text{ K}$ ,  $P = 1\text{ atm}$ , and  $\phi = 2.6$ ). (y-axes are shown in logarithmic scale).

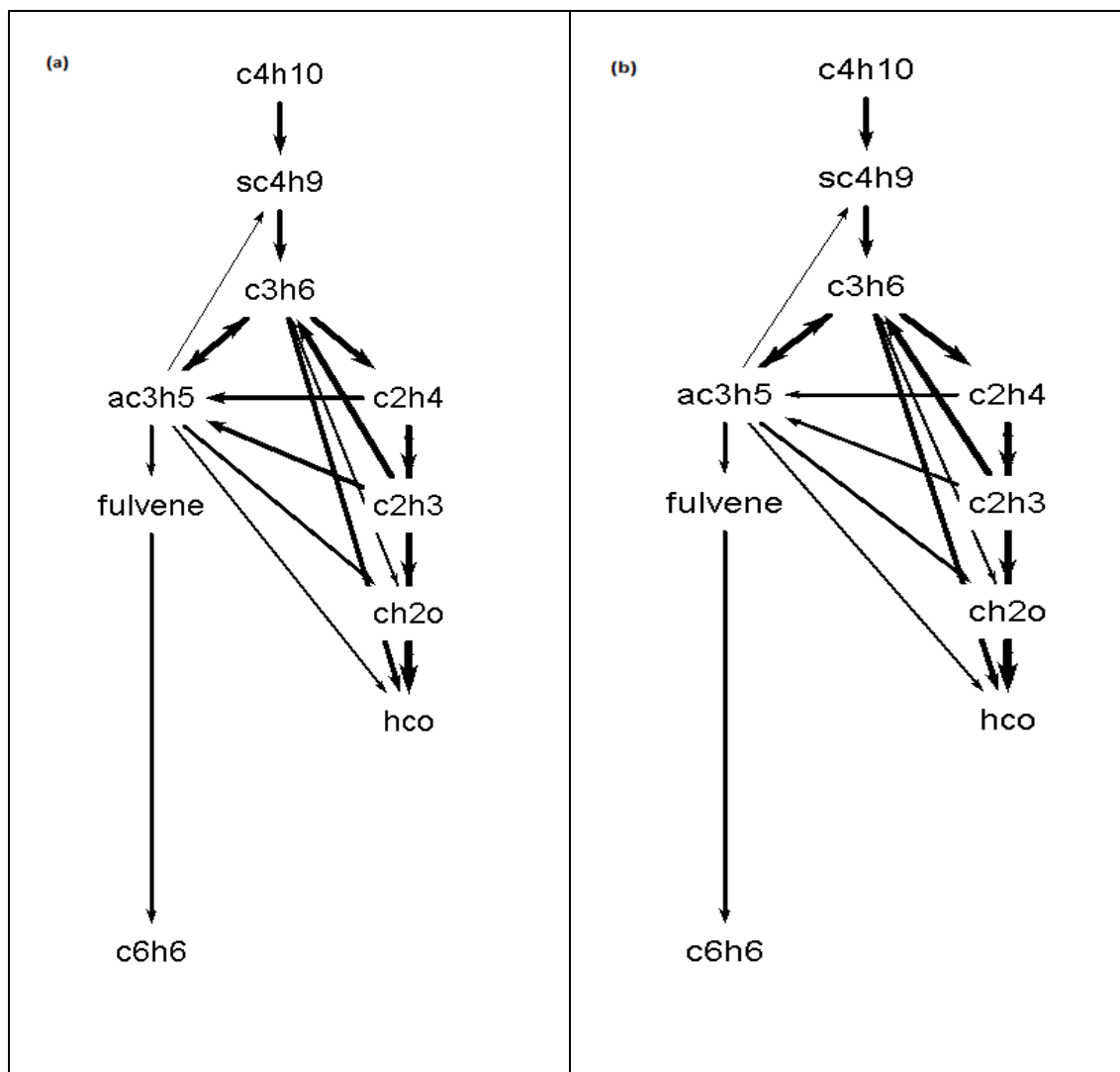


Figure 4.69. Main formation paths of  $C_6H_6$  from  $C_4H_{10}$  during the oxidations of (a) neat  $C_4H_{10}$  and (b)  $C_4H_{10}/CH_3OCH_3$  mixture at  $T=1100K$  ( $P = 1 atm$ , and  $\phi = 2.6$ ). Thicknesses of the arrows show the importance of the pathways.



The resulting path diagrams are given in Figure 4.69 for neat oxidation of n-butane (Figure 4.69.a) and the oxidation of n-butane/DME mixture (Figure 4.69.b). It is seen that the main pathways and the main precursor species are the same for the oxidations of n-butane and n-butane/DME mixture. The precursor species playing the most important roles in the formation of  $C_6H_6$  are  $C_3H_6$ ,  $C_2H_4$ ,  $aC_3H_5$  (allyl radical) and fulvene ( $C_6H_6$ ) for the oxidations of both fuel mixtures. So it can be said that the formation pathways of the first aromatic species are the same for the oxidation of n-butane, with or without DME added. At an intermediate temperature ( $T = 1100K$ ), addition of DME changes the amount of the first aromatic species formed but does not affect the pathways leading to its formation.

Reaction pathway analysis was also performed for two other temperatures values. A lower ( $T = 950K$ ) and a higher temperature ( $T = 1350K$ ) value were selected, and the remaining conditions were kept constant. The formation pathways were identified for the oxidations of neat n-butane and n-butane/DME mixture.

The pathway diagrams obtained at  $T = 950K$  are given in Figure 4.70. It can be seen that, at this temperature, the main precursor species leading to the formation of  $C_6H_6$  is  $C_3H_6$ ,  $aC_3H_5$ , and fulvene. Similar to the previous case, the pathways are almost identical for the oxidation of neat n-butane and the oxidation of n-butane/DME mixture. The only difference is, in the case of n-butane/DME mixture, the path leading to the formation of  $C_6H_6$  becomes weaker compared to the case of neat n-butane. Instead, the path leading to the formation of  $CH_2O$  becomes more dominant.

The reaction path diagrams obtained at  $T = 1350K$  are given in Figure 4.71. It can be seen that, at this temperature the main pathways of  $C_6H_6$  formation for the oxidations of neat n-butane and n-butane/DME mixture differ from each other. The main precursor species important in the formation of  $C_6H_6$  are  $C_3H_6$ ,  $C_2H_4$ ,  $C_2H_2$ , and  $C_3H_3$  for the oxidation of n-butane. In case of n-butane/DME mixture, the role of  $C_2H_2$  disappears, and the roles of  $aC_3H_4$  and  $aC_3H_5$  become important. It is also observed that in case of neat n-butane oxidation, formation of CO is an important pathway, but this pathway disappears in case of n-butane/DME oxidation. Also, it is seen that the formation of  $CH_2O$  does not occur at this temperature, which is observed at lower temperatures.

To summarize,  $C_3H_6$  is an important precursor of  $C_6H_6$  formation at the entire temperature range investigated. Other important precursor species observed at different temperatures are  $C_2H_4$ ,  $C_3H_3$ ,  $C_2H_2$ ,  $aC_3H_4$ ,  $aC_3H_5$ , and fulvene. The main pathways



leading to the formation of the first aromatic ring change with changing temperature. Addition of DME to n-butane oxidation affects these pathways at high temperature ranges.

#### 4.4. Skeletal Mechanism for n-Butane/DME Oxidation

After identification of the important pathways and species in the formations of the main oxidation products from n-butane/DME mixture, the detailed chemical kinetic mechanism used was reduced into a skeletal mechanism, taking these findings into consideration. The contribution coefficients of the elementary reactions to the formations and destructions of important reaction products were calculated. After normalization of these contribution coefficients, a threshold value needed to be specified. Various threshold values were tested. Each threshold value resulted in a skeletal mechanism with different number of total elementary reactions. These threshold values and the resulting total numbers of elementary reactions are shown in Figure 4.72.

As it can be seen from the figure, larger threshold values result in smaller number of elementary reactions, thus simpler skeletal mechanisms. However, it is important that this small number of total reactions represents the overall reaction accurately. Therefore, the resulting skeletal mechanisms were tested in accuracy, and the largest threshold value that produced an accurate set of elementary reactions was selected. This threshold value was  $\varepsilon = 0.005$ . The resulting skeletal mechanism consisted of 186 elementary reactions with 102 chemical species. Comparing to the detailed mechanism, the total number of reactions were reduced by about 80%. The skeletal mechanism produced is given Appendix B.

The accuracy of the developed skeletal mechanism was tested with comparison to the literature. The results obtained using the skeletal mechanism were compared to the results of Yoon et al. (2008), which were also used in the validation of the detailed mechanism. Mole fractions of  $\text{CH}_3$  and  $\text{C}_2\text{H}_2$  were calculated using the skeletal mechanism and compared with the findings of Yoon et al. (2008) for the oxidations of  $\text{CH}_4/\text{DME}$  and  $\text{C}_2\text{H}_6/\text{DME}$  mixtures. The results of this comparison are given in Figure 4.73. It can be observed that the orders and the trends of the mole fraction profiles of  $\text{CH}_3$  and  $\text{C}_2\text{H}_2$  are successfully predicted by the skeletal mechanism both for the  $\text{CH}_4/\text{DME}$  oxidation and the  $\text{C}_2\text{H}_6/\text{DME}$  oxidation.

The results of the skeletal mechanism were also compared with the results of the detailed mechanism. Mole fraction profiles of some species against inlet temperature were reproduced with the skeletal mechanism and compared with the previously obtained mole fraction profiles. The results of these comparisons are given in Figure 4.74. It can be seen that skeletal mechanism predicts the mole fractions of  $C_3H_3$  and  $C_{16}H_{10}$  quite well but it slightly underpredicts the mole fractions of  $C_2H_2$  and  $C_6H_6$ .

It can be said that the skeletal mechanism developed shows satisfactory accuracy and it can be used in complex multidimensional oxidation models of n-butane/DME oxidation without loss of accuracy.

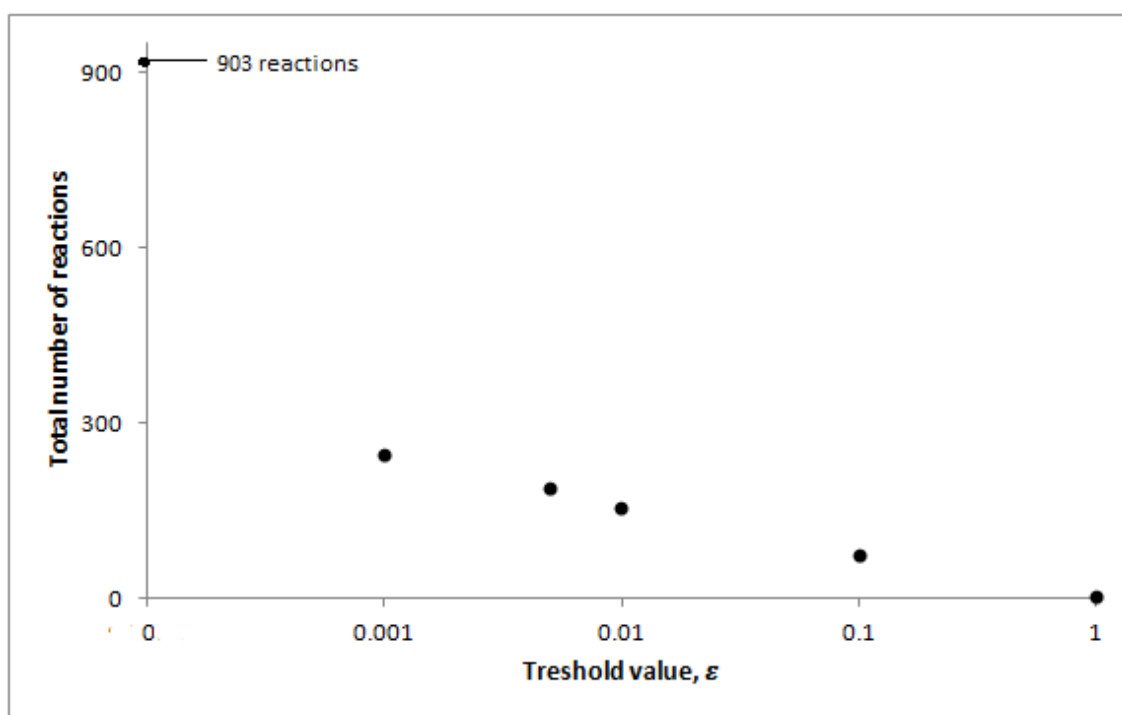


Figure 4.72. Total number of elementary reactions for different threshold values of normalized reaction contribution coefficients

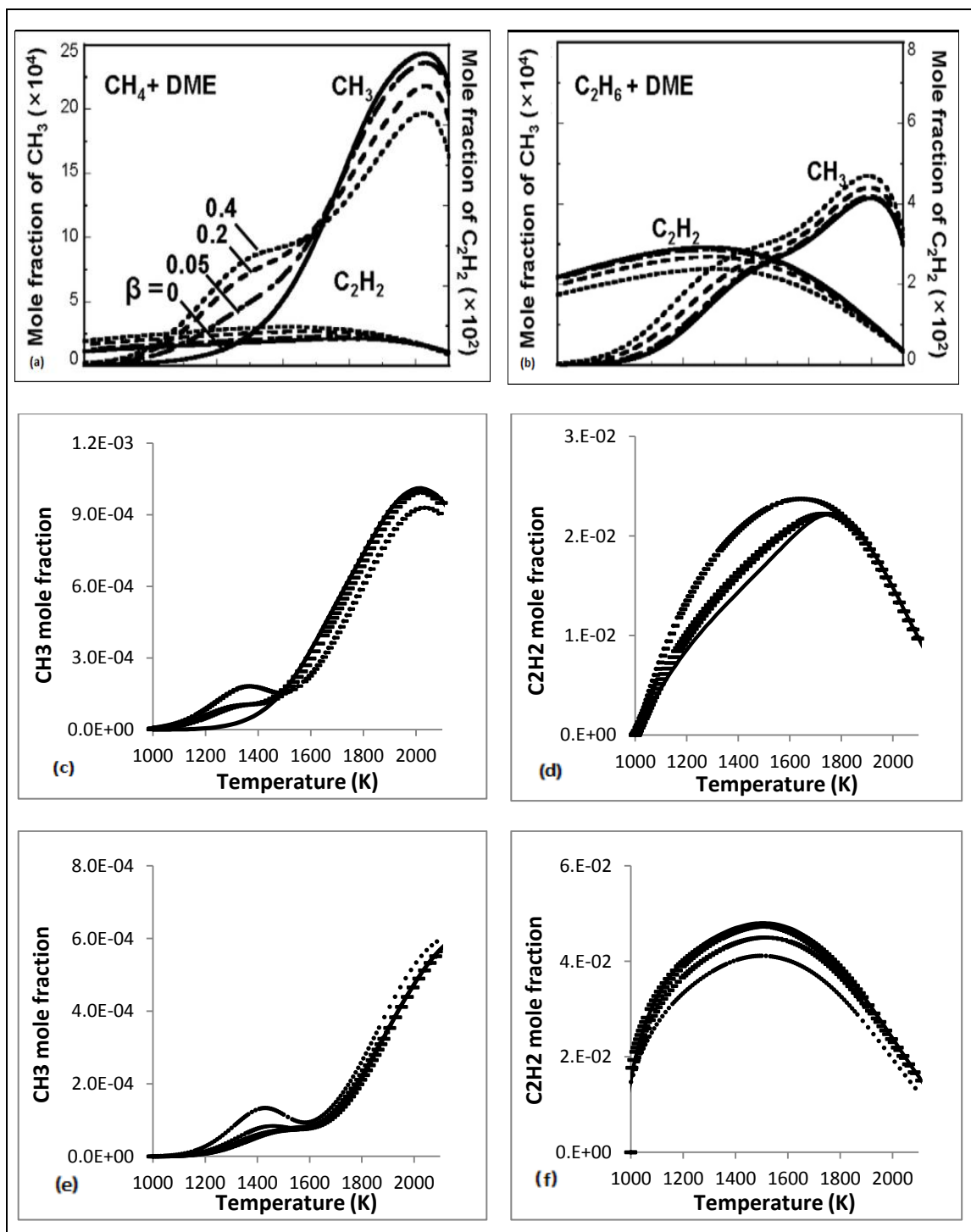


Figure 4.73. Validation of the skeletal chemical kinetic mechanism for CH<sub>4</sub>/CH<sub>3</sub>OCH<sub>3</sub> and C<sub>2</sub>H<sub>6</sub>/CH<sub>3</sub>OCH<sub>3</sub> oxidation by comparison with the results of Yoon et al. (2008) (Opposed – flow flames at 1 atm, β is the fraction of DME in the fuel mixture). Figures show the results of Yoon et al. (2008) for (a) CH<sub>4</sub>/CH<sub>3</sub>OCH<sub>3</sub> oxidation and (b) for C<sub>2</sub>H<sub>6</sub>/CH<sub>3</sub>OCH<sub>3</sub> oxidation, and the results of the skeletal mechanism for (c) CH<sub>3</sub> and (d) C<sub>2</sub>H<sub>2</sub> in CH<sub>4</sub>/CH<sub>3</sub>OCH<sub>3</sub> oxidation and (e) CH<sub>3</sub> and (f) C<sub>2</sub>H<sub>2</sub> in C<sub>2</sub>H<sub>6</sub>/CH<sub>3</sub>OCH<sub>3</sub> oxidation.

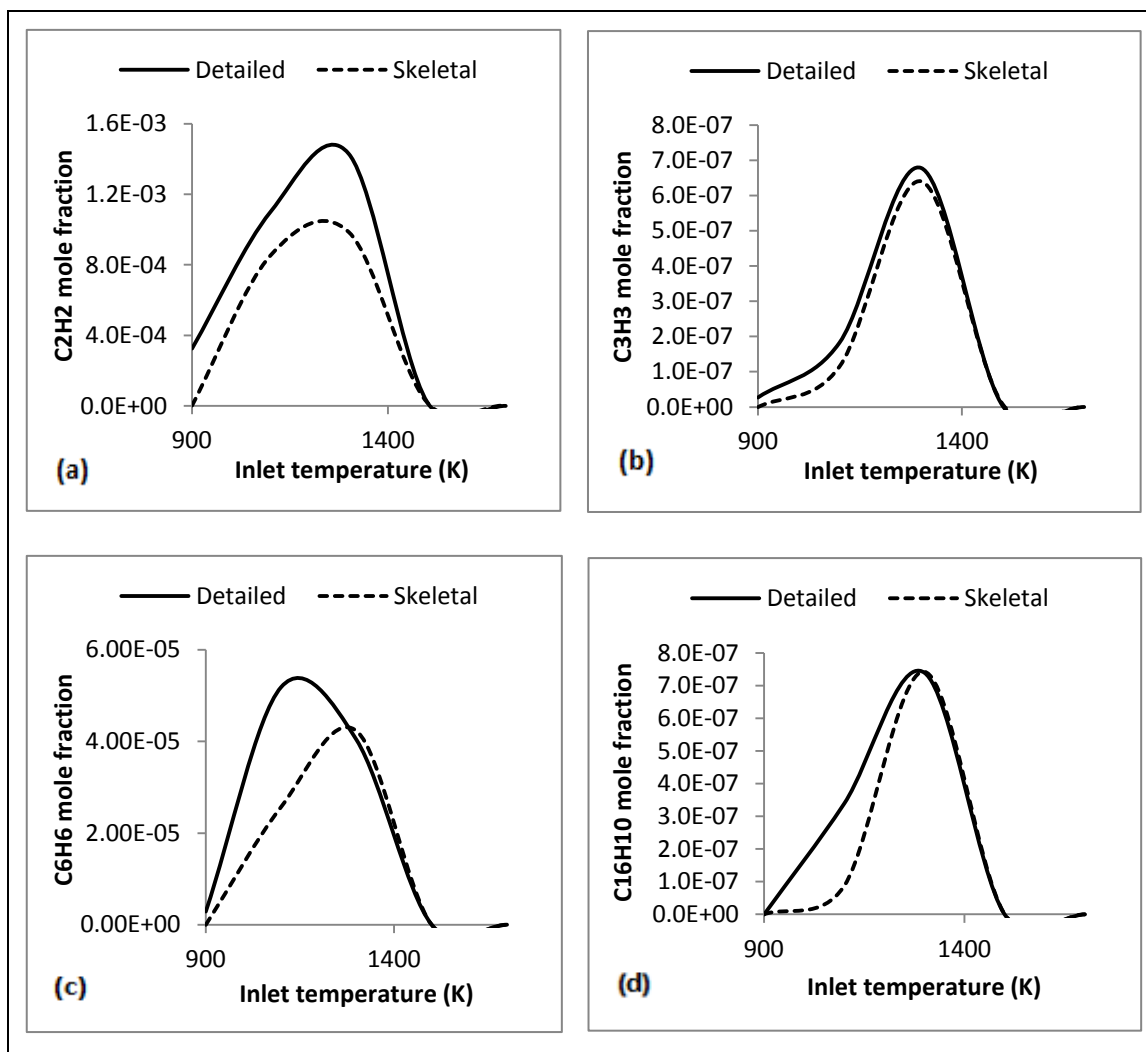


Figure 4.74. Comparison of the results of the skeletal mechanism with the results of the detailed mechanism, showing the mole fractions of (a) C<sub>2</sub>H<sub>2</sub> (b) C<sub>3</sub>H<sub>3</sub> (c) C<sub>6</sub>H<sub>6</sub> and (d) C<sub>16</sub>H<sub>10</sub> versus inlet temperatures for the oxidation of n-butane/DME(50:50) mixture. ( $T_0 = 900K$ ,  $P = 1atm$ ,  $\phi = 2.6$ ).

## CHAPTER 5

### CONCLUSIONS

The effects of DME on the oxidation of n-butane were investigated by detailed chemical kinetic modeling. The reactor model selected was the PFR model and laminar flow conditions were studied. Detailed chemical kinetic mechanisms available in the literature for the neat oxidations of n-butane and DME were combined and a new detailed chemical kinetic mechanism was obtained for the oxidation of n-butane/DME mixture. The addition of DME to n-butane in different mole fractions was tested using this kinetic mechanism. The results were compared with those of neat n-butane and neat DME oxidations. The formations of major, minor, and trace oxidation products, especially the species related to environmental problems, were analyzed.

Oxidation of pure DME resulted in higher reactions temperatures when compared to oxidation of pure n-butane. The addition of DME to n-butane in different mole fractions did not cause a significant change in the final reaction temperature. The consumption rates of the fuels and the oxidizer were observed to be faster as the mole fraction of DME in the fuel mixture was increased. This means that addition of DME to n-butane in increased amounts increased the overall rate of the reaction. DME addition also decreased the oxygen requirement at the same equivalence ratio, since DME contains oxygen in its structure.

Mole fractions of CO<sub>2</sub> and CO were not affected significantly for different mole fractions of DME added to n-butane. But for the case of pure DME oxidation, mole fraction of CO<sub>2</sub> was higher and the mole fraction of CO was lower when compared to pure n-butane oxidation. So it can be said that DME produces lower CO emissions when compared to n-butane. The mole fractions of H<sub>2</sub>O and H<sub>2</sub> were similarly not affected significantly with the addition of DME in different mole fractions. However, in the case of pure DME oxidation, H<sub>2</sub>O mole fraction was higher and H<sub>2</sub> mole fraction was lower than pure n-butane oxidation.

Mole fraction of CH<sub>4</sub>, an important environmental emission from oxidation processes, was observed to be lower for pure DME oxidation compared to pure n-butane oxidation. The addition of DME to n-butane in different amounts did not result

in a significant change in the mole fraction of  $\text{CH}_4$ . The mole fraction of  $\text{CH}_2\text{O}$ , which is an important toxic species, was observed to increase as the mole fraction of DME in the fuel mixture increased. But, mole fraction of the other aldehyde  $\text{C}_2\text{H}_4\text{O}$  was observed to decrease with increasing DME mole fraction.

Another important class of toxic species investigated was aromatic species. The precursors of these aromatic species were also investigated. It was found that as the mole fraction of DME in the fuel mixture increased, the mole fractions of these precursors and thus aromatic species were decreased. Especially in case of pure DME oxidation, mole fractions of precursors and aromatic species decreased dramatically compared to pure n-butane oxidation.

The effects of process parameters on the formations of the oxidation products of n-butane/DME mixture were investigated. Two of these process parameters were temperature and pressure. Final reaction temperature was observed to increase linearly with increasing inlet temperature. Pressure did not affect final reaction temperature under investigated conditions, due to high argon dilution.

Consumptions of the fuels and the oxidizer slightly shifted to lower temperatures with the increase in the pressure. Mole fractions of the major oxidation products ( $\text{CO}_2$ ,  $\text{CO}$ ,  $\text{H}_2\text{O}$  and  $\text{H}_2$ ) were not affected significantly with the change in pressure. The emission of  $\text{CO}$  generally increased with increasing inlet temperature. The maximum mole fractions of alkanes  $\text{CH}_4$ ,  $\text{C}_2\text{H}_6$ ,  $\text{C}_3\text{H}_8$  and oxygenated species  $\text{CH}_2\text{O}$  and  $\text{C}_2\text{H}_4\text{O}$  were observed at lower temperatures (around 800 – 900 K). Increasing pressure slightly increased the mole fraction of  $\text{CH}_4$ , while it decreased mole fractions of  $\text{C}_2\text{H}_6$ ,  $\text{C}_3\text{H}_8$ ,  $\text{CH}_2\text{O}$  and  $\text{C}_2\text{H}_4\text{O}$ . Especially, mole fractions of the two oxygenated species,  $\text{CH}_2\text{O}$  and  $\text{C}_2\text{H}_4\text{O}$ , decreased significantly with increased pressure.

Maximum mole fractions of the precursors of aromatic species were generally observed around lower temperatures, i.e. around 800 – 900 K, while some of them, such as  $\text{C}_3\text{H}_4$  isomers and  $\text{C}_2\text{H}_2$ ,  $\text{C}_3\text{H}_3$ , and  $\text{C}_4\text{H}_2$ , were delayed up to 1100 or 1300 K. Maximum mole fractions of aromatic species were generally observed around 1100 and 1300 K. Increasing pressure resulted in decrease in the mole fractions of the most of the aromatic precursors, but increased mole fractions of  $\text{C}_2\text{H}_4$ ,  $\text{C}_4\text{H}_4$ , 1,3- $\text{C}_4\text{H}_6$ , and c- $\text{C}_5\text{H}_6$ . Mole fractions of all of the aromatic species, except  $\text{C}_6\text{H}_5$  radical, increased when the pressure was increased. With the change in the pressure, roles of some of the precursors

in the formations of the aromatics might be losing importance, while roles of others becoming more dominant.

Third process parameter investigated was the equivalence ratio. Final reaction temperature was not affected with the increase in equivalence ratio under the conditions investigated, due to high argon dilution. Increasing equivalence ratio, as expected, resulted in slight decrease in the mole fractions of  $\text{CO}_2$  and  $\text{H}_2\text{O}$  and slight increase in the mole fractions of  $\text{CO}$  and  $\text{H}_2$ , at high temperatures. Increasing equivalence ratio also increased mole fractions of  $\text{CH}_4$ ,  $\text{C}_2\text{H}_6$ ,  $\text{C}_3\text{H}_8$ ,  $\text{C}_2\text{H}_4\text{O}$ , the precursor species, and the aromatics. Its effect on  $\text{CH}_2\text{O}$  was not so significant.

The formation pathways of the aromatic species were tried to be identified for the oxidations of pure n-butane and n-butane/DME mixture based on the results obtained for the concentrations of the precursors and the aromatics under different operating conditions. The effect of DME addition on these pathways was analyzed. The minor species  $\text{C}_2\text{H}_4$ ,  $\text{aC}_3\text{H}_4$ ,  $\text{pC}_3\text{H}_4$ ,  $\text{C}_3\text{H}_6$ , 1,3- $\text{C}_4\text{H}_6$ ,  $\text{C}_4\text{H}_8$ -1 and  $\text{C}_4\text{H}_8$ -2 were found to be related to the formation of the first aromatic ring  $\text{C}_6\text{H}_6$  for the oxidations of both neat n-butane and the n-butane/DME mixture. The roles of  $\text{C}_2\text{H}_2$  and  $\text{C}_4\text{H}_2$  were considered to be more related to the formations of larger aromatics.

Reaction path analysis revealed the most important species in the formation of  $\text{C}_6\text{H}_6$  at different temperatures. The most important precursor species were found to be  $\text{C}_2\text{H}_2$ ,  $\text{C}_2\text{H}_4$ ,  $\text{C}_3\text{H}_3$ ,  $\text{aC}_3\text{H}_4$ ,  $\text{aC}_3\text{H}_5$ ,  $\text{C}_3\text{H}_6$ , and fulvene for the oxidations of n-butane and n-butane/DME mixture at various temperatures. Changing temperature changed the effective pathways and the important species. It was observed that addition of DME affected the formation pathways of  $\text{C}_6\text{H}_6$  at high temperatures (around 1350K).

A skeletal kinetic mechanism was developed in order to represent the oxidation process of n-butane/DME mixture. This mechanism was validated by comparison with the available literature data and the detailed mechanism developed in this study, and satisfactory accuracy was obtained for this skeletal mechanism. The skeletal mechanism developed can be simply used in the complex mathematical modeling studies of n-butane oxidation in which DME is used as a fuel additive.

In summary, results indicate that DME can be a good candidate for an alternative fuel or a fuel additive

## REFERENCES

- Allara, D. L.; Shaw, R. *Journal of Physical and Chemical Reference Data* **1980**, *9*, 523-559.
- Arcoumanis, C.; Bae, C. Crookes, R.; Kinoshita, E. *Fuel* **2008**, *87*, 1014-1030.
- Badger, G. M.; Lewis, G. E.; Napier, I. M. *Journal of the Chemical Society* **1960**, 2825-2827.
- Bartok, W.; Sarofim, A. F. *Fossil Fuel Combustion: A Source Book*; Wiley-Interscience, 1991; p. 880.
- Basevich, V. Y.; Belyaev, A. A.; Frolov, S. M. *Russian Journal of Physical Chemistry B* **2007**, *2*, 477-484.
- Battin-Leclerc, F. *Progress in Energy and Combustion Science* **2008**, *34*, 440-498.
- Bennett, B. A. V.; McEnally, C. S.; Pfefferle, L. D.; Smooke, M. D.; Colket, M. B. *Combustion and Flame* **2009**, *156*, 1289-1302.
- Bockhorn, H.; Fetting, F.; Wenz, H. W. *Berichte der Bunsengesellschaft für physikalische Chemie* **1983**, *87*, 1067-1073.
- Buda, F.; Bounaceur, R.; Warth, V.; Glaude, P. A.; Fournet, R.; Battin-Leclerc, F. *Combustion and Flame* **2005**, *142*, 170-186.
- Carlier, M.; Corre, C.; Minetti, R.; Pauwels, J. F.; Ribaucour, M.; Sochet, L. R. *Symposium (International) on Combustion* **1991**, *23*, 1753-1758.
- Cathonnet, M.; Boettner, J. C.; James, H. *Symposium (International) on Combustion* **1981**, *18*, 903-913.
- Cernansky, N. P.; Green, R. M.; Pitz, W. J.; Westbrook, C. K. *Combustion Science and Technology* **1986**, *50*, 3-25.
- Chakir, A.; Cathonnet, M.; Boettner, J. C.; Gaillard, F. Kinetic study of n-butane oxidation. *Combustion Science and Technology* **1989**, *65*, 207-230.
- Chen, Z.; Qin, X.; Ju, Y.; Zhao, Z.; Chaos, M.; Dryer, F. L. *Proceedings of the Combustion Institute* **2007**, *31*, 1215-1222.
- Cole, J. A.; Bittner, J. D.; Longwell, J. P.; Howard, J. B. *Combustion and Flame* **1984**, *56*, 51-70.
- Colket, M. B. *Symposium (International) on Combustion* **1988**, *21*, 851-864.
- Cool, T. A.; Wang, J.; Hansen, N.; Westmoreland, P. R.; Dryer, F. L.; Zhao, Z.; Kazakov, A.; Kasper, T.; Kohse-Höinghaus, K. *Proceedings of the Combustion Institute* **2007**, *31*, 285-293.
- Corre, C.; Dryer, F. L.; Pitz, W. J.; Westbrook, C. K. *Symposium (International) on Combustion* **1992**, *24*, 843-850.



- Crookes, R.; Bob-Manuel, K. *Energy Conversion and Management* **2007**, *48*, 2971-2977.
- Curran, H. J.; Fischer, S. L.; Dryer, F. L. *International Journal of Chemical Kinetics* **2000**, *32*, 741-759.
- Curran, H. J.; Pitz, W.; Westbrook, C.; Dagaut, P.; Boettner, J. *International Journal of Chemical Kinetics* **1998**, *30*, 229-241.
- Dagaut, P.; Boettner, J.; Cathonnet, M. *Symposium (International) on Combustion* **1996**, *26*, 627-632.
- Dagaut, P.; Cathonnet, M. *Combustion and Flame* **1998**, *113*, 620-623.
- D'Anna, A.; Violi, A. *Symposium (International) on Combustion* **1998**, *27*, 425-433.
- Dean, A. M. *Journal of Physical Chemistry* **1990**, *145*, 16-37.
- Dente, M.; Ranzi, E.; Goossens, A. G. *Computers & Chemical Engineering* **1979**, *3*, 61-75.
- EPA, U.S. Environmental Protection Agency **1994**, Report No. EPA 749-F-94-003.
- EPA, U.S. Environmental Protection Agency **2011**, Report No. EPA 430-R-11-005.
- Fischer, S. L.; Dryer, F. L.; Curran, H. J. *International Journal of Chemical Kinetics* **2000**, *32*, 713-740.
- Flowers, D.; Aceves, S.; Westbrook, C. K.; Smith, J. R.; Dibble, R. *Journal of Engineering for Gas Turbines and Power* **2001**, *123*, 433-439.
- Frenklach, M.; Warnatz, J. *Combustion Science and Technology* **1987**, *51*, 265-283.
- Frye, C. A.; Boehman, A. L.; Tijm, P. J. A. *Energy & Fuels* **1999**, *13*, 650-654.
- Fu, P. P.; Beland, F. A.; Yang, S. K. *Carcinogenesis* **1980**, *1*, 725-727.
- Green, R. M.; Cernansky, N. P.; Pitz, W. J.; Westbrook, C. K. *SAE Technical Papers* **1987**, Paper no. 872108.
- Griffiths, J. F.; Mohamed, C. In *Comprehensive chemical kinetics: Low-Temperature Combustion and Autoignition*; Pilling, M. J., Ed. Elsevier: Amsterdam, 1997; Vol. 35.
- Hague, E. N.; Wheeler, R. V. *Journal of the Chemical Society* **1929**, 378-393.
- Hayashida, K.; Mogi, T.; Amagai, K.; Arai, M. *Fuel* **2011**, *90*, 493-498.
- Healy, D.; Donato, N. S.; Aul, C. J.; Petersen, E. L.; Zinner, C. M.; Bourque, G.; Curran, H. J. *Combustion and Flame* **2010**, *157*, 1526-1539.
- Hewu, W.; Longbao, Z. *Better Air Quality in Asian and Pacific Rim Cities* **2002**.
- Hidaka, Y.; Nakamura, T.; Miyauchi, A.; Shiraishi, T.; Kawano, H. *International Journal of Chemical Kinetics* **1989**, *21*, 643-666.

- Hidaka, Y.; Sato, K.; Yamane, M. *Combustion and Flame* **2000**, *123*, 1-22.
- Homann, K. H.; Wagner H.G. *Symposium (International) on Combustion* **1967**, *11*, 371-379.
- Huang, C.; Yao, M. Lu, X.; Huang, Z. *International Journal of Thermal Sciences* **2009**, *48*, 1814-1822.
- Ji, C.; Liang, C.; Wang, S. *Fuel* **2011**, *90*, 1133-1138.
- Kaden, D. A.; Hites, R. A.; Thilly, W. G. *Cancer Research* **1979**, *39*, 4152-4159.
- Kaiser, E. W.; Wallington, T. J.; Hurley, M. D.; Platz, J.; Curran, H. J.; Pitz, W. J.; Westbrook, C. K. *The Journal of Physical Chemistry A* **2000**, *104*, 8194-8206.
- Kajitani, S.; Chen, C. L.; Oguma, M.; Alam, M.; Rhee, K. T. *SAE Technical Papers* **1998**, Paper no. 982536.
- Kitamura, T.; Ito, T.; Senda, J.; Fujimoto, H. *JSAE Review* **2001**, *22*, 139-145.
- Kojima, S. *Combustion and Flame* **1994**, *99*, 87-136.
- Lafleur, A. L.; Longwell, J. P.; Marr, J. A.; Monchamp, P. A.; Plummer, E. F.; Thilly, W. G.; Mulder, P. P.; Boere, B. B.; Cornelisse, J.; Lugtenburg, J. *Environmental Health Perspectives* **1993**, *101*, 146-153.
- Lee, S.; Oh, S.; Choi, Y.; Kang, K. *Fuel* **2011**, *90*, 1674-1680.
- Liu, F.; He, X.; Ma, X.; Zhang, Q.; Thomson, M. J.; Guo, H.; Smallwood, G. J.; Shuai, S.; Wang, J. *Combustion and Flame* **2011**, *158*, 547-563.
- Lu, T.; Law, C. K. *Proceedings of the Combustion Institute* **2005**, *30*, 1333-1341.
- Marchionna, M.; Patrini, R.; Sanfilippo, D.; Migliavacca, G. *Fuel Processing Technology* **2008**, *89*, 1255-1261.
- Marinov, N. M.; Pitz, W. J.; Westbrook, C. K.; Castaldi, M. J.; Senkan, S. M. *Combustion Science and Technology* **1996**, *116*, 211-287.
- Marinov, N. M.; Pitz, W. J.; Westbrook, C. K.; Vincitore, A. M.; Castaldi, M. J.; Senkan, S. M.; Melius, C. F. *Combustion and Flame* **1998**, *114*, 192-213.
- McEnally, C. S.; Pfefferle, L. D. *Proceedings of the Combustion Institute* **2007**, *31*, 603-610.
- Miller, J. A.; Melius, C. F. *Analysis* **1992**, *91*, 21-39.
- Minetti, R.; Ribaucour, M.; Carlier, M.; Fittschen, C.; Sochet, L. R. *Combustion and Flame* **1994**, *96*, 201-211.
- Morsy, M. H. *Fuel* **2007**, *86*, 533-540.
- NIH, *U.S. National Institutes on Health* **2011**, *NTP 12<sup>th</sup> Report on Carcinogens*.
- Park, S. W. *Energy & Fuels* **2009**, *23*, 3909-3918.

- Pitz, W. J.; Westbrook, C. K.; Leppard, W. R. *SAE Technical Papers* **1988**, Paper No. 881605.
- Pitz, W. J.; Westbrook, C. K.; Proscia, W. M.; Dryer, F. L. *Symposium (International) on Combustion* **1985**, 20, 831-843.
- Pitz, W. J.; Westbrook, C. K. *Combustion and Flame* **1986**, 63, 113-133.
- Ranzi, E.; Faravelli, T.; Gaffuri, P.; Pennati, G. C.; Sogaro, A. *Combustion Science and Technology* **1994**, 100, 299-330.
- Richter, H.; Howard, J. B. *Progress in Energy and Combustion Science* **2000**, 26, 565-608.
- Rouhi, A. M. *Chemical & Engineering News* **1995**, 73, 37-39.
- Roy, K.; Christof, H.; Frank, P.; Slutsky, V.G.; Just, T. *Symposium (International) on Combustion* **1998**, 27, 329-336.
- Simmie, J. *Progress in Energy and Combustion Science* **2003**, 29, 599-634.
- Song, K. H.; Nag, P.; Litzinger, T. A.; Haworth, D. C. *Combustion and Flame* **2003**, 135, 341-349.
- Stein, S.; Walker, J.A.; Suryan, M. M.; Fahr, A. *Symposium (International) on Combustion* **1991**, 23, 85-90.
- Strelkova, M. I.; Safonov, A. A.; Sukhanov, L. P.; Umanskiy, S. Y.; Kirillov, I. A.; Potapkin, B. V.; Pasman, H. J.; Tentner, A. M. *Combustion and Flame* **2010**, 157, 641-652.
- Turns, S. R. *An Introduction to Combustion: Concepts and Applications*; 2nd ed. McGraw-Hill: Singapore, 2006; Vol. 499.
- Warnatz, J. *Combust Sci and Technol* **1983**, 34, 177.
- Warth, V.; Stef, N.; Glaude, P. A.; Battin-Leclerc, F.; Scacchi, G.; Côme, G. M. *Combustion and Flame* **1998**, 114, 81-102.
- Westbrook, C.; Dryer, F. L. *Progress in Energy and Combustion Science* **1984**, 10, 1-57.
- Westbrook, C. K.; Pitz, W. J. *SAE Technical Papers* **1989**, Paper no. 890990.
- Wilk, R. D.; Cohen, R. S.; Cernansky, N. P. *Society* **1995**, 2285-2291.
- Wu, C. H.; Kern, R. D. *Journal of Physical Chemistry* **1987**, 91, 6291-6296.
- Yamada, H.; Sakanashi, H.; Choi, N.; Tezaki, A. *SAE Transactions* **2003**, Paper No. 2003-01-1819.
- Yamasaki, Y.; Iida, N. *JSME International Journal Series B* **2003**, 46, 52-59.
- Yao, M.; Qin, J.; Zheng, Z. *Proceedings of the Institution of Mechanical Engineers Part D Journal of Automobile Engineering* **2005**, 219, 1213-1223.
- Ying, W.; Longbao, Z.; Hewu, W. *Atmospheric Environment* **2006**, 40, 2313-2320.

Ying, W.; Longbao, Z.; Zhongji, Y.; Hongyi, D. *Proceedings of the Institution of Mechanical Engineers Part D Journal of Automobile Engineering* **2005**, 219, 263–269.

Yoon, S. S.; Anh, D. H.; Chung, S. H. *Combustion and Flame* **2008**, 154, 368-377.

Zhang, J. J.; Huang, Z.; Wu, J. H.; Qiao, X. Q.; Fang, J. H. *Proceedings of the Institution of Mechanical Engineers Part D Journal of Automobile Engineering* **2008**, 222, 1691-1703.

## APPENDIX A

### DETAILED CHEMICAL KINETIC MECHANISM

Table A.1. List of species and their thermodynamic properties in the detailed chemical kinetic mechanism of C<sub>4</sub>H<sub>10</sub>/CH<sub>3</sub>OCH<sub>3</sub> oxidation. ( $H_{298}$  is the enthalpy at 298 K,  $S_{298}$  is the entropy at 298 K,  $C_p(300)$  is the heat capacity at 300 K,  $C_p(3000)$  is the heat capacity at 3000 K, and  $R$  is the gas constant)

Number	Species	$H_{298}$ (kcal/mole)	$S_{298}$ (cal/mole-K)	$C_p(300)/R$	$C_p(3000)/R$
1	AC3H4	47.6	57.9	7.2	18.3
2	AC3H5	39.6	64.7	8.1	21.0
3	ACENPHTHLN	61.6	87.0	19.0	56.1
4	ANTHRACN	55.1	92.5	22.4	67.6
5	AR	0.0	37.0	2.5	2.5
6	BIPHENYL	43.5	92.9	20.2	60.8
7	BZ(A)NDENE	56.7	90.6	20.4	64.5
8	BZ(A)NDNYL	76.8	92.0	20.1	61.6
9	BZ(A)PHNTHRN	72.8	107.0	28.7	85.1
10	BZ(GHI)FLN	99.1	94.2	26.8	79.6
11	C	171.3	37.8	2.5	2.6
12	C-2*4C6H6O	-17.0	76.7	11.9	35.5
13	C-C5H4O	14.3	73.5	10.9	29.9
14	C-C5H4OH	20.9	74.1	11.6	29.4
15	C-C5H5	63.8	63.5	9.5	26.9
16	C-C5H5O	43.4	71.4	10.6	30.0
17	C-C5H6	32.0	64.5	8.4	29.7
18	C-C5H7	52.2	50.3	11.4	32.3
19	C10H10	31.6	86.8	17.2	55.6
20	C10H6CCH	138.9	99.5	17.3	50.8
21	C10H7	94.5	81.0	15.8	47.3
22	C10H7C2H3	53.0	96.9	21.0	61.2
23	C10H7C2H5	24.8	100.6	21.8	66.2
24	C10H7CCH	80.5	100.7	17.6	53.5
25	C10H7CCH2	98.5	104.2	21.1	58.6
26	C10H7CH2	68.0	89.7	19.6	55.6
27	C10H7CH3	29.7	91.2	19.0	58.2
28	C10H7O	28.0	89.3	18.7	50.1
29	C10H7OH	-15.7	99.6	15.5	50.3
30	C10H8	37.5	79.5	16.1	50.2
31	C10H9	57.6	83.2	16.7	52.9
32	C2	200.2	47.6	5.2	4.9
33	C2H	135.0	49.6	4.5	7.7
34	C2H2	54.2	48.0	5.3	10.5
35	C2H3	68.4	55.3	4.8	12.5
36	C2H3CHO	-20.3	67.4	8.6	20.7
37	C2H3CO	16.6	68.5	8.2	17.9
38	C2H3O1-2	18.4	69.9	7.6	15.8
39	C2H4	12.5	52.4	5.2	15.1
40	C2H4O1-2	-35.8	68.2	7.6	18.6
41	C2H4O2H	8.2	79.9	10.1	22.6
42	C2H5	28.0	60.1	5.7	17.7
43	C2H5CHO	-44.5	72.7	9.7	25.7

(cont. on next page)

**Table A.1. (cont.)**

44	C2H5CO	-7.6	73.8	9.3	22.9
45	C2H5O	-4.2	65.6	7.3	20.5
46	C2H5O2	-7.0	75.3	9.4	22.9
47	C2H5O2H	-40.8	76.4	10.4	25.4
48	C2H5OH	-56.2	67.1	7.8	22.7
49	C2H6	-20.0	54.7	6.3	20.6
50	C2O	68.5	55.7	5.2	7.8
51	C3H2	129.6	64.8	7.5	11.6
52	C3H6	4.9	61.5	7.8	23.3
53	C3H8	-24.8	64.6	8.9	28.5
54	C4H10	-31.8	71.8	11.8	36.6
55	C4H2	111.7	59.8	8.9	15.9
56	C4H7	30.2	70.7	10.1	29.1
57	C4H8-1	-0.1	73.6	10.3	31.0
58	C4H8-2	-2.6	71.9	9.8	30.9
59	C5H2	165.2	63.7	10.0	19.1
60	C5H3	138.9	79.2	11.9	21.2
61	C6H2	169.7	70.9	12.4	21.8
62	C6H4C2H	137.7	81.0	13.3	35.3
63	C6H4C2H3	93.7	82.6	14.2	37.7
64	C6H5	81.4	69.2	9.5	29.8
65	C6H5C2H	76.1	79.7	13.8	38.2
66	C6H5C2H3	35.4	82.4	14.6	43.6
67	C6H5C2H5	7.1	86.2	15.5	48.8
68	C6H5CCH2	80.9	91.1	14.7	41.2
69	C6H5CCO	55.4	96.1	16.4	38.6
70	C6H5CH2	50.3	76.7	13.2	38.1
71	C6H5CH2OH	-24.0	87.4	14.2	43.1
72	C6H5CH3	12.0	78.2	12.7	40.8
73	C6H5CHCH	93.2	84.4	14.3	40.8
74	C6H5CHO	-8.7	83.5	13.0	38.0
75	C6H5CO	26.1	84.9	13.0	35.2
76	C6H5O	10.4	74.9	12.5	32.8
77	C6H5OH	-25.0	76.9	12.8	35.0
78	C6H6	19.8	64.4	10.0	33.7
79	CH	142.0	43.7	3.5	5.0
80	CH2	92.5	46.7	4.2	6.7
81	CH2(S)	101.5	45.1	4.1	6.7
82	CH2CHCCH	69.1	67.3	8.7	21.1
83	CH2CHCCH2	74.1	75.3	9.8	23.3
84	CH2CHCHCH	86.1	73.1	9.8	23.6
85	CH2CHCHCH2	28.3	70.4	9.3	26.5
86	CH2CHCHO	-16.1	67.4	8.2	20.7
87	CH2CHCO	14.8	68.1	7.7	17.9
88	CH2CHO	6.0	64.0	6.6	14.9
89	CH2CO	-12.4	57.8	6.3	12.5
90	CH2O	-27.7	52.2	4.2	9.6
91	CH2OCH2O2H	-24.0	85.9	12.3	25.2
92	CH2OCHO	-40.4	73.9	8.1	17.5
93	CH2OH	-4.1	58.9	5.7	11.9
94	CH3	34.8	46.4	4.6	9.4
95	CH3C6H4C2H3	27.5	92.8	17.5	51.8
96	CH3C6H4C2H5	-0.6	96.5	18.4	56.7
97	CH3C6H4CH2	42.5	85.7	16.1	47.0
98	CH3C6H4CH3	4.2	87.2	15.4	48.8
99	CH3CCCH2	74.3	80.4	9.9	23.4
100	CH3CH2CCH	44.8	71.4	9.9	26.2
101	CH3CHCCH	75.9	71.1	10.2	23.9

(cont. on next page)

**Table A.1. (cont.)**

102	CH3CHCCH2	37.6	69.1	9.7	26.2
103	CH3CHCO	-20.1	67.8	8.9	20.5
104	CH3CHO	-39.5	63.0	6.7	17.7
105	CH3CO	-5.4	63.7	6.2	14.9
106	CH3CO2	-51.4	63.6	7.4	17.8
107	CH3CO3	-28.6	78.0	9.7	20.3
108	CH3CO3H	-80.5	77.2	10.3	22.8
109	CH3COCH2	-7.3	72.0	9.3	23.0
110	CH3COCH2O	-19.5	91.0	13.4	26.6
111	CH3COCH2O2	-35.4	92.6	12.9	28.3
112	CH3COCH2O2H	-71.5	92.4	13.9	30.9
113	CH3COCH3	-51.6	70.1	9.0	25.8
114	CH3CY24PD	25.1	71.0	11.0	37.7
115	CH3CY24PD1	54.1	76.7	11.8	35.0
116	CH3DCY24PD	70.9	72.1	10.9	34.9
117	CH3INDENE	34.3	90.5	16.7	54.6
118	CH3INDENYL	54.2	91.9	16.6	52.1
119	CH3O	3.9	54.6	4.6	12.4
120	CH3O2	2.0	64.2	7.0	14.8
121	CH3O2H	-31.8	65.3	8.0	17.3
122	CH3OCH2	1.0	67.3	8.2	20.1
123	CH3OCH2O	-34.5	73.9	9.2	23.0
124	CH3OCH2O2	-34.6	82.6	11.0	25.5
125	CH3OCH2O2H	-68.4	83.7	12.1	28.0
126	CH3OCH2OH	-86.4	75.4	9.7	25.2
127	CH3OCH3	-43.4	63.8	7.9	22.8
128	CH3OCHO	-84.3	71.3	8.6	20.4
129	CH3OCO	-38.4	90.8	9.9	17.8
130	CH3OH	-48.1	57.3	5.3	14.7
131	CH3PHNTHRN	44.9	104.3	25.3	75.7
132	CH4	-17.9	44.5	4.2	12.2
133	CHCHCHO	37.6	68.0	8.2	17.9
134	CHOCHO	-50.6	68.2	7.5	15.1
135	CO	-26.4	47.2	3.5	4.5
136	CO2	-94.1	51.1	4.5	7.5
137	CYC6H7	49.9	72.0	10.2	35.5
138	FLRNTHN	69.8	100.6	25.1	73.3
139	FLUORENE	43.8	93.0	21.7	64.5
140	FLUORYL	71.8	94.4	21.3	61.6
141	FULVENE	56.6	70.2	10.9	32.7
142	FULVENYL	114.5	70.8	10.5	29.7
143	H	52.1	27.4	2.5	2.5
144	H2	0.0	31.2	3.5	4.5
145	H2C4O	54.6	66.4	8.7	17.4
146	H2CCCCH	116.5	72.9	10.5	18.4
147	H2CCCCH2	75.5	65.1	8.9	21.2
148	H2CCCH	83.0	61.5	8.0	15.4
149	H2O	-57.8	45.1	4.0	6.7
150	H2O2	-32.5	55.7	5.2	9.5
151	HC4-P(DEF)PTHN	60.4	110.1	15.9	56.3
152	HC4-P(DEF)PTHYL	88.3	111.4	15.7	53.4
153	HCCCHO	23.6	64.4	8.0	15.1
154	HCCCO	58.3	66.8	9.1	12.7
155	HCCHCCH	129.9	69.1	9.1	18.3
156	HCCO	42.4	60.7	6.4	9.7
157	HCCOH	20.4	58.7	6.7	12.4
158	HCO	10.4	53.7	4.1	6.9

(cont. on next page)

**Table A.1. (cont.)**

159	HCO2	-38.2	57.9	5.0	9.8
160	HCO2H	-90.2	59.4	5.5	12.2
161	HCO3	-31.3	74.1	6.7	12.2
162	HCO3H	-67.4	73.9	7.7	14.7
163	HCOH	23.3	55.4	4.9	10.5
164	HO2	3.8	54.8	4.2	6.8
165	HO2CH2OCHO	-110.3	90.9	12.9	25.5
166	HOC6H4CH3	-30.8	84.4	15.2	43.1
167	HOCH2O	-43.4	64.8	6.6	14.8
168	HOCH2O2	-42.2	74.8	8.4	17.2
169	HOCH2O2H	-76.0	75.9	9.4	19.7
170	HOCH2OCO	-81.5	101.3	11.5	20.2
171	IC3H7	21.3	69.3	8.8	25.7
172	INDENE	39.1	77.6	14.1	47.0
173	INDENYL	62.0	79.0	13.8	44.1
174	L-C5H7	53.0	74.6	11.8	31.9
175	L-C5H8	18.2	76.5	12.2	34.2
176	NC3H7	24.0	69.2	8.9	25.9
177	O	59.6	38.5	2.6	2.5
178	O2	0.0	49.0	3.5	4.8
179	O2C2H4O2H	-26.7	95.9	13.5	28.0
180	O2C2H4OH	-41.3	86.9	11.0	25.3
181	O2CH2OCH2O2H	-59.7	101.2	15.2	30.6
182	OC6H4CH3	3.6	78.2	14.5	40.6
183	OC6H4O	-30.4	75.1	13.2	32.7
184	OCH2O2H	-24.1	74.4	8.9	17.5
185	OCH2OCHO	-75.5	80.3	9.8	20.5
186	OH	9.5	43.9	3.5	4.4
187	PC2H4OH	-7.2	70.5	7.4	19.9
188	PC3H4	45.8	58.9	7.3	18.1
189	PC3H5	64.8	68.7	7.8	20.5
190	PC4H9	15.8	76.4	11.7	33.8
191	PHNTHRAN	49.5	93.9	22.4	67.6
192	PHNTHROL-1	13.0	102.6	24.9	70.1
193	PHNTHROL-9	13.0	102.6	24.9	70.1
194	PHNTHROXY-1	40.9	102.3	24.9	67.5
195	PHNTHROXY-9	40.9	102.3	24.9	67.5
196	PHNTHRYL-1	104.9	94.1	22.1	64.8
197	PHNTHRYL-9	104.9	94.1	22.1	64.8
198	PYRENE	54.0	96.1	24.5	73.6
199	SC2H4OH	-9.9	71.5	7.0	19.8
200	SC3H5	61.1	69.3	7.8	20.5
201	SC4H9	12.4	76.6	11.6	33.8



Table A.2. Chemical kinetic database for the detailed chemical kinetic mechanism of C<sub>4</sub>H<sub>10</sub>/CH<sub>3</sub>OCH<sub>3</sub> oxidation. (*A* is the pre-exponential factor,  $\beta$  is the temperature exponent, and *E* is the activation energy)

Number	Elementary reaction	A (mol.cm.sK)	$\beta$	E (cal/mole)
1	OH+H <sub>2</sub> =H+H <sub>2</sub> O	2.14E+08	1.52	3449
2	O+OH=O <sub>2</sub> +H	2.02E+14	-0.4	0
3	H+HO <sub>2</sub> =O+H <sub>2</sub> O	3.01E+13	0	1721
4	2H+H <sub>2</sub> =2H <sub>2</sub>	9.20E+16	-0.6	0
5	2H+H <sub>2</sub> O=H <sub>2</sub> +H <sub>2</sub> O	6.00E+19	-1.25	0
6	CH <sub>3</sub> O+H=CH <sub>3</sub> +OH	1.00E+14	0	0
7	CH <sub>3</sub> +OH=HCOH+H <sub>2</sub>	5.48E+13	0	2981
8	CH <sub>3</sub> +M=CH+H <sub>2</sub> +M	6.90E+14	0	82469
9	CH <sub>3</sub> OH(+M)=HCOH+H <sub>2</sub> (+M)	4.15E+16	-0.15	92285
	Third body: co /2.0/ Third body: co2 /3.0/ Third body: h2o /16.0/ Third body: h2 /2.0/ LOW/4.23E44 -7.65E0 9.2911E4/ TROE/2.5E-2 1.0E-15 8.0E3 3.0E3/			
10	CH <sub>3</sub> O+H=CH <sub>2</sub> O+H <sub>2</sub>	2.00E+13	0	0
11	CH <sub>2</sub> OH+H=CH <sub>2</sub> O+H <sub>2</sub>	2.00E+13	0	0
12	CH <sub>3</sub> O+OH=CH <sub>2</sub> O+H <sub>2</sub> O	1.00E+13	0	0
13	CH <sub>2</sub> OH+OH=CH <sub>2</sub> O+H <sub>2</sub> O	1.00E+13	0	0
14	CH <sub>3</sub> O+O=CH <sub>2</sub> O+OH	1.00E+13	0	0
15	CH <sub>2</sub> OH+O=CH <sub>2</sub> O+OH	1.00E+13	0	0
16	HCOH+OH=HCO+H <sub>2</sub> O	2.00E+13	0	0
17	HCOH+H=CH <sub>2</sub> O+H	2.00E+14	0	0
18	HCOH+O=CO <sub>2</sub> +2H	5.00E+13	0	0
19	HCOH+O=CO+OH+H	3.00E+13	0	0
20	HCOH+O <sub>2</sub> =CO <sub>2</sub> +H+OH	5.00E+12	0	0
21	HCOH+O <sub>2</sub> =CO <sub>2</sub> +H <sub>2</sub> O	3.00E+13	0	0
22	CH <sub>2</sub> +OH=CH <sub>2</sub> O+H	2.50E+13	0	0
23	CH <sub>2</sub> +CO <sub>2</sub> =CH <sub>2</sub> O+CO	1.10E+11	0	1000
24	CH <sub>2</sub> +O=CO+H <sub>2</sub>	3.00E+13	0	0
25	CH <sub>2</sub> +CH <sub>3</sub> =C <sub>2</sub> H <sub>4</sub> +H	4.00E+13	0	0
26	2CH <sub>2</sub> =C <sub>2</sub> H <sub>2</sub> +2H	4.00E+13	0	0
27	CH <sub>2</sub> +HCCO=C <sub>2</sub> H <sub>3</sub> +CO	3.00E+13	0	0
28	CH <sub>2</sub> +C <sub>2</sub> H <sub>2</sub> =H <sub>2</sub> CCCH+H	1.20E+13	0	6600
29	CH <sub>2</sub> (S)+C <sub>2</sub> H <sub>2</sub> =H <sub>2</sub> CCCH+H	1.50E+14	0	0
30	CH <sub>2</sub> (S)+C <sub>2</sub> H <sub>4</sub> =AC <sub>3</sub> H <sub>5</sub> +H	1.30E+14	0	0
31	CH+O=CO+H	5.70E+13	0	0
32	CH+OH=HCO+H	3.00E+13	0	0
33	CH+OH=C+H <sub>2</sub> O	4.00E+07	2	3000
34	CH+CO <sub>2</sub> =HCO+CO	3.40E+12	0	690
35	CH+H=C+H <sub>2</sub>	1.50E+14	0	0
36	CH+H <sub>2</sub> O=CH <sub>2</sub> O+H	1.17E+15	-0.75	0
37	CH+CH <sub>2</sub> O=CH <sub>2</sub> CO+H	9.46E+13	0	-515
38	CH+C <sub>2</sub> H <sub>2</sub> =C <sub>3</sub> H <sub>2</sub> +H	1.00E+14	0	0
39	CH+CH <sub>2</sub> =C <sub>2</sub> H <sub>2</sub> +H	4.00E+13	0	0
40	CH+CH <sub>3</sub> =C <sub>2</sub> H <sub>3</sub> +H	3.00E+13	0	0
41	C+O <sub>2</sub> =CO+O	2.00E+13	0	0
42	C+OH=CO+H	5.00E+13	0	0
43	C+CH <sub>3</sub> =C <sub>2</sub> H <sub>2</sub> +H	5.00E+13	0	0
44	C+CH <sub>2</sub> =C <sub>2</sub> H+H	5.00E+13	0	0
45	C <sub>2</sub> H <sub>5</sub> +H=C <sub>2</sub> H <sub>4</sub> +H <sub>2</sub>	1.25E+14	0	8000
46	C <sub>2</sub> H <sub>5</sub> +O=CH <sub>3</sub> +CH <sub>2</sub> O	1.00E+14	0	0
47	C <sub>2</sub> H <sub>5</sub> +HO <sub>2</sub> =CH <sub>3</sub> +CH <sub>2</sub> O+OH	3.00E+13	0	0
48	C <sub>2</sub> H <sub>5</sub> +O <sub>2</sub> =C <sub>2</sub> H <sub>4</sub> +HO <sub>2</sub>	3.00E+20	-2.86	6760
49	C <sub>2</sub> H <sub>3</sub> +O=CH <sub>2</sub> CO+H	3.00E+13	0	0
50	C <sub>2</sub> H <sub>3</sub> +OH=C <sub>2</sub> H <sub>2</sub> +H <sub>2</sub> O	2.00E+13	0	0
51	C <sub>2</sub> H <sub>3</sub> +C <sub>2</sub> H=2C <sub>2</sub> H <sub>2</sub>	3.00E+13	0	0
52	C <sub>2</sub> H <sub>3</sub> +CH=CH <sub>2</sub> +C <sub>2</sub> H <sub>2</sub>	5.00E+13	0	0

(cont. on next page)

**Table A.2. (cont.)**

53	C2H3+CH3=AC3H5+H	4.73E+02	3.7	5677
54	C2H3+CH3=C3H6	4.46E+56	-13	13865
55	C2H3+C2H2=CH2CHCCH+H	2.00E+12	0	5000
56	C2H3+C2H4=CH2CHCH2+H	5.00E+11	0	7304
57	2C2H3=CH2CHCCH2+H	7.00E+13	0	0
58	2C2H3=C2H4+C2H2	1.45E+13	0	0
59	C2H2+OH=HCCOH+H	5.04E+05	2.3	13500
60	C2H2+OH=CH3+CO	4.83E-04	4	-2000
61	HCCOH+H=CH2CO+H	1.00E+13	0	0
62	C2H2+CH3=C2H+CH4	1.81E+11	0	17289
63	CH2CHO+H=CH2CO+H2	4.00E+13	0	0
64	CH2CHO+O=CH2O+HCO	1.00E+14	0	0
65	CH2CHO+OH=CH2CO+H2O	3.00E+13	0	0
66	CH2CHO+CH3=>C2H5+CO+H	4.90E+14	-0.5	0
67	CHOCHO(+M)=CH2O+CO(+M) LOW/8.91E16 0.0E0 4.92E4/	4.27E+12	0	50600
68	CHOCHO=2CO+H2	4.07E+42	-8.5	69278
69	CHOCHO+OH=HCO+CO+H2O	1.00E+13	0	0
70	CHOCHO+O=HCO+CO+OH	7.24E+12	0	1970
71	CHOCHO+H=CH2O+HCO	1.00E+12	0	0
72	CHOCHO+HO2=HCO+CO+H2O2	1.70E+12	0	10700
73	CHOCHO+CH3=HCO+CO+CH4	1.74E+12	0	8440
74	CHOCHO+O2=HCO+CO+HO2	1.00E+14	0	37000
75	C2H+H2=C2H2+H	4.09E+05	2.39	864.3
76	C2H+OH=HCCO+H	2.00E+13	0	0
77	C2H+OH=C2+H2O	4.00E+07	2	8000
78	C2H+O2=2CO+H	9.04E+12	0	-457
79	C2H+C2H2=C4H2+H	9.64E+13	0	0
80	C2H+C2H4=CH2CHCCH+H	1.20E+13	0	0
81	HCCO+C2H2=H2CCCH+CO	1.00E+11	0	3000
82	HCCO+O=CH+CO2	2.95E+13	0	1113
83	HCCO+O2=HCO+CO+O	2.50E+08	1	0
84	HCCO+CH=C2H2+CO	5.00E+13	0	0
85	2HCCO=C2H2+2CO	1.00E+13	0	0
86	HCCO+OH=C2O+H2O	3.00E+13	0	0
87	C2O+H=CH+CO	1.00E+13	0	0
88	C2O+O=2CO	5.00E+13	0	0
89	C2O+OH=2CO+H	2.00E+13	0	0
90	C2O+O2=2CO+O	2.00E+13	0	0
91	C2+H2=C2H+H	4.00E+05	2.4	1000
92	C2+O2=2CO	5.00E+13	0	0
93	C2+OH=C2O+H	5.00E+13	0	0
94	C3H8(+M)=C2H5+CH3(+M) Third body: co /2.0/ Third body: co2 /3.0/ Third body: h2o /5.0/ Third body: h2 /2.0/ LOW/7.237E27 -2.88E0 6.7448E4/ TROE/1.0E0 1.0E-15 1.5E3 1.0E15/	7.90E+22	-1.8	88629
95	C3H8+O2=IC3H7+HO2	4.00E+13	0	48610
96	C3H8+O2=NC3H7+HO2	4.00E+13	0	51360
97	C3H8+HO2=NC3H7+H2O2	4.76E+04	2.55	16492
98	C3H8+HO2=IC3H7+H2O2	9.64E+03	2.6	13909
99	C3H8+OH=NC3H7+H2O	3.16E+07	1.8	934
100	C3H8+OH=IC3H7+H2O	7.08E+06	1.9	-159
101	C3H8+O=NC3H7+OH	3.73E+06	2.4	5504
102	C3H8+O=IC3H7+OH	5.48E+05	2.5	3139
103	C3H8+H=IC3H7+H2	1.30E+06	2.4	4471
104	C3H8+H=NC3H7+H2	1.33E+06	2.54	6756
105	C3H8+CH3=NC3H7+CH4	9.04E-01	3.65	7153
106	C3H8+CH3=IC3H7+CH4	1.51E+00	3.46	5480
107	C3H8+C2H3=IC3H7+C2H4	1.00E+03	3.1	8830
108	C3H8+C2H3=NC3H7+C2H4	6.00E+02	3.3	10500

(cont. on next page)

**Table A.2. (cont.)**

109	C3H8+C2H5=IC3H7+C2H6	1.51E+00	3.46	7470
110	C3H8+C2H5=NC3H7+C2H6	9.03E-01	3.65	9140
111	C3H8+AC3H5=C3H6+NC3H7	2.35E+02	3.3	19842
112	C3H8+AC3H5=C3H6+IC3H7	7.83E+01	3.3	18169
113	NC3H7(+M)=C2H4+CH3(+M)	1.23E+13	-0.1	30202
	Third body: co /2.0/ Third body: co2 /3.0/ Third body: h2o /5.0/ Third body: h2 /2.0/ LOW/5.485E49 -1.0E1 3.5766E4/ TROE/2.17E0 1.0E-15 2.51E2 1.185E3/			
114	NC3H7+O2=C3H6+HO2	3.58E+09	0	-3532
115	IC3H7+O2=C3H6+HO2	6.10E+20	-2.86	7910
116	C3H6+H(+M)=IC3H7(+M)	5.70E+09	1.16	874
	Third body: co /2.0/ Third body: co2 /3.0/ Third body: h2o /5.0/ Third body: h2 /2.0/ LOW/1.64E54 -1.11E1 9.364E3/ TROE/1.0E0 1.0E-15 2.6E2 3.0E3/			
117	IC3H7+H=C2H5+CH3	5.00E+13	0	0
118	NC3H7+H=C2H5+CH3	1.00E+14	0	0
119	C3H6=PC3H5+H	7.58E+14	0	101300
120	C3H6=SC3H5+H	1.45E+15	0	98060
121	C3H6=C2H2+CH4	2.50E+12	0	70000
122	C3H6=AC3H4+H2	3.00E+13	0	80000
123	C3H6+HO2=AC3H5+H2O2	9.64E+03	2.6	13910
124	C3H6+OH+O2=CH3CHO+CH2O+OH	3.00E+10	0	-8280
125	C3H6+OH=AC3H5+H2O	3.12E+06	2	-298
126	C3H6+OH=SC3H5+H2O	1.11E+06	2	1451
127	C3H6+OH=PC3H5+H2O	2.11E+06	2	2778
128	C3H6+O=CH3CHCO+2H	5.01E+07	1.76	76
129	C3H6+O=C2H5+HCO	1.58E+07	1.76	-1216
130	C3H6+O=AC3H5+OH	5.24E+11	0.7	5884
131	C3H6+O=PC3H5+OH	1.20E+11	0.7	8959
132	C3H6+O=SC3H5+OH	6.03E+10	0.7	7632
133	C3H6+H=C2H4+CH3	7.23E+12	0	1302
134	C3H6+H=AC3H5+H2	1.73E+05	2.5	2492
135	C3H6+H=SC3H5+H2	4.09E+05	2.5	9794
136	C3H6+H=PC3H5+H2	8.04E+05	2.5	12284
137	C3H6+O2=PC3H5+HO2	2.00E+13	0	47600
138	C3H6+O2=SC3H5+HO2	2.00E+13	0	44000
139	C3H6+O2=AC3H5+HO2	2.29E+12	0	39200
140	C3H6+CH3=AC3H5+CH4	2.22E+00	3.5	5675
141	C3H6+CH3=SC3H5+CH4	8.43E-01	3.5	11656
142	C3H6+CH3=PC3H5+CH4	1.35E+00	3.5	12848
143	C3H6+HCO=AC3H5+CH2O	1.08E+07	1.9	17010
144	CH3CHCO+OH=CH2CHCO+H2O	4.00E+06	2	0
145	CH3CHCO+O=CH2CHCO+OH	7.60E+08	1.5	8500
146	CH3CHCO+H=CH2CHCO+H2	2.00E+05	2.5	2500
147	CH3CHCO+H=C2H5+CO	2.00E+13	0	2000
148	CH3CHCO+O=CH3+HCO+CO	3.00E+07	2	0
149	CH2CHCHO+OH=CH2CHCO+H2O	1.00E+13	0	0
150	CH2CHCHO+O=CH2CHCO+OH	7.24E+12	0	1970
151	CH2CHCHO+O=CH2CO+HCO+H	5.01E+07	1.76	76
152	CH2CHCHO+H=CH2CHCO+H2	3.98E+13	0	4200
153	CH2CHCHO+H=C2H4+HCO	2.00E+13	0	3500
154	CH2CHCHO+O2=CH2CHCO+HO2	3.00E+13	0	36000
155	CH2CHCO=C2H3+CO	1.00E+14	0	34000
156	CH2CHCO+O=C2H3+CO2	1.00E+14	0	0
157	AC3H5+O2=CH2CHCHO+OH	1.82E+13	-0.41	22859
158	AC3H5+O2=AC3H4+HO2	4.99E+15	-1.4	22428
159	AC3H5+O2=CH2CHO+CH2O	1.06E+10	0.34	12838
160	AC3H5+O2=C2H2+CH2O+OH	2.78E+25	-4.8	15468
161	AC3H5+HO2=CH2CHCHO+H+OH	1.00E+13	0	0
162	AC3H5+OH=AC3H4+H2O	1.00E+13	0	0
163	AC3H5+H=AC3H4+H2	5.00E+13	0	0

(cont. on next page)

**Table A.2. (cont.)**

164	AC3H5+H=C3H6	1.88E+26	-3.6	5468
165	AC3H5+O=CH2CHCHO+H	1.81E+14	0	0
166	AC3H5+CH3=AC3H4+CH4	3.02E+12	-0.32	-131
167	AC3H5+C2H2=C-C5H6+H	2.95E+32	-5.83	25733
168	AC3H5+CH3=C4H8-1	1.76E+50	-11	18600
169	AC3H5+C2H3=C-C5H6+2H	1.59E+65	-14	61265
170	PC3H5+O2=CH3CHO+HCO	1.09E+23	-3.29	3892
171	PC3H5+O2=CH3CHCO+H+O	1.60E+15	-0.78	3135
172	PC3H5+O=CH3CHCO+H	1.00E+14	0	0
173	PC3H5+H=PC3H4+H2	2.00E+13	0	0
174	PC3H5+OH=PC3H4+H2O	1.00E+13	0	0
175	PC3H5+H=AC3H5+H	1.00E+14	0	0
176	SC3H5+H=AC3H5+H	1.00E+14	0	0
177	SC3H5+O2=CH3CO+CH2O	1.09E+22	-3.29	3892
178	SC3H5+O=CH2CO+CH3	1.00E+14	0	0
179	SC3H5+H=PC3H4+H2	4.00E+13	0	0
180	SC3H5+OH=PC3H4+H2O	2.00E+13	0	0
181	AC3H4+H=H2CCCH+H2	2.00E+07	2	5000
182	AC3H4+O=C2H4+CO	1.34E+07	1.88	179
183	AC3H4+OH=H2CCCH+H2O	1.00E+07	2	1000
184	AC3H4+CH3=H2CCCH+CH4	1.50E+00	3.5	5600
185	AC3H4=PC3H4	1.48E+13	0	60401
186	PC3H4+H=H2CCCH+H2	2.00E+07	2	5000
187	PC3H4+O=C2H4+CO	1.50E+13	0	2102
188	PC3H4+OH=H2CCCH+H2O	1.00E+07	2	1000
189	PC3H4+CH3=H2CCCH+CH4	1.50E+00	3.5	5600
190	PC3H4+H=CH3+C2H2	5.12E+10	1	2060
191	PC3H4+H(+M)=SC3H5(+M) LOW/8.45E39 -7.27E0 6.577E3/	6.50E+12	0	2000
192	AC3H4+H(+M)=AC3H5(+M) LOW/5.56E33 -5.0E0 4.448E3/	1.20E+11	0.69	3007
193	AC3H4+H(+M)=SC3H5(+M) LOW/1.11E34 -5.0E0 4.448E3/	8.49E+12	0	2000
194	H2CCCH+O2=CH2CO+HCO	3.00E+10	0	2868
195	H2CCCH+O=CH2O+C2H	2.00E+13	0	0
196	H2CCCH+H=C3H2+H2	5.00E+13	0	3000
197	H2CCCH+OH=C3H2+H2O	2.00E+13	0	0
198	H2CCCH+C2H3=C-C5H5+H	9.63E+40	-7.8	28820
199	H2CCCH+CH3=CH3CHCCH2	5.00E+12	0	0
200	H2CCCH+CH3=CH3CH2CCH	5.00E+12	0	0
201	H2CCCH+CH=HCCHCCH+H	7.00E+13	0	0
202	H2CCCH+CH=H2CCCH+H	7.00E+13	0	0
203	H2CCCH+H(+M)=AC3H4(+M) Third body: o2 /2.0/ Third body: co /2.0/ Third body: co2 /3.0/ Third body: h2o /5.0/ Third body: c2h2 /2.0/ Third body: h2 /2.0/ LOW/3.36E45 -8.52E0 6.293E3/	1.66E+15	-0.37	0
204	H2CCCH+H(+M)=PC3H4(+M) Third body: o2 /2.0/ Third body: co /2.0/ Third body: co2 /3.0/ Third body: h2o /5.0/ Third body: c2h2 /2.0/ Third body: h2 /2.0/ LOW/8.78E45 -8.9E0 7.974E3/	1.66E+15	-0.37	0
205	2H2CCCH=C6H6	5.56E+20	-2.535	1692
206	H2CCCH+AC3H5=FULVENE+2H	5.56E+20	-2.535	1692
207	2H2CCCH=C6H5+H	2.00E+12	0	0
208	C3H2+O2=HCCO+CO+H	5.00E+13	0	0
209	C3H2+OH=C2H2+HCO	5.00E+13	0	0
210	CHCHCHO+O2=HCO+CHOCHO	3.00E+12	0	0
211	CHCHCHO=C2H2+HCO	1.00E+14	0	33000

(cont. on next page)

**Table A.2. (cont.)**

212	CHCHCHO+H=CH2CHCO+H	1.00E+14	0	0
213	CHCHCHO+OH=HCCCHO+H2O	1.00E+13	0	0
214	CHCHCHO+H=HCCCHO+H2	2.00E+13	0	0
215	HCCCHO+H=C2H2+HCO	1.00E+14	0	3000
216	HCCCHO+OH=HCCCO+H2O	1.00E+13	0	0
217	HCCCHO+H=HCCCO+H2	4.00E+13	0	4200
218	HCCCO+O2=HCO+2CO	1.40E+09	1	0
219	HCCCO+H=C2H2+CO	1.00E+14	0	0
220	C4H10=2C2H5	2.00E+16	0	81300
221	C4H10=NC3H7+CH3	1.74E+17	0	85700
222	C4H10=PC4H9+H	1.00E+14	0	100000
223	C4H10=SC4H9+H	1.00E+14	0	100000
224	C4H10+O2=PC4H9+HO2	2.50E+13	0	49000
225	C4H10+O2=SC4H9+HO2	4.00E+13	0	47600
226	C4H10+AC3H5=PC4H9+C3H6	7.94E+11	0	20500
227	C4H10+AC3H5=SC4H9+C3H6	3.16E+11	0	16400
228	C4H10+CH3=PC4H9+CH4	5.00E+11	0	13600
229	C4H10+CH3=SC4H9+CH4	4.30E+11	0	10500
230	C4H10+H=PC4H9+H2	2.84E+05	2.54	6050
231	C4H10+H=SC4H9+H2	5.68E+05	2.4	3765
232	C4H10+OH=PC4H9+H2O	4.13E+07	1.73	753
233	C4H10+OH=SC4H9+H2O	7.23E+07	1.64	-247
234	C4H10+O=PC4H9+OH	1.13E+14	0	7850
235	C4H10+O=SC4H9+OH	5.62E+13	0	5200
236	C4H10+HO2=PC4H9+H2O2	1.70E+13	0	20460
237	C4H10+HO2=SC4H9+H2O2	1.12E+13	0	17700
238	SC4H9(+M)=C3H6+CH3(+M)	2.14E+12	0.65	30856
	Third body: co /2.0/ Third body: co2 /3.0/ Third body: h2o /5.0/ Third body: h2 /2.0/ LOW/6.323E58 -1.285E1 3.5567E4/			
239	SC4H9=C4H8-1+H	2.00E+13	0	40400
240	SC4H9=C4H8-2+H	5.01E+12	0	37900
241	PC4H9(+M)=C2H5+C2H4(+M)	1.06E+13	0	27828
	Third body: co /2.0/ Third body: co2 /3.0/ Third body: h2o /5.0/ Third body: h2 /2.0/ LOW/1.897E55 -1.191E1 3.2263E4/			
242	PC4H9=C4H8-1+H	1.26E+13	0	38600
243	C4H8-1=C2H3+C2H5	1.00E+19	-1	96770
244	C4H8-1=H+C4H7	4.11E+18	-1	97350
245	C4H8-1+CH3=C4H7+CH4	1.00E+11	0	7300
246	C4H8-1+H=C4H7+H2	5.00E+13	0	3900
247	C4H8-1+O=NC3H7+HCO	1.80E+05	2.5	-1029
248	C4H8-1+O=CH2CHCHO+CH3+H	9.67E+04	2.5	-1029
249	C4H8-1+OH=C4H7+H2O	2.25E+13	0	2217
250	C4H8-1+AC3H5=C4H7+C3H6	7.90E+10	0	12400
251	C4H8-1+O2=C4H7+HO2	4.00E+12	0	33200
252	C4H8-2=H+C4H7	4.11E+18	-1	97350
253	C4H8-2+CH3=C4H7+CH4	1.00E+11	0	8200
254	C4H8-2+H=C4H7+H2	5.00E+13	0	3800
255	C4H8-2+O=IC3H7+HCO	2.79E+06	2.12	-1775
256	C4H8-2+OH=C4H7+H2O	3.90E+13	0	2217
257	C4H8-2+O=CH3CO+C2H5	1.53E+07	1.87	-1476
258	C4H8-2+O=CH3+CH3CHCO+H	8.22E+06	1.87	-1476
259	C4H8-2+O2=C4H7+HO2	8.00E+13	0	37400
260	C4H7=CH2CHCHCH2+H	1.00E+14	0	55000
261	C4H7+OH=CH2CHCHCH2+H2O	1.00E+13	0	0
262	C4H7+CH3=CH2CHCHCH2+CH4	8.00E+12	0	0
263	C4H7+AC3H5=C3H6+CH2CHCHCH2	6.31E+12	0	0
264	C4H7+O2=CH2CHCHCH2+HO2	1.00E+09	0	0
265	C4H7+H=CH2CHCHCH2+H2	3.16E+13	0	0
266	CH2CHCHCH2+OH=CH2CHCHCH+H2O	2.00E+07	2	5000

(cont. on next page)

**Table A.2. (cont.)**

267	CH <sub>2</sub> CHCHCH <sub>2</sub> +OH=CH <sub>2</sub> CHCCH <sub>2</sub> +H <sub>2</sub> O	2.00E+07	2	2000
268	CH <sub>2</sub> CHCHCH <sub>2</sub> +O=HCO+AC <sub>3</sub> H <sub>5</sub>	6.02E+08	1.45	-858
269	CH <sub>2</sub> CHCHCH <sub>2</sub> +O=CH <sub>2</sub> CHO+C <sub>2</sub> H <sub>3</sub>	1.00E+12	0	0
270	CH <sub>2</sub> CHCHCH <sub>2</sub> +H=CH <sub>2</sub> CHCHCH+H <sub>2</sub>	3.00E+07	2	13000
271	CH <sub>2</sub> CHCHCH <sub>2</sub> +H=CH <sub>2</sub> CHCCH <sub>2</sub> +H <sub>2</sub>	3.00E+07	2	6000
272	CH <sub>3</sub> CH <sub>2</sub> CCCH+OH=CH <sub>3</sub> CHCCH+H <sub>2</sub> O	1.00E+07	2	2000
273	CH <sub>3</sub> CH <sub>2</sub> CCCH+H=C <sub>2</sub> H <sub>5</sub> +C <sub>2</sub> H <sub>2</sub>	1.00E+14	0	3000
274	CH <sub>3</sub> CHCCH <sub>2</sub> +OH=CH <sub>2</sub> CHCCH <sub>2</sub> +H <sub>2</sub> O	2.00E+07	2	1000
275	CH <sub>3</sub> CHCCH <sub>2</sub> +OH=CH <sub>3</sub> CCCH <sub>2</sub> +H <sub>2</sub> O	1.00E+07	2	2000
276	CH <sub>3</sub> CHCCH <sub>2</sub> +OH=CH <sub>3</sub> CHCCH+H <sub>2</sub> O	2.00E+07	2	2500
277	CH <sub>3</sub> CHCCH <sub>2</sub> +H=CH <sub>2</sub> CHCCH <sub>2</sub> +H <sub>2</sub>	5.00E+07	2	5000
278	CH <sub>3</sub> CHCCH <sub>2</sub> +H=CH <sub>3</sub> CCCH <sub>2</sub> +H <sub>2</sub>	1.50E+07	2	6000
279	CH <sub>3</sub> CHCCH <sub>2</sub> +H=CH <sub>3</sub> CHCCH+H <sub>2</sub>	3.00E+07	2	6500
280	CH <sub>3</sub> CHCCH <sub>2</sub> +H=CH <sub>3</sub> +AC <sub>3</sub> H <sub>4</sub>	2.00E+13	0	2000
281	CH <sub>3</sub> CHCCH+H=CH <sub>3</sub> +H <sub>2</sub> CCCH	1.00E+14	0	0
282	CH <sub>3</sub> CHCCH+O <sub>2</sub> =CH <sub>3</sub> CHCO+HCO	4.16E+10	0	2510
283	CH <sub>3</sub> CHCCH+OH=CH <sub>2</sub> CHCCH+H <sub>2</sub> O	3.00E+13	0	0
284	CH <sub>2</sub> CHCCH <sub>2</sub> +H=CH <sub>3</sub> +H <sub>2</sub> CCCH	1.00E+14	0	0
285	CH <sub>2</sub> CHCCH <sub>2</sub> +H=CH <sub>3</sub> CCCH <sub>2</sub> +H	3.00E+13	0	0
286	CH <sub>2</sub> CHCCH <sub>2</sub> +C <sub>2</sub> H <sub>2</sub> =C <sub>6</sub> H <sub>6</sub> +H	3.00E+11	0	14900
287	CH <sub>3</sub> CCCH <sub>2</sub> +H=CH <sub>3</sub> +H <sub>2</sub> CCCH	1.00E+14	0	0
288	CH <sub>3</sub> CCCH <sub>2</sub> +O <sub>2</sub> =CH <sub>3</sub> CO+CH <sub>2</sub> CO	4.16E+10	0	2510
289	CH <sub>3</sub> CCCH <sub>2</sub> +H=H <sub>2</sub> CCCH <sub>2</sub> +H <sub>2</sub>	1.00E+14	0	8000
290	CH <sub>3</sub> CCCH <sub>2</sub> +OH=H <sub>2</sub> CCCH <sub>2</sub> +H <sub>2</sub> O	1.00E+13	0	0
291	CH <sub>2</sub> CHCHCH+H=CH <sub>2</sub> CHCCH <sub>2</sub> +H	1.00E+14	0	0
292	CH <sub>2</sub> CHCHCH+OH=CH <sub>2</sub> CHCCH+H <sub>2</sub> O	2.00E+07	2	1000
293	CH <sub>2</sub> CHCHCH+H=CH <sub>2</sub> CHCCH+H <sub>2</sub>	3.00E+07	2	1000
294	CH <sub>2</sub> CHCHCH+C <sub>2</sub> H <sub>2</sub> =C <sub>6</sub> H <sub>6</sub> +H	1.60E+16	-1.33	5400
295	CH <sub>3</sub> CHCCH(+M)=CH <sub>2</sub> CHCCH+H(+M) LOW/2.0E14 0.0E0 4.1E4/	1.00E+13	0	49000
296	CH <sub>3</sub> CCCH <sub>2</sub> (+M)=H <sub>2</sub> CCCH <sub>2</sub> +H(+M) LOW/2.0E14 0.0E0 4.8E4/	1.00E+13	0	56000
297	CH <sub>2</sub> CHCCH <sub>2</sub> (+M)=CH <sub>2</sub> CHCCH+H(+M) LOW/2.0E15 0.0E0 4.2E4/	1.00E+14	0	50000
298	CH <sub>2</sub> CHCHCH(+M)=CH <sub>2</sub> CHCCH+H(+M) LOW/1.0E14 0.0E0 3.0E4/	1.00E+14	0	37000
299	CH <sub>2</sub> CHCHCH+O <sub>2</sub> =CHCHCHO+CH <sub>2</sub> O	1.00E+12	0	0
300	CH <sub>2</sub> CHCHCH+O <sub>2</sub> =CH <sub>2</sub> CHCCH+HO <sub>2</sub>	1.00E+07	2	10000
301	CH <sub>3</sub> CCCH <sub>2</sub> +H <sub>2</sub> CCCH=C <sub>6</sub> H <sub>5</sub> CH <sub>2</sub> +H	3.00E+12	0	0
302	CH <sub>3</sub> CHCCH+H <sub>2</sub> CCCH=C <sub>6</sub> H <sub>5</sub> CH <sub>2</sub> +H	3.00E+12	0	0
303	2CH <sub>3</sub> CCCH <sub>2</sub> =CH <sub>3</sub> C <sub>6</sub> H <sub>4</sub> CH <sub>2</sub> +H	3.00E+12	0	0
304	2CH <sub>3</sub> CHCCH=CH <sub>3</sub> C <sub>6</sub> H <sub>4</sub> CH <sub>2</sub> +H	3.00E+12	0	0
305	H <sub>2</sub> CCCH <sub>2</sub> +OH=H <sub>2</sub> CCCH+H <sub>2</sub> O	2.00E+07	2	2000
306	H <sub>2</sub> CCCH <sub>2</sub> +H=H <sub>2</sub> CCCH+H <sub>2</sub>	3.00E+07	2	6000
307	CH <sub>2</sub> CHCCH+OH=HCCHCCH+H <sub>2</sub> O	7.50E+06	2	5000
308	CH <sub>2</sub> CHCCH+H=HCCHCCH+H <sub>2</sub>	2.00E+07	2	15000
309	CH <sub>2</sub> CHCCH+OH=H <sub>2</sub> CCCH+H <sub>2</sub> O	1.00E+07	2	2000
310	CH <sub>2</sub> CHCCH+H=H <sub>2</sub> CCCH+H <sub>2</sub>	3.00E+07	2	5000
311	HCCHCCH+H=H <sub>2</sub> CCCH+H	1.00E+14	0	0
312	HCCHCCH+C <sub>2</sub> H <sub>2</sub> =C <sub>6</sub> H <sub>5</sub>	9.60E+70	-17.77	31300
313	HCCHCCH+O <sub>2</sub> =HCCCHO+HCO	3.00E+12	0	0
314	H <sub>2</sub> CCCH+O <sub>2</sub> =CH <sub>2</sub> CO+HCCO	1.00E+12	0	0
315	H <sub>2</sub> CCCH+OH=C <sub>4</sub> H <sub>2</sub> +H <sub>2</sub> O	3.00E+13	0	0
316	H <sub>2</sub> CCCH+O=CH <sub>2</sub> CO+C <sub>2</sub> H	2.00E+13	0	0
317	H <sub>2</sub> CCCH+O=H <sub>2</sub> C <sub>4</sub> O+H	2.00E+13	0	0
318	H <sub>2</sub> CCCH+H=C <sub>4</sub> H <sub>2</sub> +H <sub>2</sub>	5.00E+13	0	0
319	H <sub>2</sub> CCCH+CH <sub>2</sub> =AC <sub>3</sub> H <sub>4</sub> +C <sub>2</sub> H	2.00E+13	0	0
320	H <sub>2</sub> CCCH+C <sub>2</sub> H <sub>2</sub> =C <sub>6</sub> H <sub>5</sub>	3.00E+11	0	14900

(cont. on next page)

**Table A.2. (cont.)**

321	H2CCCCH(+M)=C4H2+H(+M) LOW/2.0E15 0.0E0 4.0E4/	1.00E+14	0	47000
322	HCCHCCH(+M)=C4H2+H(+M) LOW/1.0E14 0.0E0 3.0E4/	1.00E+14	0	36000
323	C4H2+CH2=C5H3+H	1.30E+13	0	4326
324	C4H2+CH=C5H2+H	1.00E+14	0	0
325	C4H2+CH2(S)=C5H3+H	3.00E+13	0	0
326	C4H2+C2H=C6H2+H	9.60E+13	0	0
327	C4H2+OH=H2C4O+H	6.66E+12	0	-410
328	C4H2+O=C3H2+CO	1.20E+12	0	0
329	H2C4O+H=C2H2+HCCO	5.00E+13	0	3000
330	H2C4O+OH=CH2CO+HCCO	1.00E+07	2	2000
331	L-C5H8+OH=L-C5H7+H2O	7.00E+06	2	0
332	L-C5H8+H=L-C5H7+H2	7.00E+06	2	5000
333	L-C5H8+H=AC3H5+C2H4	3.35E+08	1.5	2000
334	C-C5H7=C-C5H6+H	3.16E+15	0	36000
335	C-C5H7=L-C5H7	3.16E+15	0	39500
336	L-C5H7+O=CH2CHCHO+C2H3	2.00E+14	0	0
337	L-C5H7+H=L-C5H8	1.00E+14	0	0
338	C-C5H6+O2=C-C5H5+HO2	5.00E+13	0	35400
339	C-C5H6+HO2=C-C5H5+H2O2	1.99E+12	0	11660
340	C-C5H6+OH=C-C5H5+H2O	3.43E+09	1.18	-447
341	C-C5H6+O=C-C5H5+OH	1.81E+13	0	3080
342	C-C5H6+H=C-C5H5+H2	2.19E+08	1.77	3000
343	C-C5H6+CH3=C-C5H5+CH4	3.11E+11	0	5500
344	C-C5H6+C2H3=C-C5H5+C2H4	6.00E+12	0	0
345	C-C5H6+CH2CHCHCH=C-C5H5+CH2CHCHCH2	6.00E+12	0	0
346	C-C5H6+C6H5O=C-C5H5+C6H5OH	3.16E+11	0	8000
347	C-C5H5+H=C-C5H6	2.00E+14	0	0
348	C-C5H5+O=C-C5H4O+H	1.00E+14	0	0
349	C-C5H5+HO2=C-C5H5O+OH	3.00E+13	0	0
350	C-C5H5+OH=C-C5H4OH+H	3.00E+13	0	0
351	2C-C5H5=C10H8+2H	2.00E+13	0	8000
352	C-C5H5O=CH2CHCHCH+CO	2.51E+11	0	43900
353	C-C5H4OH=C-C5H4O+H	2.10E+13	0	48000
354	C-C5H4O=CO+2C2H2	1.00E+15	0	78000
355	C6H6+O2=C6H5+HO2	6.30E+13	0	60000
356	C6H6+OH=C6H5+H2O	1.63E+08	1.42	1454
357	C6H6+OH=C6H5OH+H	6.70E+12	0	10592
358	C6H6+O=C6H5O+H	2.40E+13	0	4670
359	C6H6+H=C6H5+H2	3.03E+02	3.3	5690
360	C6H5+H=C6H6	8.00E+13	0	0
361	C6H5+C2H4=C6H5C2H3+H	7.23E+01	3.5	8345
362	C6H5+C2H2=C6H5C2H+H	3.98E+13	0	10099
363	C6H5+OH=C6H5O+H	5.00E+13	0	0
364	C6H5+O=C-C5H5+CO	1.00E+14	0	0
365	C6H5+O2=C6H5O+O	2.60E+13	0	6120
366	C6H5+O2=OC6H4O+H	3.00E+13	0	8981
367	2C6H5=BIPHENYL	5.00E+12	0	0
368	C6H5+C6H6=BIPHENYL+H	4.00E+11	0	4000
369	OC6H4O=C-C5H4O+CO	1.00E+15	0	78000
370	C6H5O=CO+C-C5H5	7.40E+11	0	43850
371	C6H5O+H=C6H5OH	1.00E+14	0	0
372	C6H5O+H=C-2*4C6H6O	1.00E+14	0	0
373	C6H5OH+OH=C6H5O+H2O	2.95E+06	2	-1310
374	C6H5OH+CH3=C6H5O+CH4	1.81E+11	0	7716
375	C6H5OH+H=C6H5O+H2	1.58E+13	0	6100
376	C6H5OH+O=C6H5O+OH	2.81E+13	0	7352
377	C6H5OH+C2H3=C2H4+C6H5O	6.00E+12	0	0

(cont. on next page)

**Table A.2. (cont.)**

378	$C_6H_5OH + C_6H_5 = C_6H_6 + C_6H_5O$	4.91E+12	0	4400
379	$C-2*4C_6H_6O + H = C-C_5H_7 + CO$	2.51E+13	0	4700
380	$C_6H_5CH_3 = C_6H_5 + CH_3$	1.40E+16	0	99800
381	$C_6H_5CH_3 + O_2 = C_6H_5CH_2 + HO_2$	2.00E+12	0	39080
382	$C_6H_5CH_3 + OH = C_6H_5CH_2 + H_2O$	1.26E+13	0	2583
383	$C_6H_5CH_3 + O = C_6H_5CH_2 + OH$	5.00E+08	1.5	8000
384	$C_6H_5CH_3 + H = C_6H_5CH_2 + H_2$	3.98E+02	3.44	3120
385	$C_6H_5CH_3 + H = C_6H_6 + CH_3$	1.20E+13	0	5148
386	$C_6H_5CH_3 + O = OC_6H_4CH_3 + H$	1.63E+13	0	3418
387	$C_6H_5CH_3 + CH_3 = CH_4 + C_6H_5CH_2$	3.16E+11	0	9500
388	$C_6H_5CH_3 + C_6H_5 = C_6H_6 + C_6H_5CH_2$	2.10E+12	0	4400
389	$C_6H_5CH_2 + H = C_6H_5CH_3$	1.80E+14	0	0
390	$C_6H_5CH_2 + C_6H_5OH = C_6H_5O + C_6H_5CH_3$	1.05E+11	0	9500
391	$C_6H_5CH_2 + HOC_6H_4CH_3 = OC_6H_4CH_3 + C_6H_5CH_3$	1.05E+11	0	9500
392	$C_6H_5CH_2 + O = C_6H_5CHO + H$	2.50E+14	0	0
393	$C_6H_5CH_2 + O = C_6H_5 + CH_2O$	8.00E+13	0	0
394	$C_6H_5CH_2 + HO_2 = C_6H_5CHO + H + OH$	2.50E+14	0	0
395	$C_6H_5CH_2 + HO_2 = C_6H_5 + CH_2O + OH$	8.00E+13	0	0
396	$C_6H_5CH_2 + CH_3 = C_6H_5C_2H_5$	1.19E+13	0	221
397	$C_6H_5CH_2 + H_2CCCH = C_{10}H_{10}$	1.00E+10	0	0
398	$C_6H_5CH_2 + C_2H_2 = INDENE + H$	3.20E+11	0	7000
399	$C_6H_5CH_2 + C_6H_5CHO = C_6H_5CH_3 + C_6H_5CO$	2.77E+03	2.81	5773
400	$C_6H_5CH_2 + OH = C_6H_5CH_2OH$	6.00E+13	0	0
401	$C_6H_5CH_2OH + OH = C_6H_5CHO + H_2O + H$	8.43E+12	0	2583
402	$C_6H_5CH_2OH + H = C_6H_5CHO + H_2 + H$	8.00E+13	0	8235
403	$C_6H_5CH_2OH + H = C_6H_6 + CH_2OH$	1.20E+13	0	5148
404	$C_6H_5CH_2OH + C_6H_5CH_2 = C_6H_5CHO + C_6H_5CH_3 + H$	2.11E+11	0	9500
405	$C_6H_5CH_2OH + C_6H_5 = C_6H_5CHO + C_6H_6 + H$	1.40E+12	0	4400
406	$C_6H_5CHO + O_2 = C_6H_5CO + HO_2$	1.02E+13	0	38950
407	$C_6H_5CHO + OH = C_6H_5CO + H_2O$	1.71E+09	1.18	-447
408	$C_6H_5CHO + H = C_6H_5CO + H_2$	5.00E+13	0	4928
409	$C_6H_5CHO + H = C_6H_5 + CH_2O$	2.00E+13	0	2000
410	$C_6H_5CHO + H = C_6H_6 + HCO$	1.20E+13	0	5148
411	$C_6H_5CHO + O = C_6H_5CO + OH$	9.04E+12	0	3080
412	$C_6H_5CHO + CH_3 = CH_4 + C_6H_5CO$	2.77E+03	2.81	5773
413	$C_6H_5CHO + C_6H_5 = C_6H_6 + C_6H_5CO$	7.01E+11	0	4400
414	$C_6H_5CO = C_6H_5 + CO$	3.98E+14	0	29400
415	$OC_6H_4CH_3 + H = HOC_6H_4CH_3$	2.50E+14	0	0
416	$OC_6H_4CH_3 = C_6H_6 + H + CO$	2.51E+11	0	43900
417	$HOC_6H_4CH_3 + OH = OC_6H_4CH_3 + H_2O$	6.00E+12	0	0
418	$HOC_6H_4CH_3 + H = OC_6H_4CH_3 + H_2$	1.15E+14	0	12400
419	$HOC_6H_4CH_3 + H = C_6H_5CH_3 + OH$	2.21E+13	0	7910
420	$HOC_6H_4CH_3 + H = C_6H_5OH + CH_3$	1.20E+13	0	5148
421	$C_6H_5C_2H_5 + OH = C_6H_5C_2H_3 + H_2O + H$	8.43E+12	0	2583
422	$C_6H_5C_2H_5 + H = C_6H_5C_2H_3 + H_2 + H$	8.00E+13	0	8235
423	$C_6H_5C_2H_3 + OH = C_6H_4C_2H_3 + H_2O$	1.63E+08	1.42	1454
424	$C_6H_5C_2H_3 + H = C_6H_4C_2H_3 + H_2$	3.03E+02	3.3	5690
425	$C_6H_5C_2H_3 + OH = C_6H_5CCH_2 + H_2O$	1.00E+07	2	2000
426	$C_6H_5C_2H_3 + H = C_6H_5CCH_2 + H_2$	2.00E+07	2	6000
427	$C_6H_5CHCH + H = C_6H_5CCH_2 + H$	1.00E+14	0	0
428	$C_6H_5CCH_2 + OH = C_6H_5C_2H + H_2O$	2.00E+13	0	0
429	$C_6H_5CCH_2 + H = C_6H_5C_2H + H_2$	5.00E+13	0	0
430	$C_6H_5C_2H + O = C_6H_5CCO + H$	4.80E+09	1	0
431	$C_6H_5CCO + O_2 = C_6H_5CO + CO_2$	1.00E+12	0	0
432	$C_6H_5C_2H + OH = C_6H_4C_2H + H_2O$	1.63E+08	1.42	1454
433	$C_6H_5C_2H + H = C_6H_4C_2H + H_2$	3.03E+02	3.3	5690
434	$C_6H_5C_2H + CH_3 = C_6H_4C_2H + CH_4$	1.67E+12	0	15057
435	$C_6H_4C_2H + C_2H_2 = C_{10}H_7$	1.07E+04	2.324	-657.3
436	$C_6H_4C_2H_3 + CH_3 = INDENE + 2H$	2.00E+13	0	0

(cont. on next page)



**Table A.2. (cont.)**

437	CH3C6H4CH3+OH=CH3C6H4CH2+H2O	2.95E+13	0	2623
438	CH3C6H4CH3+O=CH3C6H4CH2+OH	5.00E+08	1.5	8000
439	CH3C6H4CH3+H=CH3C6H4CH2+H2	3.98E+02	3.44	3120
440	CH3C6H4CH2+C2H2=C10H10+H	3.20E+11	0	7000
441	CH3C6H4CH2+C2H2=CH3INDENE+H	3.20E+11	0	7000
442	CH3C6H4CH2+H=CH3C6H4CH3	7.46E+13	0	78
443	CH3C6H4CH2+CH3=CH3C6H4C2H5	6.00E+12	0	221
444	INDENE+OH=INDENYL+H2O	3.43E+09	1.18	-447
445	INDENE+O=INDENYL+OH	1.81E+13	0	3080
446	INDENE+H=INDENYL+H2	2.19E+08	1.77	3000
447	INDENYL+H=INDENE	2.00E+14	0	0
448	INDENYL+O=C6H5CHCH+CO	1.00E+14	0	0
449	INDENYL+HO2=C6H5CHCH+CO+OH	1.00E+13	0	0
450	INDENYL+C-C5H5=PHNTHRN+2H	1.00E+13	0	8000
451	CH3C6H4C2H5+OH=CH3C6H4C2H3+H2O+H	8.43E+12	0	2583
452	CH3C6H4C2H5+H=CH3C6H4C2H3+H2+H	8.00E+13	0	8235
453	CH3C6H4C2H3+OH=INDENE+H+H2O	1.26E+13	0	2583
454	CH3C6H4C2H3+H=INDENE+H+H2	3.98E+02	3.44	3120
455	CH3INDENE+OH=CH3INDENYL+H2O	3.43E+09	1.18	-447
456	CH3INDENE+O=CH3INDENYL+OH	1.81E+13	0	3080
457	CH3INDENE+H=CH3INDENYL+H2	2.19E+08	1.77	3000
458	CH3INDENE+H=INDENE+CH3	1.20E+13	0	5200
459	CH3INDENYL+H=CH3INDENE	2.00E+14	0	0
460	CH3INDENYL+C-C5H5=CH3PHNTHRN+2H	1.00E+13	0	8000
461	C10H10+OH=C10H9+H2O	5.00E+06	2	0
462	C10H10+O=C10H9+OH	7.00E+11	0.7	6000
463	C10H10+H=C10H9+H2	2.00E+05	2.5	2500
464	C10H9+H=C10H10	1.00E+14	0	0
465	C10H8+H=C10H9	5.00E+14	0	5000
466	C10H8+OH=C10H7+H2O	2.44E+08	1.42	1454
467	C10H8+OH=C10H7OH+H	9.00E+12	0	10592
468	C10H8+O=C10H7O+H	1.40E+13	0	1792
469	C10H8+H=C10H7+H2	4.55E+02	3.3	5690
470	C10H7+H=C10H8	1.00E+14	0	0
471	C10H7+O2=C10H7O+O	1.00E+13	0	0
472	C10H7+OH=C10H7O+H	5.00E+13	0	0
473	C10H7+CH3=C10H7CH2+H	2.00E+13	0	0
474	C10H7+C2H2=ACENPHTHLN+H	1.00E+20	-2.08	12000
475	C10H7+C2H2=C10H7CCH+H	1.17E-07	5.248	-9482
476	C10H7+C6H5=FLRNTHN+2H	5.00E+12	0	0
477	C10H7+C6H6=FLRNTHN+H+H2	4.00E+11	0	4000
478	C10H7O+H=C10H7OH	1.00E+14	0	0
479	C10H7OH+OH=C10H7O+H2O	2.95E+06	2	-1312
480	C10H7OH+H=C10H7O+H2	1.58E+13	0	6100
481	C10H7O=INDENYL+CO	7.40E+11	0	43850
482	C10H7CH3+OH=C10H7CH2+H2O	1.27E+13	0	2583
483	C10H7CH3+O=C10H7CH2+OH	5.00E+08	1.5	8000
484	C10H7CH3+H=C10H7CH2+H2	3.98E+02	3.44	3120
485	C10H7CH3+H=C10H8+CH3	1.20E+13	0	5148
486	C10H7CH2+H=C10H7CH3	1.00E+14	0	0
487	C10H7CH2+O=C10H7+CH2O	1.00E+14	0	0
488	C10H7CH2+HO2=>C10H7+CH2O+OH	1.00E+13	0	0
489	C10H7CH2+C2H2=BZ(A)NDENE+H	3.20E+11	0	7000
490	C10H7CH2+CH3=C10H7C2H5	1.19E+13	0	221
491	C10H7C2H5+OH=C10H7C2H3+H2O+H	8.44E+12	0	2583
492	C10H7C2H5+H=C10H7C2H3+H2+H	8.00E+13	0	8235
493	C10H7C2H3+OH=C10H7CCH2+H2O	1.00E+07	2	2000
494	C10H7C2H3+H=C10H7CCH2+H2	2.00E+07	2	6000
495	C10H7CCH2+OH=C10H7CCH+H2O	2.00E+13	0	0

(cont. on next page)

**Table A.2. (cont.)**

496	C10H7CCH2+H=C10H7CCH+H2	5.00E+13	0	0
497	C10H7CCH+OH=C10H6CCH+H2O	1.63E+08	1.42	1454
498	C10H7CCH+H=C10H6CCH+H2	3.03E+02	3.3	5690
499	C10H7CCH+H=ACENPHTHLN+H	8.46E+21	-2.614	7062.6
500	C10H6CCH+C2H2=PHNTHRYL-1	1.07E+04	2.324	-657.3
501	FLUORENE+OH=FLUORYL+H2O	3.43E+09	1.18	-447
502	FLUORENE+O=FLUORYL+OH	1.81E+13	0	3080
503	FLUORENE+H=FLUORYL+H2	2.19E+08	1.77	3000
504	FLUORYL+H=FLUORENE	2.00E+14	0	0
505	BZ(A)NDNYL+H=BZ(A)NDENE	2.00E+14	0	0
506	BZ(A)NDENE+OH=BZ(A)NDNYL+H2O	3.43E+09	1.18	-447
507	BZ(A)NDENE+O=BZ(A)NDNYL+OH	1.81E+13	0	3080
508	BZ(A)NDENE+H=BZ(A)NDNYL+H2	2.19E+08	1.77	3000
509	BZ(A)NDNYL+C-C5H5=BZ(A)PHNTHRN+2H	1.00E+13	0	8000
510	PHNTHRN+OH=PHNTHRYL-1+H2O	2.17E+08	1.42	1454
511	PHNTHRN+OH=PHNTHRYL-9+H2O	5.43E+07	1.42	1454
512	PHNTHRN+OH=PHNTHROL-1+H	9.00E+12	0	10592
513	PHNTHRN+OH=PHNTHROL-9+H	9.00E+12	0	10592
514	PHNTHRN+H=PHNTHRYL-1+H2	4.04E+02	3.3	5690
515	PHNTHRN+H=PHNTHRYL-9+H2	1.01E+02	3.3	5690
516	ANTHRACN=PHNTHRN	8.00E+12	0	65000
517	PHNTHRYL-1+H=PHNTHRN	8.00E+13	0	0
518	PHNTHRYL-9+H=PHNTHRN	8.00E+13	0	0
519	PHNTHRYL-1+O2=PHNTHROXY-1+O	1.00E+13	0	0
520	PHNTHRYL-9+O2=PHNTHROXY-9+O	1.00E+13	0	0
521	PHNTHROL-1+OH=PHNTHROXY-1+H2O	2.95E+06	2	-1310
522	PHNTHROL-1+H=PHNTHROXY-1+H2	1.59E+13	0	6100
523	PHNTHROXY-1+H=PHNTHROL-1	1.00E+14	0	0
524	PHNTHROL-9+OH=PHNTHROXY-9+H2O	2.95E+06	2	-1310
525	PHNTHROL-9+H=PHNTHROXY-9+H2	1.59E+13	0	6100
526	PHNTHROXY-9+H=PHNTHROL-9	1.00E+14	0	0
527	PHNTHROXY-1=BZ(A)NDNYL+CO	7.40E+11	0	43850
528	PHNTHROXY-9=FLUORYL+CO	7.40E+11	0	43850
529	PHNTHRYL-1+C2H2=PYRENE+H	3.49E+10	0.557	5658
530	PHNTHRYL-1+CH3=HC4-P(DEF)PTHN+2H	2.00E+13	0	0
531	CH3PHNTHRN+OH=HC4-P(DEF)PTHN+H2O+H	1.27E+13	0	2583
532	CH3PHNTHRN+H=HC4-P(DEF)PTHN+H2+H	3.98E+02	3.44	3120
533	CH3PHNTHRN+H=PHNTHRN+CH3	1.20E+13	0	5148
534	HC4-P(DEF)PTHN+OH=HC4-P(DEF)PTHYL+H2O	3.43E+09	1.18	-447
535	HC4-P(DEF)PTHN+O=HC4-P(DEF)PTHYL+OH	1.81E+13	0	3080
536	HC4-P(DEF)PTHN+H=HC4-P(DEF)PTHYL+H2	2.19E+08	1.77	3000
537	HC4-P(DEF)PTHYL+H=HC4-P(DEF)PTHN	2.00E+14	0	0
538	BZ(A)PHNTHRN+H=BZ(GHI)FLN+H2+H	3.03E+02	3.3	5690
539	BZ(A)PHNTHRN+OH=BZ(GHI)FLN+H2O+H	1.63E+08	1.42	1454
540	H2CCCH+CH2=CH2CHCCH+H	4.00E+13	0	0
541	C-C5H5+CH3=CH3CY24PD	1.76E+50	-11	18600
542	CH3CY24PD+H=C-C5H6+CH3	1.00E+13	0	1300
543	C6H6+H=CH3CY24PD1	2.39E+27	-3.92	29200
544	CYC6H7=CH3CY24PD1	5.00E+12	0	38100
545	CH3CY24PD1+H=CH3CY24PD	1.00E+14	0	0
546	CH3CY24PD1+H=C-C5H5+CH3	1.00E+14	0	0
547	CYC6H7=CH3DCY24PD	5.50E+10	0	23500
548	C6H6+H=CYC6H7	4.87E+56	-12.73	26800
549	CH3DCY24PD+H2=CH3CY24PD+H	4.00E+12	0	15000
550	FULVENE=C6H6	9.84E+37	-7.4	76979
551	FULVENE+H=C6H6+H	3.00E+12	0.5	2000
552	FULVENE+H=FULVENYL+H2	3.03E+02	3.3	5690
553	FULVENE+OH=FULVENYL+H2O	1.63E+08	1.42	1454
554	FULVENYL+H=C6H5+H	1.00E+14	0	0

(cont. on next page)

**Table A.2. (cont.)**

555	FULVENYL+O2=C-C5H4O+HCO	1.00E+12	0	0
556	CH2O+CH3=HCO+CH4	3.64E-06	5.42	998
557	HCO+CH3=CH4+CO	1.21E+14	0	0
558	HCO+HO2=CH2O+O2	2.97E+10	0.33	-3861
559	CH2O+HO2=HCO+H2O2	5.82E-03	4.53	6557
560	C2H5+C2H3=2C2H4	3.00E+12	0	0
561	CH3OH+CH3=CH2OH+CH4	3.19E+01	3.17	7172
562	HCCO+OH=2HCO	1.00E+13	0	0
563	C2H6+O2=C2H5+HO2	4.00E+13	0	50900
564	C2H6+HO2=C2H5+H2O2	1.70E+13	0	20460
565	CH3+C2H5=CH4+C2H4	1.95E+13	-0.5	0
566	CH3OH+CH2O=2CH3O	3.84E+13	0.05	84720
567	CH2O+CH3O=CH3OH+HCO	1.15E+11	0	1280
568	CH4+CH3O=CH3+CH3OH	1.57E+11	0	8842
569	C2H6+CH3O=C2H5+CH3OH	3.00E+11	0	7000
570	CH3O+CH3OH=CH2OH+CH3OH	3.00E+11	0	4074
571	C2H5OH(+M)=CH2OH+CH3(+M)	5.71E+23	-1.68	94410
	Third body: co /2.0/ Third body: co2 /3.0/ Third body: h2o /5.0/ Third body: h2 /2.0/ LOW/3.11E85 -1.884E1 1.131E5/ TROE/5.0E-1 5.5E2 8.25E2 6.1E3/			
572	C2H5OH(+M)=C2H5+OH(+M)	2.40E+23	-1.62	99540
	Third body: co /2.0/ Third body: co2 /3.0/ Third body: h2o /5.0/ Third body: h2 /2.0/ LOW/5.11E85 -1.88E1 1.1877E5/ TROE/5.0E-1 6.5E2 8.0E2 1.0E15/			
573	C2H5OH(+M)=C2H4+H2O(+M)	2.79E+13	0.09	66140
	Third body: h2o /5.0/ LOW/2.57E83 -1.885E1 8.6453E4/ TROE/7.0E-1 3.5E2 8.0E2 3.8E3/			
574	C2H5OH(+M)=CH3CHO+H2(+M)	7.24E+11	0.1	91010
	Third body: h2o /5.0/ LOW/4.46E87 -1.942E1 1.1559E5/ TROE/9.0E-1 9.0E2 1.1E3 3.5E3/			
575	C2H5OH+O2=PC2H4OH+HO2	2.00E+13	0	52800
576	C2H5OH+O2=SC2H4OH+HO2	1.50E+13	0	50150
577	C2H5OH+OH=PC2H4OH+H2O	1.74E+11	0.27	600
578	C2H5OH+OH=SC2H4OH+H2O	4.64E+11	0.15	0
579	C2H5OH+H=PC2H4OH+H2	1.23E+07	1.8	5098
580	C2H5OH+H=SC2H4OH+H2	2.58E+07	1.65	2827
581	C2H5OH+HO2=PC2H4OH+H2O2	1.23E+04	2.55	15750
582	C2H5OH+HO2=SC2H4OH+H2O2	8.20E+03	2.55	10750
583	C2H5OH+HO2=C2H5O+H2O2	2.50E+12	0	24000
584	C2H5OH+O=PC2H4OH+OH	9.41E+07	1.7	5459
585	C2H5OH+O=SC2H4OH+OH	1.88E+07	1.85	1824
586	C2H5OH+CH3=PC2H4OH+CH4	1.33E+02	3.18	9362
587	C2H5OH+CH3=SC2H4OH+CH4	4.44E+02	2.9	7690
588	C2H5OH+C2H5=PC2H4OH+C2H6	5.00E+10	0	13400
589	C2H5OH+C2H5=SC2H4OH+C2H6	5.00E+10	0	10400
590	PC2H4OH=C2H4+OH	1.29E+12	-0.37	26850
591	SC2H4OH+M=CH3CHO+H+M	1.00E+14	0	25000
592	CH3CHO=CH3+HCO	2.61E+15	0.15	80550
593	CH3CHO+O2=CH3CO+HO2	3.01E+13	0	39150
594	CH3CHO+OH=CH3CO+H2O	2.00E+06	1.8	1300
595	CH3CHO+H=CH3CO+H2	1.34E+13	0	3300
596	CH3CHO+O=CH3CO+OH	5.94E+12	0	1868
597	CH3CHO+HO2=CH3CO+H2O2	3.01E+12	0	11930
598	CH3CHO+CH3=CH3CO+CH4	2.61E+06	1.78	5911
599	C2H4+O2=C2H3+HO2	4.00E+13	0	58200
600	CH2O+M=CO+H2+M	1.83E+32	-4.42	87120
601	C2H4+CH3O=C2H3+CH3OH	1.20E+11	0	6750
602	CH3COCH3=CH3CO+CH3	1.22E+23	-1.99	83950
603	CH3COCH3+OH=CH3COCH2+H2O	1.05E+10	0.97	1586
604	CH3COCH3+H=CH3COCH2+H2	5.63E+07	2	7700

(cont. on next page)

**Table A.2. (cont.)**

605	CH <sub>3</sub> COCH <sub>3</sub> +O=CH <sub>3</sub> COCH <sub>2</sub> +OH	1.13E+14	0	7850
606	CH <sub>3</sub> COCH <sub>3</sub> +CH <sub>3</sub> =CH <sub>3</sub> COCH <sub>2</sub> +CH <sub>4</sub>	3.96E+11	0	9784
607	CH <sub>3</sub> COCH <sub>3</sub> +CH <sub>3</sub> O=CH <sub>3</sub> COCH <sub>2</sub> +CH <sub>3</sub> OH	1.00E+11	0	7000
608	CH <sub>3</sub> COCH <sub>2</sub> =CH <sub>2</sub> CO+CH <sub>3</sub>	1.00E+14	0	31000
609	CH <sub>3</sub> COCH <sub>3</sub> +O <sub>2</sub> =CH <sub>3</sub> COCH <sub>2</sub> +HO <sub>2</sub>	1.20E+14	0	46000
610	CH <sub>3</sub> COCH <sub>3</sub> +HO <sub>2</sub> =CH <sub>3</sub> COCH <sub>2</sub> +H <sub>2</sub> O <sub>2</sub>	1.70E+13	0	20460
611	C <sub>2</sub> H <sub>5</sub> CO=C <sub>2</sub> H <sub>5</sub> +CO	1.83E+15	-0.73	12910
612	C <sub>2</sub> H <sub>5</sub> CHO+H=C <sub>2</sub> H <sub>5</sub> CO+H <sub>2</sub>	3.98E+13	0	4200
613	C <sub>2</sub> H <sub>5</sub> CHO+O=C <sub>2</sub> H <sub>5</sub> CO+OH	5.01E+12	0	1790
614	C <sub>2</sub> H <sub>5</sub> CHO+OH=C <sub>2</sub> H <sub>5</sub> CO+H <sub>2</sub> O	9.24E+06	1.5	-962
615	C <sub>2</sub> H <sub>5</sub> CHO+CH <sub>3</sub> =C <sub>2</sub> H <sub>5</sub> CO+CH <sub>4</sub>	2.61E+06	1.78	5911
616	C <sub>2</sub> H <sub>5</sub> CHO+HO <sub>2</sub> =C <sub>2</sub> H <sub>5</sub> CO+H <sub>2</sub> O <sub>2</sub>	1.00E+12	0	11000
617	C <sub>2</sub> H <sub>5</sub> CHO+CH <sub>3</sub> O=C <sub>2</sub> H <sub>5</sub> CO+CH <sub>3</sub> OH	1.00E+12	0	3300
618	C <sub>2</sub> H <sub>5</sub> CHO+C <sub>2</sub> H <sub>5</sub> =C <sub>2</sub> H <sub>5</sub> CO+C <sub>2</sub> H <sub>6</sub>	1.00E+12	0	8000
619	C <sub>2</sub> H <sub>5</sub> CHO=C <sub>2</sub> H <sub>5</sub> +HCO	9.85E+18	-0.73	81710
620	C <sub>2</sub> H <sub>5</sub> CHO+O <sub>2</sub> =C <sub>2</sub> H <sub>5</sub> CO+HO <sub>2</sub>	2.00E+13	0.5	42200
621	C <sub>2</sub> H <sub>5</sub> CHO+C <sub>2</sub> H <sub>3</sub> =C <sub>2</sub> H <sub>5</sub> CO+C <sub>2</sub> H <sub>4</sub>	1.70E+12	0	8440
622	CH <sub>3</sub> OH(+M)=CH <sub>2</sub> OH+H(+M)	2.69E+16	-0.08	98940
	LOW/2.34E40 -6.33E0 1.031E5/ TROE/7.73E-1 6.93E2 5.333E3/			
623	CH <sub>3</sub> CO+H=CH <sub>2</sub> CO+H <sub>2</sub>	2.00E+13	0	0
624	CH <sub>3</sub> CO+O=CH <sub>2</sub> CO+OH	2.00E+13	0	0
625	CH <sub>3</sub> CO+CH <sub>3</sub> =CH <sub>2</sub> CO+CH <sub>4</sub>	5.00E+13	0	0
626	C <sub>2</sub> H <sub>5</sub> +O=CH <sub>3</sub> CHO+H	5.00E+13	0	0
627	C <sub>2</sub> H <sub>6</sub> +CH=C <sub>2</sub> H <sub>5</sub> +CH <sub>2</sub>	1.10E+14	0	-260
628	CH <sub>2</sub> OH+CH <sub>2</sub> O=CH <sub>3</sub> OH+HCO	1.29E-01	4.56	6596
629	C <sub>2</sub> H <sub>5</sub> OH+OH=C <sub>2</sub> H <sub>5</sub> O+H <sub>2</sub> O	7.46E+11	0.3	1634
630	C <sub>2</sub> H <sub>5</sub> OH+H=C <sub>2</sub> H <sub>5</sub> O+H <sub>2</sub>	1.50E+07	1.6	3038
631	C <sub>2</sub> H <sub>5</sub> OH+O=C <sub>2</sub> H <sub>5</sub> O+OH	1.58E+07	2	4448
632	C <sub>2</sub> H <sub>5</sub> OH+CH <sub>3</sub> =C <sub>2</sub> H <sub>5</sub> O+CH <sub>4</sub>	1.34E+02	2.92	7452
633	SC <sub>2</sub> H <sub>4</sub> OH+O <sub>2</sub> =CH <sub>3</sub> CHO+HO <sub>2</sub>	3.81E+06	2	1641
634	C <sub>2</sub> H <sub>5</sub> O+O <sub>2</sub> =CH <sub>3</sub> CHO+HO <sub>2</sub>	4.28E+10	0	1097
635	C <sub>2</sub> H <sub>5</sub> O <sub>2</sub> =C <sub>2</sub> H <sub>5</sub> +O <sub>2</sub>	4.93E+50	-11.5	42250
636	CH <sub>3</sub> O <sub>2</sub> +M=CH <sub>3</sub> +O <sub>2</sub> +M	4.34E+27	-3.42	30470
637	CH <sub>3</sub> O <sub>2</sub> H=CH <sub>3</sub> O+OH	6.31E+14	0	42300
638	C <sub>2</sub> H <sub>5</sub> O <sub>2</sub> H=C <sub>2</sub> H <sub>5</sub> O+OH	6.31E+14	0	42300
639	C <sub>2</sub> H <sub>5</sub> O+M=CH <sub>3</sub> +CH <sub>2</sub> O+M	1.35E+38	-6.96	23800
640	CH <sub>3</sub> O <sub>2</sub> +CH <sub>2</sub> O=CH <sub>3</sub> O <sub>2</sub> H+HCO	1.99E+12	0	11670
641	C <sub>2</sub> H <sub>5</sub> O <sub>2</sub> +CH <sub>2</sub> O=C <sub>2</sub> H <sub>5</sub> O <sub>2</sub> H+HCO	1.99E+12	0	11670
642	C <sub>2</sub> H <sub>4</sub> +CH <sub>3</sub> O <sub>2</sub> =C <sub>2</sub> H <sub>3</sub> +CH <sub>3</sub> O <sub>2</sub> H	1.13E+13	0	30430
643	C <sub>2</sub> H <sub>4</sub> +C <sub>2</sub> H <sub>5</sub> O <sub>2</sub> =C <sub>2</sub> H <sub>3</sub> +C <sub>2</sub> H <sub>5</sub> O <sub>2</sub> H	1.13E+13	0	30430
644	CH <sub>4</sub> +CH <sub>3</sub> O <sub>2</sub> =CH <sub>3</sub> +CH <sub>3</sub> O <sub>2</sub> H	1.81E+11	0	18480
645	CH <sub>4</sub> +C <sub>2</sub> H <sub>5</sub> O <sub>2</sub> =CH <sub>3</sub> +C <sub>2</sub> H <sub>5</sub> O <sub>2</sub> H	1.81E+11	0	18480
646	CH <sub>3</sub> OH+CH <sub>3</sub> O <sub>2</sub> =CH <sub>2</sub> OH+CH <sub>3</sub> O <sub>2</sub> H	1.81E+12	0	13710
647	CH <sub>3</sub> OH+C <sub>2</sub> H <sub>5</sub> O <sub>2</sub> =CH <sub>2</sub> OH+C <sub>2</sub> H <sub>5</sub> O <sub>2</sub> H	1.81E+12	0	13710
648	C <sub>2</sub> H <sub>5</sub> +HO <sub>2</sub> =C <sub>2</sub> H <sub>5</sub> O+OH	3.20E+13	0	0
649	CH <sub>3</sub> O <sub>2</sub> +CH <sub>3</sub> =2CH <sub>3</sub> O	7.00E+12	0	-1000
650	CH <sub>3</sub> O <sub>2</sub> +C <sub>2</sub> H <sub>5</sub> =CH <sub>3</sub> O+C <sub>2</sub> H <sub>5</sub> O	7.00E+12	0	-1000
651	CH <sub>3</sub> O <sub>2</sub> +HO <sub>2</sub> =CH <sub>3</sub> O <sub>2</sub> H+O <sub>2</sub>	1.75E+10	0	-3275
652	CH <sub>3</sub> OH+O <sub>2</sub> =CH <sub>2</sub> OH+HO <sub>2</sub>	2.05E+13	0	44900
653	C <sub>2</sub> H <sub>5</sub> O <sub>2</sub> +HO <sub>2</sub> =C <sub>2</sub> H <sub>5</sub> O <sub>2</sub> H+O <sub>2</sub>	1.75E+10	0	-3275
654	2CH <sub>3</sub> O <sub>2</sub> =>CH <sub>2</sub> O+CH <sub>3</sub> OH+O <sub>2</sub>	3.11E+14	-1.61	-1051
655	2CH <sub>3</sub> O <sub>2</sub> =>O <sub>2</sub> +2CH <sub>3</sub> O	1.40E+16	-1.61	1860
656	C <sub>2</sub> H <sub>6</sub> +CH <sub>3</sub> O <sub>2</sub> =C <sub>2</sub> H <sub>5</sub> +CH <sub>3</sub> O <sub>2</sub> H	1.70E+13	0	20460
657	C <sub>2</sub> H <sub>6</sub> +C <sub>2</sub> H <sub>5</sub> O <sub>2</sub> =C <sub>2</sub> H <sub>5</sub> +C <sub>2</sub> H <sub>5</sub> O <sub>2</sub> H	1.70E+13	0	20460
658	O <sub>2</sub> C <sub>2</sub> H <sub>4</sub> OH=PC <sub>2</sub> H <sub>4</sub> OH+O <sub>2</sub>	3.90E+16	-1	30000
659	O <sub>2</sub> C <sub>2</sub> H <sub>4</sub> OH=>OH+2CH <sub>2</sub> O	1.25E+10	0	18900
660	C <sub>2</sub> H <sub>5</sub> O <sub>2</sub> =C <sub>2</sub> H <sub>4</sub> O <sub>2</sub> H	5.64E+47	-11.44	37320
661	C <sub>2</sub> H <sub>4</sub> O <sub>2</sub> H=>C <sub>2</sub> H <sub>4</sub> O <sub>1</sub> -2+OH	4.25E+22	-4.18	22350
662	CH <sub>3</sub> CO <sub>3</sub> =CH <sub>3</sub> CO+O <sub>2</sub>	4.73E+19	-1.93	25900

(cont. on next page)

**Table A.2. (cont.)**

663	CH <sub>3</sub> CO <sub>2</sub> +M=CH <sub>3</sub> +CO <sub>2</sub> +M	4.40E+15	0	10500
664	CH <sub>3</sub> CO <sub>3</sub> H=CH <sub>3</sub> CO <sub>2</sub> +OH	5.01E+14	0	40150
665	CH <sub>3</sub> CO <sub>3</sub> +HO <sub>2</sub> =CH <sub>3</sub> CO <sub>3</sub> H+O <sub>2</sub>	1.75E+10	0	-3275
666	C <sub>2</sub> H <sub>5</sub> O+M=CH <sub>3</sub> CHO+H+M	1.16E+35	-5.89	25270
667	H <sub>2</sub> O <sub>2</sub> +CH <sub>3</sub> CO <sub>3</sub> =HO <sub>2</sub> +CH <sub>3</sub> CO <sub>3</sub> H	2.41E+12	0	9936
668	CH <sub>4</sub> +CH <sub>3</sub> CO <sub>3</sub> =CH <sub>3</sub> +CH <sub>3</sub> CO <sub>3</sub> H	1.81E+11	0	18480
669	C <sub>2</sub> H <sub>4</sub> +CH <sub>3</sub> CO <sub>3</sub> =C <sub>2</sub> H <sub>3</sub> +CH <sub>3</sub> CO <sub>3</sub> H	1.13E+13	0	30430
670	C <sub>2</sub> H <sub>6</sub> +CH <sub>3</sub> CO <sub>3</sub> =C <sub>2</sub> H <sub>5</sub> +CH <sub>3</sub> CO <sub>3</sub> H	1.70E+13	0	20460
671	CH <sub>2</sub> O+CH <sub>3</sub> CO <sub>3</sub> =HCO+CH <sub>3</sub> CO <sub>3</sub> H	1.99E+12	0	11670
672	CH <sub>3</sub> O <sub>2</sub> +CH <sub>3</sub> CHO=CH <sub>3</sub> O <sub>2</sub> H+CH <sub>3</sub> CO	3.01E+12	0	11930
673	CH <sub>3</sub> CHO+CH <sub>3</sub> CO <sub>3</sub> =CH <sub>3</sub> CO+CH <sub>3</sub> CO <sub>3</sub> H	3.01E+12	0	11930
674	C <sub>2</sub> H <sub>3</sub> CO=C <sub>2</sub> H <sub>3</sub> +CO	2.04E+14	-0.4	31450
675	C <sub>2</sub> H <sub>3</sub> CHO+OH=C <sub>2</sub> H <sub>3</sub> CO+H <sub>2</sub> O	9.24E+06	1.5	-962
676	C <sub>2</sub> H <sub>3</sub> CHO+H=C <sub>2</sub> H <sub>3</sub> CO+H <sub>2</sub>	1.34E+13	0	3300
677	C <sub>2</sub> H <sub>3</sub> CHO+O=C <sub>2</sub> H <sub>3</sub> CO+OH	5.94E+12	0	1868
678	C <sub>2</sub> H <sub>3</sub> CHO+HO <sub>2</sub> =C <sub>2</sub> H <sub>3</sub> CO+H <sub>2</sub> O <sub>2</sub>	3.01E+12	0	11930
679	C <sub>2</sub> H <sub>3</sub> CHO+CH <sub>3</sub> =C <sub>2</sub> H <sub>3</sub> CO+CH <sub>4</sub>	2.61E+06	1.78	5911
680	C <sub>2</sub> H <sub>3</sub> CHO+CH <sub>3</sub> O <sub>2</sub> =C <sub>2</sub> H <sub>3</sub> CO+CH <sub>3</sub> O <sub>2</sub> H	3.01E+12	0	11930
681	C <sub>2</sub> H <sub>4</sub> O <sub>2</sub> H=C <sub>2</sub> H <sub>4</sub> +HO <sub>2</sub>	9.29E+30	-6.1	19930
682	C <sub>2</sub> H <sub>4</sub> +CH <sub>3</sub> O <sub>2</sub> =>C <sub>2</sub> H <sub>4</sub> O <sub>1</sub> -2+CH <sub>3</sub> O	2.82E+12	0	17110
683	C <sub>2</sub> H <sub>4</sub> +C <sub>2</sub> H <sub>5</sub> O <sub>2</sub> =>C <sub>2</sub> H <sub>4</sub> O <sub>1</sub> -2+C <sub>2</sub> H <sub>5</sub> O	2.82E+12	0	17110
684	C <sub>2</sub> H <sub>4</sub> O <sub>1</sub> -2=CH <sub>3</sub> +HCO	3.63E+13	0	57200
685	C <sub>2</sub> H <sub>4</sub> O <sub>1</sub> -2=CH <sub>3</sub> CHO	7.41E+12	0	53800
686	C <sub>2</sub> H <sub>4</sub> O <sub>1</sub> -2+OH=C <sub>2</sub> H <sub>3</sub> O <sub>1</sub> -2+H <sub>2</sub> O	1.78E+13	0	3610
687	C <sub>2</sub> H <sub>4</sub> O <sub>1</sub> -2+H=C <sub>2</sub> H <sub>3</sub> O <sub>1</sub> -2+H <sub>2</sub>	8.00E+13	0	9680
688	C <sub>2</sub> H <sub>4</sub> O <sub>1</sub> -2+HO <sub>2</sub> =C <sub>2</sub> H <sub>3</sub> O <sub>1</sub> -2+H <sub>2</sub> O <sub>2</sub>	1.13E+13	0	30430
689	C <sub>2</sub> H <sub>4</sub> O <sub>1</sub> -2+CH <sub>3</sub> O <sub>2</sub> =C <sub>2</sub> H <sub>3</sub> O <sub>1</sub> -2+CH <sub>3</sub> O <sub>2</sub> H	1.13E+13	0	30430
690	C <sub>2</sub> H <sub>4</sub> O <sub>1</sub> -2+C <sub>2</sub> H <sub>5</sub> O <sub>2</sub> =C <sub>2</sub> H <sub>3</sub> O <sub>1</sub> -2+C <sub>2</sub> H <sub>5</sub> O <sub>2</sub> H	1.13E+13	0	30430
691	C <sub>2</sub> H <sub>4</sub> O <sub>1</sub> -2+CH <sub>3</sub> =C <sub>2</sub> H <sub>3</sub> O <sub>1</sub> -2+CH <sub>4</sub>	1.07E+12	0	11830
692	C <sub>2</sub> H <sub>4</sub> O <sub>1</sub> -2+CH <sub>3</sub> O=C <sub>2</sub> H <sub>3</sub> O <sub>1</sub> -2+CH <sub>3</sub> OH	1.20E+11	0	6750
693	CH <sub>3</sub> COCH <sub>2</sub> O <sub>2</sub> =CH <sub>3</sub> COCH <sub>2</sub> +O <sub>2</sub>	8.09E+15	-1.11	27450
694	CH <sub>3</sub> COCH <sub>3</sub> +CH <sub>3</sub> COCH <sub>2</sub> O <sub>2</sub> =CH <sub>3</sub> COCH <sub>2</sub> +CH <sub>3</sub> COC H <sub>2</sub> O <sub>2</sub> H	1.00E+11	0	5000
695	CH <sub>2</sub> O+CH <sub>3</sub> COCH <sub>2</sub> O <sub>2</sub> =HCO+CH <sub>3</sub> COCH <sub>2</sub> O <sub>2</sub> H	1.29E+11	0	9000
696	HO <sub>2</sub> +CH <sub>3</sub> COCH <sub>2</sub> O <sub>2</sub> =>CH <sub>3</sub> COCH <sub>2</sub> O <sub>2</sub> H+O <sub>2</sub>	1.00E+12	0	0
697	CH <sub>3</sub> COCH <sub>2</sub> O <sub>2</sub> H=CH <sub>3</sub> COCH <sub>2</sub> O+OH	1.00E+16	0	43000
698	CH <sub>3</sub> COCH <sub>2</sub> O=CH <sub>3</sub> CO+CH <sub>2</sub> O	4.16E+16	-1.03	13960
699	C <sub>2</sub> H <sub>5</sub> CHO+CH <sub>3</sub> O <sub>2</sub> =C <sub>2</sub> H <sub>5</sub> CO+CH <sub>3</sub> O <sub>2</sub> H	3.01E+12	0	11930
700	C <sub>2</sub> H <sub>5</sub> CHO+C <sub>2</sub> H <sub>5</sub> O=C <sub>2</sub> H <sub>5</sub> CO+C <sub>2</sub> H <sub>5</sub> OH	6.03E+11	0	3300
701	C <sub>2</sub> H <sub>5</sub> CHO+C <sub>2</sub> H <sub>5</sub> O <sub>2</sub> =C <sub>2</sub> H <sub>5</sub> CO+C <sub>2</sub> H <sub>5</sub> O <sub>2</sub> H	3.01E+12	0	11930
702	C <sub>2</sub> H <sub>5</sub> CHO+CH <sub>3</sub> CO <sub>3</sub> =C <sub>2</sub> H <sub>5</sub> CO+CH <sub>3</sub> CO <sub>3</sub> H	3.01E+12	0	11930
703	CH <sub>3</sub> CHO+OH=CH <sub>3</sub> +HCO <sub>2</sub> H	3.00E+15	-1.08	0
704	C <sub>2</sub> H <sub>3</sub> O <sub>1</sub> -2=CH <sub>3</sub> CO	8.50E+14	0	14000
705	C <sub>2</sub> H <sub>3</sub> O <sub>1</sub> -2=CH <sub>2</sub> CHO	1.00E+14	0	14000
706	CH <sub>2</sub> CHO=CH <sub>2</sub> CO+H	3.09E+15	-0.26	50820
707	CH <sub>2</sub> CHO+O <sub>2</sub> =>CH <sub>2</sub> O+CO+OH	2.00E+13	0	4200
708	HCO <sub>3</sub> =HCO+O <sub>2</sub>	7.77E+26	-3.96	44230
709	CH <sub>2</sub> O+HCO <sub>3</sub> =HCO+HCO <sub>3</sub> H	1.99E+12	0	11670
710	HCO <sub>3</sub> H=HCO <sub>2</sub> +OH	5.01E+14	0	40150
711	HCO <sub>2</sub> +M=H+CO <sub>2</sub> +M	2.44E+15	-0.5	26500
712	CH <sub>3</sub> CHO+OH=CH <sub>2</sub> CHO+H <sub>2</sub> O	1.72E+05	2.4	815
713	C <sub>2</sub> H <sub>4</sub> +H <sub>2</sub> =2CH <sub>3</sub>	3.77E+12	0.83	84710
714	C <sub>2</sub> H <sub>4</sub> +HO <sub>2</sub> =C <sub>2</sub> H <sub>4</sub> O <sub>1</sub> -2+OH	2.23E+12	0	17190
715	CH <sub>3</sub> OCH <sub>3</sub> =CH <sub>3</sub> +CH <sub>3</sub> O	4.86E+55	-11.56	102100
716	CH <sub>3</sub> OCH <sub>3</sub> +OH=CH <sub>3</sub> OCH <sub>2</sub> +H <sub>2</sub> O	9.35E+05	2.29	-780
717	CH <sub>3</sub> OCH <sub>3</sub> +H=CH <sub>3</sub> OCH <sub>2</sub> +H <sub>2</sub>	7.72E+06	2.09	3384
718	CH <sub>3</sub> OCH <sub>3</sub> +O=CH <sub>3</sub> OCH <sub>2</sub> +OH	1.86E-03	5.29	-109
719	CH <sub>3</sub> OCH <sub>3</sub> +HO <sub>2</sub> =CH <sub>3</sub> OCH <sub>2</sub> +H <sub>2</sub> O <sub>2</sub>	1.68E+13	0	17690
720	CH <sub>3</sub> OCH <sub>3</sub> +CH <sub>3</sub> O <sub>2</sub> =CH <sub>3</sub> OCH <sub>2</sub> +CH <sub>3</sub> O <sub>2</sub> H	1.68E+13	0	17690

(cont. on next page)

**Table A.2. (cont.)**

721	$\text{CH}_3\text{OCH}_3+\text{CH}_3=\text{CH}_3\text{OCH}_2+\text{CH}_4$	1.45E-06	5.73	5699
722	$\text{CH}_3\text{OCH}_3+\text{O}_2=\text{CH}_3\text{OCH}_2+\text{HO}_2$	4.10E+13	0	44910
723	$\text{CH}_3\text{OCH}_3+\text{CH}_3\text{O}=\text{CH}_3\text{OCH}_2+\text{CH}_3\text{OH}$	6.02E+11	0	4074
724	$\text{CH}_3\text{OCH}_2=\text{CH}_2\text{O}+\text{CH}_3$	1.60E+13	0	25500
725	$\text{CH}_3\text{OCH}_2+\text{CH}_3\text{O}=\text{CH}_3\text{OCH}_3+\text{CH}_2\text{O}$	2.41E+13	0	0
726	$\text{CH}_3\text{OCH}_2+\text{CH}_2\text{O}=\text{CH}_3\text{OCH}_3+\text{HCO}$	5.49E+03	2.8	5862
727	$\text{CH}_3\text{OCH}_2+\text{CH}_3\text{CHO}=\text{CH}_3\text{OCH}_3+\text{CH}_3\text{CO}$	1.26E+12	0	8499
728	$\text{CH}_3\text{OCH}_2+\text{HO}_2=\text{CH}_3\text{OCH}_2\text{O}+\text{OH}$	9.00E+12	0	0
729	$\text{CH}_3\text{OCH}_2\text{O}_2=\text{CH}_3\text{OCH}_2+\text{O}_2$	4.44E+19	-1.59	36240
730	$\text{CH}_3\text{OCH}_3+\text{CH}_3\text{OCH}_2\text{O}_2=\text{CH}_3\text{OCH}_2+\text{CH}_3\text{OCH}_2\text{O}_2\text{H}$	5.00E+12	0	17690
731	$\text{CH}_3\text{OCH}_2\text{O}_2+\text{CH}_2\text{O}=\text{CH}_3\text{OCH}_2\text{O}_2\text{H}+\text{HCO}$	1.00E+12	0	11670
732	$\text{CH}_3\text{OCH}_2\text{O}_2+\text{CH}_3\text{CHO}=\text{CH}_3\text{OCH}_2\text{O}_2\text{H}+\text{CH}_3\text{CO}$	2.80E+12	0	13600
733	$\text{CH}_3\text{OCH}_2\text{O}_2\text{H}=\text{CH}_3\text{OCH}_2\text{O}+\text{OH}$	4.38E+21	-1.94	43870
734	$\text{CH}_3\text{OCH}_2\text{O}=\text{CH}_3\text{O}+\text{CH}_2\text{O}$	5.18E+12	-0.13	19370
735	$\text{CH}_3\text{OCH}_2\text{O}_2=\text{CH}_2\text{OCH}_2\text{O}_2\text{H}$	6.00E+10	0	21580
736	$\text{CH}_2\text{OCH}_2\text{O}_2\text{H}=\text{OH}+2\text{CH}_2\text{O}$	1.50E+13	0	20760
737	$\text{O}_2\text{CH}_2\text{OCH}_2\text{O}_2\text{H}=\text{CH}_2\text{OCH}_2\text{O}_2\text{H}+\text{O}_2$	1.92E+19	-1.62	36270
738	$\text{O}_2\text{CH}_2\text{OCH}_2\text{O}_2\text{H}=\text{HO}_2\text{CH}_2\text{OCHO}+\text{OH}$	4.00E+10	0	18580
739	$\text{HO}_2\text{CH}_2\text{OCHO}=\text{OCH}_2\text{OCHO}+\text{OH}$	2.00E+16	0	40500
740	$\text{OCH}_2\text{OCHO}=\text{CH}_2\text{O}+\text{HCO}_2$	5.96E+16	-1.5	19620
741	$\text{C}_2\text{H}_5\text{O}_2=\text{C}_2\text{H}_4+\text{HO}_2$	3.37E+55	-13.42	44670
742	$\text{C}_2\text{H}_4\text{O}_2\text{H}=\text{C}_2\text{H}_5+\text{O}_2$	2.15E+37	-8.21	28020
743	$\text{CH}_3\text{O}+\text{CH}_3=\text{CH}_2\text{O}+\text{CH}_4$	2.40E+13	0	0
744	$\text{CH}_3\text{OCH}_3+\text{HCO}_3=\text{CH}_3\text{OCH}_2+\text{HCO}_3\text{H}$	4.43E+04	2.6	13910
745	$\text{OCH}_2\text{OCHO}=\text{HOCH}_2\text{OCO}$	1.00E+11	0	14000
746	$\text{HOCH}_2\text{OCO}=\text{HOCH}_2\text{O}+\text{CO}$	2.18E+16	-2.69	17200
747	$\text{HOCH}_2\text{OCO}=\text{CH}_2\text{OH}+\text{CO}_2$	8.67E+17	-3.45	19080
748	$\text{CH}_2\text{OH}+\text{HO}_2=\text{HOCH}_2\text{O}+\text{OH}$	1.00E+13	0	0
749	$\text{HOCH}_2\text{O}=\text{CH}_2\text{O}+\text{OH}$	1.48E+17	-1.21	21240
750	$\text{HOCH}_2\text{O}=\text{HCO}_2\text{H}+\text{H}$	1.00E+14	0	14900
751	$\text{HCO}_2\text{H}+\text{M}=\text{CO}+\text{H}_2\text{O}+\text{M}$	2.30E+13	0	50000
752	$\text{HCO}_2\text{H}+\text{M}=\text{CO}_2+\text{H}_2+\text{M}$	1.50E+16	0	57000
753	$2\text{CH}_3\text{OCH}_2\text{O}_2=\text{CH}_3\text{OCHO}+\text{CH}_3\text{OCH}_2\text{OH}+\text{O}_2$	6.63E+22	-4.5	0
754	$2\text{CH}_3\text{OCH}_2\text{O}_2=\text{O}_2+2\text{CH}_3\text{OCH}_2\text{O}$	1.55E+23	-4.5	0
755	$\text{CH}_3\text{OCH}_2\text{O}=\text{CH}_3\text{OCHO}+\text{H}$	1.75E+16	-0.66	11720
756	$\text{CH}_3\text{OCHO}=\text{CH}_3+\text{HCO}_2$	1.39E+18	-0.99	79140
757	$\text{CH}_3\text{OCHO}+\text{O}_2=\text{CH}_3\text{OCO}+\text{HO}_2$	1.00E+13	0	49700
758	$\text{CH}_3\text{OCHO}+\text{OH}=\text{CH}_3\text{OCO}+\text{H}_2\text{O}$	2.34E+07	1.61	-35
759	$\text{CH}_3\text{OCHO}+\text{HO}_2=\text{CH}_3\text{OCO}+\text{H}_2\text{O}_2$	1.22E+12	0	17000
760	$\text{CH}_3\text{OCHO}+\text{O}=\text{CH}_3\text{OCO}+\text{OH}$	2.35E+05	2.5	2230
761	$\text{CH}_3\text{OCHO}+\text{H}=\text{CH}_3\text{OCO}+\text{H}_2$	4.55E+06	2	5000
762	$\text{CH}_3\text{OCHO}+\text{CH}_3=\text{CH}_3\text{OCO}+\text{CH}_4$	7.55E-01	3.46	5481
763	$\text{CH}_3\text{OCHO}+\text{CH}_3\text{O}=\text{CH}_3\text{OCO}+\text{CH}_3\text{OH}$	5.48E+11	0	5000
764	$\text{CH}_3\text{OCHO}+\text{CH}_3\text{O}_2=\text{CH}_3\text{OCO}+\text{CH}_3\text{O}_2\text{H}$	1.22E+12	0	17000
765	$\text{CH}_3\text{OCO}=\text{CH}_3\text{O}+\text{CO}$	7.45E+12	-1.76	17150
766	$\text{CH}_3\text{OCO}=\text{CH}_3+\text{CO}_2$	1.51E+12	-1.78	13820
767	$\text{OCH}_2\text{O}_2\text{H}=\text{CH}_2\text{O}+\text{HO}_2$	1.28E+18	-1.8	10460
768	$\text{OCH}_2\text{O}_2\text{H}=\text{HOCH}_2\text{O}_2$	3.00E+11	0	8600
769	$\text{HOCH}_2\text{O}_2+\text{HO}_2=\text{HOCH}_2\text{O}_2\text{H}+\text{O}_2$	3.50E+10	0	-3275
770	$\text{CH}_3\text{OCH}_3+\text{HCO}_2=\text{CH}_3\text{OCH}_2+\text{HCO}_2\text{H}$	1.00E+13	0	17690
771	$\text{HCO}_2\text{H}=\text{HCO}+\text{OH}$	4.59E+18	-0.46	108300
772	$\text{CH}_2\text{O}+\text{HCO}_2=\text{HCO}+\text{HCO}_2\text{H}$	5.60E+12	0	13600
773	$\text{HCO}_2+\text{HO}_2=\text{HCO}_2\text{H}+\text{O}_2$	3.50E+10	0	-3275
774	$\text{HCO}_2+\text{H}_2\text{O}_2=\text{HCO}_2\text{H}+\text{HO}_2$	2.40E+12	0	10000
775	$\text{HCO}_2\text{H}+\text{OH}=\text{H}_2\text{O}+\text{CO}_2+\text{H}$	2.62E+06	2.06	916
776	$\text{HCO}_2\text{H}+\text{OH}=\text{H}_2\text{O}+\text{CO}+\text{OH}$	1.85E+07	1.51	-962
777	$\text{HCO}_2\text{H}+\text{H}=\text{H}_2+\text{CO}_2+\text{H}$	4.24E+06	2.1	4868
778	$\text{HCO}_2\text{H}+\text{H}=\text{H}_2+\text{CO}+\text{OH}$	6.03E+13	-0.35	2988
779	$\text{HCO}_2\text{H}+\text{CH}_3=\text{CH}_4+\text{CO}+\text{OH}$	3.90E-07	5.8	2200

(cont. on next page)

**Table A.2. (cont.)**

780	$\text{HCO}_2\text{H}+\text{HO}_2\Rightarrow\text{H}_2\text{O}_2+\text{CO}+\text{OH}$	1.00E+12	0	11920
781	$\text{HCO}_2\text{H}+\text{O}\Rightarrow\text{CO}+2\text{OH}$	1.77E+18	-1.9	2975
782	$\text{CH}_3+\text{H}(+\text{M})=\text{CH}_4(+\text{M})$	2.14E+15	-0.4	0
	Third body: co /2.0/ Third body: co2 /3.0/ Third body: h2o /5.0/ Third body: h2 /2.0/ LOW/3.31E30 -4.0E0 2.108E3/ TROE/0.0E0 1.0E-15 1.0E-15 4.0E1/			
783	$\text{CH}_4+\text{H}=\text{CH}_3+\text{H}_2$	1.73E+04	3	8224
784	$\text{HCO}+\text{OH}=\text{CO}+\text{H}_2\text{O}$	1.02E+14	0	0
785	$\text{O}+\text{H}_2=\text{H}+\text{OH}$	5.08E+04	2.67	6292
786	$\text{HCO}+\text{M}=\text{H}+\text{CO}+\text{M}$	1.86E+17	-1	17000
	Third body: co /1.9/ Third body: co2 /3.8/ Third body: h2o /12.0/ Third body: h2 /2.5/			
787	$\text{C}_2\text{H}_4+\text{O}=\text{CH}_3+\text{HCO}$	1.02E+07	1.88	179
788	$\text{H}+\text{C}_2\text{H}_4(+\text{M})=\text{C}_2\text{H}_5(+\text{M})$	1.08E+12	0.45	1822
	Third body: co /2.0/ Third body: co2 /3.0/ Third body: h2o /5.0/ Third body: h2 /2.0/ LOW/1.112E34 -5.0E0 4.448E3/ TROE/1.0E0 1.0E-15 9.5E1 2.0E2/			
789	$\text{C}_2\text{H}_6+\text{H}=\text{C}_2\text{H}_5+\text{H}_2$	5.54E+02	3.5	5167
790	$\text{C}_2\text{H}_6+\text{OH}=\text{C}_2\text{H}_5+\text{H}_2\text{O}$	5.13E+06	2.06	855
791	$\text{CH}_3+\text{HO}_2=\text{CH}_3\text{O}+\text{OH}$	1.10E+13	0	0
792	$\text{CO}+\text{HO}_2=\text{CO}_2+\text{OH}$	3.01E+13	0	23000
793	$2\text{CH}_3(+\text{M})=\text{C}_2\text{H}_6(+\text{M})$	9.21E+16	-1.17	635.8
	Third body: co /2.0/ Third body: co2 /3.0/ Third body: h2o /5.0/ Third body: h2 /2.0/ LOW/1.135E36 -5.246E0 1.705E3/ TROE/4.05E-1 1.12E3 6.96E1 1.0E15/			
794	$\text{H}+\text{O}_2(+\text{M})=\text{HO}_2(+\text{M})$	1.48E+12	0.6	0
	Third body: co /1.9/ Third body: co2 /3.8/ Third body: h2o /12.0/ Third body: h2 /2.5/ LOW/3.5E16 -4.1E-1 -1.116E3/ TROE/5.0E-1 1.0E-30 1.0E30/			
795	$\text{HCO}+\text{H}=\text{CO}+\text{H}_2$	7.34E+13	0	0
796	$\text{HCO}+\text{O}=\text{CO}+\text{OH}$	3.02E+13	0	0
797	$\text{CH}_2\text{O}+\text{OH}=\text{HCO}+\text{H}_2\text{O}$	3.43E+09	1.18	-447
798	$\text{CH}_2\text{O}+\text{H}=\text{HCO}+\text{H}_2$	9.33E+08	1.5	2976
799	$\text{CH}_3+\text{OH}=\text{CH}_2\text{O}+\text{H}_2$	2.25E+13	0	4300
800	$\text{CH}_3+\text{O}=\text{CH}_2\text{O}+\text{H}$	8.00E+13	0	0
801	$\text{CH}_3\text{O}(+\text{M})=\text{CH}_2\text{O}+\text{H}(+\text{M})$	5.45E+13	0	13500
	LOW/2.344E25 -2.7E0 3.06E4/			
802	$\text{C}_2\text{H}_4(+\text{M})=\text{C}_2\text{H}_2+\text{H}_2(+\text{M})$	1.80E+13	0	76000
	LOW/1.5E15 0.0E0 5.5443E4/			
803	$\text{HO}_2+\text{O}=\text{OH}+\text{O}_2$	3.25E+13	0	0
804	$\text{CH}_3\text{O}+\text{O}_2=\text{CH}_2\text{O}+\text{HO}_2$	5.50E+10	0	2424
805	$\text{CH}_3+\text{HO}_2=\text{CH}_4+\text{O}_2$	3.00E+12	0	0
806	$\text{HCO}+\text{O}_2=\text{CO}+\text{HO}_2$	7.58E+12	0	410
807	$\text{HO}_2+\text{OH}=\text{H}_2\text{O}+\text{O}_2$	2.89E+13	0	-500
808	$2\text{OH}(+\text{M})=\text{H}_2\text{O}_2(+\text{M})$	1.24E+14	-0.37	0
	Third body: co /1.9/ Third body: co2 /3.8/ Third body: h2o /12.0/ Third body: h2 /2.5/ LOW/3.041E30 -4.63E0 2.049E3/ TROE/4.7E-1 1.0E2 2.0E3 1.0E15/			
809	$\text{H}_2\text{O}_2+\text{H}=\text{H}_2\text{O}+\text{OH}$	2.41E+13	0	3970
810	$\text{C}_2\text{H}_2+\text{H}(+\text{M})=\text{C}_2\text{H}_3(+\text{M})$	3.11E+11	0.58	2589
	Third body: co /2.0/ Third body: co2 /3.0/ Third body: h2o /5.0/ Third body: h2 /2.0/ LOW/2.254E40 -7.269E0 6.577E3/ TROE/1.0E0 1.0E-15 6.75E2 1.0E15/			
811	$\text{C}_2\text{H}_4+\text{OH}=\text{C}_2\text{H}_3+\text{H}_2\text{O}$	2.05E+13	0	5955
812	$\text{C}_2\text{H}_2+\text{M}=\text{C}_2\text{H}+\text{H}+\text{M}$	4.20E+16	0	107000
813	$\text{CH}_2+\text{O}_2=\text{CO}+\text{H}_2\text{O}$	7.28E+19	-2.54	1809
814	$\text{C}_2\text{H}_2+\text{OH}=\text{C}_2\text{H}+\text{H}_2\text{O}$	3.37E+07	2	14000
815	$\text{O}+\text{C}_2\text{H}_2=\text{C}_2\text{H}+\text{OH}$	3.16E+15	-0.6	15000
816	$\text{C}_2\text{H}_2+\text{O}=\text{CH}_2+\text{CO}$	6.12E+06	2	1900
817	$\text{C}_2\text{H}+\text{O}_2=\text{HCO}+\text{CO}$	2.41E+12	0	0
818	$\text{C}_2\text{H}+\text{O}=\text{CO}+\text{CH}$	1.81E+13	0	0

(cont. on next page)

**Table A.2. (cont.)**

819	CH <sub>2</sub> +O <sub>2</sub> =HCO+OH	1.29E+20	-3.3	284
820	CH <sub>2</sub> +O=>CO+2H	5.00E+13	0	0
821	CH <sub>2</sub> +H=CH+H <sub>2</sub>	1.00E+18	-1.56	0
822	CH <sub>2</sub> +OH=CH+H <sub>2</sub> O	1.13E+07	2	3000
823	CH <sub>2</sub> +O <sub>2</sub> =>CO <sub>2</sub> +2H	3.29E+21	-3.3	2868
824	CH+O <sub>2</sub> =HCO+O	3.30E+13	0	0
825	CH <sub>3</sub> OH+O=CH <sub>2</sub> OH+OH	3.88E+05	2.5	3080
826	H <sub>2</sub> O <sub>2</sub> +O=OH+HO <sub>2</sub>	9.55E+06	2	3970
827	C <sub>2</sub> H <sub>2</sub> +O=HCCO+H	1.43E+07	2	1900
828	CH <sub>2</sub> CO+O=CH <sub>2</sub> +CO <sub>2</sub>	1.75E+12	0	1350
829	CH <sub>2</sub> +O <sub>2</sub> =CH <sub>2</sub> O+O	3.29E+21	-3.3	2868
830	CH <sub>2</sub> CO(+M)=CH <sub>2</sub> +CO(+M)	3.00E+14	0	70980
	LOW/3.6E15 0.0E0 5.927E4/			
831	CH <sub>2</sub> CO+O=HCCO+OH	1.00E+13	0	8000
832	CH <sub>2</sub> CO+OH=HCCO+H <sub>2</sub> O	1.00E+13	0	2000
833	CH <sub>2</sub> CO+H=HCCO+H <sub>2</sub>	2.00E+14	0	8000
834	HCCO+H=CH <sub>2</sub> (S)+CO	1.10E+14	0	0
835	HCCO+O=>H+2CO	8.00E+13	0	0
836	CH <sub>2</sub> +O <sub>2</sub> =CO <sub>2</sub> +H <sub>2</sub>	1.01E+21	-3.3	1508
837	CH <sub>3</sub> OH+OH=CH <sub>3</sub> O+H <sub>2</sub> O	1.00E+06	2.1	496.7
838	C <sub>2</sub> H <sub>5</sub> +H=2CH <sub>3</sub>	3.61E+13	0	0
839	C <sub>2</sub> H <sub>3</sub> +O <sub>2</sub> =CH <sub>2</sub> O+HCO	1.70E+29	-5.31	6500
840	C <sub>2</sub> H <sub>4</sub> +CH <sub>3</sub> =C <sub>2</sub> H <sub>3</sub> +CH <sub>4</sub>	6.62E+00	3.7	9500
841	CH <sub>3</sub> CO(+M)=CH <sub>3</sub> +CO(+M)	3.00E+12	0	16720
	LOW/1.2E15 0.0E0 1.2518E4/			
842	HCO+O=CO <sub>2</sub> +H	3.00E+13	0	0
843	CH <sub>3</sub> +M=CH <sub>2</sub> +H+M	1.97E+16	0	92520
844	CH <sub>3</sub> +H=CH <sub>2</sub> +H <sub>2</sub>	9.00E+13	0	15100
845	CH <sub>3</sub> +OH=CH <sub>2</sub> +H <sub>2</sub> O	3.00E+06	2	2500
846	CH+CH <sub>4</sub> =C <sub>2</sub> H <sub>4</sub> +H	6.00E+13	0	0
847	C <sub>2</sub> H <sub>4</sub> +O=CH <sub>2</sub> CHO+H	3.39E+06	1.88	179
848	HCCO+O <sub>2</sub> =CO <sub>2</sub> +HCO	2.40E+11	0	-854
849	CH <sub>2</sub> CO+OH=CH <sub>2</sub> OH+CO	3.73E+12	0	-1013
850	CH <sub>3</sub> +O <sub>2</sub> =CH <sub>2</sub> O+OH	7.47E+11	0	14250
851	CH <sub>3</sub> +OH=CH <sub>2</sub> (S)+H <sub>2</sub> O	2.65E+13	0	2186
852	CH <sub>2</sub> (S)+M=CH <sub>2</sub> +M	1.00E+13	0	0
853	CH <sub>2</sub> (S)+CH <sub>4</sub> =2CH <sub>3</sub>	4.00E+13	0	0
854	CH <sub>2</sub> (S)+C <sub>2</sub> H <sub>6</sub> =CH <sub>3</sub> +C <sub>2</sub> H <sub>5</sub>	1.20E+14	0	0
855	CH <sub>2</sub> (S)+O <sub>2</sub> =>CO+OH+H	7.00E+13	0	0
856	CH <sub>2</sub> (S)+H <sub>2</sub> =CH <sub>3</sub> +H	7.00E+13	0	0
857	CH <sub>2</sub> (S)+H=CH+H <sub>2</sub>	3.00E+13	0	0
858	CH <sub>2</sub> (S)+O=>CO+2H	3.00E+13	0	0
859	CH <sub>2</sub> (S)+OH=CH <sub>2</sub> O+H	3.00E+13	0	0
860	CH <sub>2</sub> (S)+CO <sub>2</sub> =CH <sub>2</sub> O+CO	3.00E+12	0	0
861	CH <sub>2</sub> (S)+CH <sub>3</sub> =C <sub>2</sub> H <sub>4</sub> +H	2.00E+13	0	0
862	CH <sub>2</sub> (S)+CH <sub>2</sub> CO=C <sub>2</sub> H <sub>4</sub> +CO	1.60E+14	0	0
863	C <sub>2</sub> H <sub>3</sub> +O <sub>2</sub> =CH <sub>2</sub> CHO+O	3.50E+14	-0.61	5260
864	CH <sub>4</sub> +OH=CH <sub>3</sub> +H <sub>2</sub> O	4.19E+06	2	2547
865	CH <sub>4</sub> +O=CH <sub>3</sub> +OH	6.92E+08	1.56	8485
866	C <sub>2</sub> H <sub>6</sub> +CH <sub>3</sub> =C <sub>2</sub> H <sub>5</sub> +CH <sub>4</sub>	6.14E+06	1.74	10450
867	CO+OH=CO <sub>2</sub> +H	1.40E+05	1.95	-1347
868	O+H <sub>2</sub> O=2OH	2.97E+06	2.02	13400
869	H <sub>2</sub> O <sub>2</sub> +OH=H <sub>2</sub> O+HO <sub>2</sub>	1.00E+12	0	0
870	H <sub>2</sub> O <sub>2</sub> +OH=H <sub>2</sub> O+HO <sub>2</sub>	5.80E+14	0	9560
871	CH <sub>3</sub> OH(+M)=CH <sub>3</sub> +OH(+M)	1.90E+16	0	91730
	Third body: co /2.0/ Third body: co2 /3.0/ Third body: h2o /16.0/ Third body: h2 /2.0/			
	LOW/2.95E44 -7.35E0 9.546E4/ TROE/4.14E-1 2.79E2 5.459E3/			
872	CH <sub>3</sub> OH+HO <sub>2</sub> =CH <sub>2</sub> OH+H <sub>2</sub> O <sub>2</sub>	3.98E+13	0	19400

(cont. on next page)



**Table A.2. (cont.)**

873	$C_2H_6+O=C_2H_5+OH$	3.00E+07	2	5115
874	$H+OH+M=H_2O+M$	2.21E+22	-2	0
	Third body: h2o /6.4/			
875	$CO+O(+M)=CO_2(+M)$	1.80E+10	0	2384
	Third body: co /1.9/ Third body: co2 /3.8/ Third body: h2o /12.0/ Third body: h2 /2.5/ LOW/1.35E24 -2.788E0 4.191E3/			
876	$CO+O_2=CO_2+O$	2.53E+12	0	47688
877	$CH_2O+M=HCO+H+M$	6.28E+29	-3.57	93200
878	$CH_2O+O=HCO+OH$	6.26E+09	1.15	2260
879	$CH_3+O_2=CH_3O+O$	2.00E+18	-1.57	29230
880	$HO_2+H=2OH$	7.08E+13	0	300
881	$HO_2+H=H_2+O_2$	1.66E+13	0	820
882	$2HO_2=H_2O_2+O_2$	4.20E+14	0	11982
883	$2HO_2=H_2O_2+O_2$	1.30E+11	0	-1629
884	$CH_4+HO_2=CH_3+H_2O_2$	3.42E+11	0	19290
885	$H+O+M=OH+M$	4.71E+18	-1	0
	Third body: h2o /6.4/			
886	$2O+M=O_2+M$	6.17E+15	-0.5	0
	Third body: co /1.9/ Third body: co2 /3.8/ Third body: h2o /12.0/ Third body: h2 /2.5/			
887	$H_2+M=2H+M$	4.57E+19	-1.4	104400
	Third body: co /1.9/ Third body: co2 /3.8/ Third body: h2o /12.0/ Third body: h2 /2.5/			
888	$C_2H_3+H(+M)=C_2H_4(+M)$	6.10E+12	0.27	280
	Third body: co /1.9/ Third body: co2 /3.8/ Third body: h2o /12.0/ Third body: h2 /2.5/ LOW/9.8E29 -3.86E0 3.32E3/ TROE/7.82E-1 2.08E2 2.663E3 6.095E3/			
889	$C_2H_4+H=C_2H_3+H_2$	1.33E+06	2.53	12240
890	$C_2H_3+O_2=HO_2+C_2H_2$	1.34E+06	1.61	-384
891	$C_2H_2+O_2=HCCO+OH$	2.00E+08	1.5	30100
892	$CH_3OH+OH=CH_2OH+H_2O$	7.10E+06	1.8	-596
893	$CH_3OH+H=CH_3O+H_2$	3.60E+12	0	6095
894	$CH_3OH+H=CH_2OH+H_2$	1.44E+13	0	6095
895	$CH_2OH+O_2=CH_2O+HO_2$	2.41E+14	0	5017
896	$CH_2OH+O_2=CH_2O+HO_2$	1.51E+15	-1	0
897	$C_2H_2+OH=CH_2CO+H$	2.18E-04	4.5	-1000
898	$C_2H_2+OH=CH_2CO+H$	2.00E+11	0	0
899	$CH_2CO+H=CH_3+CO$	2.71E+04	2.75	714
900	$CH_3+C_2H_3=CH_4+C_2H_2$	3.92E+11	0	0
901	$C_2H_3+H=C_2H_2+H_2$	4.00E+13	0	0
902	$C_2H_5+H(+M)=C_2H_6(+M)$	5.21E+17	-0.99	1580
	Third body: ch4 /2.0/ Third body: co /1.5/ Third body: co2 /2.0/ Third body: c2h6 /3.0/ Third body: h2o /6.0/ Third body: h2 /2.0/ LOW/1.99E41 -7.08E0 6.685E3/ TROE/8.422E-1 1.25E2 2.219E3 6.882E3/			

## APPENDIX B

### SKELETAL CHEMICAL KINETIC MECHANISM

Table B.1. List of species and their thermodynamic properties in the skeletal chemical kinetic mechanism of C<sub>4</sub>H<sub>10</sub>/CH<sub>3</sub>OCH<sub>3</sub> oxidation. (*H*<sub>298</sub> is the enthalpy at 298 K, *S*<sub>298</sub> is the entropy at 298 K, *C<sub>p</sub>*(300) is the heat capacity at 300 K, *C<sub>p</sub>*(3000) is the heat capacity at 3000 K, and *R* is the gas constant)

Number	Species	H298 (kcal/mole)	S298 (cal/mole-K)	Cp(300)/R	Cp(3000)/R
1	AC3H4	47.6347	57.9411	7.1698	18.303
2	AC3H5	39.6017	64.7287	8.0663	21.0195
3	ACENPHTHLN	61.6008	86.9901	19.038	56.0809
4	ANTHRACN	55.1191	92.5374	22.4279	67.6239
5	AR	-0.0007	36.9794	2.5	2.5
6	BIPHENYL	43.53	92.9207	20.1702	60.8346
7	C-C5H5	63.8038	63.5172	9.4635	26.9009
8	C-C5H6	31.9977	64.4537	8.3893	29.6948
9	C10H7	94.5052	81.0227	15.7949	47.3349
10	C10H7CCH	80.5032	100.693	17.6102	53.4928
11	C10H7CH3	29.6675	91.2406	18.968	58.2171
12	C10H7OH	-15.7062	99.605	15.459	50.3315
13	C10H8	37.4591	79.4822	16.1347	50.1614
14	C10H9	57.6011	83.1621	16.663	52.8792
15	C2H	135.0143	49.5587	4.4807	7.7061
16	C2H2	54.1979	48.0153	5.3456	10.4758
17	C2H3	68.4153	55.3304	4.8153	12.4519
18	C2H4	12.5379	52.3786	5.1503	15.1328
19	C2H4O1-2	-35.786	68.1996	7.5558	18.6382
20	C2H5	28.0164	60.1377	5.6976	17.6617
21	C2H5O	-4.2426	65.6396	7.2883	20.461
22	C2H5O2	-7.0035	75.2585	9.3614	22.9213
23	C2H6	-20.045	54.7211	6.3287	20.5748
24	C3H2	129.6103	64.8169	7.5143	11.5881
25	C3H6	4.8865	61.5133	7.782	23.33
26	C3H8	-24.8246	64.5655	8.8936	28.5272
27	C4H10	-31.8434	71.7967	11.8324	36.6187
28	C4H2	111.7139	59.7801	8.9303	15.9499
29	C4H7	30.2332	70.73	10.0763	29.0966
30	C4H8-1	-0.1331	73.5848	10.3192	30.956
31	C4H8-2	-2.6259	71.8711	9.8064	30.8971
32	C5H3	138.8709	79.1964	11.8609	21.2406
33	C6H2	169.6772	70.9256	12.3931	21.8315
34	C6H4C2H	137.6904	80.9952	13.3327	35.2534
35	C6H5	81.3956	69.2177	9.5375	29.7888
36	C6H5C2H	76.1038	79.7145	13.839	38.1832
37	C6H5C2H3	35.4394	82.3941	14.6014	43.6325
38	C6H5CCH2	80.874	91.1348	14.7343	41.1521
39	C6H5CCO	55.4109	96.0637	16.3723	38.6436
40	C6H5CH2	50.3113	76.7348	13.2438	38.0902
41	C6H5CH3	11.9975	78.1856	12.6635	40.75
42	C6H5O	10.3547	74.874	12.4752	32.7591
43	C6H5OH	-25.0122	76.9387	12.7996	34.9759

(cont. on next page)

**Table B.1. (cont.)**

44	C6H6	19.8118	64.3608	10.023	33.7267
45	CH2	92.4928	46.718	4.1504	6.6552
46	CH2(S)	101.5117	45.1	4.0638	6.6852
47	CH2CHCCH	69.149	67.3371	8.715	21.0774
48	CH2CHCCH2	74.1446	75.3201	9.809	23.3415
49	CH2CHCHCH	86.1	73.0716	9.7543	23.6125
50	CH2CHCHCH2	28.2901	70.4453	9.3495	26.5491
51	CH2CHO	5.9976	64.0012	6.6308	14.9021
52	CH2CO	-12.3994	57.7883	6.2566	12.5282
53	CH2O	-27.7059	52.2449	4.2282	9.5671
54	CH2OH	-4.1049	58.8745	5.6991	11.8792
55	CH3	34.8218	46.3748	4.6459	9.4186
56	CH3CCCH2	74.3475	80.3594	9.9137	23.4185
57	CH3CH2CCH	44.7549	71.4409	9.9478	26.1878
58	CH3CHCCH	75.9049	71.1272	10.191	23.9248
59	CH3CHCCH2	37.551	69.0775	9.7273	26.2113
60	CH3CHO	-39.5147	63.0474	6.6671	17.71
61	CH3CO	-5.404	63.7403	6.2483	14.8808
62	CH3CY24PD1	54.1121	76.6863	11.7739	34.9937
63	CH3O	3.8953	54.6045	4.5693	12.4166
64	CH3OCH2	0.9977	67.2788	8.2051	20.1382
65	CH3OCH3	-43.4069	63.7587	7.9244	22.8474
66	CH3OCO	-38.3969	90.8396	9.8758	17.7572
67	CH3PHNTHR N	44.9472	104.2957	25.2691	75.6717
68	CH4	-17.9014	44.4653	4.241	12.1923
69	CO	-26.4211	47.212	3.4973	4.4758
70	CO2	-94.0618	51.0801	4.4838	7.4803
71	CYC6H7	49.9322	72.0073	10.2478	35.4978
72	FULVENE	56.6144	70.2241	10.9031	32.65
73	H	52.0979	27.3889	2.5	2.5
74	H2	-0.0005	31.2096	3.4731	4.4635
75	H2C4O	54.5936	66.4338	8.6898	17.3844
76	H2CCCCH	116.509	72.9371	10.4847	18.3583
77	H2CCCH	83.0457	61.485	7.9713	15.3539
78	H2O	-57.8039	45.1003	4.0253	6.7088
79	H2O2	-32.5323	55.6547	5.2413	9.4918
80	HCCHCCH	129.8936	69.0633	9.0713	18.3274
81	HCCO	42.447	60.7393	6.3662	9.7152
82	HCO	10.3997	53.6602	4.1492	6.8613
83	HCOH	23.331	55.4209	4.9454	10.5034
84	HO2	3.7991	54.8015	4.1919	6.7748
85	IC3H7	21.2996	69.2584	8.7967	25.6665
86	INDENE	39.0799	77.5741	14.1155	47.0086
87	INDENYL	61.9824	78.9545	13.823	44.0963
88	NC3H7	24.0499	69.1683	8.8893	25.8561
89	O	59.5592	38.4644	2.6327	2.519
90	O2	-0.0013	49.0034	3.5277	4.7925
91	OC6H4O	-30.4471	75.1347	13.207	32.6762
92	OH	9.4899	43.8811	3.4923	4.35
93	PC3H4	45.7713	58.8964	7.3048	18.1062
94	PC3H5	64.7544	68.7423	7.8219	20.5147
95	PC4H9	15.8182	76.3863	11.6762	33.8198
96	PHNTHR N	49.4985	93.9075	22.4279	67.6239
97	PHNTHR YL-1	104.9044	94.0878	22.088	64.7971
98	PHNTHR YL-9	104.9044	94.0878	22.088	64.7971
99	PYRENE	54.0384	96.1357	24.4759	73.5525
100	SC2H4OH	-9.8531	71.5405	7.009	19.7944
101	SC3H5	61.0938	69.2502	7.7772	20.4882
102	SC4H9	12.4479	76.6064	11.599	33.8149

Table B.2. Chemical kinetic database for the skeletal chemical kinetic mechanism of C<sub>4</sub>H<sub>10</sub>/CH<sub>3</sub>OCH<sub>3</sub> oxidation. (*A* is the pre-exponential factor, *b* is the temperature exponent, and *E* is the activation energy)

No	Elementary Reaction	A	b	E
1	OH+H <sub>2</sub> =H+H <sub>2</sub> O	2.14E+08	1.5	3449
2	O+OH=O <sub>2</sub> +H	2.02E+14	-0.4	0
3	HCOH+O <sub>2</sub> =CO <sub>2</sub> +H <sub>2</sub> O	3.00E+13	0	0
4	CH <sub>2</sub> +CO <sub>2</sub> =CH <sub>2</sub> O+CO	1.10E+11	0	1000
5	CH <sub>2</sub> +C <sub>2</sub> H <sub>2</sub> =H <sub>2</sub> CCCH+H	1.20E+13	0	6600
6	CH <sub>2</sub> (S)+C <sub>2</sub> H <sub>2</sub> =H <sub>2</sub> CCCH+H	1.50E+14	0	0
7	C <sub>2</sub> H <sub>3</sub> +CH <sub>3</sub> =C <sub>3</sub> H <sub>6</sub>	4.46E+56	-13	13865
8	C <sub>2</sub> H <sub>3</sub> +C <sub>2</sub> H <sub>2</sub> =CH <sub>2</sub> CHCCH+H	2.00E+12	0	5000
9	C <sub>2</sub> H <sub>3</sub> +C <sub>2</sub> H <sub>4</sub> =CH <sub>2</sub> CHCHCH <sub>2</sub> +H	5.00E+11	0	7304
10	C <sub>2</sub> H+C <sub>2</sub> H <sub>2</sub> =C <sub>4</sub> H <sub>2</sub> +H	9.64E+13	0	0
11	HCCO+C <sub>2</sub> H <sub>2</sub> =H <sub>2</sub> CCCH+CO	1.00E+11	0	3000
12	C <sub>3</sub> H <sub>8</sub> (+M)=C <sub>2</sub> H <sub>5</sub> +CH <sub>3</sub> (+M)	7.90E+22	-1.8	88629
	Third body: H <sub>2</sub> /2.0/ Third body: H <sub>2</sub> O /5.0/ Third body: CO <sub>2</sub> /3.0/ Third body: CO /2.0/ LOW/7.237E27 -2.88E0 6.7448E4/ TROE/1.0E0 1.0E-15 1.5E3 1.0E15/			
13	C <sub>3</sub> H <sub>8</sub> +H=IC <sub>3</sub> H <sub>7</sub> +H <sub>2</sub>	1.30E+06	2.4	4471
14	C <sub>3</sub> H <sub>8</sub> +H=NC <sub>3</sub> H <sub>7</sub> +H <sub>2</sub>	1.33E+06	2.5	6756
15	C <sub>3</sub> H <sub>6</sub> =C <sub>2</sub> H <sub>2</sub> +CH <sub>4</sub>	2.50E+12	0	70000
16	C <sub>3</sub> H <sub>6</sub> =AC <sub>3</sub> H <sub>4</sub> +H <sub>2</sub>	3.00E+13	0	80000
17	C <sub>3</sub> H <sub>6</sub> +OH=AC <sub>3</sub> H <sub>5</sub> +H <sub>2</sub> O	3.12E+06	2	-298
18	C <sub>3</sub> H <sub>6</sub> +H=C <sub>2</sub> H <sub>4</sub> +CH <sub>3</sub>	7.23E+12	0	1302
19	C <sub>3</sub> H <sub>6</sub> +H=AC <sub>3</sub> H <sub>5</sub> +H <sub>2</sub>	1.73E+05	2.5	2492
20	C <sub>3</sub> H <sub>6</sub> +H=SC <sub>3</sub> H <sub>5</sub> +H <sub>2</sub>	4.09E+05	2.5	9794
21	C <sub>3</sub> H <sub>6</sub> +CH <sub>3</sub> =AC <sub>3</sub> H <sub>5</sub> +CH <sub>4</sub>	2.22E+00	3.5	5675
22	AC <sub>3</sub> H <sub>5</sub> +H=AC <sub>3</sub> H <sub>4</sub> +H <sub>2</sub>	5.00E+13	0	0
23	AC <sub>3</sub> H <sub>5</sub> +H=C <sub>3</sub> H <sub>6</sub>	1.88E+26	-3.6	5468
24	AC <sub>3</sub> H <sub>5</sub> +C <sub>2</sub> H <sub>2</sub> =C-C <sub>5</sub> H <sub>6</sub> +H	2.95E+32	-5.8	25733
25	AC <sub>3</sub> H <sub>5</sub> +CH <sub>3</sub> =C <sub>4</sub> H <sub>8</sub> -1	1.76E+50	-11	18600
26	PC <sub>3</sub> H <sub>5</sub> +O <sub>2</sub> =CH <sub>3</sub> CHO+HCO	1.09E+23	-3.3	3892
27	AC <sub>3</sub> H <sub>4</sub> +H=H <sub>2</sub> CCCH+H <sub>2</sub>	2.00E+07	2	5000
28	AC <sub>3</sub> H <sub>4</sub> +OH=H <sub>2</sub> CCCH+H <sub>2</sub> O	1.00E+07	2	1000
29	AC <sub>3</sub> H <sub>4</sub> =PC <sub>3</sub> H <sub>4</sub>	1.48E+13	0	60401
30	PC <sub>3</sub> H <sub>4</sub> +H=H <sub>2</sub> CCCH+H <sub>2</sub>	2.00E+07	2	5000
31	PC <sub>3</sub> H <sub>4</sub> +OH=H <sub>2</sub> CCCH+H <sub>2</sub> O	1.00E+07	2	1000
32	PC <sub>3</sub> H <sub>4</sub> +CH <sub>3</sub> =H <sub>2</sub> CCCH+CH <sub>4</sub>	1.50E+00	3.5	5600
33	PC <sub>3</sub> H <sub>4</sub> +H=CH <sub>3</sub> +C <sub>2</sub> H <sub>2</sub>	5.12E+10	1	2060
34	AC <sub>3</sub> H <sub>4</sub> +H(+M)=AC <sub>3</sub> H <sub>5</sub> (+M)	1.20E+11	0.7	3007
	LOW/5.56E33 -5.0E0 4.448E3/			
35	AC <sub>3</sub> H <sub>4</sub> +H(+M)=SC <sub>3</sub> H <sub>5</sub> (+M)	8.49E+12	0	2000
	LOW/1.11E34 -5.0E0 4.448E3/			
36	H <sub>2</sub> CCCH+O <sub>2</sub> =CH <sub>2</sub> CO+HCO	3.00E+10	0	2868
37	H <sub>2</sub> CCCH+H=C <sub>3</sub> H <sub>2</sub> +H <sub>2</sub>	5.00E+13	0	3000
38	H <sub>2</sub> CCCH+CH <sub>3</sub> =CH <sub>3</sub> CHCCH <sub>2</sub>	5.00E+12	0	0
39	H <sub>2</sub> CCCH+CH <sub>3</sub> =CH <sub>3</sub> CH <sub>2</sub> CCH	5.00E+12	0	0
	H <sub>2</sub> CCCH+H(+M)=AC <sub>3</sub> H <sub>4</sub> (+M)	1.66E+15	-0.4	0
40	Third body: C <sub>2</sub> H <sub>2</sub> /2.0/ Third body: H <sub>2</sub> /2.0/ Third body: H <sub>2</sub> O /5.0/ Third body: CO <sub>2</sub> /3.0/ Third body: CO /2.0/ Third body: O <sub>2</sub> /2.0/ LOW/3.36E45 -8.52E0 6.293E3/			
41	2H <sub>2</sub> CCCH=C <sub>6</sub> H <sub>6</sub>	5.56E+20	-2.5	1692
42	H <sub>2</sub> CCCH+AC <sub>3</sub> H <sub>5</sub> =FULVENE+2H	5.56E+20	-2.5	1692
43	2H <sub>2</sub> CCCH=C <sub>6</sub> H <sub>5</sub> +H	2.00E+12	0	0
44	C <sub>3</sub> H <sub>2</sub> +O <sub>2</sub> =HCCO+CO+H	5.00E+13	0	0
45	C <sub>4</sub> H <sub>10</sub> =2C <sub>2</sub> H <sub>5</sub>	2.00E+16	0	81300
46	C <sub>4</sub> H <sub>10</sub> =NC <sub>3</sub> H <sub>7</sub> +CH <sub>3</sub>	1.74E+17	0	85700
47	C <sub>4</sub> H <sub>10</sub> +H=PC <sub>4</sub> H <sub>9</sub> +H <sub>2</sub>	2.84E+05	2.5	6050
48	C <sub>4</sub> H <sub>10</sub> +H=SC <sub>4</sub> H <sub>9</sub> +H <sub>2</sub>	5.68E+05	2.4	3765

(cont. on next page)

**Table B.2. (cont.)**

49	SC4H9=C4H8-1+H	2.00E+13	0	40400
50	SC4H9=C4H8-2+H	5.01E+12	0	37900
51	PC4H9=C4H8-1+H	1.26E+13	0	38600
52	C4H8-1+H=C4H7+H2	5.00E+13	0	3900
53	C4H8-2+H=C4H7+H2	5.00E+13	0	3800
54	C4H8-2+O2=C4H7+HO2	8.00E+13	0	37400
55	C4H7=CH2CHCHCH2+H	1.00E+14	0	55000
56	CH2CHCHCH2+H=CH2CHCHCH+H2	3.00E+07	2	13000
57	CH2CHCHCH2+H=CH2CHCCH2+H2	3.00E+07	2	6000
58	CH3CH2CCH+H=C2H5+C2H2	1.00E+14	0	3000
59	CH3CHCCH2+H=CH3+AC3H4	2.00E+13	0	2000
60	CH2CHCCH2+H=CH3+H2CCCH	1.00E+14	0	0
61	CH3CCCH2+H=CH3+H2CCCH	1.00E+14	0	0
62	CH2CHCCH2(+M)=CH2CHCCH+H(+M)	1.00E+14	0	50000
	LOW/2.0E15 0.0E0 4.2E4/			
63	CH3CCCH2+H2CCCH=C6H5CH2+H	3.00E+12	0	0
64	CH2CHCCH+OH=H2CCCCH+H2O	1.00E+07	2	2000
65	CH2CHCCH+H=H2CCCCH+H2	3.00E+07	2	5000
66	H2CCCCH+O2=CH2CO+HCCO	1.00E+12	0	0
67	H2CCCCH+H=C4H2+H2	5.00E+13	0	0
68	H2CCCCH+C2H2=C6H5	3.00E+11	0	14900
69	H2CCCCH(+M)=C4H2+H(+M)	1.00E+14	0	47000
	LOW/2.0E15 0.0E0 4.0E4/			
70	C4H2+OH=H2C4O+H	6.66E+12	0	-410
71	C-C5H6+OH=C-C5H5+H2O	3.43E+09	1.2	-447
72	C-C5H6+H=C-C5H5+H2	2.19E+08	1.8	3000
73	C-C5H5+H=C-C5H6	2.00E+14	0	0
74	2C-C5H5=C10H8+2H	2.00E+13	0	8000
75	C6H6+OH=C6H5+H2O	1.63E+08	1.4	1454
76	C6H6+OH=C6H5OH+H	6.70E+12	0	10592
77	C6H6+O=C6H5O+H	2.40E+13	0	4670
78	C6H6+H=C6H5+H2	3.03E+02	3.3	5690
79	C6H5+C2H4=C6H5C2H3+H	7.23E+01	3.5	8345
80	C6H5+C2H2=C6H5C2H+H	3.98E+13	0	10099
81	C6H5+O2=C6H5O+O	2.60E+13	0	6120
82	C6H5+C6H6=BIPHENYL+H	4.00E+11	0	4000
83	C6H5CH3=C6H5+CH3	1.40E+16	0	99800
84	C6H5CH3+H=C6H5CH2+H2	3.98E+02	3.4	3120
85	C6H5CH3+H=C6H6+CH3	1.20E+13	0	5148
86	C6H5CH2+H=C6H5CH3	1.80E+14	0	0
87	C6H5CH2+C2H2=INDENE+H	3.20E+11	0	7000
88	C6H5CCH2+H=C6H5C2H+H2	5.00E+13	0	0
89	C6H5C2H+O=C6H5CCO+H	4.80E+09	1	0
90	C6H5C2H+H=C6H4C2H+H2	3.03E+02	3.3	5690
91	INDENE+OH=INDENYL+H2O	3.43E+09	1.2	-447
92	INDENE+H=INDENYL+H2	2.19E+08	1.8	3000
93	INDENYL+H=INDENE	2.00E+14	0	0
94	INDENYL+C-C5H5=PHNTHRN+2H	1.00E+13	0	8000
95	C10H8+H=C10H9	5.00E+14	0	5000
96	C10H8+OH=C10H7OH+H	9.00E+12	0	10592
97	C10H8+H=C10H7+H2	4.55E+02	3.3	5690
98	C10H7+C2H2=ACENPHTHLN+H	1.00E+20	-2.1	12000
99	C10H7CH3+H=C10H8+CH3	1.20E+13	0	5148
100	C10H7CCH+H=ACENPHTHLN+H	8.46E+21	-2.6	7062.6
101	PHNTHRN+H=PHNTHRYL-1+H2	4.04E+02	3.3	5690
102	PHNTHRN+H=PHNTHRYL-9+H2	1.01E+02	3.3	5690
103	ANTHRACN=PHNTHRN	8.00E+12	0	65000
104	PHNTHRYL-1+C2H2=PYRENE+H	3.49E+10	0.6	5658
105	CH3PHNTHRN+H=PHNTHRN+CH3	1.20E+13	0	5148

(cont. on next page)

**Table B.2. (cont.)**

106	$C_6H_6+H=CH_3CY_24PD1$	2.39E+27	-3.9	29200
107	$CH_2O+CH_3=HCO+CH_4$	3.64E-06	5.4	998
108	$SC_2H_4OH+M=CH_3CHO+H+M$	1.00E+14	0	25000
109	$CH_3CHO=CH_3+HCO$	2.61E+15	0.1	80550
110	$CH_3CHO+H=CH_3CO+H_2$	1.34E+13	0	3300
111	$C_2H_5O_2=C_2H_5+O_2$	4.93E+50	-11.5	42250
112	$C_2H_5O+M=CH_3CHO+H+M$	1.16E+35	-5.9	25270
113	$C_2H_4O_1-2=CH_3CHO$	7.41E+12	0	53800
114	$CH_3OCH_3=CH_3+CH_3O$	4.86E+55	-11.6	102100
115	$CH_3OCH_3+OH=CH_3OCH_2+H_2O$	9.35E+05	2.3	-780
116	$CH_3OCH_3+H=CH_3OCH_2+H_2$	7.72E+06	2.1	3384
117	$CH_3OCH_3+CH_3=CH_3OCH_2+CH_4$	1.44E-06	5.7	5699
118	$CH_3+H(+M)=CH_4(+M)$	2.14E+15	-0.4	0
	Third body: H <sub>2</sub> /2.0/ Third body: H <sub>2</sub> O /5.0/ Third body: CO <sub>2</sub> /3.0/ Third body: CO /2.0/ LOW/3.31E30 -4.0E0 2.108E3/ TROE/0.0E0 1.0E-15 1.0E-15 4.0E1/			
119	$CH_4+H=CH_3+H_2$	1.73E+04	3	8224
120	$HCO+M=H+CO+M$	1.86E+17	-1	17000
	Third body: H <sub>2</sub> /2.5/ Third body: H <sub>2</sub> O /12.0/ Third body: CO <sub>2</sub> /3.8/ Third body: CO /1.9/			
121	$H+C_2H_4(+M)=C_2H_5(+M)$	1.08E+12	0.5	1822
	Third body: H <sub>2</sub> /2.0/ Third body: H <sub>2</sub> O /5.0/ Third body: CO <sub>2</sub> /3.0/ Third body: CO /2.0/ LOW/1.112E34 -5.0E0 4.448E3/ TROE/1.0E0 1.0E-15 9.5E1 2.0E2/			
122	$C_2H_6+H=C_2H_5+H_2$	5.54E+02	3.5	5167
123	$C_2H_6+OH=C_2H_5+H_2O$	5.12E+06	2.1	855
124	$2CH_3(+M)=C_2H_6(+M)$	9.21E+16	-1.2	635.8
	Third body: H <sub>2</sub> /2.0/ Third body: H <sub>2</sub> O /5.0/ Third body: CO <sub>2</sub> /3.0/ Third body: CO /2.0/ LOW/1.135E36 -5.246E0 1.705E3/ TROE/4.05E-1 1.12E3 6.96E1 1.0E15/			
125	$H+O_2(+M)=HO_2(+M)$	1.48E+12	0.6	0
	Third body: H <sub>2</sub> /2.5/ Third body: H <sub>2</sub> O /12.0/ Third body: CO <sub>2</sub> /3.8/ Third body: CO /1.9/ LOW/3.5E16 -4.1E-1 -1.116E3/ TROE/5.0E-1 1.0E-30 1.0E30/			
126	$CH_2O+OH=HCO+H_2O$	3.43E+09	1.2	-447
127	$CH_2O+H=HCO+H_2$	9.33E+08	1.5	2976
128	$CH_3+OH=CH_2O+H_2$	2.25E+13	0	4300
129	$CH_3O(+M)=CH_2O+H(+M)$	5.45E+13	0	13500
	LOW/2.344E25 -2.7E0 3.06E4/			
130	$C_2H_4(+M)=C_2H_2+H_2(+M)$	1.80E+13	0	76000
	LOW/1.5E15 0.0E0 5.5443E4/			
131	$C_2H_2+H(+M)=C_2H_3(+M)$	3.11E+11	0.6	2589
	Third body: H <sub>2</sub> /2.0/ Third body: H <sub>2</sub> O /5.0/ Third body: CO <sub>2</sub> /3.0/ Third body: CO /2.0/ LOW/2.254E40 -7.269E0 6.577E3/ TROE/1.0E0 1.0E-15 6.75E2 1.0E15/			
132	$C_2H_4+OH=C_2H_3+H_2O$	2.05E+13	0	5955
133	$C_2H_2+OH=C_2H+H_2O$	3.37E+07	2	14000
134	$C_2H_2+O=CH_2+CO$	6.12E+06	2	1900
135	$C_2H_2+O=HCCO+H$	1.43E+07	2	1900
136	$CH_2CO(+M)=CH_2+CO(+M)$	3.00E+14	0	70980
	LOW/3.6E15 0.0E0 5.927E4/			
137	$CH_2CO+H=HCCO+H_2$	2.00E+14	0	8000
138	$C_2H_3+O_2=CH_2O+HCO$	1.70E+29	-5.3	6500
139	$C_2H_4+CH_3=C_2H_3+CH_4$	6.62E+00	3.7	9500
140	$CH_3CO(+M)=CH_3+CO(+M)$	3.00E+12	0	16720
	LOW/1.2E15 0.0E0 1.2518E4/			
141	$CH_3+O_2=CH_2O+OH$	7.47E+11	0	14250
142	$CH_2(S)+H_2=CH_3+H$	7.00E+13	0	0
143	$CH_2(S)+CO_2=CH_2O+CO$	3.00E+12	0	0
144	$C_2H_3+O_2=CH_2CHO+O$	3.50E+14	-0.6	5260
145	$CH_4+OH=CH_3+H_2O$	4.19E+06	2	2547
146	$C_2H_6+CH_3=C_2H_5+CH_4$	6.14E+06	1.7	10450
147	$CO+OH=CO_2+H$	1.40E+05	1.9	-1347
148	$2HO_2=H_2O_2+O_2$	4.20E+14	0	11982
149	$C_2H_4+H=C_2H_3+H_2$	1.32E+06	2.5	12240

(cont. on next page)

**Table B.2. (cont.)**

150	$C_2H_2+O_2=HCCO+OH$	2.00E+08	1.5	30100
151	$CH_2OH+O_2=CH_2O+HO_2$	2.41E+14	0	5017
152	$C_2H_2+OH=CH_2CO+H$	2.00E+11	0	0
153	$CH_2CO+H=CH_3+CO$	2.71E+04	2.8	714
154	$H+HO_2=O+H_2O$	3.01E+13	0	1721
155	$C_3H_6+H=PC_3H_5+H_2$	8.04E+05	2.5	12284
156	$AC_3H_5+O_2=CH_2CHO+CH_2O$	1.06E+10	0.3	12838
157	$AC_3H_5+CH_3=AC_3H_4+CH_4$	3.02E+12	-0.3	-131
158	$AC_3H_4+CH_3=H_2CCCH+CH_4$	1.50E+00	3.5	5600
159	$H_2CCCH+OH=C_3H_2+H_2O$	2.00E+13	0	0
160	$H_2CCCH+H(+M)=PC_3H_4(+M)$	1.66E+15	-0.4	0
	Third body: $C_2H_2$ /2.0/ Third body: $H_2$ /2.0/ Third body: $H_2O$ /5.0/ Third body: $CO_2$ /3.0/ Third body: $CO$ /2.0/ Third body: $O_2$ /2.0/ LOW/8.78E45 -8.9E0 7.974E3/			
161	$C_4H_8-1+OH=C_4H_7+H_2O$	2.25E+13	0	2217
162	$C_4H_8-2+OH=C_4H_7+H_2O$	3.90E+13	0	2217
163	$CH_2CHCHCH_2+OH=CH_2CHCCH_2+H_2O$	2.00E+07	2	2000
164	$CH_2CHCCH_2+C_2H_2=C_6H_6+H$	3.00E+11	0	14900
165	$CH_3CHCCH(+M)=CH_2CHCCH+H(+M)$	1.00E+13	0	49000
166	$HCCHCCH+C_2H_2=C_6H_5$	9.60E+70	-17.8	31300
167	$HCCHCCH(+M)=C_4H_2+H(+M)$	1.00E+14	0	36000
168	$C_4H_2+CH_2=C_5H_3+H$	1.30E+13	0	4326
169	$C_4H_2+C_2H=C_6H_2+H$	9.60E+13	0	0
170	$C-C_5H_6+CH_3=C-C_5H_5+CH_4$	3.11E+11	0	5500
171	$C_6H_5+O_2=OC_6H_4O+H$	3.00E+13	0	8981
172	$C_6H_5CH_3+CH_3=CH_4+C_6H_5CH_2$	3.16E+11	0	9500
173	$C_6H_5C_2H+OH=C_6H_4C_2H+H_2O$	1.63E+08	1.4	1454
174	$C_6H_6+H=CYC_6H_7$	4.87E+56	-12.7	26800
175	$FULVENE=C_6H_6$	9.84E+37	-7.4	76979
176	$FULVENE+H=C_6H_6+H$	3.00E+12	0.5	2000
177	$CH_3CHO+CH_3=CH_3CO+CH_4$	2.61E+06	1.8	5911
178	$CH_3OCO=CH_3+CO_2$	1.51E+12	-1.8	13820
179	$O+H_2=H+OH$	5.08E+04	2.7	6292
180	$CO+HO_2=CO_2+OH$	3.01E+13	0	23000
181	$CH_3+H=CH_2+H_2$	9.00E+13	0	15100
182	$CH_3+OH=CH_2(S)+H_2O$	2.65E+13	0	2186
183	$CH_2(S)+CH_4=2CH_3$	4.00E+13	0	0
184	$CH_4+O=CH_3+OH$	6.92E+08	1.6	8485
185	$CH_2OH+O_2=CH_2O+HO_2$	1.51E+15	-1	0
186	$C_2H_2+OH=CH_2CO+H$	2.18E-04	4.5	-1000